TOPICS ON ENVIRONMENTAL AND PHYSICAL GEODESY

Compiled by Jose M. Redondo

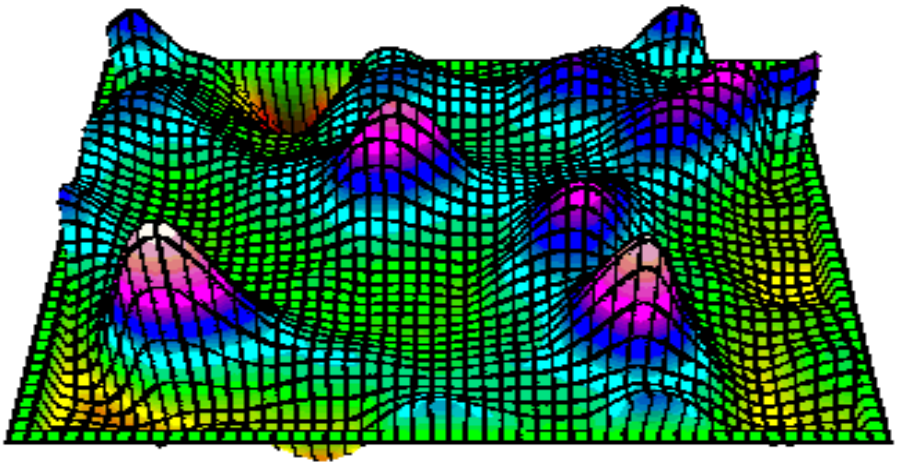

Dept. Fisica Aplicada UPC, Barcelona Tech.
November 2014

Contents

Chapter 1

Vector calculus identities

See also: Vector algebra relations

The following identities are important in vector calculus:

1.1 Operator notations

1.1.1 Gradient

Main article: Gradient

Gradient of a tensor field, $\mathfrak{T}$, of order n, is generally written as

$$\operatorname{grad}(\mathfrak{T}) = \nabla\mathfrak{T}$$

and is a tensor field of order $n + 1$. In particular, if the tensor field has order 0 (i.e. a scalar), ψ , the resulting gradient,

$$\operatorname{grad}(\psi) = \nabla\psi$$

is a vector field.

1.1.2 Divergence

Main article: Divergence

The divergence of a tensor field, $\mathfrak{T}$, of non-zero order n, is generally written as

$$\operatorname{div}(\mathfrak{T}) = \nabla \cdot \mathfrak{T}$$

and is a contraction to a tensor field of order $n - 1$. Specifically, the divergence of a vector is a scalar. The divergence of a higher order tensor field may be found by decomposing the tensor field into a sum of outer products, thereby allowing the use of the identity,

$$\nabla \cdot (\mathbf{a} \otimes \hat{\mathfrak{T}}) = \hat{\mathfrak{T}}(\nabla \cdot \mathbf{a}) + (\mathbf{a} \cdot \nabla)\hat{\mathfrak{T}}$$

where $\mathbf{a} \cdot \nabla$ is the directional derivative in the direction of $\mathbf{a}$ multiplied by its magnitude. Specifically, for the outer product of two vectors,

$$\nabla \cdot (\mathbf{a}\mathbf{b}^{\mathrm{T}}) = \mathbf{b}(\nabla \cdot \mathbf{a}) + (\mathbf{a} \cdot \nabla)\mathbf{b} \,.$$

1.1.3 Curl

Main article: Curl (mathematics)

For a 3-dimensional vector field $\mathbf{v}$, curl is generally written as:

$$\operatorname{curl}(\mathbf{v}) = \nabla \times \mathbf{v}$$

and is also a 3-dimensional vector field.

1.1.4 Laplacian

Main article: Laplace operator

For a tensor field, $\mathfrak{T}$, the laplacian is generally written as:

$$\Delta\mathfrak{T} = \nabla^2\mathfrak{T} = (\nabla \cdot \nabla)\mathfrak{T}$$

and is a tensor field of the same order.

1.1.5 Special notations

In *Feynman subscript notation*,

$$\nabla_{\mathbf{B}}\,(\mathbf{A} \cdot \mathbf{B}) = \mathbf{A} \times (\nabla \times \mathbf{B}) + (\mathbf{A} \cdot \nabla)\,\mathbf{B}$$

where the notation $\nabla\mathbf{B}$ means the subscripted gradient operates on only the factor $\mathbf{B}$.[1][2]

A less general but similar idea is used in *geometric algebra* where the so-called Hestenes *overdot notation* is employed.[3] The above identity is then expressed as:

$$\dot{\nabla}\left(\mathbf{A}\cdot\dot{\mathbf{B}}\right) = \mathbf{A}\times(\nabla\times\mathbf{B}) + (\mathbf{A}\cdot\nabla)\,\mathbf{B}$$

where overdots define the scope of the vector derivative. The dotted vector, in this case **B**, is differentiated, while the (undotted) **A** is held constant.

For the remainder of this article, Feynman subscript notation will be used where appropriate.

1.2 Properties

1.2.1 Distributive properties

$$\nabla(\psi+\phi) = \nabla\psi + \nabla\phi$$

$$\nabla\cdot(\mathbf{A}+\mathbf{B}) = \nabla\cdot\mathbf{A} + \nabla\cdot\mathbf{B}$$

$$\nabla\times(\mathbf{A}+\mathbf{B}) = \nabla\times\mathbf{A} + \nabla\times\mathbf{B}$$

1.2.2 Product rule for the gradient

The gradient of the product of two scalar fields ψ and ϕ follows the same form as the product rule in single variable calculus.

$$\nabla(\psi\,\phi) = \phi\,\nabla\psi + \psi\,\nabla\phi$$

1.2.3 Product of a scalar and a vector

$$\nabla\cdot(\psi\mathbf{A}) = \mathbf{A}\cdot\nabla\psi + \psi\nabla\cdot\mathbf{A}$$

$$\nabla\times(\psi\mathbf{A}) = \psi(\nabla\times\mathbf{A}) + (\nabla\psi)\times\mathbf{A}$$

1.2.4 Quotient rule

$$\nabla\left(\frac{f}{g}\right) = \frac{g\nabla f - f\nabla g}{g^2}$$

$$\nabla\cdot\left(\frac{\mathbf{A}}{g}\right) = \frac{(\nabla\cdot\mathbf{A})g - \mathbf{A}\cdot\nabla g}{g^2}$$

$$\nabla\times\left(\frac{\mathbf{A}}{g}\right) = \frac{(\nabla\times\mathbf{A})g + \mathbf{A}\times\nabla g}{g^2}$$

1.2.5 Chain rule

$$\nabla(f\circ g) = (f'\circ g)\nabla g$$

$$\nabla(f\circ\mathbf{A}) = (\nabla f\circ\mathbf{A})\nabla\mathbf{A}$$

$$\nabla\cdot(\mathbf{A}\circ f) = (\mathbf{A}'\circ f)\cdot\nabla f$$

$$\nabla\times(\mathbf{A}\circ f) = -(\mathbf{A}'\circ f)\times\nabla f$$

1.2.6 Vector dot product

$$\begin{aligned}\nabla(\mathbf{A}\cdot\mathbf{B}) &= \mathbf{J}_{\mathbf{A}}^{\mathrm{T}}\mathbf{B} + \mathbf{J}_{\mathbf{B}}^{\mathrm{T}}\mathbf{A}\\ &= (\mathbf{A}\cdot\nabla)\mathbf{B} + (\mathbf{B}\cdot\nabla)\mathbf{A} + \mathbf{A}\times(\nabla\times\mathbf{B}) + \mathbf{B}\times(\nabla\times\mathbf{A})\,.\end{aligned}$$

where **JA** denotes the Jacobian of **A**.

Alternatively, using Feynman subscript notation,

$$\nabla(\mathbf{A}\cdot\mathbf{B}) = \nabla_{\mathbf{A}}(\mathbf{A}\cdot\mathbf{B}) + \nabla_{\mathbf{B}}(\mathbf{A}\cdot\mathbf{B})\,.$$

As a special case, when **A** = **B**,

$$\begin{aligned}\frac{1}{2}\nabla\left(\mathbf{A}\cdot\mathbf{A}\right) &= \mathbf{J}_{\mathbf{A}}^{\mathrm{T}}\mathbf{A}\\ &= (\mathbf{A}\cdot\nabla)\mathbf{A} + \mathbf{A}\times(\nabla\times\mathbf{A})\,.\end{aligned}$$

1.2.7 Vector cross product

$$\nabla\cdot(\mathbf{A}\times\mathbf{B}) = \mathbf{B}\cdot(\nabla\times\mathbf{A}) - \mathbf{A}\cdot(\nabla\times\mathbf{B})$$

$$\begin{aligned}\nabla\times(\mathbf{A}\times\mathbf{B}) &= \mathbf{A}(\nabla\cdot\mathbf{B}) - \mathbf{B}(\nabla\cdot\mathbf{A}) + (\mathbf{B}\cdot\nabla)\mathbf{A} - (\mathbf{A}\cdot\nabla)\mathbf{B}\\ &= (\nabla\cdot\mathbf{B} + \mathbf{B}\cdot\nabla)\mathbf{A} - (\nabla\cdot\mathbf{A} + \mathbf{A}\cdot\nabla)\mathbf{B}\\ &= \nabla\cdot(\mathbf{B}\mathbf{A}^{\mathrm{T}}) - \nabla\cdot(\mathbf{A}\mathbf{B}^{\mathrm{T}})\\ &= \nabla\cdot(\mathbf{B}\mathbf{A}^{\mathrm{T}} - \mathbf{A}\mathbf{B}^{\mathrm{T}})\end{aligned}$$

1.3 Second derivatives

1.3.1 Curl of the gradient

The curl of the gradient of *any* scalar field ϕ is always the zero vector:

$$\nabla\times(\nabla\phi) = \mathbf{0}$$

1.3.2 Divergence of the curl

The divergence of the curl of *any* vector field **A** is always zero:

$$\nabla\cdot(\nabla\times\mathbf{A}) = 0$$

1.3.3 Divergence of the gradient

The Laplacian of a scalar field is defined as the divergence of the gradient:

$$\nabla^2\psi = \nabla\cdot(\nabla\psi)$$

Note that the result is a scalar quantity.

1.3.4 Curl of the curl

$\nabla \times (\nabla \times \mathbf{A}) = \nabla(\nabla \cdot \mathbf{A}) - \nabla^2 \mathbf{A}$

Here,∇^2 is the vector Laplacian operating on the vector field $\mathbf{A}$.

1.4 Summary of important identities

1.4.1 Addition and multiplication

- $\mathbf{A} + \mathbf{B} = \mathbf{B} + \mathbf{A}$
- $\mathbf{A} \cdot \mathbf{B} = \mathbf{B} \cdot \mathbf{A}$
- $\mathbf{A} \times \mathbf{B} = -\mathbf{B} \times \mathbf{A}$
- $(\mathbf{A} + \mathbf{B}) \cdot \mathbf{C} = \mathbf{A} \cdot \mathbf{C} + \mathbf{B} \cdot \mathbf{C}$
- $(\mathbf{A} + \mathbf{B}) \times \mathbf{C} = \mathbf{A} \times \mathbf{C} + \mathbf{B} \times \mathbf{C}$
- $\mathbf{A} \cdot (\mathbf{B} \times \mathbf{C}) = \mathbf{B} \cdot (\mathbf{C} \times \mathbf{A}) = \mathbf{C} \cdot (\mathbf{A} \times \mathbf{B})$ (scalar triple product)
- $\mathbf{A} \times (\mathbf{B} \times \mathbf{C}) = (\mathbf{A} \cdot \mathbf{C})\,\mathbf{B} - (\mathbf{A} \cdot \mathbf{B})\,\mathbf{C}$ (vector triple product)
- $(\mathbf{A} \times \mathbf{B}) \times \mathbf{C} = (\mathbf{A} \cdot \mathbf{C})\,\mathbf{B} - (\mathbf{B} \cdot \mathbf{C})\,\mathbf{A}$ (vector triple product)
- $(\mathbf{A} \times \mathbf{B}) \cdot (\mathbf{C} \times \mathbf{D}) = (\mathbf{A} \cdot \mathbf{C})\,(\mathbf{B} \cdot \mathbf{D}) - (\mathbf{B} \cdot \mathbf{C})\,(\mathbf{A} \cdot \mathbf{D})$
- $(\mathbf{A} \cdot (\mathbf{B} \times \mathbf{C}))\,\mathbf{D} = (\mathbf{A} \cdot \mathbf{D})\,(\mathbf{B} \times \mathbf{C}) + (\mathbf{B} \cdot \mathbf{D})\,(\mathbf{C} \times \mathbf{A}) + (\mathbf{C} \cdot \mathbf{D})\,(\mathbf{A} \times \mathbf{B})$
- $(\mathbf{A} \times \mathbf{B}) \times (\mathbf{C} \times \mathbf{D}) = (\mathbf{A} \cdot (\mathbf{B} \times \mathbf{D}))\,\mathbf{C} - (\mathbf{A} \cdot (\mathbf{B} \times \mathbf{C}))\,\mathbf{D}$

1.4.2 Differentiation

Gradient

- $\nabla(\psi + \phi) = \nabla\psi + \nabla\phi$
- $\nabla(\psi\,\phi) = \phi\,\nabla\psi + \psi\,\nabla\phi$
- $\nabla\,(\mathbf{A} \cdot \mathbf{B}) = (\mathbf{A} \cdot \nabla)\,\mathbf{B} + (\mathbf{B} \cdot \nabla)\,\mathbf{A} + \mathbf{A} \times (\nabla \times \mathbf{B}) + \mathbf{B} \times (\nabla \times \mathbf{A})$

Divergence

- $\nabla \cdot (\mathbf{A} + \mathbf{B}) = \nabla \cdot \mathbf{A} + \nabla \cdot \mathbf{B}$
- $\nabla \cdot (\psi\mathbf{A}) = \psi\nabla \cdot \mathbf{A} + \mathbf{A} \cdot \nabla\psi$
- $\nabla \cdot (\mathbf{A} \times \mathbf{B}) = \mathbf{B} \cdot (\nabla \times \mathbf{A}) - \mathbf{A} \cdot (\nabla \times \mathbf{B})$

Curl

- $\nabla \times (\mathbf{A} + \mathbf{B}) = \nabla \times \mathbf{A} + \nabla \times \mathbf{B}$
- $\nabla \times (\psi\mathbf{A}) = \psi\nabla \times \mathbf{A} + \nabla\psi \times \mathbf{A}$
- $\nabla \times (\mathbf{A} \times \mathbf{B}) = \mathbf{A}\,(\nabla \cdot \mathbf{B}) - \mathbf{B}\,(\nabla \cdot \mathbf{A}) + (\mathbf{B} \cdot \nabla)\,\mathbf{A} - (\mathbf{A} \cdot \nabla)\,\mathbf{B}$

Second derivatives

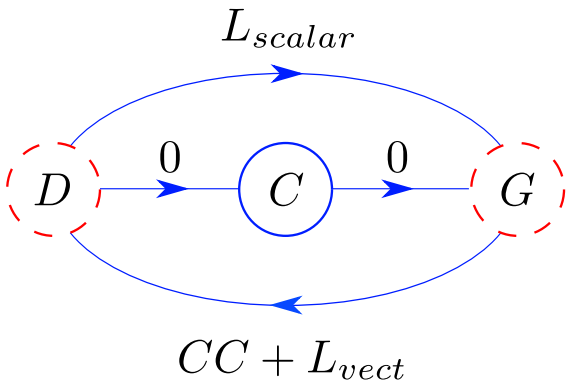

DCG chart: A simple chart depicting all rules pertaining to second derivatives. D, C, G, L and CC stand for divergence, curl, gradient, Laplacian and curl of curl, respectively. Arrows indicate existence of second derivatives. Blue circle in the middle represents curl of curl, whereas the other two red circles(dashed) mean that DD and GG do not exist.

- $\nabla \cdot (\nabla \times \mathbf{A}) = 0$
- $\nabla \times (\nabla\psi) = \mathbf{0}$
- $\nabla \cdot (\nabla\psi) = \nabla^2\psi$ (scalar Laplacian)
- $\nabla\,(\nabla \cdot \mathbf{A}) - \nabla \times (\nabla \times \mathbf{A}) = \nabla^2\mathbf{A}$ (vector Laplacian)
- $\nabla \cdot (\phi\nabla\psi) = \phi\nabla^2\psi + \nabla\phi \cdot \nabla\psi$
- $\psi\nabla^2\phi - \phi\nabla^2\psi = \nabla \cdot (\psi\nabla\phi - \phi\nabla\psi)$
- $\nabla^2(\phi\psi) = \phi\nabla^2\psi + 2\nabla\phi \cdot \nabla\psi + \psi\nabla^2\phi$
- $\nabla^2(\psi\mathbf{A}) = \mathbf{A}\nabla^2\psi + 2(\nabla\psi \cdot \nabla)\mathbf{A} + \psi\nabla^2\mathbf{A}$
- $\nabla^2(\mathbf{A} \cdot \mathbf{B}) = \mathbf{A} \cdot \nabla^2\mathbf{B} - \mathbf{B} \cdot \nabla^2\mathbf{A} + 2\nabla \cdot ((\mathbf{B} \cdot \nabla)\mathbf{A} + \mathbf{B} \times \nabla \times \mathbf{A})$ (Green's vector identity)

Third derivatives

- $\nabla^2(\nabla\psi) = \nabla(\nabla \cdot (\nabla\psi)) = \nabla(\nabla^2\psi)$
- $\nabla^2(\nabla \cdot \mathbf{A}) = \nabla \cdot (\nabla(\nabla \cdot \mathbf{A})) = \nabla \cdot (\nabla^2\mathbf{A})$
- $\nabla^2(\nabla \times \mathbf{A}) = -\nabla \times (\nabla \times (\nabla \times \mathbf{A})) = \nabla \times (\nabla^2\mathbf{A})$

1.4.3 Integration

Below, the curly symbol ∂ means "boundary of".

Surface–volume integrals

In the following surface–volume integral theorems, V denotes a 3d volume with a corresponding 2d boundary $S = \partial V$ (a closed surface):

- $\oiint_{\partial V} \mathbf{A} \cdot d\mathbf{S} = \iiint_V (\nabla \cdot \mathbf{A})\, dV$ (Divergence theorem)
- $\oiint_{\partial V} \psi d\mathbf{S} = \iiint_V \nabla\psi\, dV$
- $\oiint_{\partial V} (\hat{\mathbf{n}} \times \mathbf{A})\, dS = \iiint_V (\nabla \times \mathbf{A})\, dV$
- $\oiint_{\partial V} \psi\, (\nabla\varphi \cdot \hat{\mathbf{n}})\, dS = \iiint_V \left(\psi\nabla^2\varphi + \nabla\varphi \cdot \nabla\psi\right) dV$ (Green's first identity)
- $\oiint_{\partial V} [(\psi\nabla\varphi - \varphi\nabla\psi) \cdot \hat{\mathbf{n}}]\, dS = \oiint_{\partial V} \left[\psi\frac{\partial\varphi}{\partial n} - \varphi\frac{\partial\psi}{\partial n}\right] dS = \iiint_V \left(\psi\nabla^2\varphi - \varphi\nabla^2\psi\right) dV$ (Green's second identity)

Curve–surface integrals

In the following curve–surface integral theorems, S denotes a 2d open surface with a corresponding 1d boundary $C = \partial S$ (a closed curve):

- $\oint_{\partial S} \mathbf{A} \cdot d\boldsymbol{\ell} = \iint_S (\nabla \times \mathbf{A}) \cdot d\mathbf{s}$ (Stokes' theorem)
- $\oint_{\partial S} \psi d\boldsymbol{\ell} = \iint_S (\hat{\mathbf{n}} \times \nabla\psi)\, dS$

Integration around a closed curve in the clockwise sense is the negative of the same line integral in the counterclockwise sense (analogous to interchanging the limits in a definite integral):

$$\oint_{\partial S} \mathbf{A} \cdot \mathrm{d}\boldsymbol{\ell} = -\oint_{\partial S} \mathbf{A} \cdot \mathrm{d}\boldsymbol{\ell}.$$

1.5 See also

- Exterior derivative
- Vector calculus
- Del in cylindrical and spherical coordinates
- Comparison of vector algebra and geometric algebra

1.6 Notes and references

[1] Feynman, R. P.; Leighton, R. B.; Sands, M. (1964). *The Feynman Lecture on Physics*. Addison-Wesley. Vol II, p. 27–4. ISBN 0-8053-9049-9.

[2] Kholmetskii, A. L.; Missevitch, O. V. (2005). "The Faraday induction law in relativity theory". arXiv:physics/0504223 [physics.class-ph].

[3] Doran, C.; Lasenby, A. (2003). *Geometric algebra for physicists*. Cambridge University Press. p. 169. ISBN 978-0-521-71595-9.

1.7 Further reading

- Balanis, Constantine A. *Advanced Engineering Electromagnetics*. ISBN 0-471-62194-3.
- Schey, H. M. (1997). *Div Grad Curl and all that: An informal text on vector calculus*. W. W. Norton & Company. ISBN 0-393-96997-5.
- Griffiths, David J. (1999). *Introduction to Electrodynamics*. Prentice Hall. ISBN 0-13-805326-X.

Chapter 2

Flow velocity

In continuum mechanics the **macroscopic velocity**,[1][2] also **flow velocity** in fluid dynamics or **drift velocity** in electromagnetism, of a fluid is a vector field which is used to mathematically describe the motion of a fluid. The length of the flow velocity vector is the **flow speed**.

2.1 Definition

The flow velocity ***u*** of a fluid is a vector field

$$\mathbf{u} = \mathbf{u}(\mathbf{x}, t)$$

which gives the velocity of an *element of fluid* at a position $\mathbf{x}$ and time t .

The flow speed q is the length of the flow velocity vector[3]

$$q = ||\mathbf{u}||$$

and is a scalar field.

2.2 Uses

The flow velocity of a fluid effectively describes everything about the motion of a fluid. Many physical properties of a fluid can be expressed mathematically in terms of the flow velocity. Some common examples follow:

2.2.1 Steady flow

Main article: Steady flow

The flow of a fluid is said to be *steady* if $\mathbf{u}$ does not vary with time. That is if

$$\frac{\partial \mathbf{u}}{\partial t} = 0.$$

2.2.2 Incompressible flow

Main article: Incompressible flow

If a fluid is incompressible the divergence of $\mathbf{u}$ is zero:

$$\nabla \cdot \mathbf{u} = 0.$$

That is, if $\mathbf{u}$ is a solenoidal vector field.

2.2.3 Irrotational flow

Main article: Irrotational flow

A flow is *irrotational* if the curl of $\mathbf{u}$ is zero:

$$\nabla \times \mathbf{u} = 0.$$

That is, if $\mathbf{u}$ is an irrotational vector field.

A flow in a simply-connected domain which is irrotational can be described as a potential flow, through the use of a velocity potential Φ, with $\mathbf{u} = \nabla\Phi$. If the flow is both irrotational and incompressible, the Laplacian of the velocity potential must be zero: $\Delta\Phi = 0$.

2.2.4 Vorticity

Main article: Vorticity

The *vorticity*, ω , of a flow can be defined in terms of its flow velocity by

$$\omega = \nabla \times \mathbf{u}.$$

Thus in irrotational flow the vorticity is zero.

2.3 The velocity potential

Main article: Potential flow

If an irrotational flow occupies a simply-connected fluid region then there exists a scalar field ϕ such that

$$\mathbf{u} = \nabla\phi$$

The scalar field ϕ is called the velocity potential for the flow. (See Irrotational vector field.)

2.4 References

[1] Duderstadt, James J., Martin, William R. (1979). "Chapter 4:The derivation of continuum description from transport equations". In Wiley-Interscience Publications. *Transport theory*. New York. p. 218. ISBN 978-0471044925.

[2] Freidberg, Jeffrey P. (2008). "Chapter 10:A self-consistent two-fluid model". In Cambridge University Press. *Plasma Physics and Fusion Energy* (1 ed.). Cambridge. p. 225. ISBN 978-0521733175.

[3] Courant, R.; Friedrichs, K.O. (1999) [First published in 1948]. *Supersonic Flow and Shock Waves*. Applied mathematical sciences (5th ed.). Springer-Verlag New York Inc. p. 24. ISBN 0387902325. OCLC 44071435.

Chapter 3

Laminar flow

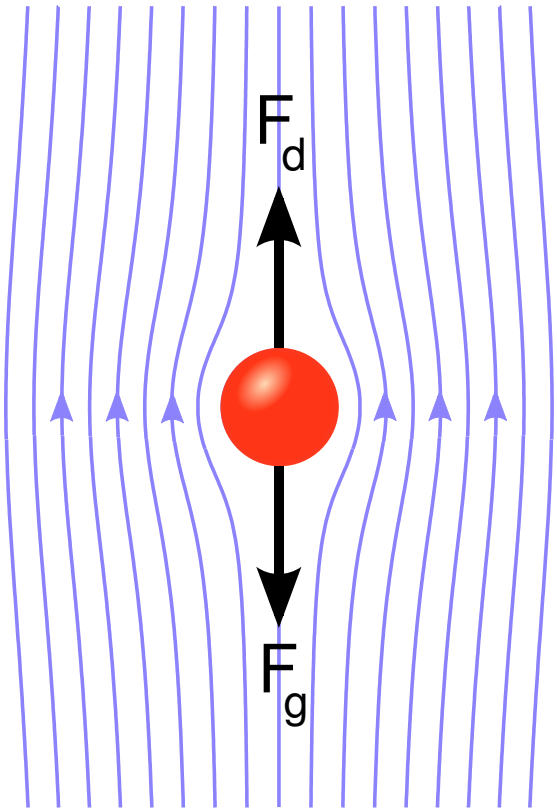

A sphere in Stokes flow, at very low Reynolds number. An object moving through a fluid experiences a force in the direction opposite to its motion.

In fluid dynamics, **laminar flow** (or streamline flow) occurs when a fluid flows in parallel layers, with no disruption between the layers.[1] At low velocities, the fluid tends to flow without lateral mixing, and adjacent layers slide past one another like playing cards. There are no cross-currents perpendicular to the direction of flow, nor eddies or swirls of fluids.[2] In laminar flow, the motion of the particles of the fluid is very orderly with all particles moving in straight lines parallel to the pipe walls.[3] Laminar flow is a flow regime characterized by high momentum diffusion and low momentum convection.

When a fluid is flowing through a closed channel such as a pipe or between two flat plates, either of two types of flow may occur depending on the velocity of the fluid: laminar flow or turbulent flow. Laminar flow tends to occur at lower velocities, below a threshold at which it becomes turbulent. Turbulent flow is a less orderly flow regime that is characterised by eddies or small packets of fluid particles which result in lateral mixing.[2] In non-scientific terms, laminar flow is *smooth* while turbulent flow is *rough*.

3.1 Relationship with the Reynolds number

The type of flow occurring in a fluid in a channel is important in fluid dynamics problems. The dimensionless Reynolds number is an important parameter in the equations that describe whether flow conditions lead to laminar or turbulent flow. The Reynolds number delimiting laminar and turbulent flow depends on the particular flow geometry, and moreover, the transition from laminar to turbulent flow can be sensitive to disturbance levels and imperfections present in a given configuration.

In the case of flow through a straight pipe with a circular cross-section, at a Reynolds number below a critical value of approximately 2040,[4] fluid motion will ultimately be laminar, whereas at larger Reynolds numbers, the flow can be turbulent. When the Reynolds number is much less than 1, Stokes flow occurs. This is an extreme case of laminar flow whereby viscous (frictional) effects are much greater than inertial forces.

3.2 Examples

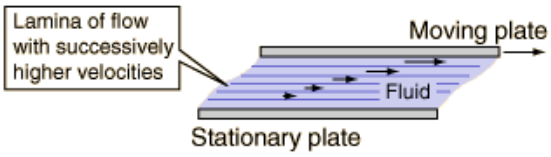

In the case of a moving plate in a liquid, it is found that there is a layer (lamina) that moves with the plate, and a layer next to any stationary plate that is stationary.

A common application of laminar flow is in the smooth

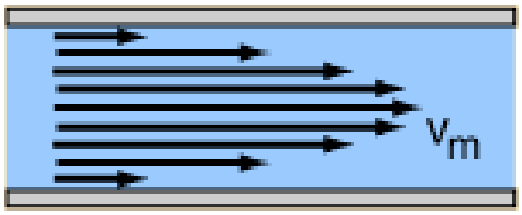

The streamlines associated with laminar flow resemble a deck of cards. This flow profile of a fluid in a pipe shows that the fluid acts in layers that slide over one another.

flow of a viscous liquid through a tube or pipe. In that case, the velocity of flow varies from zero at the walls to a maximum along the cross-sectional centre of the vessel. The flow profile of laminar flow in a tube can be calculated by dividing the flow into thin cylindrical elements and applying the viscous force to them.[5]

Another example is the flow of air over an aircraft wing. The boundary layer is a very thin sheet of air lying over the surface of the wing (and all other surfaces of the aircraft). Because air has viscosity, this layer of air tends to adhere to the wing. As the wing moves forward through the air, the boundary layer at first flows smoothly over the streamlined shape of the airfoil. Here, the flow is laminar and the boundary layer is a laminar layer. Prandtl applied the concept of the laminar boundary layer to airfoils in 1904.[6][7]

3.3 Laminar flow barriers

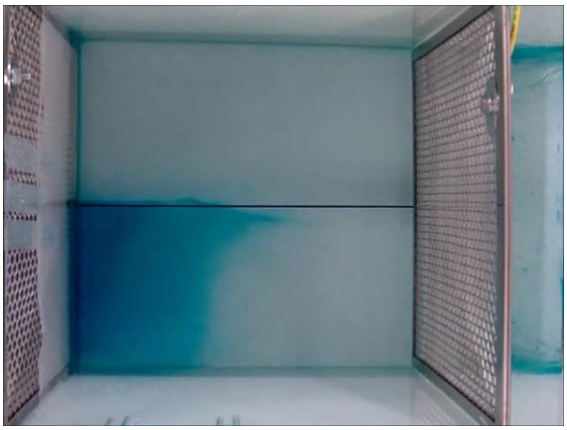

Experimental chamber for studying chemotaxis in response to laminar flow.

Laminar airflow is used to separate volumes of air, or prevent airborne contaminants from entering an area. Laminar flow hoods are used to exclude contaminants from sensitive processes in science, electronics and medicine. Air curtains are frequently used in commercial settings to keep heated or refrigerated air from passing through doorways. A laminar flow reactor (LFR) is a reactor that uses laminar flow to study chemical reactions and process mechanisms.

3.4 See also

- Chaos theory
- Laminar flow reactor

3.5 References

[1] Batchelor, G. (2000). *Introduction to Fluid Mechanics*.

[2] Geankoplis, Christie John (2003). *Transport Processes and Separation Process Principles*. Prentice Hall Professional Technical Reference. ISBN 0-13-101367-X.

[3] Noakes, Cath & Sleigh, Andrew (January 2009). "Real Fluids". *An Introduction to Fluid Mechanics*. University of Leeds. Retrieved 23 November 2010.

[4] Avila, K.; D. Moxey; A. de Lozar; M. Avila; D. Barkley; B. Hof (July 2011). "The Onset of Turbulence in Pipe Flow". *Science* **333** (6039): 192–196. Bibcode:2011Sci...333..192A. doi:10.1126/science.1203223.

[5] Nave, R. (2005). "Laminar Flow". *HyperPhysics*. Georgia State University. Retrieved 23 November 2010.

[6] Anderson, J.D. (1997). *A history of aerodynamics and its impact on flying machines*. Cambridge U. Press. ISBN 0-521-66955-3.

[7] Rogers, D.F. (1992). *Laminar flow analysis*. Cambridge U. Press. ISBN 0-521-41152-1.

3.6 External links

- Laminar Flow on YouTube
- Laminar flow in a pipe on YouTube

Chapter 4

Chaos theory

For other uses, see Chaos Theory (disambiguation).

Chaos theory is a field of study in mathematics, with applications in several disciplines including meteorology, sociology, physics, engineering, economics, biology, and philosophy. Chaos theory studies the behavior of dynamical systems that are highly sensitive to initial conditions—a response popularly referred to as the butterfly effect. Small differences in initial conditions (such as those due to rounding errors in numerical computation) yield widely diverging outcomes for such dynamical systems, rendering long-term prediction difficult in general.[1] This happens even though these systems are deterministic, meaning that their future behavior is fully determined by their initial conditions, with no random elements involved.[2] In other words, the deterministic nature of these systems does not make them predictable.[3][4] This behavior is known as *deterministic chaos*, or simply *chaos*. The theory was summarized by Edward Lorenz as follows:[5]

> Chaos: When the present determines the future, but the approximate present does not approximately determine the future.

Chaotic behavior can be observed in many natural systems, such as weather and climate.[6][7] This behavior can be studied through analysis of a chaotic mathematical model, or through analytical techniques such as recurrence plots and Poincaré maps.

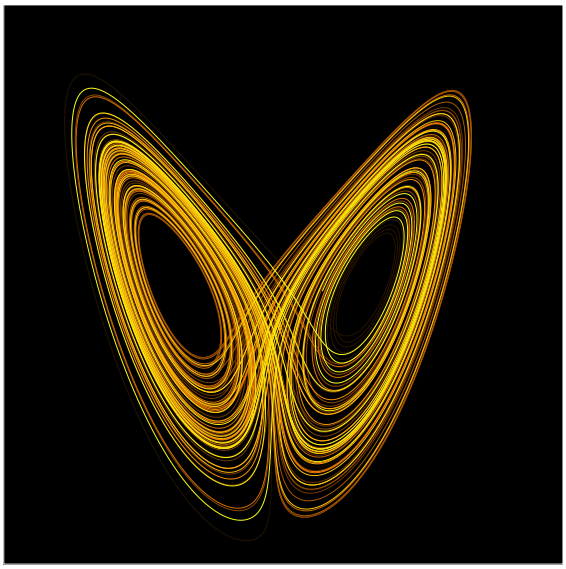

A plot of the Lorenz attractor for values r = 28, σ = 10, b = 8/3

A double rod pendulum animation showing chaotic behavior. Starting the pendulum from a slightly different initial condition would result in a completely different trajectory. The double rod pendulum is one of the simplest dynamical systems that has chaotic solutions.

4.1 Introduction

Chaos theory concerns deterministic systems whose behavior can in principle be predicted. Chaotic systems are predictable for a while and then *appear* to become random. The amount of time for which the behavior of a chaotic system can be effectively predicted depends on three things: How much uncertainty we are willing to tolerate in the forecast; how accurately we are able to measure its current state; and a time scale depending on the dynamics of the system, called the Lyapunov time. Some examples of Lyapunov times are: chaotic electrical circuits, ~1 millisecond; weather systems, a couple of days (unproven); the solar system, 50 million years. In chaotic systems the uncertainty in a forecast increases exponentially with elapsed time. Hence doubling the forecast time

squares the proportional uncertainty in the forecast. This means that in practice a meaningful prediction cannot be made over an interval of more than two or three times the Lyapunov time. When meaningful predictions cannot be made, the system appears to be random.[8]

4.2 Chaotic dynamics

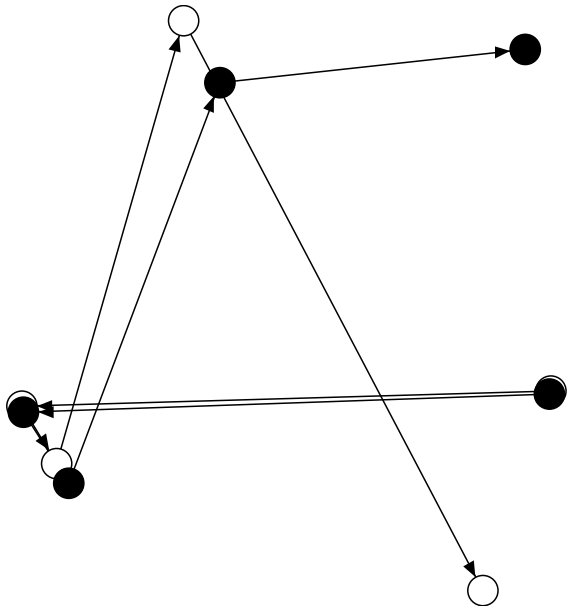

The map defined by $x \to 4\ x\ (1 - x)$ *and* $y \to x + y \mod 1$ *displays sensitivity to initial conditions. Here two series of* x *and* y *values diverge markedly over time from a tiny initial difference.*

In common usage, "chaos" means "a state of disorder".[9] However, in chaos theory, the term is defined more precisely. Although there is no universally accepted mathematical definition of chaos, a commonly used definition says that, for a dynamical system to be classified as chaotic, it must have the following properties:[10]

1. it must be sensitive to initial conditions;
2. it must be topologically mixing; and
3. it must have dense periodic orbits.

4.2.1 Sensitivity to initial conditions

Main article: Butterfly effect

Sensitivity to initial conditions means that each point in a chaotic system is arbitrarily closely approximated by other points with significantly different future paths, or trajectories. Thus, an arbitrarily small change, or perturbation, of the current trajectory may lead to significantly different future behavior.

It has been shown that in some cases the last two properties in the above actually imply sensitivity to initial conditions,[11][12] and if attention is restricted to intervals, the second property implies the other two[13] (an alternative, and in general weaker, definition of chaos uses only the first two properties in the above list).[14] It is interesting that the most practically significant property, that of sensitivity to initial conditions, is redundant in the definition, being implied by two (or for intervals, one) purely topological properties, which are therefore of greater interest to mathematicians.

Sensitivity to initial conditions is popularly known as the "butterfly effect", so called because of the title of a paper given by Edward Lorenz in 1972 to the American Association for the Advancement of Science in Washington, D.C., entitled *Predictability: Does the Flap of a Butterfly's Wings in Brazil set off a Tornado in Texas?*.[15] The flapping wing represents a small change in the initial condition of the system, which causes a chain of events leading to large-scale phenomena. Had the butterfly not flapped its wings, the trajectory of the system might have been vastly different.

A consequence of sensitivity to initial conditions is that if we start with only a finite amount of information about the system (as is usually the case in practice), then beyond a certain time the system will no longer be predictable. This is most familiar in the case of weather, which is generally predictable only about a week ahead.[16] Of course this does not mean that we cannot say anything about events far in the future; there are some restrictions on the system. With weather, we know that the temperature will never reach 100 degrees Celsius or fall to −130 degrees Celsius on earth, but we are not able to say exactly what day we will have the hottest temperature of the year.

In more mathematical terms, the Lyapunov exponent measures the sensitivity to initial conditions. Given two starting trajectories in the phase space that are infinitesimally close, with initial separation $\delta \mathbf{Z}_0$ end up diverging at a rate given by

$$|\delta \mathbf{Z}(t)| \approx e^{\lambda t} |\delta \mathbf{Z}_0|$$

where t is the time and λ is the Lyapunov exponent. The rate of separation depends on the orientation of the initial separation vector, so there is a whole spectrum of Lyapunov exponents. The number of Lyapunov exponents is equal to the number of dimensions of the phase space, though it is common to just refer to the largest one. For example, the maximal Lyapunov exponent (MLE) is most often used because it determines the overall predictability of the system. A positive MLE is usually taken as an indication that the system is chaotic.

There are also other properties that relate to sensitivity of initial conditions, such as measure-theoretical mixing (as discussed in ergodic theory) and properties of a K-system.[4]

4.2.2 Topological mixing

The map defined by x → 4 x *(1 –* x*) and* y → x + y *mod 1 also displays topological mixing. Here the blue region is transformed by the dynamics first to the purple region, then to the pink and red regions, and eventually to a cloud of points scattered across the space.*

Topological mixing (or *topological transitivity*) means that the system will evolve over time so that any given region or open set of its phase space will eventually overlap with any other given region. This mathematical concept of "mixing" corresponds to the standard intuition, and the mixing of colored dyes or fluids is an example of a chaotic system.

Topological mixing is often omitted from popular accounts of chaos, which equate chaos with only sensitivity to initial conditions. However, sensitive dependence on initial conditions alone does not give chaos. For example, consider the simple dynamical system produced by repeatedly doubling an initial value. This system has sensitive dependence on initial conditions everywhere, since any pair of nearby points will eventually become widely separated. However, this example has no topological mixing, and therefore has no chaos. Indeed, it has extremely simple behavior: all points except 0 will tend to positive or negative infinity.

4.2.3 Density of periodic orbits

For a chaotic system to have a *dense periodic orbit* means that every point in the space is approached arbitrarily closely by periodic orbits.[17] The one-dimensional logistic map defined by $x \to 4\ x\ (1 - x)$ is one of the simplest systems with density of periodic orbits. For example, $\frac{5-\sqrt{5}}{8} \to \frac{5+\sqrt{5}}{8} \to \frac{5-\sqrt{5}}{8}$ (or approximately 0.3454915 → 0.9045085 → 0.3454915) is an (unstable) orbit of period 2, and similar orbits exist for periods 4, 8, 16, etc. (indeed, for all the periods specified by Sharkovskii's theorem).[18]

Sharkovskii's theorem is the basis of the Li and Yorke[19] (1975) proof that any one-dimensional system that exhibits a regular cycle of period three will also display regular cycles of every other length as well as completely chaotic orbits.

4.2.4 Strange attractors

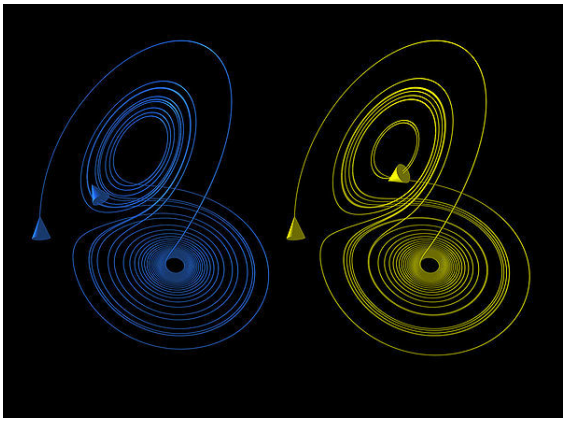

The Lorenz attractor displays chaotic behavior. These two plots demonstrate sensitive dependence on initial conditions within the region of phase space occupied by the attractor.

Some dynamical systems, like the one-dimensional logistic map defined by $x \to 4\ x\ (1 - x)$, are chaotic everywhere, but in many cases chaotic behavior is found only in a subset of phase space. The cases of most interest arise when the chaotic behavior takes place on an attractor, since then a large set of initial conditions will lead to orbits that converge to this chaotic region.

An easy way to visualize a chaotic attractor is to start with a point in the basin of attraction of the attractor, and then simply plot its subsequent orbit. Because of the topological transitivity condition, this is likely to produce a picture of the entire final attractor, and indeed both orbits shown in the figure on the right give a picture of the general shape of the Lorenz attractor. This attractor results from a simple three-dimensional model of the Lorenz weather system. The Lorenz attractor is perhaps one of the best-known chaotic system diagrams, probably because it was not only one of the first, but it is also one of the most complex and as such gives rise to a very interesting pattern, that with a little imagination, looks like the wings of a butterfly.

Unlike fixed-point attractors and limit cycles, the attractors that arise from chaotic systems, known as *strange attractors*, have great detail and complexity. Strange attractors occur in both continuous dynamical systems (such as the Lorenz system) and in some discrete systems (such as the Hénon map). Other discrete dynamical systems have a repelling structure called a Julia set which forms at the boundary between basins of attraction of fixed points –

Julia sets can be thought of as strange *repellers*. Both strange attractors and Julia sets typically have a fractal structure, and the fractal dimension can be calculated for them.

4.2.5 Minimum complexity of a chaotic system

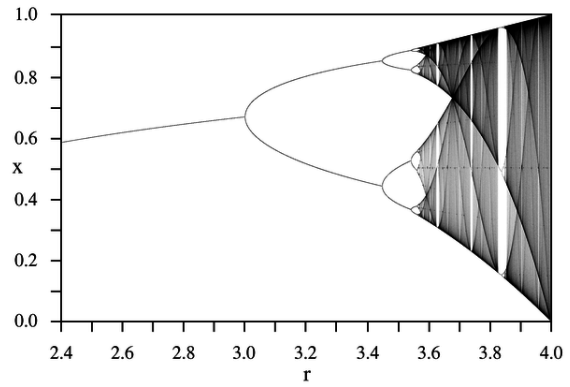

Bifurcation diagram of the logistic map $x \to r\,x\,(1-x)$. *Each vertical slice shows the attractor for a specific value of* r. *The diagram displays period-doubling as* r *increases, eventually producing chaos.*

Discrete chaotic systems, such as the logistic map, can exhibit strange attractors whatever their dimensionality. In contrast, for continuous dynamical systems, the Poincaré–Bendixson theorem shows that a strange attractor can only arise in three or more dimensions. Finite-dimensional linear systems are never chaotic; for a dynamical system to display chaotic behavior, it has to be either nonlinear or infinite-dimensional.

The Poincaré–Bendixson theorem states that a two-dimensional differential equation has very regular behavior. The Lorenz attractor discussed above is generated by a system of three differential equations such as:

$$\begin{aligned}\frac{\mathrm{d}x}{\mathrm{d}t} &= \sigma y - \sigma x,\\ \frac{\mathrm{d}y}{\mathrm{d}t} &= \rho x - xz - y,\\ \frac{\mathrm{d}z}{\mathrm{d}t} &= xy - \beta z.\end{aligned}$$

where x , y , and z make up the system state, t is time, and σ , ρ , β are the system parameters. Five of the terms on the right hand side are linear, while two are quadratic; a total of seven terms. Another well-known chaotic attractor is generated by the Rossler equations which have only one nonlinear term out of seven. Sprott [20] found a three-dimensional system with just five terms, that had only one nonlinear term, which exhibits chaos for certain parameter values. Zhang and Heidel [21][22] showed that, at least for dissipative and conservative quadratic systems, three-dimensional quadratic systems with only three or four terms on the right-hand side cannot exhibit chaotic behavior. The reason is, simply put, that solutions to such systems are asymptotic to a two-dimensional surface and therefore solutions are well behaved.

While the Poincaré–Bendixson theorem shows that a continuous dynamical system on the Euclidean plane cannot be chaotic, two-dimensional continuous systems with non-Euclidean geometry can exhibit chaotic behavior.[23] Perhaps surprisingly, chaos may occur also in linear systems, provided they are infinite dimensional.[24] A theory of linear chaos is being developed in a branch of mathematical analysis known as functional analysis.

4.2.6 Jerk systems

In physics, jerk is the third derivative of position, and such, in mathematics differential equations of the form

$$J\left(\dddot{x}, \ddot{x}, \dot{x}, x\right) = 0$$

are sometimes called *Jerk equations*. It has been shown, that a jerk equation, which is equivalent to a system of three first order, ordinary, non-linear differential equation is in a certain sense the minimal setting for solutions showing chaotic behaviour. This motivates mathematical interest in *jerk systems*. Systems involving a fourth or higher derivative are called accordingly *hyperjerk systems*.[25]

A *jerk system* is a system whose behavior is described by a *jerk equation*, and for certain jerk equations simple electronic circuits may be designed which model the solutions to this equation. These circuits are known as *jerk circuits*.

One of the most interesting properties of jerk circuits is the possibility of chaotic behavior. In fact, certain well-known chaotic systems, such as the Lorenz attractor and the Rössler map, are conventionally described as a system of three first-order differential equations, but which may be combined into a single (although rather complicated) jerk equation. It has been shown, that non-linear jerk systems are in a sense minimally complex systems to show chaotic behaviour, there is no chaotic system involving only *two* first order, ordinary differential equations (the system resulting in an equation of *second* order only).

An example of a jerk equation with non-linearity in the magnitude of x , is:

$$\frac{\mathrm{d}^3x}{\mathrm{d}t^3} + A\frac{\mathrm{d}^2x}{\mathrm{d}t^2} + \frac{\mathrm{d}x}{\mathrm{d}t} - |x| + 1 = 0.$$

Here A is an adjustable parameter. This equation has a chaotic solution for A=3/5 and can be implemented with the following jerk circuit; the required non-linearity is brought about by the two diodes:

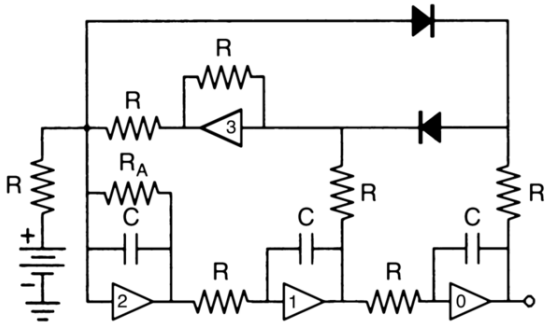

In the above circuit, all resistors are of equal value, except $R_A = R/A = 5R/3$, and all capacitors are of equal size. The dominant frequency will be $1/2\pi RC$. The output of op amp 0 will correspond to the x variable, the output of 1 will correspond to the first derivative of x and the output of 2 will correspond to the second derivative.

4.3 Spontaneous order

Under the right conditions chaos will spontaneously evolve into a lockstep pattern. In the Kuramoto model, four conditions suffice to produce synchronization in a chaotic system. Examples include the coupled oscillation of Christiaan Huygens' pendulums, fireflies, neurons, the London Millenium Bridge resonance, and large arrays of Josephson junctions.[26]

4.4 History

Barnsley fern created using the chaos game. Natural forms (ferns, clouds, mountains, etc.) may be recreated through an Iterated function system (IFS).

An early proponent of chaos theory was Henri Poincaré. In the 1880s, while studying the three-body problem, he found that there can be orbits that are nonperiodic, and yet not forever increasing nor approaching a fixed point.[27][28] In 1898 Jacques Hadamard published an influential study of the chaotic motion of a free particle gliding frictionlessly on a surface of constant negative curvature, called "Hadamard's billiards".[29] Hadamard was able to show that all trajectories are unstable, in that all particle trajectories diverge exponentially from one another, with a positive Lyapunov exponent.

Chaos Theory got its start in the field of ergodic theory. Later studies, also on the topic of nonlinear differential equations, were carried out by George David Birkhoff,[30] Andrey Nikolaevich Kolmogorov,[31][32][33] Mary Lucy Cartwright and John Edensor Littlewood,[34] and Stephen Smale.[35] Except for Smale, these studies were all directly inspired by physics: the three-body problem in the case of Birkhoff, turbulence and astronomical problems in the case of Kolmogorov, and radio engineering in the case of Cartwright and Littlewood. Although chaotic planetary motion had not been observed, experimentalists had encountered turbulence in fluid motion and nonperiodic oscillation in radio circuits without the benefit of a theory to explain what they were seeing.

Despite initial insights in the first half of the twentieth century, chaos theory became formalized as such only after mid-century, when it first became evident to some scientists that linear theory, the prevailing system theory at that time, simply could not explain the observed behavior of certain experiments like that of the logistic map. What had been attributed to measure imprecision and simple "noise" was considered by chaos theorists as a full component of the studied systems.

The main catalyst for the development of chaos theory was the electronic computer. Much of the mathematics of chaos theory involves the repeated iteration of simple mathematical formulas, which would be impractical to do by hand. Electronic computers made these repeated calculations practical, while figures and images made it possible to visualize these systems. As a graduate student in Chihiro Hayashi's laboratory at Kyoto University, Yoshisuke Ueda was experimenting with analog computers and noticed, on Nov. 27, 1961, what he called “randomly transitional phenomena”. Yet his advisor did not agree with his conclusions at the time, and did not allow him to report his findings until 1970.[36][37]

An early pioneer of the theory was Edward Lorenz whose interest in chaos came about accidentally through his work on weather prediction in 1961.[6] Lorenz was using a simple digital computer, a Royal McBee LGP-30, to run his weather simulation. He wanted to see a sequence of data again and to save time he started the simulation in the middle of its course. He was able to do this by entering a printout of the data corresponding to conditions in the middle of his simulation which he had calculated last time. To his surprise the weather that the

Turbulence in the tip vortex from an airplane wing. Studies of the critical point beyond which a system creates turbulence were important for chaos theory, analyzed for example by the Soviet physicist Lev Landau, who developed the Landau-Hopf theory of turbulence. David Ruelle and Floris Takens later predicted, against Landau, that fluid turbulence could develop through a strange attractor, a main concept of chaos theory.

machine began to predict was completely different from the weather calculated before. Lorenz tracked this down to the computer printout. The computer worked with 6-digit precision, but the printout rounded variables off to a 3-digit number, so a value like 0.506127 was printed as 0.506. This difference is tiny and the consensus at the time would have been that it should have had practically no effect. However, Lorenz had discovered that small changes in initial conditions produced large changes in the long-term outcome.[38] Lorenz's discovery, which gave its name to Lorenz attractors, showed that even detailed atmospheric modelling cannot, in general, make precise long-term weather predictions.

In 1963, Benoît Mandelbrot found recurring patterns at every scale in data on cotton prices.[39] Beforehand he had studied information theory and concluded noise was patterned like a Cantor set: on any scale the proportion of noise-containing periods to error-free periods was a constant – thus errors were inevitable and must be planned for by incorporating redundancy.[40] Mandelbrot described both the "Noah effect" (in which sudden discontinuous changes can occur) and the "Joseph effect" (in which persistence of a value can occur for a while, yet suddenly change afterwards).[41][42] This challenged the idea that changes in price were normally distributed. In 1967, he published "How long is the coast of Britain? Statistical self-similarity and fractional dimension", showing that a coastline's length varies with the scale of the measuring instrument, resembles itself at all scales, and is infinite in length for an infinitesimally small measuring device.[43] Arguing that a ball of twine appears to be a point when viewed from far away (0-dimensional), a ball when viewed from fairly near (3-dimensional), or a curved strand (1-dimensional), he argued that the dimensions of an object are relative to the observer and may be fractional. An object whose irregularity is constant over different scales ("self-similarity") is a fractal (examples include the Menger sponge, the Sierpiński gasket, and the Koch curve or "snowflake", which is infinitely long yet encloses a finite space and has a fractal dimension of circa 1.2619). In 1982 Mandelbrot published *The Fractal Geometry of Nature*, which became a classic of chaos theory. Biological systems such as the branching of the circulatory and bronchial systems proved to fit a fractal model.[44]

In December 1977, the New York Academy of Sciences organized the first symposium on Chaos, attended by David Ruelle, Robert May, James A. Yorke (coiner of the term "chaos" as used in mathematics), Robert Shaw, and the meteorologist Edward Lorenz. The following year, independently Pierre Coullet and Charles Tresser with the article "Iterations d'endomorphismes et groupe de renormalisation" and Mitchell Feigenbaum with the article "Quantitative Universality for a Class of Nonlinear Transformations" described logistic maps.[45][46] They notably discovered the universality in chaos, permitting the application of chaos theory to many different phenomena.

In 1979, Albert J. Libchaber, during a symposium organized in Aspen by Pierre Hohenberg, presented his experimental observation of the bifurcation cascade that leads to chaos and turbulence in Rayleigh–Bénard convection systems. He was awarded the Wolf Prize in Physics in 1986 along with Mitchell J. Feigenbaum for their inspiring achievements.[47]

In 1986, the New York Academy of Sciences co-organized with the National Institute of Mental Health and the Office of Naval Research the first important conference on chaos in biology and medicine. There, Bernardo Huberman presented a mathematical model of the eye tracking disorder among schizophrenics.[48] This led to a renewal of physiology in the 1980s through the application of chaos theory, for example, in the study of pathological cardiac cycles.

In 1987, Per Bak, Chao Tang and Kurt Wiesenfeld published a paper in *Physical Review Letters*[49] describing for the first time self-organized criticality (SOC), considered to be one of the mechanisms by which complexity arises in nature.

Alongside largely lab-based approaches such as the Bak–Tang–Wiesenfeld sandpile, many other investigations have focused on large-scale natural or social systems that are known (or suspected) to display scale-invariant behavior. Although these approaches were not always welcomed (at least initially) by specialists in the subjects examined, SOC has nevertheless become established as a strong candidate for explaining a number of natural phenomena, including earthquakes (which, long before SOC was discovered, were known as a source of scale-invariant behavior such as the Gutenberg–Richter law de-

scribing the statistical distribution of earthquake sizes, and the Omori law[50] describing the frequency of aftershocks), solar flares, fluctuations in economic systems such as financial markets (references to SOC are common in econophysics), landscape formation, forest fires, landslides, epidemics, and biological evolution (where SOC has been invoked, for example, as the dynamical mechanism behind the theory of "punctuated equilibria" put forward by Niles Eldredge and Stephen Jay Gould). Given the implications of a scale-free distribution of event sizes, some researchers have suggested that another phenomenon that should be considered an example of SOC is the occurrence of wars. These investigations of SOC have included both attempts at modelling (either developing new models or adapting existing ones to the specifics of a given natural system), and extensive data analysis to determine the existence and/or characteristics of natural scaling laws.

In the same year, James Gleick published *Chaos: Making a New Science*, which became a best-seller and introduced the general principles of chaos theory as well as its history to the broad public, though his history underemphasized important Soviet contributions.[51] Initially the domain of a few, isolated individuals, chaos theory progressively emerged as a transdisciplinary and institutional discipline, mainly under the name of nonlinear systems analysis. Alluding to Thomas Kuhn's concept of a paradigm shift exposed in *The Structure of Scientific Revolutions* (1962), many "chaologists" (as some described themselves) claimed that this new theory was an example of such a shift, a thesis upheld by Gleick.

The availability of cheaper, more powerful computers broadens the applicability of chaos theory. Currently, chaos theory continues to be a very active area of research,[52] involving many different disciplines (mathematics, topology, physics, social systems, population modeling, biology, meteorology, astrophysics, information theory, computational neuroscience, etc.).

4.5 Distinguishing random from chaotic data

It can be difficult to tell from data whether a physical or other observed process is random or chaotic, because in practice no time series consists of a pure "signal". There will always be some form of corrupting noise, even if it is present as round-off or truncation error. Thus any real time series, even if mostly deterministic, will contain some randomness.[53][54]

All methods for distinguishing deterministic and stochastic processes rely on the fact that a deterministic system always evolves in the same way from a given starting point.[53][55] Thus, given a time series to test for determinism, one can

1. pick a test state;
2. search the time series for a similar or nearby state; and
3. compare their respective time evolutions.

Define the error as the difference between the time evolution of the test state and the time evolution of the nearby state. A deterministic system will have an error that either remains small (stable, regular solution) or increases exponentially with time (chaos). A stochastic system will have a randomly distributed error.[56]

Essentially, all measures of determinism taken from time series rely upon finding the closest states to a given test state (e.g., correlation dimension, Lyapunov exponents, etc.). To define the state of a system, one typically relies on phase space embedding methods.[57] Typically one chooses an embedding dimension and investigates the propagation of the error between two nearby states. If the error looks random, one increases the dimension. If the dimension can be increased to obtain a deterministically looking error, then analysis is done. Though it may sound simple, one complication is that as the dimension increases, the search for a nearby state requires a lot more computation time and a lot of data (the amount of data required increases exponentially with embedding dimension) to find a suitably close candidate. If the embedding dimension (number of measures per state) is chosen too small (less than the "true" value), deterministic data can appear to be random, but in theory there is no problem choosing the dimension too large – the method will work.

When a nonlinear deterministic system is attended by external fluctuations, its trajectories present serious and permanent distortions. Furthermore, the noise is amplified due to the inherent nonlinearity and reveals totally new dynamical properties. Statistical tests attempting to separate noise from the deterministic skeleton or inversely isolate the deterministic part risk failure. Things become worse when the deterministic component is a nonlinear feedback system.[58] In presence of interactions between nonlinear deterministic components and noise, the resulting nonlinear series can display dynamics that traditional tests for nonlinearity are sometimes not able to capture.[59]

The question of how to distinguish deterministic chaotic systems from stochastic systems has also been discussed in philosophy. It has been shown that they might be observationally equivalent.[60]

4.6 Applications

Chaos theory was born from observing weather patterns, but it has become applicable to a variety of other situations. Some areas benefiting from chaos theory today are geology, mathematics, microbiology,

A conus textile shell, similar in appearance to Rule 30, a cellular automaton with chaotic behaviour.[61]

biology, computer science, economics,[62][63][64] engineering,[65] finance,[66][67] algorithmic trading,[68][69][70] meteorology, philosophy, physics, politics, population dynamics,[71] psychology, and robotics. A few categories are listed below with examples, but this is by no means a comprehensive list as new applications are appearing every day.

4.6.1 Computer science

Chaos theory is not new to computer science and has been used for many years in cryptography. One type of encryption, secret key or symmetric key, relies on diffusion and confusion, which is modeled well by chaos theory.[72] Another type of computing, DNA computing, when paired with chaos theory, offers a more efficient way to encrypt images and other information.[73] Robotics is another area that has recently benefited from chaos theory. Instead of robots acting in a trial-and-error type of refinement to interact with their environment, chaos theory has been used to build a predictive model.[74]

4.6.2 Biology

For over a hundred years, biologists have been keeping track of populations of different species with population models. Most models are deterministic systems, but recently scientists have been able to implement chaotic models in certain populations.[75] For example, a study on models of Canadian lynx showed there was chaotic behavior in the population growth.[76] Chaos can also be found in ecological systems, such as hydrology. While a chaotic model for hydrology has its shortcomings, there is still much to be learned from looking at the data through the lens of chaos theory.[77] Another biological application is found in cardiotocography. Fetal surveillance is a delicate balance of obtaining accurate information while being as noninvasive as possible. Better models of warning signs of fetal hypoxia can be obtained through chaotic modeling.[78]

4.6.3 Other areas

In chemistry, predicting gas solubility is essential to manufacturing polymers, but models using particle swarm optimization (PSO) tend to converge to the wrong points. An improved version of PSO has been created by introducing chaos, which keeps the simulations from getting stuck.[79] In celestial mechanics, especially when observing asteroids, applying chaos theory leads to better predictions about when these objects will come in range of Earth and other planets.[80] In quantum physics and electrical engineering, the study of large arrays of Josephson junctions benefitted greatly from chaos theory.[81] Closer to home, coal mines have always been dangerous places where frequent natural gas leaks cause many deaths. Until recently, there was no reliable way to predict when they would occur. But these gas leaks have chaotic tendencies that, when properly modeled, can be predicted fairly accurately.[82]

Chaos theory can be applied outside of the natural sciences. By adapting a model of career counseling to include a chaotic interpretation of the relationship between employees and the job market, better suggestions can be made to people struggling with career decisions.:[83] Modern organizations are increasingly seen as open complex adaptive systems, with fundamental natural nonlinear structures, subject to internal and external forces which may be sources of chaos. The chaos metaphor—used in verbal theories—grounded on mathematical models and psychological aspects of human behavior provides helpful insights to describing the complexity of small work groups, that go beyond the metaphor itself.[84]

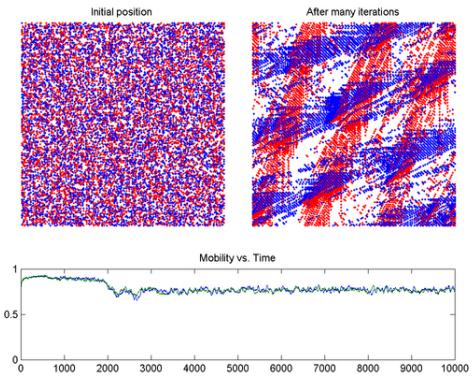

The red cars and blue cars take turns to move; the red ones only move upwards, and the blue ones move rightwards. Every time, all the cars of the same colour try to move one step if there is no car in front of it. Here, the model has self-organized in a somewhat geometric pattern where there are some traffic jams and some areas where cars can move at top speed.
Source: https://en.wikipedia.org/wiki/File:BML_N%3D200_P%3D32.png

It is possible that economic models can also be improved through an application of chaos theory, but predicting the health of an economic system and what factors influence it most is an extremely complex task.[85] Economic and financial systems are fundamentally different from those in the physical and natural sciences since the former are inherently stochastic in nature, as they result from the interactions of people, and thus pure deterministic models are unlikely to provide accurate representations of the data. The empirical literature that tests for chaos in economics and finance presents very mixed results, in part due to confusion between specific tests for chaos and more general tests for non-linear relationships.[86]

Traffic forecasting is another area that greatly benefits from applications of chaos theory. Better predictions of when traffic will occur would allow measures to be taken for it to be dispersed before the traffic starts, rather than after. Combining chaos theory principles with a few other methods has led to a more accurate short-term prediction model (see the plot of the BML traffic model at right).[87]

Chaos theory also finds applications in psychology. For example, in modeling group behavior in which heterogeneous members may behave as if sharing to different degrees what in Wilfred Bion's theory is a basic assumption, the group dynamics is the result of the individual dynamics of the members: each individual reproduces the group dynamics in a different scale, and the chaotic behavior of the group is reflected in each member.[88]

4.7 See also

4.8 References

[1] Kellert, Stephen H. (1993). *In the Wake of Chaos: Unpredictable Order in Dynamical Systems*. University of Chicago Press. p. 32. ISBN 0-226-42976-8.

[2] Kellert 1993, p. 56

[3] Kellert 1993, p. 62

[4] Werndl, Charlotte (2009). "What are the New Implications of Chaos for Unpredictability?". *The British Journal for the Philosophy of Science* **60** (1): 195–220. doi:10.1093/bjps/axn053.

[5] Danforth, Christopher M. (April 2013). "Chaos in an Atmosphere Hanging on a Wall". *Mathematics of Planet Earth 2013*. Retrieved 4 April 2013.

[6] Lorenz, Edward N. (1963). "Deterministic non-periodic flow". *Journal of the Atmospheric Sciences* **20** (2): 130–141. Bibcode:1963JAtS...20..130L. doi:10.1175/1520-0469(1963)020<0130:DNF>2.0.CO;2.

[7] Ivancevic, Vladimir G.; Tijana T. Ivancevic (2008). *Complex nonlinearity: chaos, phase transitions, topology change, and path integrals*. Springer. ISBN 978-3-540-79356-4.

[8] *Sync: The Emerging Science of Spontaneous Order*, Steven Strogatz, Hyperion, New York, 2003, pages 189-190.

[9] Definition of chaos at Wiktionary;

[10] Hasselblatt, Boris; Anatole Katok (2003). *A First Course in Dynamics: With a Panorama of Recent Developments*. Cambridge University Press. ISBN 0-521-58750-6.

[11] Elaydi, Saber N. (1999). *Discrete Chaos*. Chapman & Hall/CRC. p. 117. ISBN 1-58488-002-3.

[12] Basener, William F. (2006). *Topology and its applications*. Wiley. p. 42. ISBN 0-471-68755-3.

[13] Vellekoop, Michel; Berglund, Raoul (April 1994). "On Intervals, Transitivity = Chaos". *The American Mathematical Monthly* **101** (4): 353–5. doi:10.2307/2975629. JSTOR 2975629.

[14] Medio, Alfredo; Lines, Marji (2001). *Nonlinear Dynamics: A Primer*. Cambridge University Press. p. 165. ISBN 0-521-55874-3.

[15] Wikiversity (28 July 2011). "1972/Lorenz". Wikipedia. Retrieved 8 April 2014.

[16] Watts, Robert G. (2007). *Global Warming and the Future of the Earth*. Morgan & Claypool. p. 17.

[17] Devaney 2003

[18] Alligood, Sauer & Yorke 1997

[19] Li, T.Y.; Yorke, J.A. (1975). "Period Three Implies Chaos" (PDF). *American Mathematical Monthly* **82** (10): 985–92. doi:10.2307/2318254.

[20] Sprott, J.C. (1997). "Simplest dissipative chaotic flow". *Physics Letters A* **228** (4–5): 271. Bibcode:1997PhLA..228..271S. doi:10.1016/S0375-9601(97)00088-1.

[21] Fu, Z.; Heidel, J. (1997). "Non-chaotic behaviour in three-dimensional quadratic systems". *Nonlinearity* **10** (5): 1289. Bibcode:1997Nonli..10.1289F. doi:10.1088/0951-7715/10/5/014.

[22] Heidel, J.; Fu, Z. (1999). "Nonchaotic behaviour in three-dimensional quadratic systems II. The conservative case". *Nonlinearity* **12** (3): 617. Bibcode:1999Nonli..12..617H. doi:10.1088/0951-7715/12/3/012.

[23] Rosario, Pedro (2006). *Underdetermination of Science: Part I*. Lulu.com. ISBN 1411693914.

[24] Bonet, J.; Martínez-Giménez, F.; Peris, A. (2001). "A Banach space which admits no chaotic operator". *Bulletin of the London Mathematical Society* **33** (2): 196–8. doi:10.1112/blms/33.2.196.

[25] K. E. Chlouverakis and J. C. Sprott, Chaos Solitons & Fractals 28, 739-746 (2005), Chaotic Hyperjerk Systems, http://sprott.physics.wisc.edu/pubs/paper297.htm

[26] Steven Strogatz, *Sync: The Emerging Science of Spontaneous Order*, Hyperion, 2003.

[27] Poincaré, Jules Henri (1890). "Sur le problème des trois corps et les équations de la dynamique. Divergence des séries de M. Lindstedt". *Acta Mathematica* **13**: 1–270. doi:10.1007/BF02392506.

[28] Diacu, Florin; Holmes, Philip (1996). *Celestial Encounters: The Origins of Chaos and Stability*. Princeton University Press.

[29] Hadamard, Jacques (1898). "Les surfaces à courbures opposées et leurs lignes géodesiques". *Journal de Mathématiques Pures et Appliquées* **4**: 27–73.

[30] George D. Birkhoff, *Dynamical Systems,* vol. 9 of the American Mathematical Society Colloquium Publications (Providence, Rhode Island: American Mathematical Society, 1927)

[31] Kolmogorov, Andrey Nikolaevich (1941). "Local structure of turbulence in an incompressible fluid for very large Reynolds numbers". *Doklady Akademii Nauk SSSR* **30** (4): 301–5. Bibcode:1941DoSSR..30..301K. Reprinted in: Kolmogorov, A. N. (1991). "The Local Structure of Turbulence in Incompressible Viscous Fluid for Very Large Reynolds Numbers". *Proceedings of the Royal Society A* **434** (1890): 9–13. Bibcode:1991RSPSA.434....9K. doi:10.1098/rspa.1991.0075.

[32] Kolmogorov, A. N. (1941). "On degeneration of isotropic turbulence in an incompressible viscous liquid". *Doklady Akademii Nauk SSSR* **31** (6): 538–540. Reprinted in: Kolmogorov, A. N. (1991). "Dissipation of Energy in the Locally Isotropic Turbulence". *Proceedings of the Royal Society A* **434** (1890): 15–17. Bibcode:1991RSPSA.434...15K. doi:10.1098/rspa.1991.0076.

[33] Kolmogorov, A. N. (1954). "Preservation of conditionally periodic movements with small change in the Hamiltonian function". *Doklady Akademii Nauk SSSR*. Lecture Notes in Physics **98**: 527–530. Bibcode:1979LNP....93...51K. doi:10.1007/BFb0021737. ISBN 3-540-09120-3. See also Kolmogorov–Arnold–Moser theorem

[34] Cartwright, Mary L.; Littlewood, John E. (1945). "On non-linear differential equations of the second order, I: The equation $y'' + k(1-y^2)y' + y = b\lambda k\cos(\lambda t + a)$, k large". *Journal of the London Mathematical Society* **20** (3): 180–9. doi:10.1112/jlms/s1-20.3.180. See also: Van der Pol oscillator

[35] Smale, Stephen (January 1960). "Morse inequalities for a dynamical system". *Bulletin of the American Mathematical Society* **66**: 43–49. doi:10.1090/S0002-9904-1960-10386-2.

[36] Abraham & Ueda 2001, See Chapters 3 and 4

[37] Sprott 2003, p. 89

[38] Gleick, James (1987). *Chaos: Making a New Science*. London: Cardinal. p. 17. ISBN 0-434-29554-X.

[39] Mandelbrot, Benoît (1963). "The variation of certain speculative prices". *Journal of Business* **36** (4): 394–419. doi:10.1086/294632.

[40] Berger J.M., Mandelbrot B. (1963). "A new model for error clustering in telephone circuits". *I.B.M. Journal of Research and Development* **7**: 224–236. doi:10.1147/rd.73.0224.

[41] Mandelbrot, B. (1977). *The Fractal Geometry of Nature*. New York: Freeman. p. 248.

[42] See also: Mandelbrot, Benoît B.; Hudson, Richard L. (2004). *The (Mis)behavior of Markets: A Fractal View of Risk, Ruin, and Reward*. New York: Basic Books. p. 201.

[43] Mandelbrot, Benoît (5 May 1967). "How Long Is the Coast of Britain? Statistical Self-Similarity and Fractional Dimension". *Science* **156** (3775): 636–8. Bibcode:1967Sci...156..636M. doi:10.1126/science.156.3775.636. PMID 17837158.

[44] Buldyrev, S.V.; Goldberger, A.L.; Havlin, S.; Peng, C.K.; Stanley, H.E. (1994). "Fractals in Biology and Medicine: From DNA to the Heartbeat". In Bunde, Armin; Havlin, Shlomo. *Fractals in Science*. Springer. pp. 49–89. ISBN 3-540-56220-6.

[45] Feigenbaum, Mitchell (July 1978). "Quantitative universality for a class of nonlinear transformations". *Journal of Statistical Physics* **19** (1): 25–52. Bibcode:1978JSP....19...25F. doi:10.1007/BF01020332.

[46] Coullet, Pierre, and Charles Tresser. "Iterations d'endomorphismes et groupe de renormalisation." Le Journal de Physique Colloques 39.C5 (1978): C5-25

[47] "The Wolf Prize in Physics in 1986.".

[48] Huberman, B.A. (July 1987). "A Model for Dysfunctions in Smooth Pursuit Eye Movement". *Annals of the New York Academy of Sciences.* 504 Perspectives in Biological Dynamics and Theoretical Medicine: 260–273. Bibcode:1987NYASA.504..260H. doi:10.1111/j.1749-6632.1987.tb48737.x.

[49] Bak, Per; Tang, Chao; Wiesenfeld, Kurt; Tang; Wiesenfeld (27 July 1987). "Self-organized criticality: An explanation of the 1/f noise". *Physical Review Letters* **59** (4): 381–4. Bibcode:1987PhRvL..59..381B. doi:10.1103/PhysRevLett.59.381. However, the conclusions of this article have been subject to dispute. "?".. See especially: Laurson, Lasse; Alava, Mikko J.; Zapperi, Stefano (15 September 2005). "Letter: Power spectra of self-organized critical sand piles". *Journal of Statistical Mechanics: Theory and Experiment* **0511**. L001.

[50] Omori, F. (1894). "On the aftershocks of earthquakes". *Journal of the College of Science, Imperial University of Tokyo* **7**: 111–200.

[51] Gleick, James (August 26, 2008). *Chaos: Making a New Science*. Penguin Books. ISBN 0143113453.

[52] Motter A. E. and Campbell D. K., Chaos at fifty, Phys. Today 66(5), 27-33 (2013).

[53] Provenzale, A., et al.; Smith; Vio; Murante (1992). "Distinguishing between low-dimensional dynamics and randomness in measured time-series". *Physica D* **58**: 31–49. Bibcode:1992PhyD...58...31P. doi:10.1016/0167-2789(92)90100-2.

[54] Brock, W.A. (October 1986). "Distinguishing random and deterministic systems: Abridged version". *Journal of Economic Theory* **40**: 168–195. doi:10.1016/0022-0531(86)90014-1.

[55] Sugihara G., May R.; May (1990). "Nonlinear forecasting as a way of distinguishing chaos from measurement error in time series" (PDF). *Nature* **344** (6268): 734–741. Bibcode:1990Natur.344..734S. doi:10.1038/344734a0. PMID 2330029.

[56] Casdagli, Martin (1991). "Chaos and Deterministic *versus* Stochastic Non-linear Modelling". *Journal of the Royal Statistical Society, Series B* **54** (2): 303–328. JSTOR 2346130.

[57] Broomhead, D.S.; King, G.P.; King (June–July 1986). "Extracting qualitative dynamics from experimental data". *Physica D* **20** (2–3): 217–236. Bibcode:1986PhyD...20..217B. doi:10.1016/0167-2789(86)90031-X.

[58] Kyrtsou C (2008). "Re-examining the sources of heteroskedasticity: the paradigm of noisy chaotic models". *Physica A* **387** (27): 6785–9. Bibcode:2008PhyA..387.6785K. doi:10.1016/j.physa.2008.09.008.

[59] Kyrtsou, C. (2005). "Evidence for neglected linearity in noisy chaotic models". *International Journal of Bifurcation and Chaos* **15** (10): 3391–4. Bibcode:2005IJBC...15.3391K. doi:10.1142/S0218127405013964.

[60] Werndl, Charlotte (2009). "Are Deterministic Descriptions and Indeterministic Descriptions Observationally Equivalent?". *Studies in History and Philosophy of Modern Physics* **40** (3): 232–242. doi:10.1016/j.shpsb.2009.06.004.

[61] Stephen Coombes (February 2009). "The Geometry and Pigmentation of Seashells". *www.maths.nottingham.ac.uk*. University of Nottingham. Retrieved 2013-04-10.

[62] Kyrtsou C., Labys W. (2006). "Evidence for chaotic dependence between US inflation and commodity prices". *Journal of Macroeconomics* **28** (1): 256–266. doi:10.1016/j.jmacro.2005.10.019.

[63] Kyrtsou C., Labys W.; Labys (2007). "Detecting positive feedback in multivariate time series: the case of metal prices and US inflation". *Physica A* **377** (1): 227–229. Bibcode:2007PhyA..377..227K. doi:10.1016/j.physa.2006.11.002.

[64] Kyrtsou, C.; Vorlow, C. (2005). "Complex dynamics in macroeconomics: A novel approach". In Diebolt, C.; Kyrtsou, C. *New Trends in Macroeconomics*. Springer Verlag.

[65] Applying Chaos Theory to Embedded Applications

[66] Hristu-Varsakelis, D.; Kyrtsou, C. (2008). "Evidence for nonlinear asymmetric causality in US inflation, metal and stock returns". *Discrete Dynamics in Nature and Society* **2008**: 1. doi:10.1155/2008/138547. 138547.

[67] Kyrtsou, C. and M. Terraza, (2003). "Is it possible to study chaotic and ARCH behaviour jointly? Application of a noisy Mackey-Glass equation with heteroskedastic errors to the Paris Stock Exchange returns series". *Computational Economics* **21** (3): 257–276. doi:10.1023/A:1023939610962.

[68] Williams, Bill Williams, Justine (2004). *Trading chaos : maximize profits with proven technical techniques* (2nd ed.). New York: Wiley. ISBN 9780471463085.

[69] Peters, Edgar E. (1994). *Fractal market analysis : applying chaos theory to investment and economics* (2. print. ed.). New York u.a.: Wiley. ISBN 978-0471585244.

[70] Peters, / Edgar E. (1996). *Chaos and order in the capital markets : a new view of cycles, prices, and market volatility* (2nd ed.). New York: John Wiley & Sons. ISBN 978-0471139386.

[71] Dilão, R.; Domingos, T. (2001). "Periodic and Quasi-Periodic Behavior in Resource Dependent Age Structured Population Models". *Bulletin of Mathematical Biology* **63** (2): 207–230. doi:10.1006/bulm.2000.0213. PMID 11276524.

[72] Wang, Xingyuan; Zhao, Jianfeng (2012). "An improved key agreement protocol based on chaos". *Commun. Nonlinear Sci. Numer. Simul.* **15** (12): 4052–4057. Bibcode:2010CNSNS..15.4052W. doi:10.1016/j.cnsns.2010.02.014.

[73] Babaei, Majid (2013). "A novel text and image encryption method based on chaos theory and DNA computing". *Natural Computing. an International Journal* **12** (1): 101–107. doi:10.1007/s11047-012-9334-9.

[74] Nehmzow, Ulrich; Keith Walker (Dec 2005). "Quantitative description of robot–environment interaction using chaos theory". *Robotics and Autonomous Systems* **53** (3–4): 177–193. doi:10.1016/j.robot.2005.09.009.

[75] Eduardo, Liz; Ruiz-Herrera, Alfonso (2012). "Chaos in discrete structured population models". *SIAM Journal on Applied Dynamical Systems* **11** (4): 1200–1214. doi:10.1137/120868980.

[76] Lai, Dejian (1996). "Comparison study of AR models on the Canadian lynx data: a close look at BDS statistic". *Computational Statistics \& Data Analysis* **22** (4): 409–423. doi:10.1016/0167-9473(95)00056-9.

[77] Sivakumar, B (31 January 2000). "Chaos theory in hydrology: important issues and interpretations". *Journal of Hydrology* **227** (1–4): 1–20. Bibcode:2000JHyd..227....1S. doi:10.1016/S0022-1694(99)00186-9.

[78] Bozóki, Zsolt (February 1997). "Chaos theory and power spectrum analysis in computerized cardiotocography". *European Journal of Obstetrics & Gynecology and Reproductive Biology* **71** (2): 163–168. doi:10.1016/s0301-2115(96)02628-0.

[79] Li, Mengshan; Xingyuan Huanga; Hesheng Liua; Bingxiang Liub; Yan Wub; Aihua Xiongc; Tianwen Dong (25

October 2013). "Prediction of gas solubility in polymers by back propagation artificial neural network based on self-adaptive particle swarm optimization algorithm and chaos theory". *Fluid Phase Equilibria* **356**: 11–17. doi:10.1016/j.fluid.2013.07.017.

[80] Morbidelli, A. (2001). "Chaotic diffusion in celestial mechanics". *Regular & Chaotic Dynamics. International Scientific Journal* **6** (4): 339–353.

[81] Steven Strogatz, *Sync: The Emerging Science of Spontaneous Order, Hyperion, 2003*

[82] Dingqi, Li; Yuanping Chenga; Lei Wanga; Haifeng Wanga; Liang Wanga; Hongxing Zhou (May 2011). "Prediction method for risks of coal and gas outbursts based on spatial chaos theory using gas desorption index of drill cuttings". *Mining Science and Technology* **21** (3): 439–443.

[83] Pryor, Robert G. L.; Norman E. Aniundson; Jim E. H. Bright (June 2008). "Probabilities and Possibilities: The Strategic Counseling Implications of the Chaos Theory of Careers". *The Career Development Quarterly* **56**: 309–318. doi:10.1002/j.2161-0045.2008.tb00096.x.

[84] Dal Forno, Arianna; Merlone, Ugo (2013). "Chaotic Dynamics in Organization Theory". In Bischi, Gian Italo; Chiarella, Carl; Shusko, Irina. *Global Analysis of Dynamic Models in Economics and Finance*. Springer-Verlag. pp. 185–204. ISBN 978-3-642-29503-4.

[85] Juárez, Fernando (2011). "Applying the theory of chaos and a complex model of health to establish relations among financial indicators". *Procedia Computer Science* **3**: 982–986. doi:10.1016/j.procs.2010.12.161.

[86] Brooks, Chris (1998). "Chaos in foreign exchange markets: a sceptical view". *Computational Economics* **11**: 265–281. doi:10.1023/A:1008650024944. ISSN 1572-9974.

[87] Wang, Jin; Qixin Shi (February 2013). "Short-term traffic speed forecasting hybrid model based on Chaos–Wavelet Analysis-Support Vector Machine theory". *Transportation Research Part C: Emerging Technologies* **27**: 219–232. doi:10.1016/j.trc.2012.08.004.

[88] Dal Forno, Arianna; Merlone, Ugo (2013). "Nonlinear dynamics in work groups with Bion's basic assumptions". *Nonlinear Dynamics, Psychology, and Life Sciences* **17** (2): 295–315. ISSN 1090-0578.

4.9 Scientific literature

4.9.1 Articles

- Sharkovskii, A.N. (1964). "Co-existence of cycles of a continuous mapping of the line into itself". *Ukrainian Math. J.* **16**: 61–71.
- Li, T.Y.; Yorke, J.A. (1975). "Period Three Implies Chaos". *American Mathematical Monthly* **82** (10): 985–92. Bibcode:1975AmMM...82..985L. doi:10.2307/2318254.
- Crutchfield, Tucker, Morrison, J.D., Packard, N.H., Shaw, R.S (December 1986). "Chaos". *Scientific American* **255** (6): 38–49 (bibliography p.136). Bibcode:1986SciAm.255...38T. Online version (Note: the volume and page citation cited for the online text differ from that cited here. The citation here is from a photocopy, which is consistent with other citations found online, but which don't provide article views. The online content is identical to the hardcopy text. Citation variations will be related to country of publication).
- Kolyada, S.F. (2004). "Li-Yorke sensitivity and other concepts of chaos". *Ukrainian Math. J.* **56** (8): 1242–57. doi:10.1007/s11253-005-0055-4.
- Strelioff, C.; Hübler, A. (2006). "Medium-Term Prediction of Chaos" (PDF). *Phys. Rev. Lett.* **96** (4): 044101. Bibcode:2006PhRvL..96d4101S. doi:10.1103/PhysRevLett.96.044101. PMID 16486826. 044101.
- Hübler, A.; Foster, G.; Phelps, K. (2007). "Managing Chaos: Thinking out of the Box" (PDF). *Complexity* **12** (3): 10–13. doi:10.1002/cplx.20159.

4.9.2 Textbooks

- Alligood, K.T.; Sauer, T.; Yorke, J.A. (1997). *Chaos: an introduction to dynamical systems*. Springer-Verlag. ISBN 0-387-94677-2.
- Baker, G. L. (1996). *Chaos, Scattering and Statistical Mechanics*. Cambridge University Press. ISBN 0-521-39511-9.
- Badii, R.; Politi A. (1997). *Complexity: hierarchical structures and scaling in physics*. Cambridge University Press. ISBN 0-521-66385-7.
- Bunde; Havlin, Shlomo, eds. (1996). *Fractals and Disordered Systems*. Springer. ISBN 3642848702. and Bunde; Havlin, Shlomo, eds. (1994). *Fractals in Science*. Springer. ISBN 3-540-56220-6.
- Collet, Pierre, and Eckmann, Jean-Pierre (1980). *Iterated Maps on the Interval as Dynamical Systems*. Birkhauser. ISBN 0-8176-4926-3.
- Devaney, Robert L. (2003). *An Introduction to Chaotic Dynamical Systems* (2nd ed.). Westview Press. ISBN 0-8133-4085-3.
- Gollub, J. P.; Baker, G. L. (1996). *Chaotic dynamics*. Cambridge University Press. ISBN 0-521-47685-2.
- Guckenheimer, John; Holmes, Philip (1983). *Nonlinear Oscillations, Dynamical Systems, and Bifurcations of Vector Fields*. Springer-Verlag. ISBN 0-387-90819-6.

- Gulick, Denny (1992). *Encounters with Chaos*. McGraw-Hill. ISBN 0-07-025203-3.
- Gutzwiller, Martin (1990). *Chaos in Classical and Quantum Mechanics*. Springer-Verlag. ISBN 0-387-97173-4.
- Hoover, William Graham (2001) [1999]. *Time Reversibility, Computer Simulation, and Chaos*. World Scientific. ISBN 981-02-4073-2.
- Kautz, Richard (2011). *Chaos: The Science of Predictable Random Motion*. Oxford University Press. ISBN 978-0-19-959458-0.
- Kiel, L. Douglas; Elliott, Euel W. (1997). *Chaos Theory in the Social Sciences*. Perseus Publishing. ISBN 0-472-08472-0.
- Moon, Francis (1990). *Chaotic and Fractal Dynamics*. Springer-Verlag. ISBN 0-471-54571-6.
- Ott, Edward (2002). *Chaos in Dynamical Systems*. Cambridge University Press. ISBN 0-521-01084-5.
- Strogatz, Steven (2000). *Nonlinear Dynamics and Chaos*. Perseus Publishing. ISBN 0-7382-0453-6.
- Sprott, Julien Clinton (2003). *Chaos and Time-Series Analysis*. Oxford University Press. ISBN 0-19-850840-9.
- Tél, Tamás; Gruiz, Márton (2006). *Chaotic dynamics: An introduction based on classical mechanics*. Cambridge University Press. ISBN 0-521-83912-2.
- Teschl, Gerald (2012). *Ordinary Differential Equations and Dynamical Systems*. Providence: American Mathematical Society. ISBN 978-0-8218-8328-0.
- Thompson J M T, Stewart H B (2001). *Nonlinear Dynamics And Chaos*. John Wiley and Sons Ltd. ISBN 0-471-87645-3.
- Tufillaro; Reilly (1992). *An experimental approach to nonlinear dynamics and chaos*. Addison-Wesley. ISBN 0-201-55441-0.
- Wiggins, Stephen (2003). *Introduction to Applied Dynamical Systems and Chaos*. Springer. ISBN 0-387-00177-8.
- Zaslavsky, George M. (2005). *Hamiltonian Chaos and Fractional Dynamics*. Oxford University Press. ISBN 0-19-852604-0.

4.9.3 Semitechnical and popular works

- Christophe Letellier, *Chaos in Nature*, World Scientific Publishing Company, 2012, ISBN 978-981-4374-42-2.
- Abraham, Ralph H.; Ueda, Yoshisuke, eds. (2000). *The Chaos Avant-Garde: Memoirs of the Early Days of Chaos Theory*. World Scientific. ISBN 978-981-238-647-2.
- Barnsley, Michael F. (2000). *Fractals Everywhere*. Morgan Kaufmann. ISBN 978-0-12-079069-2.
- Bird, Richard J. (2003). *Chaos and Life: Complexit and Order in Evolution and Thought*. Columbia University Press. ISBN 978-0-231-12662-5.
- John Briggs and David Peat, *Turbulent Mirror: : An Illustrated Guide to Chaos Theory and the Science of Wholeness*, Harper Perennial 1990, 224 pp.
- John Briggs and David Peat, *Seven Life Lessons of Chaos: Spiritual Wisdom from the Science of Change*, Harper Perennial 2000, 224 pp.
- Cunningham, Lawrence A. (1994). "From Random Walks to Chaotic Crashes: The Linear Genealogy of the Efficient Capital Market Hypothesis". *George Washington Law Review* **62**: 546.
- Predrag Cvitanović, *Universality in Chaos*, Adam Hilger 1989, 648 pp.
- Leon Glass and Michael C. Mackey, *From Clocks to Chaos: The Rhythms of Life,* Princeton University Press 1988, 272 pp.
- James Gleick, *Chaos: Making a New Science*, New York: Penguin, 1988. 368 pp.
- John Gribbin. *Deep Simplicity*. Penguin Press Science. Penguin Books.
- L Douglas Kiel, Euel W Elliott (ed.), *Chaos Theory in the Social Sciences: Foundations and Applications*, University of Michigan Press, 1997, 360 pp.
- Arvind Kumar, *Chaos, Fractals and Self-Organisation; New Perspectives on Complexity in Nature* , National Book Trust, 2003.
- Hans Lauwerier, *Fractals*, Princeton University Press, 1991.
- Edward Lorenz, *The Essence of Chaos*, University of Washington Press, 1996.
- Alan Marshall (2002) The Unity of Nature: Wholeness and Disintegration in Ecology and Science, Imperial College Press: London
- Heinz-Otto Peitgen and Dietmar Saupe (Eds.), *The Science of Fractal Images*, Springer 1988, 312 pp.
- Clifford A. Pickover, *Computers, Pattern, Chaos, and Beauty: Graphics from an Unseen World* , St Martins Pr 1991.
- Ilya Prigogine and Isabelle Stengers, *Order Out of Chaos*, Bantam 1984.

- Heinz-Otto Peitgen and P. H. Richter, *The Beauty of Fractals : Images of Complex Dynamical Systems*, Springer 1986, 211 pp.
- David Ruelle, *Chance and Chaos*, Princeton University Press 1993.
- Ivars Peterson, *Newton's Clock: Chaos in the Solar System*, Freeman, 1993.
- Ian Roulstone and John Norbury (2013). *Invisible in the Storm: the role of mathematics in understanding weather*. Princeton University Press. ISBN 0691152721.
- David Ruelle, *Chaotic Evolution and Strange Attractors*, Cambridge University Press, 1989.
- Peter Smith, *Explaining Chaos*, Cambridge University Press, 1998.
- Ian Stewart, *Does God Play Dice?: The Mathematics of Chaos* , Blackwell Publishers, 1990.
- Steven Strogatz, *Sync: The emerging science of spontaneous order*, Hyperion, 2003.
- Yoshisuke Ueda, *The Road To Chaos*, Aerial Pr, 1993.
- M. Mitchell Waldrop, *Complexity : The Emerging Science at the Edge of Order and Chaos*, Simon & Schuster, 1992.
- Sawaya, Antonio (2010). *Financial time series analysis : Chaos and neurodynamics approach*.

4.10 External links

- Hazewinkel, Michiel, ed. (2001), "Chaos", *Encyclopedia of Mathematics*, Springer, ISBN 978-1-55608-010-4
- Nonlinear Dynamics Research Group with Animations in Flash
- The Chaos group at the University of Maryland
- The Chaos Hypertextbook. An introductory primer on chaos and fractals
- ChaosBook.org An advanced graduate textbook on chaos (no fractals)
- Society for Chaos Theory in Psychology & Life Sciences
- Nonlinear Dynamics Research Group at CSDC, Florence Italy
- Interactive live chaotic pendulum experiment, allows users to interact and sample data from a real working damped driven chaotic pendulum
- Nonlinear dynamics: how science comprehends chaos, talk presented by Sunny Auyang, 1998.
- Nonlinear Dynamics. Models of bifurcation and chaos by Elmer G. Wiens
- Gleick's *Chaos* (excerpt)
- Systems Analysis, Modelling and Prediction Group at the University of Oxford
- A page about the Mackey-Glass equation
- High Anxieties — The Mathematics of Chaos (2008) BBC documentary directed by David Malone
- The chaos theory of evolution - article published in Newscientist featuring similarities of evolution and non-linear systems including fractal nature of life and chaos.
- Jos Leys, Étienne Ghys et Aurélien Alvarez, *Chaos, A Mathematical Adventure*. Nine films about dynamical systems, the butterfly effect and chaos theory, intended for a wide audience.

Chapter 5

Fractal

For other uses, see Fractal (disambiguation).

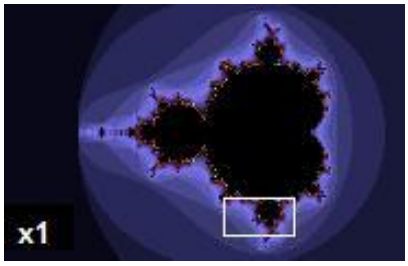

Figure 1a. The Mandelbrot set illustrates self-similarity. As the image is enlarged, the same pattern re-appears so that it is virtually impossible to determine the scale being examined.

Figure 1b. The same fractal magnified six times.

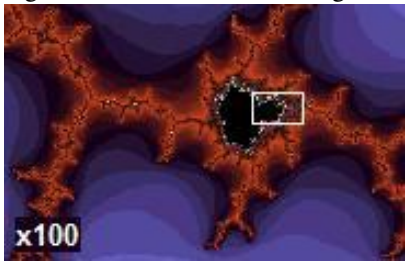

Figure 1c. The same fractal magnified a hundred times.

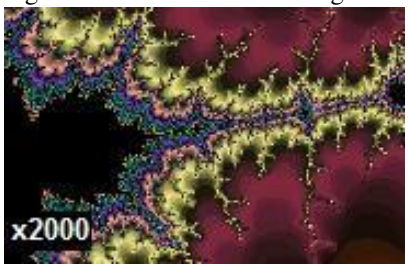

Figure 1d. Even at a magnification of 2,000, the Mandelbrot set displays fine detail resembling the full set.

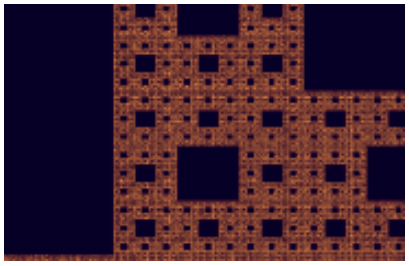

Figure 1e. Another example highlighting how scale is a key feature of a fractal.

A ***fractal*** is a natural phenomenon or a mathematical set that exhibits a repeating pattern that displays at every scale. If the replication is exactly the same at every scale, it is called a self-similar pattern.[1] Fractals can also be nearly the same at different levels. This latter pattern is illustrated in Figure 1.[2][3][4][5] Fractals also includes the idea of a *detailed pattern* that repeats itself.[2]:166; 18[3][6]

Fractals are different from other geometric figures because of the way in which they scale. Doubling the edge lengths of a polygon multiplies its area by four, which is two (the ratio of the new to the old side length) raised to the power of two (the dimension of the space the polygon resides in). Likewise, if the radius of a sphere is doubled, its volume scales by eight, which is two (the ratio of the new to the old radius) to the power of three (the dimension that the sphere resides in). But if a fractal's one-dimensional lengths are all doubled, the spatial content of the fractal scales by a power of two that is not necessarily an integer.[2] This power is called the fractal dimension of the fractal, and it usually exceeds the fractal's topological dimension.[7]

As mathematical equations, fractals are usually nowhere differentiable.[2][5][8] An infinite fractal curve can be conceived of as winding through space differently from an ordinary line, still being a 1-dimensional line yet having a fractal dimension indicating it also resembles a surface.[2]:15[7]:48

The mathematical roots of the idea of fractals have been traced throughout the years as a formal path of published works, starting in the 17th century with notions of recursion, then moving through increasingly rigorous mathematical treatment of the concept to the study of

continuous but not differentiable functions in the 19th century, and on to the coining of the word *fractal* in the 20th century with a subsequent burgeoning of interest in fractals and computer-based modelling in the 21st century.[9][10] The term "fractal" was first used by mathematician Benoît Mandelbrot in 1975. Mandelbrot based it on the Latin *frāctus* meaning "broken" or "fractured", and used it to extend the concept of theoretical fractional dimensions to geometric patterns in nature.[2]:405[6]

There is some disagreement amongst authorities about how the concept of a fractal should be formally defined. Mandelbrot himself summarized it as "beautiful, damn hard, increasingly useful. That's fractals."[11] The general consensus is that theoretical fractals are infinitely self-similar, iterated, and detailed mathematical constructs having fractal dimensions, of which many examples have been formulated and studied in great depth.[2][3][4] Fractals are not limited to geometric patterns, but can also describe processes in time.[1][5][12] Fractal patterns with various degrees of self-similarity have been rendered or studied in images, structures and sounds[13] and found in nature,[14][15][16][17][18] technology,[19][20][21][22] art,[23][24][25] and law.[26]

5.1 Introduction

The word "fractal" often has different connotations for laypeople than for mathematicians, where the layperson is more likely to be familiar with fractal art than a mathematical conception. The mathematical concept is difficult to define formally even for mathematicians, but key features can be understood with little mathematical background.

The feature of "self-similarity", for instance, is easily understood by analogy to zooming in with a lens or other device that zooms in on digital images to uncover finer, previously invisible, new structure. If this is done on fractals, however, no new detail appears; nothing changes and the same pattern repeats over and over, or for some fractals, nearly the same pattern reappears over and over. Self-similarity itself is not necessarily counter-intuitive (e.g., people have pondered self-similarity informally such as in the infinite regress in parallel mirrors or the homunculus, the little man inside the head of the little man inside the head...). The difference for fractals is that the pattern reproduced must be detailed.[2]:166; 18[3][6]

This idea of being detailed relates to another feature that can be understood without mathematical background: Having a fractional or fractal dimension greater than its topological dimension, for instance, refers to how a fractal scales compared to how geometric shapes are usually perceived. A regular line, for instance, is conventionally understood to be 1-dimensional; if such a curve is divided into pieces each 1/3 the length of the original, there are always 3 equal pieces. In contrast, consider the curve in Figure 2. It is also 1-dimensional for the same reason as the ordinary line, but it has, in addition, a fractal dimension greater than 1 because of how its detail can be measured. The fractal curve divided into parts 1/3 the length of the original line becomes 4 pieces rearranged to repeat the original detail, and this unusual relationship is the basis of its fractal dimension.

This also leads to understanding a third feature, that fractals as mathematical equations are "nowhere differentiable". In a concrete sense, this means fractals cannot be measured in traditional ways.[2][5][8] To elaborate, in trying to find the length of a wavy non-fractal curve, one could find straight segments of some measuring tool small enough to lay end to end over the waves, where the pieces could get small enough to be considered to conform to the curve in the normal manner of measuring with a tape measure. But in measuring a wavy fractal curve such as the one in Figure 2, one would never find a small enough straight segment to conform to the curve, because the wavy pattern would always re-appear, albeit at a smaller size, essentially pulling a little more of the tape measure into the total length measured each time one attempted to fit it tighter and tighter to the curve. This is perhaps counter-intuitive, but it is how fractals behave.[2]

5.2 History

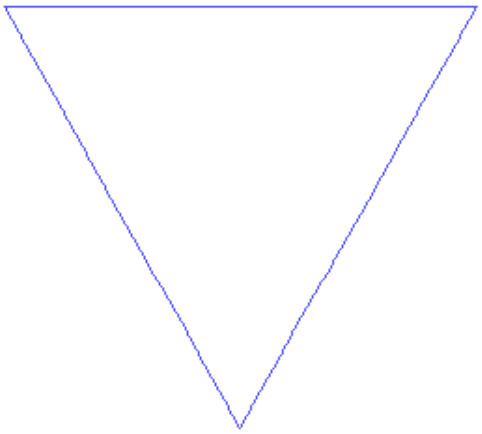

Figure 2a. Koch snowflake, a fractal that begins with an equilateral triangle and then replaces the middle third of every line segment with a pair of line segments that form an equilateral "bump"

The history of fractals traces a path from chiefly theoretical studies to modern applications in computer graphics, with several notable people contributing canonical fractal forms along the way.[9][10] According to Pickover,

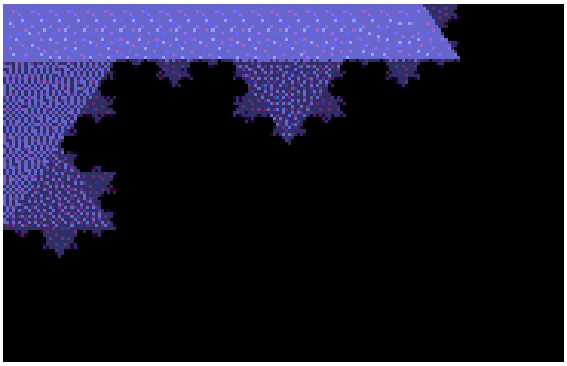

Figure 2b. Koch snowflake, a zoom out of the Koch Snowflake

the mathematics behind fractals began to take shape in the 17th century when the mathematician and philosopher Gottfried Leibniz pondered recursive self-similarity (although he made the mistake of thinking that only the straight line was self-similar in this sense).[27] In his writings, Leibniz used the term "fractional exponents", but lamented that "Geometry" did not yet know of them.[2]:405 Indeed, according to various historical accounts, after that point few mathematicians tackled the issues and the work of those who did remained obscured largely because of resistance to such unfamiliar emerging concepts, which were sometimes referred to as mathematical "monsters".[8][9][10] Thus, it was not until two centuries had passed that in 1872 Karl Weierstrass presented the first definition of a function with a graph that would today be considered fractal, having the non-intuitive property of being everywhere continuous but nowhere differentiable.[9]:7[10] Not long after that, in 1883, Georg Cantor, who attended lectures by Weierstrass,[10] published examples of subsets of the real line known as Cantor sets, which had unusual properties and are now recognized as fractals.[9]:11–24 Also in the last part of that century, Felix Klein and Henri Poincaré introduced a category of fractal that has come to be called "self-inverse" fractals.[2]:166

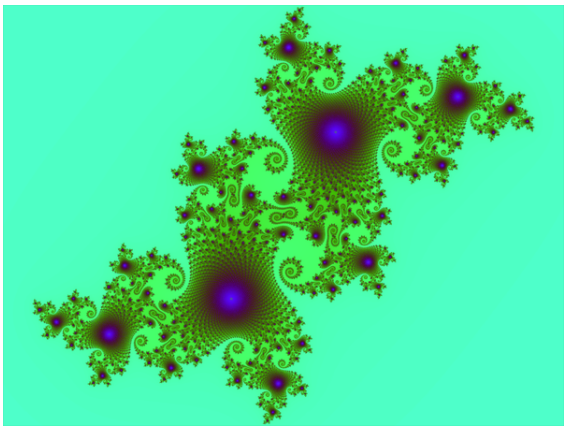

Figure 3. A Julia set, a fractal related to the Mandelbrot set

One of the next milestones came in 1904, when Helge von Koch, extending ideas of Poincaré and dissatisfied with Weierstrass's abstract and analytic definition, gave a more geometric definition including hand drawn images of a similar function, which is now called the Koch curve (see Figure 2).[9]:25[10] Another milestone came a decade later in 1915, when Wacław Sierpiński constructed his famous triangle then, one year later, his carpet. By 1918, two French mathematicians, Pierre Fatou and Gaston Julia, though working independently, arrived essentially simultaneously at results describing what are now seen as fractal behaviour associated with mapping complex numbers and iterative functions and leading to further ideas about attractors and repellors (i.e., points that attract or repel other points), which have become very important in the study of fractals (see Figure 3 and Figure 4).[5][9][10] Very shortly after that work was submitted, by March 1918, Felix Hausdorff expanded the definition of "dimension", significantly for the evolution of the definition of fractals, to allow for sets to have noninteger dimensions.[10] The idea of self-similar curves was taken further by Paul Lévy, who, in his 1938 paper *Plane or Space Curves and Surfaces Consisting of Parts Similar to the Whole* described a new fractal curve, the Lévy C curve.[notes 1]

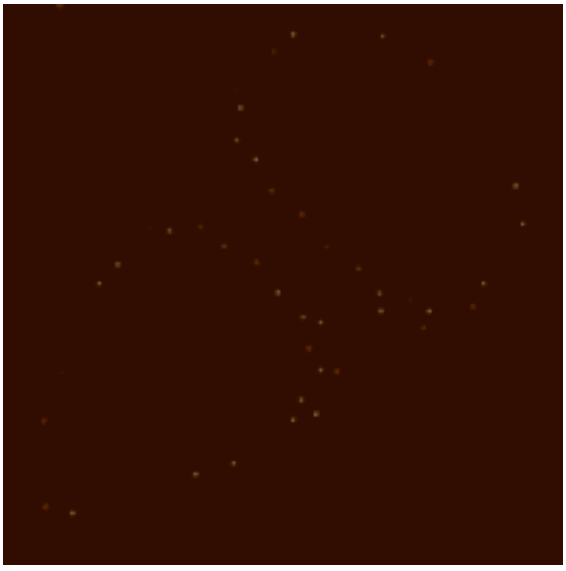

Figure 4. A strange attractor that exhibits multifractal scaling

Different researchers have postulated that without the aid of modern computer graphics, early investigators were limited to what they could depict in manual drawings, so lacked the means to visualize the beauty and appreciate some of the implications of many of the patterns they had discovered (the Julia set, for instance, could only be visualized through a few iterations as very simple drawings hardly resembling the image in Figure 3).[2]:179[8][10] That changed, however, in the 1960s, when Benoît Mandelbrot started writing about self-similarity in papers such as *How Long Is the Coast of Britain? Statistical Self-Similarity and Fractional Dimension*,[28] which built on earlier work by Lewis Fry Richardson. In 1975[6] Mandelbrot solidified hundreds of years of thought and mathematical development in coining the word "fractal"

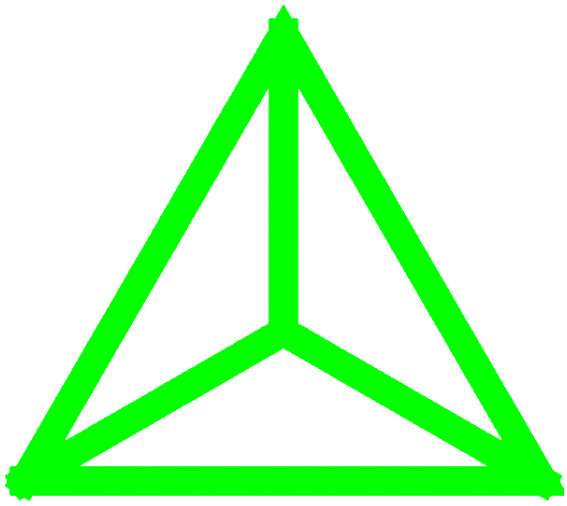

Uniform Mass Center Triangle Fractal

and illustrated his mathematical definition with striking computer-constructed visualizations. These images, such as of his canonical Mandelbrot set pictured in Figure 1, captured the popular imagination; many of them were based on recursion, leading to the popular meaning of the term "fractal".[29] Currently, fractal studies are essentially exclusively computer-based.[8][9][27]

5.3 Characteristics

One often cited description that Mandelbrot published to describe geometric fractals is "a rough or fragmented geometric shape that can be split into parts, each of which is (at least approximately) a reduced-size copy of the whole";[2] this is generally helpful but limited. Authorities disagree on the exact definition of *fractal*, but most usually elaborate on the basic ideas of self-similarity and an unusual relationship with the space a fractal is embedded in.[1][2][3][5][30] One point agreed on is that fractal patterns are characterized by fractal dimensions, but whereas these numbers quantify complexity (i.e., changing detail with changing scale), they neither uniquely describe nor specify details of how to construct particular fractal patterns.[31] In 1975 when Mandelbrot coined the word "fractal", he did so to denote an object whose Hausdorff–Besicovitch dimension is greater than its topological dimension.[6] It has been noted that this dimensional requirement is not met by fractal space-filling curves such as the Hilbert curve.[notes 2]

According to Falconer, rather than being strictly defined, fractals should, in addition to being nowhere differentiable and able to have a fractal dimension, be generally characterized by a gestalt of the following features;[3]

- Self-similarity, which may be manifested as:
  - Exact self-similarity: *identical at all scales; e.g. Koch snowflake*
  - Quasi self-similarity: *approximates the same pattern at different scales; may contain small copies of the entire fractal in distorted and degenerate forms; e.g., the Mandelbrot set's satellites are approximations of the entire set, but not exact copies, as shown in Figure 1*
  - Statistical self-similarity: *repeats a pattern stochastically so numerical or statistical measures are preserved across scales; e.g., randomly generated fractals; the well-known example of the coastline of Britain, for which one would not expect to find a segment scaled and repeated as neatly as the repeated unit that defines, for example, the Koch snowflake[5]*
  - Qualitative self-similarity: *as in a time series*[12]
  - Multifractal scaling: *characterized by more than one fractal dimension or scaling rule*
- Fine or detailed structure at arbitrarily small scales. A consequence of this structure is fractals may have emergent properties[32] (related to the next criterion in this list).
- Irregularity locally and globally that is not easily described in traditional Euclidean geometric language. For images of fractal patterns, this has been expressed by phrases such as "smoothly piling up surfaces" and "swirls upon swirls".[7]
- Simple and "perhaps recursive" definitions *see Common techniques for generating fractals*

As a group, these criteria form guidelines for excluding certain cases, such as those that may be self-similar without having other typically fractal features. A straight line, for instance, is self-similar but not fractal because it lacks detail, is easily described in Euclidean language, has the same Hausdorff dimension as topological dimension, and is fully defined without a need for recursion.[2][5]

5.4 Brownian motion

A path generated by a one dimensional Wiener process is a fractal curve of dimension 1.5, and Brownian motion is a finite version of this.[33]

5.5 Common techniques for generating fractals

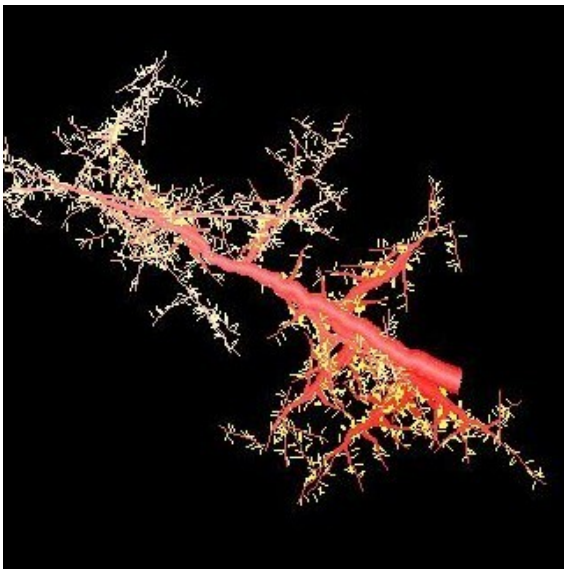

Figure 5. Self-similar branching pattern modeled in silico using L-systems principles[18]

Images of fractals can be created by fractal generating programs.

- *Iterated function systems* – use fixed geometric replacement rules; may be stochastic or deterministic;[34] e.g., Koch snowflake, Cantor set, Haferman carpet,[35] Sierpinski carpet, Sierpinski gasket, Peano curve, Harter-Heighway dragon curve, T-Square, Menger sponge
- *Strange attractors* – use iterations of a map or solutions of a system of initial-value differential equations that exhibit chaos (e.g., see multifractal image)
- *L-systems* - use string rewriting; may resemble branching patterns, such as in plants, biological cells (e.g., neurons and immune system cells[18]), blood vessels, pulmonary structure,[36] etc. (e.g., see Figure 5) or turtle graphics patterns such as space-filling curves and tilings
- *Escape-time fractals* – use a formula or recurrence relation at each point in a space (such as the complex plane); usually quasi-self-similar; also known as "orbit" fractals; e.g., the Mandelbrot set, Julia set, Burning Ship fractal, Nova fractal and Lyapunov fractal. The 2d vector fields that are generated by one or two iterations of escape-time formulae also give rise to a fractal form when points (or pixel data) are passed through this field repeatedly.
- *Random fractals* – use stochastic rules; e.g., Lévy flight, percolation clusters, self avoiding walks, fractal landscapes, trajectories of Brownian motion and the Brownian tree (i.e., dendritic fractals generated by modeling diffusion-limited aggregation or reaction-limited aggregation clusters).[5]

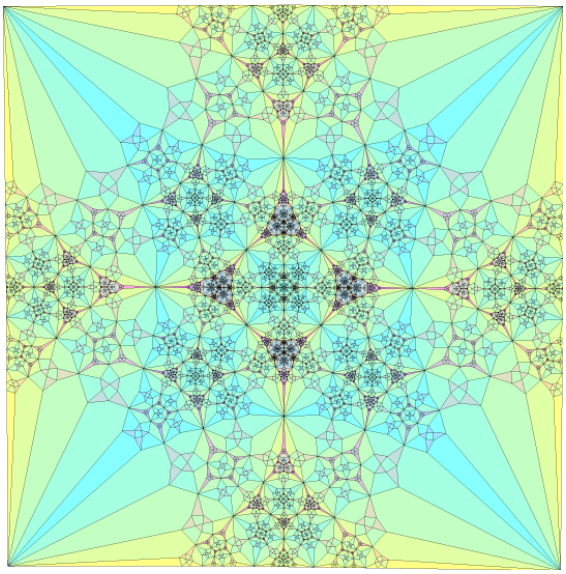

A fractal generated by a finite subdivision rule for an alternating link

- *Finite subdivision rules* use a recursive topological algorithm for refining tilings[37] and they are similar to the process of cell division.[38] The iterative processes used in creating the Cantor set and the Sierpinski carpet are examples of finite subdivision rules, as is barycentric subdivision.

5.6 Simulated fractals

Fractal patterns have been modeled extensively, albeit within a range of scales rather than infinitely, owing to the practical limits of physical time and space. Models may simulate theoretical fractals or natural phenomena

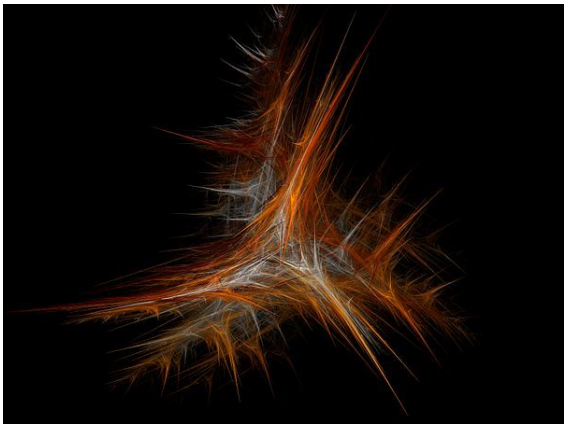

A fractal flame

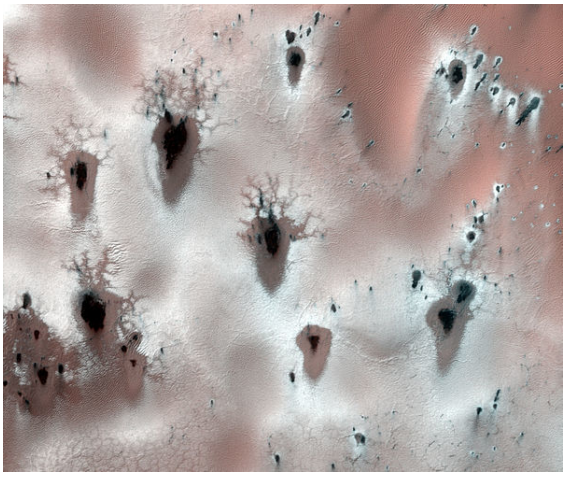

Fractal defrosting patterns, polar Mars. The patterns are formed by sublimation of frozen CO_2. Width of image is about a kilometer.

with fractal features. The outputs of the modelling process may be highly artistic renderings, outputs for investigation, or benchmarks for fractal analysis. Some specific applications of fractals to technology are listed elsewhere. Images and other outputs of modelling are normally referred to as being “fractals” even if they do not have strictly fractal characteristics, such as when it is possible to zoom into a region of the fractal image that does not exhibit any fractal properties. Also, these may include calculation or display artifacts which are not characteristics of true fractals.

Modeled fractals may be sounds,[13] digital images, electrochemical patterns, circadian rhythms,[39] etc. Fractal patterns have been reconstructed in physical 3-dimensional space[21]:10 and virtually, often called "in silico" modeling.[36] Models of fractals are generally created using fractal-generating software that implements techniques such as those outlined above.[5][12][21] As one illustration, trees, ferns, cells of the nervous system,[18] blood and lung vasculature,[36] and other branching patterns in nature can be modeled on a computer by using recursive algorithms and L-systems techniques.[18] The recursive nature of some patterns is obvious in certain examples—a branch from a tree or a frond from a fern is a miniature replica of the whole: not identical, but similar in nature. Similarly, random fractals have been used to describe/create many highly irregular real-world objects. A limitation of modeling fractals is that resemblance of a fractal model to a natural phenomenon does not prove that the phenomenon being modeled is formed by a process similar to the modeling algorithms.

5.7 Natural phenomena with fractal features

Further information: Patterns in nature

Approximate fractals found in nature display self-similarity over extended, but finite, scale ranges. The connection between fractals and leaves, for instance, is currently being used to determine how much carbon is contained in trees.[40]

Examples of phenomena known or anticipated to have fractal features are listed below:

5.8 In creative works

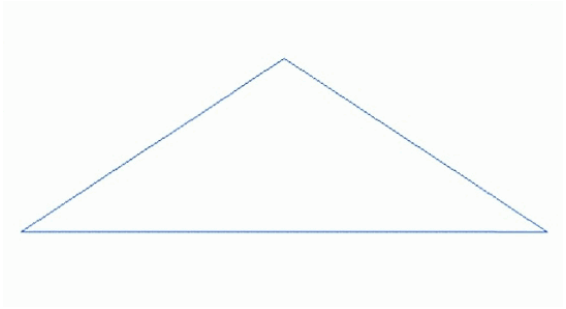

A fractal that models the surface of a mountain (animation)

Further information: Fractal art

Fractal patterns have been found in the paintings of American artist Jackson Pollock. While Pollock’s paintings appear to be composed of chaotic dripping and splattering, computer analysis has found fractal patterns in his work.[25]

Decalcomania, a technique used by artists such as Max Ernst, can produce fractal-like patterns.[49] It involves pressing paint between two surfaces and pulling them apart.

Cyberneticist Ron Eglash has suggested that fractal geometry and mathematics are prevalent in African art, games, divination, trade, and architecture. Circular

houses appear in circles of circles, rectangular houses in rectangles of rectangles, and so on. Such scaling patterns can also be found in African textiles, sculpture, and even cornrow hairstyles.[24][50]

In a 1996 interview with Michael Silverblatt, David Foster Wallace admitted that the structure of the first draft of *Infinite Jest* he gave to his editor Michael Pietsch was inspired by fractals, specifically the Sierpinski triangle (aka Sierpinski gasket) but that the edited novel is "more like a lopsided Sierpinsky Gasket".[23]

5.9 Applications in technology

Main article: Fractal analysis

5.10 See also

5.10.1 Fractal-generating programs

There are many fractal generating programs available, both free and commercial. Some of the fractal generating programs include:

- Apophysis - open source software for Microsoft Windows based systems
- Electric Sheep - open source distributed computing software
- Fractint - freeware with available source code
- Sterling - Freeware software for Microsoft Windows based systems
- SpangFract - For Mac OS
- Ultra Fractal - A proprietary fractal generator for Microsoft Windows and Mac OS X based systems
- XaoS - A cross platform open source fractal zooming program
- Chaotica - a commercial software for Microsoft Windows, Linux and Mac OS
- Terragen - a fractal terrain generator.

Most of the above programs make two-dimensional fractals, with a few creating three-dimensional fractal objects, such as quaternions, mandelbulbs and mandelboxes.

5.11 Notes

[1] The original paper, Lévy, Paul (1938). "Les Courbes planes ou gauches et les surfaces composées de parties semblables au tout". *Journal de l'École Polytechnique*: 227–247, 249–291., is translated in Edgar, pages 181-239.

[2] The Hilbert curve map is not a homeomorphism, so it does not preserve topological dimension. The topological dimension and Hausdorff dimension of the image of the Hilbert map in $\mathbf{R}^2$ are both 2. Note, however, that the topological dimension of the *graph* of the Hilbert map (a set in $\mathbf{R}^3$) is 1.

5.12 References

[1] Gouyet, Jean-François (1996). *Physics and fractal structures*. Paris/New York: Masson Springer. ISBN 978-0-387-94153-0.

[2] Mandelbrot, Benoît B. (1983). *The fractal geometry of nature*. Macmillan. ISBN 978-0-7167-1186-5. Retrieved 1 February 2012.

[3] Falconer, Kenneth (2003). *Fractal Geometry: Mathematical Foundations and Applications*. John Wiley & Sons, Ltd. xxv. ISBN 0-470-84862-6.

[4] Briggs, John (1992). *Fractals:The Patterns of Chaos*. London, UK: Thames and Hudson. p. 148. ISBN 0-500-27693-5.

[5] Vicsek, Tamás (1992). *Fractal growth phenomena*. Singapore/New Jersey: World Scientific. pp. 31; 139–146. ISBN 978-981-02-0668-0.

[6] Albers, Donald J.; Alexanderson, Gerald L. (2008). "Benoît Mandelbrot: In his own words". *Mathematical people : profiles and interviews*. Wellesley, MA: AK Peters. p. 214. ISBN 978-1-56881-340-0.

[7] Mandelbrot, Benoît B. (2004). *Fractals and Chaos*. Berlin: Springer. p. 38. ISBN 978-0-387-20158-0. "A fractal set is one for which the fractal (Hausdorff-Besicovitch) dimension strictly exceeds the topological dimension"

[8] Gordon, Nigel (2000). *Introducing fractal geometry*. Duxford, UK: Icon. p. 71. ISBN 978-1-84046-123-7.

[9] Edgar, Gerald (2004). *Classics on Fractals*. Boulder, CO: Westview Press. ISBN 978-0-8133-4153-8.

[10] Trochet, Holly (2009). "A History of Fractal Geometry". *MacTutor History of Mathematics*. Archived from the original on 4 February 2012.

[11] Mandelbrot, Benoit. "24/7 Lecture on Fractals". *2006 Ig Nobel Awards*. Improbable Research.

[12] Peters, Edgar (1996). *Chaos and order in the capital markets : a new view of cycles, prices, and market volatility*. New York: Wiley. ISBN 0-471-13938-6.

[13] Brothers, Harlan J. (2007). "Structural Scaling in Bach's Cello Suite No. 3". *Fractals* **15**: 89–95. doi:10.1142/S0218348X0700337X.

[14] Tan, Can Ozan; Cohen, Michael A.; Eckberg, Dwain L.; Taylor, J. Andrew (2009). "Fractal properties of human heart period variability: Physiological and methodological implications". *The Journal of Physiology* **587** (15): 3929. doi:10.1113/jphysiol.2009.169219.

[15] Buldyrev, Sergey V.; Goldberger, Ary L.; Havlin, Shlomo; Peng, Chung-Kang; Stanley, H. Eugene (1995). "3". In Bunde, Armin; Havlin, Shlomo. "Fractals in Science". Springer.

[16] Liu, Jing Z.; Zhang, Lu D.; Yue, Guang H. (2003). "Fractal Dimension in Human Cerebellum Measured by Magnetic Resonance Imaging". *Biophysical Journal* **85** (6): 4041–4046. doi:10.1016/S0006-3495(03)74817-6. PMC 1303704. PMID 14645092.

[17] Karperien, Audrey L.; Jelinek, Herbert F.; Buchan, Alastair M. (2008). "Box-Counting Analysis of Microglia Form in Schizophrenia, Alzheimer's Disease and Affective Disorder". *Fractals* **16** (2): 103. doi:10.1142/S0218348X08003880.

[18] Jelinek, Herbert F.; Karperien, Audrey; Cornforth, David; Cesar, Roberto; Leandro, Jorge de Jesus Gomes (2002). "MicroMod-an L-systems approach to neural modelling". In Sarker, Ruhul. *Workshop proceedings: the Sixth Australia-Japan Joint Workshop on Intelligent and Evolutionary Systems, University House, ANU,*. University of New South Wales. ISBN 9780731705054. OCLC 224846454. http://researchoutput.csu.edu.au/R/-?func=dbin-jump-full&object_id=6595&local_base=GEN01-CSU01. Retrieved 3 February 2012. "Event location: Canberra, Australia"

[19] Hu, Shougeng; Cheng, Qiuming; Wang, Le; Xie, Shuyun (2012). "Multifractal characterization of urban residential land price in space and time". *Applied Geography* **34**: 161. doi:10.1016/j.apgeog.2011.10.016.

[20] Karperien, Audrey; Jelinek, Herbert F.; Leandro, Jorge de Jesus Gomes; Soares, João V. B.; Cesar Jr, Roberto M.; Luckie, Alan (2008). "Automated detection of proliferative retinopathy in clinical practice". *Clinical ophthalmology (Auckland, N.Z.)* **2** (1): 109–122. doi:10.2147/OPTH.S1579. PMC 2698675. PMID 19668394.

[21] Losa, Gabriele A.; Nonnenmacher, Theo F. (2005). *Fractals in biology and medicine*. Springer. ISBN 978-3-7643-7172-2. Retrieved 1 February 2012.

[22] Vannucchi, Paola; Leoni, Lorenzo (2007). "Structural characterization of the Costa Rica décollement: Evidence for seismically-induced fluid pulsing". *Earth and Planetary Science Letters* **262** (3–4): 413. Bibcode:2007E&PSL.262..413V. doi:10.1016/j.epsl.2007.07.056.

[23] Wallace, David Foster. "Bookworm on KCRW". Kcrw.com. Retrieved 2010-10-17.

[24] Eglash, Ron (1999). "African Fractals: Modern Computing and Indigenous Design". New Brunswick: Rutgers University Press. Retrieved 2010-10-17.

[25] Taylor, Richard; Micolich, Adam P.; Jonas, David. "Fractal Expressionism: Can Science Be Used To Further Our Understanding Of Art?". Phys.unsw.edu.au. Retrieved 2010-10-17.

[26] Stumpff, Andrew (2013). "The Law is a Fractal: The Attempt to Anticipate Everything" **44**. Loyola University Chicago Law Journal. p. 649.

[27] Pickover, Clifford A. (2009). *The Math Book: From Pythagoras to the 57th Dimension, 250 Milestones in the History of Mathematics*. Sterling Publishing Company, Inc. p. 310. ISBN 978-1-4027-5796-9. Retrieved 2011-02-05.

[28] Batty, Michael (1985-04-04). "Fractals - Geometry Between Dimensions". *New Scientist* (Holborn Publishing Group) **105** (1450): 31.

[29] Russ, John C. (1994). *Fractal surfaces* **1**. Springer. p. 1. ISBN 978-0-306-44702-0. Retrieved 2011-02-05.

[30] Edgar, Gerald (2008). *Measure, topology, and fractal geometry*. New York, NY: Springer-Verlag. p. 1. ISBN 978-0-387-74748-4.

[31] Karperien, Audrey (2004). http://www.webcitation.org/65DyLbmF1 *Defining microglial morphology: Form, Function, and Fractal Dimension*. Charles Sturt University. Retrieved 2012-02-05.

[32] Spencer, John; Thomas, Michael S. C.; McClelland, James L. (2009). *Toward a unified theory of development : connectionism and dynamic systems theory re-considered*. Oxford/New York: Oxford University Press. ISBN 978-0-19-530059-8.

[33] Falconer, Kenneth (2013). *Fractals, A Very Short Introduction*. Oxford University Press.

[34] Frame, Angus (3 August 1998). "Iterated Function Systems". In Pickover, Clifford A. *Chaos and fractals: a computer graphical journey : ten year compilation of advanced research*. Elsevier. pp. 349–351. ISBN 978-0-444-50002-1. Retrieved 4 February 2012.

[35] "Haferman Carpet". WolframAlpha. Retrieved 18 October 2012.

[36] Hahn, Horst K.; Georg, Manfred; Peitgen, Heinz-Otto (2005). "Fractal aspects of three-dimensional vascular constructive optimization". In Losa, Gabriele A.; Nonnenmacher, Theo F. *Fractals in biology and medicine*. Springer. pp. 55–66. ISBN 978-3-7643-7172-2.

[37] J. W. Cannon, W. J. Floyd, W. R. Parry. *Finite subdivision rules*. Conformal Geometry and Dynamics, vol. 5 (2001), pp. 153–196.

[38] J. W. Cannon, W. Floyd and W. Parry. *Crystal growth, biological cell growth and geometry*. Pattern Formation in Biology, Vision and Dynamics, pp. 65–82. World Scientific, 2000. ISBN 981-02-3792-8,ISBN 978-981-02-3792-9.

[39] Fathallah-Shaykh, Hassan M. (2011). "Fractal Dimension of the Drosophila Circadian Clock". *Fractals* **19** (4): 423–430. doi:10.1142/S0218348X11005476.

[40] "Hunting the Hidden Dimension." *Nova*. PBS. WPMB-Maryland. 28 October 2008.

[41] Sornette, Didier (2004). *Critical phenomena in natural sciences: chaos, fractals, selforganization, and disorder : concepts and tools*. Springer. pp. 128–140. ISBN 978-3-540-40754-6.

[42] Meyer, Yves; Roques, Sylvie (1993). *Progress in wavelet analysis and applications: proceedings of the International Conference "Wavelets and Applications," Toulouse, France - June 1992*. Atlantica Séguier Frontières. p. 25. ISBN 978-2-86332-130-0. Retrieved 2011-02-05.

[43] Pincus, David (September 2009). "The Chaotic Life: Fractal Brains Fractal Thoughts". *psychologytoday.com*.

[44] Carbone, Alessandra; Gromov, Mikhael; Prusinkiewicz, Przemyslaw (2000). *Pattern formation in biology, vision and dynamics*. World Scientific. p. 78. ISBN 978-981-02-3792-9.

[45] Addison, Paul S. (1997). *Fractals and chaos: an illustrated course*. CRC Press. pp. 44–46. ISBN 978-0-7503-0400-9. Retrieved 2011-02-05.

[46] Ozhovan M.I., Dmitriev I.E., Batyukhnova O.G. Fractal structure of pores of clay soil. Atomic Energy, 74, 241-243 (1993)

[47] Takayasu, H. (1990). *Fractals in the physical sciences*. Manchester: Manchester University Press. p. 36. ISBN 9780719034343.

[48] Jun, Li; Ostoja-Starzewski, Martin. "Saturn's Rings are Fractal". Retrieved 28 June 2014.

[49] Frame, Michael; and Mandelbrot, Benoît B.; *A Panorama of Fractals and Their Uses*

[50] Nelson, Bryn; *Sophisticated Mathematics Behind African Village Designs Fractal patterns use repetition on large, small scale*, San Francisco Chronicle, Wednesday, February 23, 2009

[51] Hohlfeld, Robert G.; Cohen, Nathan (1999). "Self-similarity and the geometric requirements for frequency independence in Antennae". *Fractals* **7** (1): 79–84. doi:10.1142/S0218348X99000098.

[52] Reiner, Richard; Waltereit, Patrick; Benkhelifa, Fouad; Müller, Stefan; Walcher, Herbert; Wagner, Sandrine; Quay, Rüdiger; Schlechtweg, Michael; Ambacher, Oliver; Ambacher, O. (2012). "Fractal structures for low-resistance large area AlGaN/GaN power transistors". *Proceedings of ISPSD*: 341. doi:10.1109/ISPSD.2012.6229091. ISBN 978-1-4577-1596-9.

[53] Chen, Yanguang (2011). "Modeling Fractal Structure of City-Size Distributions Using Correlation Functions". *PLoS ONE* **6** (9): e24791. doi:10.1371/journal.pone.0024791. PMC 3176775. PMID 21949753.

[54] "Applications". Retrieved 2007-10-21.

[55] Smith, Robert F.; Mohr, David N.; Torres, Vicente E.; Offord, Kenneth P.; Melton III, L. Joseph (1989). "Renal insufficiency in community patients with mild asymptomatic microhematuria". *Mayo Clinic proceedings. Mayo Clinic* **64** (4): 409–414. PMID 2716356.

[56] Landini, Gabriel (2011). "Fractals in microscopy". *Journal of Microscopy* **241** (1): 1–8. doi:10.1111/j.1365-2818.2010.03454.x. PMID 21118245.

[57] Cheng, Qiuming (1997). "Multifractal Modeling and Lacunarity Analysis". *Mathematical Geology* **29** (7): 919–932. doi:10.1023/A:1022355723781.

[58] Chen, Yanguang (2011). "Modeling Fractal Structure of City-Size Distributions Using Correlation Functions". *PLoS ONE* **6** (9): e24791. doi:10.1371/journal.pone.0024791. PMC 3176775. PMID 21949753.

[59] Burkle-Elizondo, Gerardo; Valdéz-Cepeda, Ricardo David (2006). "Fractal analysis of Mesoamerican pyramids". *Nonlinear dynamics, psychology, and life sciences* **10** (1): 105–122. PMID 16393505.

[60] Brown, Clifford T.; Witschey, Walter R. T.; Liebovitch, Larry S. (2005). "The Broken Past: Fractals in Archaeology". *Journal of Archaeological Method and Theory* **12**: 37. doi:10.1007/s10816-005-2396-6.

[61] Saeedi, Panteha; Sorensen, Soren A. "An Algorithmic Approach to Generate After-disaster Test Fields for Search and Rescue Agents". *Proceedings of the World Congress on Engineering 2009*: 93–98. ISBN 978-988-17-0125-1.

[62] Bunde, A.; Havlin, S. (2009). "Fractal Geometry, A Brief Introduction to". "Encyclopedia of Complexity and Systems Science". p. 3700. doi:10.1007/978-0-387-30440-3_218. ISBN 978-0-387-75888-6.

5.13 Further reading

- Barnsley, Michael F.; and Rising, Hawley; *Fractals Everywhere*. Boston: Academic Press Professional, 1993. ISBN 0-12-079061-0
- Duarte, German A.; *Fractal Narrative. About the Relationship Between Geometries and Technology and Its Impact on Narrative Spaces*. Bielefeld: Transcript, 2014. ISBN 978-3-8376-2829-6
- Falconer, Kenneth; *Techniques in Fractal Geometry*. John Wiley and Sons, 1997. ISBN 0-471-92287-0
- Jürgens, Hartmut; Peitgen, Heins-Otto; and Saupe, Dietmar; *Chaos and Fractals: New Frontiers of Science*. New York: Springer-Verlag, 1992. ISBN 0-387-97903-4
- Mandelbrot, Benoit B.; *The Fractal Geometry of Nature*. New York: W. H. Freeman and Co., 1982. ISBN 0-7167-1186-9

- Peitgen, Heinz-Otto; and Saupe, Dietmar; eds.; *The Science of Fractal Images*. New York: Springer-Verlag, 1988. ISBN 0-387-96608-0
- Pickover, Clifford A.; ed.; *Chaos and Fractals: A Computer Graphical Journey - A 10 Year Compilation of Advanced Research*. Elsevier, 1998. ISBN 0-444-50002-2
- Jones, Jesse; *Fractals for the Macintosh*, Waite Group Press, Corte Madera, CA, 1993. ISBN 1-878739-46-8.
- Lauwerier, Hans; *Fractals: Endlessly Repeated Geometrical Figures*, Translated by Sophia Gill-Hoffstadt, Princeton University Press, Princeton NJ, 1991. ISBN 0-691-08551-X, cloth. ISBN 0-691-02445-6 paperback. "This book has been written for a wide audience..." Includes sample BASIC programs in an appendix.
- Sprott, Julien Clinton (2003). *Chaos and Time-Series Analysis*. Oxford University Press. ISBN 978-0-19-850839-7.
- Wahl, Bernt; Van Roy, Peter; Larsen, Michael; and Kampman, Eric; *Exploring Fractals on the Macintosh*, Addison Wesley, 1995. ISBN 0-201-62630-6
- Lesmoir-Gordon, Nigel; "The Colours of Infinity: The Beauty, The Power and the Sense of Fractals." ISBN 1-904555-05-5 (The book comes with a related DVD of the Arthur C. Clarke documentary introduction to the fractal concept and the Mandelbrot set).
- Liu, Huajie; *Fractal Art*, Changsha: Hunan Science and Technology Press, 1997, ISBN 9787535722348.
- Gouyet, Jean-François; *Physics and Fractal Structures* (Foreword by B. Mandelbrot); Masson, 1996. ISBN 2-225-85130-1, and New York: Springer-Verlag, 1996. ISBN 978-0-387-94153-0. Out-of-print. Available in PDF version at."Physics and Fractal Structures" (in French). Jfgouyet.fr. Retrieved 2010-10-17.
- Bunde, Armin; Havlin, Shlomo (1996). *Fractals and Disordered Systems*. Springer.
- Bunde, Armin; Havlin, Shlomo (1995). *Fractals in Science*. Springer.
- ben-Avraham, Daniel; Havlin, Shlomo (2000). *Diffusion and Reactions in Fractals and Disordered Systems*. Cambridge University Press.
- Falconer, Kenneth (2013). *Fractals, A Very Short Introduction*. Oxford University Press.

5.14 External links

- Fractals at DMOZ
- Scaling and Fractals presented by Shlomo Havlin, Bar-Ilan University
- Hunting the Hidden Dimension, *PBS NOVA*, first aired August 24, 2011
- Benoit Mandelbrot: Fractals and the Art of Roughness, TED (conference), February 2010
- Zoom Video in Mandelbox on YouTube (Example of 3D fractal)
- Video fly through of an animated Mandelbulb world on YouTube
- Technical Library on Fractals for controlling fluid
- Equations of self-similar fractal measure based on the fractional-order calculus(2007)

Chapter 6

Wind wave

"Ocean wave" redirects here. For the film, see Ocean Waves (film).

In fluid dynamics, **wind waves**, or **wind-generated**

Hurricane Marie storm waves

Video of large waves from Hurricane Marie along the coast of Newport Beach CA.

waves, are surface waves that occur on the free surface of oceans, seas, lakes, rivers, and canals or even on small puddles and ponds. They result from the wind blowing over an area of fluid surface. Waves in the oceans can travel thousands of miles before reaching land. Wind waves range in size from small ripples, to waves over 100ft (30m) high.[1]

When directly generated and affected by local winds, a wind wave system is called a **wind sea**. After the wind ceases to blow, wind waves are called *swells*. More generally, a swell consists of wind-generated waves that are not significantly affected by the local wind at that time.

Ocean waves

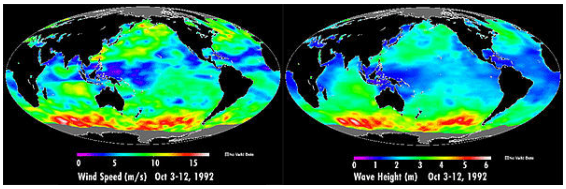

The image shows the global distribution of wind speed and wave height as observed by NASA's TOPEX/Poseidon's dual-frequency radar altimeter from October 3 to October 12, 1992. Simultaneous observations of wind speed and wave height are helping scientists to predict ocean waves . Wind speed is determined by the strength of the radar signal after it has bounced off the ocean surface and returned to the satellite. A calm sea serves as a good reflector and returns a strong signal; a rough sea tends to scatter the signals and returns a weak pulse. Wave height is determined by the shape of the return radar pulse. A calm sea with low waves returns a condensed pulse whereas a rough sea with high waves returns a stretched pulse. Comparing the two images above shows a high degree of correlation between wind speed and wave height. The strongest winds (33.6mph; 54km/h) and highest waves are found in the Southern Ocean. The weakest winds—shown as areas of magenta and dark blue—are generally found in the tropical Oceans.

They have been generated elsewhere or some time ago.[2] Wind waves in the ocean are called **ocean surface waves**.

Wind waves have a certain amount of randomness: subsequent waves differ in height, duration, and shape with limited predictability. They can be described as a stochastic process, in combination with the physics gov-

erning their generation, growth, propagation and decay—as well as governing the interdependence between flow quantities such as: the water surface movements, flow velocities and water pressure. The key statistics of wind waves (both seas and swells) in evolving sea states can be predicted with wind wave models.

Although waves are usually considered in the water seas of Earth, the hydrocarbon seas of Titan may also have wind-driven waves.[3]

6.1 Wave formation

NOAA ship Delaware II *in bad weather on Georges Bank.*

The great majority of large breakers one observes on a beach result from distant winds. Five factors influence the formation of wind waves:[4]

- Wind speed or strength relative to wave speed- the wind must be moving faster than the wave crest for energy transfer
- The uninterrupted distance of open water over which the wind blows without significant change in direction (called the *fetch*)
- Width of area affected by fetch
- Wind duration - the time over which the wind has blown over a given area
- Water depth

All of these factors work together to determine the size of wind waves:

- Wave height (from high trough to crest)
- Wave length (from crest to crest)
- Wave period (time interval between arrival of consecutive crests at a stationary point)
- Wave propagation direction

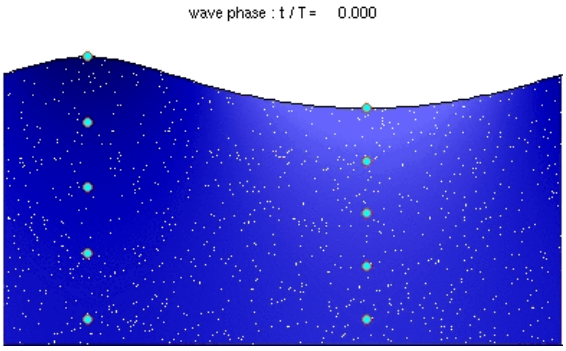

water particles movements of deep a water wave.

A fully developed sea has the maximum wave size theoretically possible for a wind of a specific strength, duration, and fetch. Further exposure to that specific wind could only cause a loss of energy due to the breaking of wave tops and formation of "whitecaps". Waves in a given area typically have a range of heights. For weather reporting and for scientific analysis of wind wave statistics, their characteristic height over a period of time is usually expressed as *significant wave height*. This figure represents an average height of the highest one-third of the waves in a given time period (usually chosen somewhere in the range from 20 minutes to twelve hours), or in a specific wave or storm system. The significant wave height is also the value a "trained observer" (e.g. from a ship's crew) would estimate from visual observation of a sea state. Given the variability of wave height, the largest individual waves are likely to be somewhat less than twice the reported significant wave height for a particular day or storm.[5]

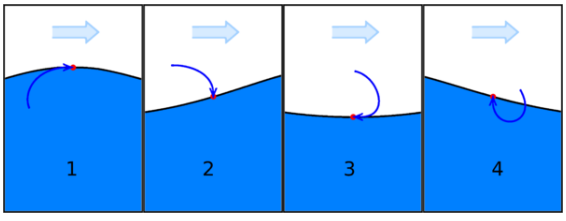

The phases of an ocean surface wave: 1. Wave Crest, where the water masses of the surface layer are moving horizontally in the same direction as the propagating wave front. 2. Falling wave. 3. Trough, where the water masses of the surface layer are moving horizontally in the opposite direction of the wave front direction. 4. Rising wave.

• **Sources of wind wave generation:** Sea water wave is generated by many kinds of disturbances such as Seis-

mic events, gravity, and crossing wind. The generation of wind wave is initiated by the disturbances of cross wind field on the surface of the sea water. Two major Mechanisms of surface wave formation by winds (a.k.a.'The Miles-Phillips Mechanism') and other sources (ex. earthquakes) of wave formation can explain the generation of wind waves.

However, if one set a flat water surface (Beaufort Point,0) and abrupt cross wind flows on the surface of the water,then the generation of surface wind waves can be explained by following two mechanisms which initiated by normal pressure fluctuations of turbulent winds and parallel wind shear flows.

• **The mechanism of the surface wave generation by winds**

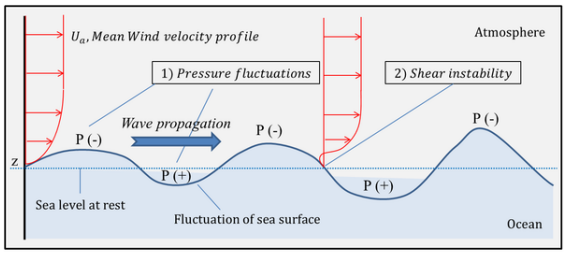

the simple picture of the wave formation mechanism

1) Starts from "Fluctuations of wind" (O.M.Phillips) : the wind wave formation on water surface by wind is started by a random distribution of normal pressure acting on the water from the wind. By the mechanism developed by O.M. Phillips (in 1957), the water surface is initially at rest and the generation of wave is initiated by adding turbulent wind flows and then, by the fluctuations of the wind, normal pressure acting on the water surface. This pressure fluctuation arise normal and tangential stresses to the surface water, and generates wave behavior on the water surface. {*Assumptions* 1. water originally at rest 2. water is inviscid 3. Water is irrotational 4. Random distribution of normal pressure to the water surface from the turbulent wind 5. Correlations between air and Water motions are neglected}[6]

2) starts from "wind shear forces" on the water surface (J.W.Miles, applied to mainly 2D deep water gravity waves) ; John W. Miles suggested a surface wave generation mechanism which is initiated by turbulent wind shear flows Ua(y), based on the inviscid Orr-Sommerfeld equation in 1957. He found the energy transfer from wind to water surface as a wave speed, c is proportional to the curvature of the velocity profile of wind Ua"(y) at point where the mean wind speed is equal to the wave speed (Ua=c, where, Ua is the Mean turbulent wind speed). Since the wind profile Ua(y) is logarithmic to the water surface, the curvature Ua"(y) have negative sign at the point of Ua=c. This relations show the wind flow transferring its kinetic energy to the water surface at their interface, and arises wave speed, c.

the growth-rate can be determined by the curvature of the winds ((d^2 Ua)/(dz^2)) at the steering height (Ua (z=z_h)=c) for a given wind speed Ua {*Assumptions*; 1. 2D parallel shear flow, Ua(y) 2. incompressible, inviscid water / wind 3. irrotational water 4. slope of the displacement of surface is small}[7]

• **Generally**, these wave formation mechanisms occur together on the ocean surface and arise wind waves and grows up to the fully developed waves.

For example,[8]

If we suppose a very flat sea surface (Beaufort number, 0), and sudden wind flow blows steadily across the sea surface, physical wave generation process will be like;

1. Turbulent wind flows form random pressure fluctuations at the sea surface. Small waves with a few centimeters order of wavelengths is generated by the pressure fluctuations. (The Phillips mechanism[6])

2. The cross wind keep acting on the initially fluctuated sea surface, then the wave become larger. As the wave become larger, the pressure differences get larger along to the wave growing, then the wave growth rate is getting faster. Then the shear instability expedites the wave growing exponentially. (The Miles mechanism[6])

3. The interactions between the waves on the surface generate longer waves (Hasselmann et al., 1973[9]) and the interaction will transfer wave energy from the shorter waves generated by the Miles mechanism to the waves have slightly lower frequencies than the frequency at the peak wave magnitudes, then finally the waves will be faster than the cross wind speed (Pierson & Moskowitz[10]).

((NOTE: Most of the wave speeds calculated from the wave length divided by the period are proportional to sqrt (length). Thus, except for the shortest wave length, the waves follow the deep water theory described in the next section. The 28 ft long wave must be either in shallow water or between deep and shallow.))

6.2 Types of wind waves

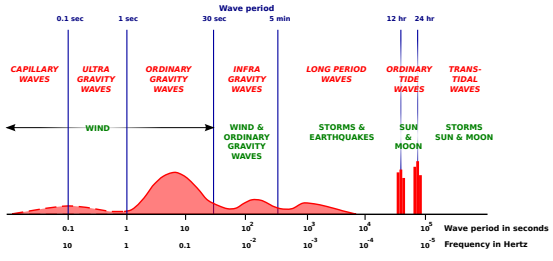

Classification of the spectrum of ocean waves according to wave period.[11]

Three different types of wind waves develop over time:

- Capillary waves, or ripples

Surf on a rocky irregular bottom. Porto Covo, west coast of Portugal

- Seas
- Swells

Ripples appear on smooth water when the wind blows, but will die quickly if the wind stops. The restoring force that allows them to propagate is surface tension. Seas are the larger-scale, often irregular motions that form under sustained winds. These waves tend to last much longer, even after the wind has died, and the restoring force that allows them to propagate is gravity. As waves propagate away from their area of origin, they naturally separate into groups of common direction and wavelength. The sets of waves formed in this way are known as swells.

Individual "rogue waves" (also called “freak waves”, “monster waves”, “killer waves”, and “king waves”) much higher than the other waves in the sea state can occur. In the case of the Draupner wave, its 25 m (82 ft) height was 2.2 times the significant wave height. Such waves are distinct from tides, caused by the Moon and Sun's gravitational pull, tsunamis that are caused by underwater earthquakes or landslides, and waves generated by underwater explosions or the fall of meteorites—all having far longer wavelengths than wind waves.

Yet, the largest ever recorded wind waves are common — not rogue — waves in extreme sea states. For example: 29.1 m (95 ft) high waves have been recorded on the RRS Discovery in a sea with 18.5 m (61 ft) significant wave height, so the highest wave is only 1.6 times the significant wave height.[12] The biggest recorded by a buoy (as of 2011) was 32.3 m (106 ft) high during the 2007 typhoon Krosa near Taiwan.[13]

Ocean waves can be classified based on: the disturbing force(s) that create(s) them; the extent to which the disturbing force(s) continue(s) to influence them after formation; the extent to which the restoring force(s) weaken(s) (or flatten) them; and their wavelength or period. Seismic Sea waves have a period of ~20 minutes, and speeds of 760km/h (470mph). Wind waves (deep-water waves) have a period of about 20 seconds.

The speed of all ocean waves is controlled by gravity, wavelength, and water depth. Most characteristics of ocean waves depend on the relationship between their wavelength and water depth. Wavelength determines the size of the orbits of water molecules within a wave, but water depth determines the shape of the orbits. The paths of water molecules in a wind wave are circular only when the wave is traveling in deep water. A wave cannot “feel” the bottom when it moves through water deeper than half its wavelength because too little wave energy is contained in the small circles below that depth. Waves moving through water deeper than half their wavelength are known as deep-water waves. On the other hand, the orbits of water molecules in waves moving through shallow water are flattened by the proximity of the sea surface bottom. Waves in water shallower than 1/20 their original wavelength are known as shallow-water waves. Transitional waves travel through water deeper than 1/20 their original wavelength but shallower than half their original wavelength.

In general, the longer the wavelength, the faster the wave energy will move through the water. For deep-water waves, this relationship is represented with the following formula:

$$C = L/T$$

where C is speed (celerity), L is wavelength, and T is time, or period (in seconds).

The speed of a deep-water wave may also be approximated by:

$$C = \sqrt{gL/2\pi}$$

where g is the acceleration due to gravity, 9.8 meters (32.2 feet) per second squared. Because g and π (3.14) are constants, the equation can be reduced to:

$$C = 1.251\sqrt{L}$$

when C is measured in meters per second and L in meters. Note that in both instances that wave speed is proportional to wavelength.

The speed of shallow-water waves is described by a different equation that may be written as:

$$C = \sqrt{gd} = 3.1\sqrt{d}$$

where C is speed (in meters per second), g is the acceleration due to gravity, and d is the depth of the water (in meters). The period of a wave remains unchanged regardless of the depth of water through which it is moving. As deep-water waves enter the shallows and feel the bottom, however, their speed is reduced and their crests “bunch up,” so their wavelength shortens.

6.3 Wave shoaling and refraction

See also: wave shoaling and refraction

As waves travel from deep to shallow water, their shape alters (wave height increases, speed decreases, and length decreases as wave orbits become asymmetrical). This process is called shoaling.

Wave refraction is the process by which wave crests realign themselves as a result of decreasing water depths. Varying depths along a wave crest cause the crest to travel at different phase speeds, with those parts of the wave in deeper water moving faster than those in shallow water. This process continues until the crests become (nearly) parallel to the depth contours. Rays—lines normal to wave crests between which a fixed amount of energy flux is contained—converge on local shallows and shoals. Therefore, the wave energy between rays is concentrated as they converge, with a resulting increase in wave height.

Because these effects are related to a spatial variation in the phase speed, and because the phase speed also changes with the ambient current – due to the Doppler shift – the same effects of refraction and altering wave height also occur due to current variations. In the case of meeting an adverse current the wave *steepens*, i.e. its wave height increases while the wave length decreases, similar to the shoaling when the water depth decreases.[15]

6.4 Wave breaking

Big wave breaking

See also: surf wave, breaking wave and Iribarren number

Some waves undergo a phenomenon called "breaking". A breaking wave is one whose base can no longer support its top, causing it to collapse. A wave breaks when it runs into shallow water, or when two wave systems oppose and combine forces. When the slope, or steepness ratio, of a wave is too great, breaking is inevitable.

Individual waves in deep water break when the wave steepness—the ratio of the wave height H to the wavelength λ—exceeds about 0.07, so for $H > 0.07\ \lambda$. In shallow water, with the water depth small compared to the wavelength, the individual waves break when their wave height H is larger than 0.8 times the water depth h, that is $H > 0.8\ h$.[16] Waves can also break if the wind grows strong enough to blow the crest off the base of the wave.

Three main types of breaking waves are identified by surfers or surf lifesavers. Their varying characteristics make them more or less suitable for surfing, and present different dangers.

- **Spilling**, or **rolling**: these are the safest waves on which to surf. They can be found in most areas with relatively flat shorelines. They are the most common type of shorebreak
- **Plunging**, or **dumping**: these break suddenly and can "dump" swimmers—pushing them to the bottom with great force. These are the preferred waves for experienced surfers. Strong offshore winds and long wave periods can cause dumpers. They are often found where there is a sudden rise in the sea floor, such as a reef or sandbar.
- **Surging**: these may never actually break as they approach the water's edge, as the water below them is very deep. They tend to form on steep shorelines. These waves can knock swimmers over and drag them back into deeper water.

6.5 Science of waves

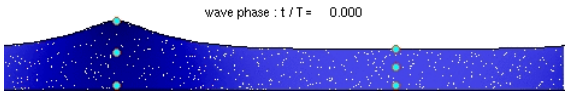

Stokes drift in shallow water waves (Animation)

Wind waves are mechanical waves that propagate along the interface between water and air; the restoring force is provided by gravity, and so they are often referred to as surface gravity waves. As the wind blows, pressure and friction forces perturb the equilibrium of the water surface. These forces transfer energy from the air to the water, forming waves. The initial formation of waves by the wind is described in the theory of Phillips from 1957, and the subsequent growth of the small waves has been modeled by Miles, also in 1957.[17][18]

See also: Airy wave theory

In the case of monochromatic linear plane waves in deep water, particles near the surface move in circular paths, making wind waves a combination of longitudinal (back and forth) and transverse (up and down) wave motions.

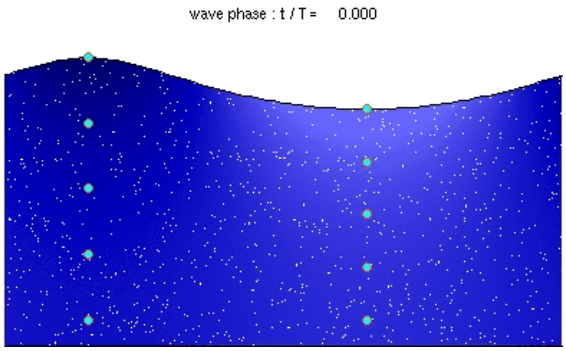

Stokes drift in a deeper water wave (Animation)

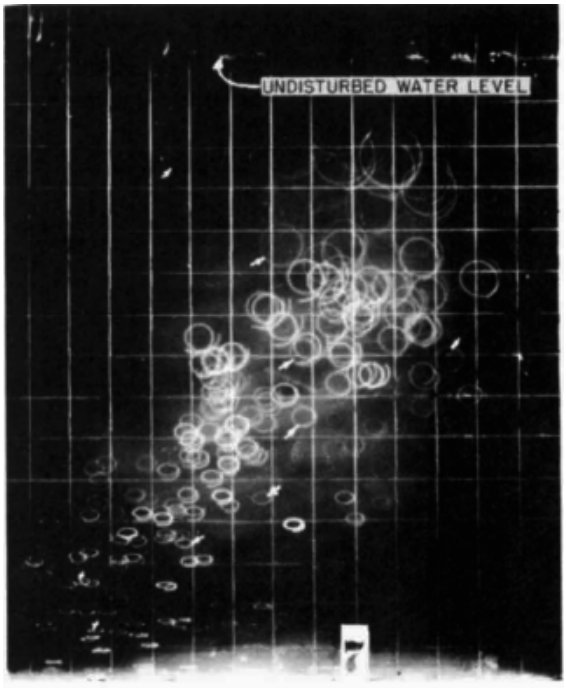

Photograph of the water particle orbits under a – progressive and periodic – surface gravity wave in a wave flume. The wave conditions are: mean water depth d = *2.50 ft (0.76 m), wave height* H = *0.339 ft (0.103 m), wavelength* λ = *6.42 ft (1.96 m), period* T = *1.12 s.*[19]

When waves propagate in shallow water, (where the depth is less than half the wavelength) the particle trajectories are compressed into ellipses.[20][21]

As the wave amplitude (height) increases, the particle paths no longer form closed orbits; rather, after the passage of each crest, particles are displaced slightly from their previous positions, a phenomenon known as Stokes drift.[22][23]

As the depth below the free surface increases, the radius of the circular motion decreases. At a depth equal to half the wavelength λ, the orbital movement has decayed to less than 5% of its value at the surface. The phase speed (also called the celerity) of a surface gravity wave is – for pure periodic wave motion of small-amplitude waves – well approximated by

$$c = \sqrt{\frac{g\lambda}{2\pi}\tanh\left(\frac{2\pi d}{\lambda}\right)}$$

where

c = phase speed;

λ = wavelength;

d = water depth;

g = acceleration due to gravity at the Earth's surface.

In deep water, where $d \geq \frac{1}{2}\lambda$, so $\frac{2\pi d}{\lambda} \geq \pi$ and the hyperbolic tangent approaches 1 , the speed c approximates

$$c_{\text{deep}} = \sqrt{\frac{g\lambda}{2\pi}}.$$

In SI units, with c_{deep} in m/s, $c_{\text{deep}} \approx 1.25\sqrt{\lambda}$, when λ is measured in metres. This expression tells us that waves of different wavelengths travel at different speeds. The fastest waves in a storm are the ones with the longest wavelength. As a result, after a storm, the first waves to arrive on the coast are the long-wavelength swells.

For intermediate and shallow water, the Boussinesq equations are applicable, combining frequency dispersion and nonlinear effects. And in very shallow water, the shallow water equations can be used.

If the wavelength is very long compared to the water depth, the phase speed (by taking the limit of c when the wavelength approaches infinity) can be approximated by

$$c_{\text{shallow}} = \lim_{\lambda\to\infty} c = \sqrt{gd}.$$

On the other hand, for very short wavelengths, surface tension plays an important role and the phase speed of these gravity-capillary waves can (in deep water) be approximated by

$$c_{\text{gravity-capillary}} = \sqrt{\frac{g\lambda}{2\pi} + \frac{2\pi S}{\rho\lambda}}$$

where

S = surface tension of the air-water interface;

ρ = density of the water.[24]

When several wave trains are present, as is always the case in nature, the waves form groups. In deep water the groups travel at a group velocity which is half of the phase

speed.[25] Following a single wave in a group one can see the wave appearing at the back of the group, growing and finally disappearing at the front of the group.

As the water depth d decreases towards the coast, this will have an effect: wave height changes due to wave shoaling and refraction. As the wave height increases, the wave may become unstable when the crest of the wave moves faster than the trough. This causes *surf*, a breaking of the waves.

The movement of wind waves can be captured by wave energy devices. The energy density (per unit area) of regular sinusoidal waves depends on the water density ρ , gravity acceleration g and the wave height H (which, for regular waves, is equal to twice the amplitude, a):

$$E = \frac{1}{8}\rho g H^2 = \frac{1}{2}\rho g a^2.$$

The velocity of propagation of this energy is the group velocity.

6.6 Wind wave models

Main article: Wind wave model

Surfers are very interested in the wave forecasts. There are many websites that provide predictions of the surf quality for the upcoming days and weeks. Wind wave models are driven by more general weather models that predict the winds and pressures over the oceans, seas and lakes.

Wind wave models are also an important part of examining the impact of shore protection and beach nourishment proposals. For many beach areas there is only patchy information about the wave climate, therefore estimating the effect of wind waves is important for managing littoral environments.

6.7 Seismic signals

Main article: microseism

Ocean water waves generate land seismic waves that propagate hundreds of kilometers into the land.[26] These seismic signals usually have the period of 6 ± 2 seconds. Such recordings were first reported and understood in about 1900.

There are two types of seismic "ocean waves". The primary waves are generated in shallow waters by direct water wave-land interaction and have the same period as the water waves (10 to 16 seconds). The more powerful secondary waves are generated by the superposition of ocean waves of equal period traveling in opposite directions, thus generating standing gravity waves – with an associated pressure oscillation at half the period, which is not diminishing with depth. The theory for microseism generation by standing waves was provided by Michael Longuet-Higgins in 1950, after in 1941 Pierre Bernard suggested this relation with standing waves on the basis of observations.[27][28]

6.8 Internal waves

Internal waves can form at the boundary between water layers of different densities. These sub-surface waves are called internal waves. As is the case with ocean waves at the air-ocean interface, internal waves possess troughs, crests, wavelength, and period. Internal waves move very slowly because the density difference between the joined media is very small. Internal waves occur in the ocean at the base of the pycnocline, especially at the bottom edge of a steep thermocline. The wave height of internal waves may be greater than 30 meters (100 feet), causing the pycnocline to undulate slowly through a considerable depth. Their wavelength often exceeds 0.8 kilometres (0.50 mi) and their periods are typically 5 to 8 minutes. Internal waves are generated by wind energy, tidal energy, and ocean currents. Surface manifestations of internal waves have been photographed from space.

Internal waves may mix nutrients into surface water and trigger plankton blooms. They can also affect submarines and oil platforms.

6.9 See also

6.10 Notes

[1] Tolman, H.L. (23 June 2010), "Practical wind wave modeling", in Mahmood, M.F., *CBMS Conference Proceedings on Water Waves: Theory and Experiment*, Howard University, US, 13–18 May 2008: World Scientific Publications, ISBN 978-981-4304-23-8

[2] Holthuijsen (2007), page 5.

[3] Lorenz, R. D. and A. G. Hayes, The Growth of Wind-Waves in Titan's Hydrocarbon Seas, Icarus, 219, 468–475, 2012

[4] Young, I. R. (1999). *Wind generated ocean waves*. Elsevier. ISBN 0-08-043317-0. p. 83.

[5] Weisse, Ralf; von Storch, Hans (2008). *Marine climate change: Ocean waves, storms and surges in the perspective of climate change*. Springer. p. 51. ISBN 978-3-540-25316-7.

[6] Phillips, O. M. (1957), "On the generation of waves by turbulent wind", Journal of Fluid Mechanics 2

(5): 417–445, Bibcode:1957JFM.....2..417P, doi:10.1017/S0022112057000233

[7] Miles, J. W. (1957), "On the generation of surface waves by shear flows", Journal of Fluid Mechanics 3 (2): 185–204, Bibcode:1957JFM.....3..185M, doi:10.1017/S0022112057000567

[8] Chapter 16 - Ocean Waves

[9] Hasselmann K., T.P. Barnett, E. Bouws, H. Carlson, D.E. Cartwright, K. Enke, J.A. Ewing, H. Gienapp, D.E. Hasselmann, P. Kruseman, A. Meerburg, P. Mller, D.J. Olbers, K. Richter, W. Sell, and H. Walden. Measurements of wind-wave growth and swell decay during the Joint North Sea Wave Project (JONSWAP)' Ergnzungsheft zur Deutschen Hydrographischen Zeitschrift Reihe, A(8) (Nr. 12), p.95, 1973.

[10] Pierson, Willard J., Jr. and Moskowitz, Lionel A. Proposed Spectral Form for Fully Developed Wind Seas Based on the Similarity Theory of S. A. Kitaigorodskii, Journal of Geophysical Research, Vol. 69, p.5181-5190, 1964.

[11] Munk, Walter H. (1950), "Origin and generation of waves", *Proceedings 1st International Conference on Coastal Engineering*, Long Beach, California: ASCE, pp. 1–4

[12] Holliday, Naomi P.; Yelland, Margaret J.; Pascal, Robin; Swail, Val R.; Taylor, Peter K.; Griffiths, Colin R.; Kent, Elizabeth (2006), *Were extreme waves in the Rockall Trough the largest ever recorded?*, *Geophysical Research Letters* **33** (L05613), Bibcode:2006GeoRL..3305613H, doi:10.1029/2005GL025238

[13] P. C. Liu; H. S. Chen; D.-J. Doong; C. C. Kao; Y.-J. G. Hsu (11 June 2008), *Monstrous ocean waves during typhoon Krosa*, *Annales Geophysicae* (European Geosciences Union) **26**: 1327–1329, Bibcode:2008AnGeo..26.1327L, doi:10.5194/angeo-26-1327-2008

[14] Tom Garrison (2009). *Oceanography: An Invitation to Marine Science (7th Edition)*. Yolanda Cossio. ISBN 978-0495391937.

[15] Longuet-Higgins, M.S.; Stewart, R.W. (1964), *Radiation stresses in water waves; a physical discussion, with applications*, *Deep Sea Research* **11** (4): 529–562, doi:10.1016/0011-7471(64)90001-4

[16] R.J. Dean and R.A. Dalrymple (2002). *Coastal processes with engineering applications*. Cambridge University Press. ISBN 0-521-60275-0. p. 96–97.

[17] Phillips, O. M. (1957), *On the generation of waves by turbulent wind*, *Journal of Fluid Mechanics* **2** (5): 417–445, Bibcode:1957JFM.....2..417P, doi:10.1017/S0022112057000233

[18] Miles, J. W. (1957), *On the generation of surface waves by shear flows*, *Journal of Fluid Mechanics* **3** (2): 185–204, Bibcode:1957JFM.....3..185M, doi:10.1017/S0022112057000567

[19] Figure 6 from: Wiegel, R.L.; Johnson, J.W. (1950), "Elements of wave theory", *Proceedings 1st International Conference on Coastal Engineering*, Long Beach, California: ASCE, pp. 5–21

[20] For the particle trajectories within the framework of linear wave theory, see for instance:
Phillips (1977), page 44.
Lamb, H. (1994). *Hydrodynamics* (6th edition ed.). Cambridge University Press. ISBN 978-0-521-45868-9. Originally published in 1879, the 6th extended edition appeared first in 1932. See §229, page 367.
L. D. Landau and E. M. Lifshitz (1986). *Fluid mechanics*. Course of Theoretical Physics **6** (Second revised edition ed.). Pergamon Press. ISBN 0-08-033932-8. See page 33.

[21] A good illustration of the wave motion according to linear theory is given by Prof. Robert Dalrymple's Java applet.

[22] For nonlinear waves, the particle paths are not closed, as found by George Gabriel Stokes in 1847, see the original paper by Stokes. Or in Phillips (1977), page 44: *"To this order, it is evident that the particle paths are not exactly closed … pointed out by Stokes (1847) in his classical investigation"*.

[23] Solutions of the particle trajectories in fully nonlinear periodic waves and the Lagrangian wave period they experience can for instance be found in:
J.M. Williams (1981). "Limiting gravity waves in water of finite depth". *Philosophical Transactions of the Royal Society A* **302** (1466): 139–188. Bibcode:1981RSPTA.302..139W. doi:10.1098/rsta.1981.0159.
J.M. Williams (1985). *Tables of progressive gravity waves*. Pitman. ISBN 978-0-273-08733-5.

[24] Carl Nordling, Jonny Östermalm (2006). *Physics Handbook for Science and Engineering* (Eight edition ed.). Studentliteratur. p. 263. ISBN 978-91-44-04453-8.

[25] In deep water, the group velocity is half the phase velocity, as is shown here. Another reference is .

[26] Peter Bormann. Seismic Signals and Noise

[27] Bernard, P. (1941), *Sur certaines proprietes de la boule etudiees a l'aide des enregistrements seismographiques*, *Bull. Inst. Oceanogr. Monaco* **800**: 1–19

[28] Longuet-Higgins, M.S. (1950), *A theory of the origin of microseisms*, *Philosophical Transactions of the Royal Society A* **243** (857): 1–35, Bibcode:1950RSPTA.243....1L, doi:10.1098/rsta.1950.0012

6.11 References

6.11.1 Scientific

- Stokes, G.G. (1847). "On the theory of oscillatory waves". *Transactions of the Cambridge Philosophical Society* **8**: 441–455.
Reprinted in: G.G. Stokes (1880). *Mathematical*

and Physical Papers, Volume I. Cambridge University Press. pp. 197–229.

- Phillips, O.M. (1977). *The dynamics of the upper ocean* (2nd ed.). Cambridge University Press. ISBN 0-521-29801-6.
- Holthuijsen, Leo H. (2007). *Waves in oceanic and coastal waters*. Cambridge University Press. ISBN 0-521-86028-8.
- Janssen, Peter (2004). *The interaction of ocean waves and wind*. Cambridge University Press. ISBN 978-0-521-46540-3.

6.11.2 Other

- Rousmaniere, John (1989). *The Annapolis Book of Seamanship* (2nd revised ed.). Simon & Schuster. ISBN 0-671-67447-1.
- Carr, Michael (Oct 1998). "Understanding Waves". *Sail*: 38–45.

6.12 External links

- "Anatomy of a Wave" Holben, Jay boatsafe.com captured 5/23/06
- NOAA National Weather Service
- ESA press release on swell tracking with ASAR onboard ENVISAT
- Introductory oceanography chapter 10 – Ocean Waves
- HyperPhysics – Ocean Waves

Chapter 7

Mixing (process engineering)

In industrial process engineering, **mixing** is a unit operation that involves manipulation of a heterogeneous physical system with the intent to make it more homogeneous. Familiar examples include pumping of the water in a swimming pool to homogenize the water temperature, and the stirring of pancake batter to eliminate lumps (deagglomeration). Mixing is performed to allow heat and/or mass transfer to occur between one or more steams, components or phases. Modern industrial processing almost always involves some form of mixing.[1] Some classes of chemical reactors are also mixers. With the right equipment, it is possible to mix a solid, liquid or gas into another solid, liquid or gas. A biofuel fermenter may require the mixing of microbes, gases and liquid medium for optimal yield; organic nitration requires concentrated (liquid) nitric and sulfuric acids to be mixed with a hydrophobic organic phase; production of pharmaceutical tablets requires blending of solid powders. The opposite of mixing is segregation. A classical example of segregation is the brazil nut effect.

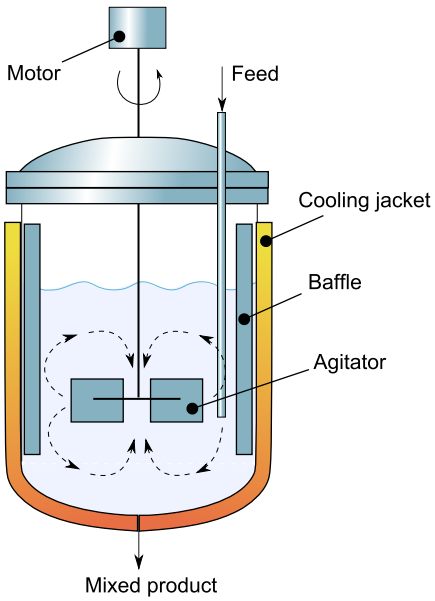

Schematics of an agitated vessel with a Rushton turbine and baffles

7.1 Mixing classification

The type of operation and equipment used during mixing depends on the state of materials being mixed (liquid, semi-solid, or solid) and the miscibility of the materials being processed. In this context, the act of mixing may be synonymous with stirring-, or kneading-processes.[1]

7.2 Liquid–liquid mixing

Mixing of liquids is an operation which occurs frequently in process engineering. The nature of the liquid(s) to be blended determines the equipment used for mixing; single-phase blending tends to involve low-shear, high-flow mixers to cause liquid engulfment, while multi-phase mixing generally requires the use of high-shear, low-flow mixers to create droplets of one liquid in another. Liquid–liquid mixers operate in laminar, turbulent or transitional flow regimes, depending on the Reynolds number of the flow. Turbulent or transitional mixing is frequently conducted with turbines or impellers; laminar mixing is conducted with helical ribbon or anchor mixers.[2]

7.2.1 Single-phase blending

Mixing of liquids that are miscible or at least soluble in each other occurs frequently in process engineering (and in everyday life). An everyday example would be the addition of milk or cream to tea or coffee. Since both liquids are water-based, they dissolve easily in one another. The momentum of the liquid being added is sometimes enough to cause enough turbulence to mix the two, since the viscosity of both liquids is relatively low. If necessary, a spoon or paddle could be used to complete the mixing process. Blending in a more viscous liquid, such as honey, requires more mixing power per unit volume to achieve the same homogeneity in the same amount of time.

7.2.2 Multi-phase mixing

Mixing of liquids that are not miscible or soluble in each other often necessitates different equipment than is used for single-phase blending. An everyday example would be the mixing of oil into water (or vinegar), which necessitates the use of a whisk or fork rather than a spoon or paddle mixer. Specialized mixers for this purpose, called high shear devices, or **HSD**s, rotate at high speeds and generate intense shear which breaks up liquid into droplets.

7.3 Gas–gas mixing

Main article: Gas blending

7.4 Solid–solid mixing

Blending powders is one of the oldest unit-operations in the solids handling industries. For many decades powder blending has been used just to homogenize bulk materials. Many different machines have been designed to handle materials with various bulk solids properties. On the basis of the practical experience gained with these different machines, engineering knowledge has been developed to construct reliable equipment and to predict scale-up and mixing behavior. Nowadays the same mixing technologies are used for many more applications: to improve product quality, to coat particles, to fuse materials, to wet, to disperse in liquid, to agglomerate, to alter functional material properties, etc. This wide range of applications of mixing equipment requires a high level of knowledge, long time experience and extended test facilities to come to the optimal selection of equipment and processes.

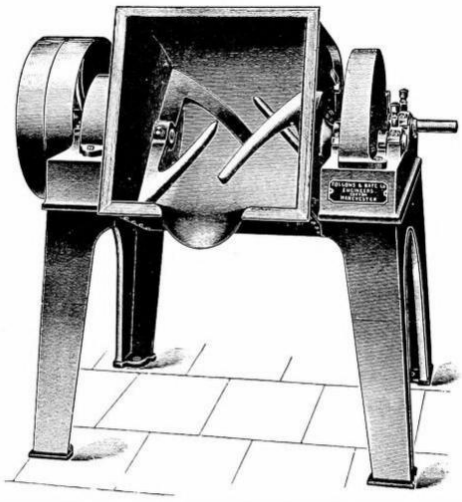

Fig. 43.—Machine for incorporating Liquids and finely-ground Solids.

Machine for incorporating liquids and finely ground solids

One example of a solid–solid mixing process is mulling foundry molding sand, where sand, bentonite clay, fine coal dust and water are mixed to a plastic, moldable and reusable mass, applied for molding and pouring molten metal to obtain sand castings that are metallic parts for automobile, machine building, construction or other industries.

7.4.1 Mixing mechanisms

In powder two different dimensions in the mixing process can be determined: convective mixing and intensive mixing. In the case of convective mixing material in the mixer is transported from one location to another. This type of mixing process will lead to a less ordered state inside the mixer, the components which have to be mixed will be distributed over the other components. With progressing time the mixture will become more and more randomly ordered. After a certain mixing time the ultimate random state is reached. Usually this type of mixing is applied for free-flowing and coarse materials. Possible threat during macro mixing is the de-mixing of the components, since differences in size, shape or density of the different particles can lead to segregation. In the convective mixing range, Hosokawa has several processes available from silo mixers to horizontal mixers and conical mixers. When materials are cohesive, which is the case with e.g. fine particles and also with wet material, convective mixing is no longer sufficient to obtain a randomly ordered mixture. The relative strong inter-particle forces will form lumps, which are not broken up by the mild transportation forces in the convective mixer. To decrease the lump size additional forces are necessary; i.e. more energy intensive mixing is required. These additional forces can either be impact forces or shear forces.

7.5 Liquid–solid mixing

Liquid–solid mixing is typically done to suspend coarse free-flowing solids, or to break up lumps of fine agglomerated solids. An example of the former is the mixing granulated sugar into water; an example of the latter is the mixing of flour or powdered milk into water. In the first case, the particles can be lifted into suspension (and separated from one another) by bulk motion of the fluid; in the second, the mixer itself (or the high shear field near it) must destabilize the lumps and cause them to disintegrate.

One example of a solid–liquid mixing process in industry is concrete mixing, where cement, sand, small stones or gravel and water are commingled to a homogeneous self-hardening mass, used in the construction industry.

7.5.1 Solid suspension

Suspension of solids into a liquid is done to improve the rate of mass transfer between the solid and the liquid. Examples include dissolving a solid reactant into a solvent, or suspending catalyst particles in liquid to improve the flow of reactants and products to and from the particles. The associated eddy diffusion increases the rate of mass transfer within the bulk of the fluid, and the convection of material away from the particles decreases the size of the boundary layer, where most of the resistance to mass transfer occurs. Axial-flow impellers are preferred for solid suspension, although radial-flow impellers can be used in a tank with baffles, which converts some of the rotational motion into vertical motion. When the solid is denser than the liquid (and therefore collects at the bottom of the tank), the impeller is rotated so that the fluid is pushed downwards; when the solid is less dense than the liquid (and therefore floats on top), the impeller is rotated so that the fluid is pushed upwards (though this is relatively rare). The equipment preferred for solid suspension produces large volumetric flows but not necessarily high shear; high flow-number turbine impellers, such as hydrofoils, are typically used. Multiple turbines mounted on the same shaft can reduce power draw.[3]

7.5.2 Solid deagglomeration

Very fine powders, such as titanium dioxide pigments, and materials that have been spray dried may agglomerate or form lumps during transportation and storage. Starchy materials or those which form gels when exposed to solvent may form lumps which are wetted on the outside but are dry on the inside. These types of materials are not easily mixed into liquid with the types of mixers preferred for solid suspension because the agglomerate particles must be subjected to intense shear to be broken up. In some ways, deagglomeration of solids is similar to the blending of immiscible liquids, except for the fact that coalescence is usually not a problem. An everyday example of this type of mixing is the production of milkshakes from liquid milk and solid ice cream. The type of mixer preferred for solid deagglomeration is a high-shear disperser or a low-power number turbine that can be spun at high speed to produce intense shear fields which rip agglomerates into particles.

7.6 Liquid–gas mixing

Liquids and gases are typically mixed to allow mass transfer to occur. For instance, in the case of air stripping, gas is used to remove volatiles from a liquid. Typically, a packed column is used for this purpose, with the packing acting as a motionless mixer and the air pump providing the driving force. When a tank and impeller are used, the objective is typically to ensure that the gas bubbles remain in contact with the liquid for as long as possible. This is especially important if the gas is expensive, such as pure oxygen, or diffuses slowly into the liquid. Mixing in a tank is also useful when a (relatively) slow chemical reaction is occurring in the liquid phase, and so the concentration difference in the thin layer near the bubble is close to that of the bulk. This reduces the driving force for mass transfer. If there is a (relatively) fast chemical reaction in the liquid phase, it is sometimes advantageous to disperse but not recirculate the gas bubbles, ensuring that they are in plug flow and can transfer mass more efficiently.

Rushton turbines have been traditionally used do disperse gases into liquids, but newer options, such as the Smith turbine and Bakker turbine are becoming more prevalent.[4] One of the issues is that as the gas flow increases, more and more of the gas accumulates in the low pressure zones behind the impeller blades, which reduces the power drawn by the mixer (and therefore its effectiveness). Newer designs, such as the GDX impeller, have nearly eliminated this problem.

7.7 Gas–solid mixing

Main article: Fluidization

Gas–solid mixing may be conducted to transport powders or small particulate solids from one place to another, or to mix gaseous reactants with solid catalyst particles. In either case, the turbulent eddies of the gas must provide enough force to suspend the solid particles, which will otherwise sink under the force of gravity. The size and shape of the particles is an important consideration, since different particles will have different drag coefficients, and particles made of different materials will have different densities. A common unit operation the process industry to separate gases and solids is the cyclone which slows the gas and causes the particles to settle out.

7.8 Multiphase mixing

Multiphase mixing occurs when solids, liquids and gases are combined in one step. This may occur as part of a catalytic chemical process, in which liquid and gaseous reagents must be combined with a solid catalyst (such as hydrogenation); or in fermentation, where solid microbes and the gases they require must be well-distributed in a liquid medium. The type of mixer used depends upon the properties of the phases. In some cases, the mixing power is provided by the gas itself as it moves up through the liquid, entraining liquid with the bubble plume. This draws liquid upwards inside the plume, and causes liquid to fall outside the plume. If the viscosity of the liquid is too high to allow for this (or if the solid particles are

too heavy), an impeller may be needed to keep the solid particles suspended.

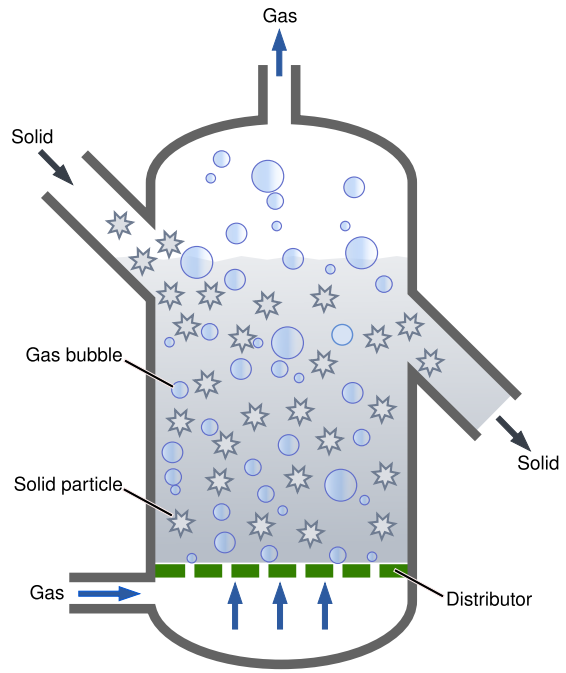

Schematic drawing of a fluidized bed reactor

7.9 Constitutive equations

Many of the equations used for determining the output of mixers are empirically derived, or contain empirically-derived constants. Since mixers operate in the turbulent regime, many of the equations are approximations that are considered acceptable for most engineering purposes.

When a mixing impeller rotates in the fluid, it generates a combination of flow and shear. The impeller generated flow can be calculated with the following equation:

$Q = Fl * N * D^3$

Flow numbers for impellers have been published in the North American Mixing Forum sponsored Handbook of Industrial Mixing.[5]

The power required to rotate an impeller can be calculated using the following equations:

$P = Po\rho N^3 D^5$ (Turbulent regime)[6]

$P = K_p \mu N^2 D^3$ (Laminar regime)

Po is the (dimensionless) power number, which is a function of impeller geometry; ρ is the density of the fluid; N is the rotational speed, typically rotations per second; D is the diameter of the impeller; K_p is the laminar power constant; and μ is the viscosity of the fluid. Note that the mixer power is strongly dependent upon the rotational speed and impeller diameter, and linearly dependent upon either the density or viscosity of the fluid, depending on which flow regime is present. In the transitional regime, flow near the impeller is turbulent and so the turbulent power equation is used.

The time required to blend a fluid to within 5% of the final concentration, θ_{95} , can be calculated with the following correlations:

$\theta_{95} = \frac{5.40}{Po^{\frac{1}{3}} N}(\frac{T}{D})^2$ (Turbulent regime)

$\theta_{95} = \frac{34596}{Po^{\frac{1}{3}} N^2 D^2}(\frac{\mu}{\rho})(\frac{T}{D})^2$ (Transitional region)

$\theta_{95} = \frac{896 * 10^3 K_p^{-1.69}}{N}$ (Laminar regime)

The Transitional/Turbulent boundary occurs at $Po^{\frac{1}{3}} Re = 6404$

The Laminar/Transitional boundary occurs at $Po^{\frac{1}{3}} Re = 186$

7.10 Laboratory mixing

A magnetic stirrer

At a laboratory scale, mixing is achieved by magnetic stirrers or by simple hand-shaking. Sometimes mixing in laboratory vessels is more thorough and occurs faster than is possible industrially. Magnetic stir bars are radial-flow mixers that induce solid body rotation in the fluid being mixed. This is acceptable on a small scale, since the vessels are small and mixing therefore occurs rapidly (short blend time). A variety of stir bar configurations exist, but because of the small size and (typically) low viscosity of the fluid, it is possible to use one configuration

for nearly all mixing tasks. The cylindrical stir bar can be used for suspension of solids, as seen in iodometry, deagglomeration (useful for preparation of microbiology growth medium from powders), and liquid–liquid blending. Another peculiarity of laboratory mixing is that the mixer rests on the bottom of the vessel instead of being suspended near the center. Furthermore, the vessels used for laboratory mixing are typically more widely varied than those used for industrial mixing; for instance, Erlenmeyer flasks, or Florence flasks may be used in addition to the more cylindrical beaker.

7.11 Mixing in microfluidics

When scaled down to the microscale, fluid mixing behaves radically different.[7] This is typically at sizes from a couple (2 or 3) millimeters down to the nanometer range. At this size range normal convection does not happen unless you force it. Diffusion is the dominate mechainism whereby two different fluids come together. Diffusion is a relatively slow process. Hence a number of researchers had to devise ways to get the two fluids to mix. This involved Y junctions, T junctions, three-way intersections and designs where the interfacial area between the two fluids is maximized. Beyond just interfacing the two liquids people also made twisting channels to force the two fluids to mix. These included multilayered devices where the fluids would corkscrew, looped devices where the fluids would flow around obstructions and wavy devices where the channel would constrict and flare out. Additionally channels with features on the walls like notches or groves were tried.

One way to tell if mixing is happening due to convection or diffusion is by finding the Peclet number. It is the ratio of convection to diffusion. At high Peclet numbers, convection dominates. At low Peclet numbers, diffusion dominates.

Peclet = flow velocity * mixing path / diffusion coefficient

7.12 Industrial mixing equipment

At an industrial scale, efficient mixing can be difficult to achieve. A great deal of engineering effort goes into designing and improving mixing processes. Mixing at industrial scale is done in batches (dynamic mixing) or with help of static mixers. Moving mixers are powered with electric motors which operate at standard speeds of 1800 or 1500 RPM, which is typically much faster than necessary. Gearboxes are used to reduce speed and increase torque. Some applications require the use of multi-shaft mixers, in which a combination of mixer types are used to completely blend the product.[8]

7.12.1 Turbines

A selection of turbine geometries and power numbers are shown below.

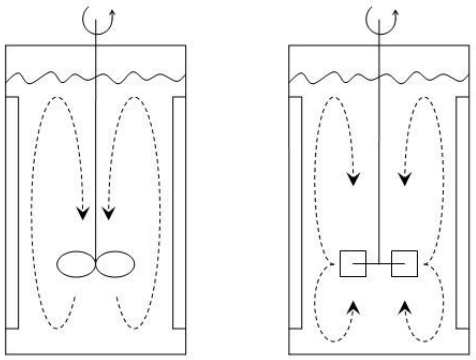

Axial flow impeller (left) and radial flow impeller (right).

Different types of impellers are used for different tasks; for instance, Rushton turbines are useful for dispersing gases into liquids, but are not very helpful for dispersing settled solids into liquid. Newer turbines have largely supplanted the Rushton turbine for gas–liquid mixing, such as the Smith turbine and Bakker turbine.[9] The power number is an empirical measure of the amount of torque needed to drive different impellers in the same fluid at constant power per unit volume; impellers with higher power numbers will require more torque but operate at lower speed than impellers with lower power numbers, which will operate at lower torque but higher speeds.

7.12.2 Close-clearance mixers

There are two main types of close-clearance mixers: anchors and helical ribbons. Anchor mixers induce solid-body rotation and do not promote vertical mixing, but helical ribbons do. Close clearance mixers are used in the laminar regime, because the viscosity of the fluid overwhelms the inertial forces of the flow and prevents the fluid leaving the impeller from entraining the fluid next to it. Helical ribbon mixers are typically rotated to push material at the wall downwards, which helps circulate the fluid and refresh the surface at the wall.[10]

7.12.3 High shear dispersers

Main article: high-shear mixer

High shear dispersers create intense shear near the impeller but relatively little flow in the bulk of the vessel. Such devices typically resemble circular saw blades and are rotated at high speed. Because of their shape,

they have a relatively low drag coefficient and therefore require comparatively little torque to spin at high speed. High shear dispersers are used for forming emulsions (or suspensions) of immiscible liquids and solid deagglomeration.[11]

7.12.4 Static mixers

Main article: static mixer

Static mixers are used when a mixing tank would be too large, too slow, or too expensive to use in a given process.

7.13 See also

- Banbury mixer
- Industrial mixer

7.14 References

For an in-depth resource covering mixing theory, technology, and a very broad range of applications please refer to the **Handbook of Industrial Mixing: Science and Practice**.[5]

[1] Ullmann, Fritz (2005). Ullmann's Chemical Engineering and Plant Design, Volumes 1–2. John Wiley & Sons. http://app.knovel.com/hotlink/toc/id:kpUCEPDV02/ullmanns-chemical-engineering

[2] http://www.bakker.org/cfm/webdoc13.htm

[3] http://www.bakker.org/cfm/webdoc4.htm

[4] http://cercell.com/support/bactovessel-details/turbine-principles/

[5] Edward L. Paul, Victor Atiemo-Obeng, and Suzanne M. Kresta, ed. (2003). *Handbook of Industrial Mixing: Science and Practice*. Wiley. ISBN 978-0-471-26919-9.

[6] http://cercell.com/support/bactovessel-details/turbine-power/

[7] Nguyen, Nam-Trung; Wu, Zhigang (1 February 2005). "Micromixers—a review". *Journal of Micromechanics and Microengineering* **15** (2): R1–R16. Bibcode:2005JMiMi..15R...1N. doi:10.1088/0960-1317/15/2/R01.

[8] http://www.hockmeyer.com/products/high-viscosity-mixers/dual-triple-shaft-mixer-detail.html

[9] http://www.bakker.org/cfm/bt6.htm

[10] http://www.bakker.org/cfm/webdoc10.htm

[11] http://www.hockmeyer.com/technical/publications/73-dispersion-tips-help.html

7.15 External links

- Wiki on equipment for mixing bulk solids and powders
- Visualizations of fluid dynamics in mixing processes
- A textbook chapter on mixing in the food industry

Chapter 8

Liquid bubble

For specific types of bubbles, and metaphors of the word "bubble", see Bubble (disambiguation).

A **bubble** is a globule of one substance in another, usually gas in a liquid. Due to the Marangoni effect, bubbles may remain intact when they reach the surface of the immersive substance.

Air bubbles as a man surfaces in a pool.

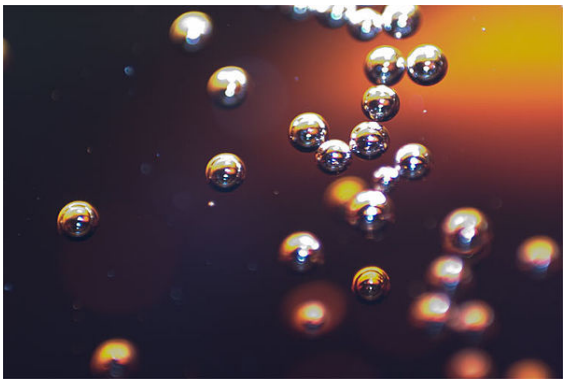

Bubbles of gas in a soft drink

8.1 Common examples

Bubbles are seen in many places in everyday life, for example:

- As spontaneous nucleation of supersaturated carbon dioxide in soft drinks
- As water vapor in boiling water
- As air mixed into agitated water, such as below a waterfall
- As sea foam
- As given off in chemical reactions, e.g. baking soda + vinegar
- As a gas trapped in glass during its manufacture
- An air bubble in a solution of fluorescein and water (or alcohol) is the essential part of a spirit level

Bubble of gas in a mudpot

A bubble of gas in a tar pit

8.2 Physics and chemistry

Bubbles form, and coalesce, into globular shapes, because those shapes are at a lower energy state. For the physics and chemistry behind it, see nucleation.

8.2.1 Appearance

Humans can see bubbles because they have a different refractive index (IR) than the surrounding substance. For example, the IR of air is approximately 1.0003 and the IR of water is approximately 1.333. Snell's Law describes how electromagnetic waves change direction at the interface between two mediums with different IR; thus bubbles can be identified from the accompanying refraction and internal reflection even though both the immersed and immersing mediums are transparent.

The above explanation only holds for bubbles of one medium submerged in another medium (e.g. bubbles of air in a soft drink); the volume of a membrane bubble (e.g. soap bubble) will not distort light very much, and one can only see a membrane bubble due to thin-film diffraction and reflection.

8.2.2 Applications

Nucleation can be intentionally induced, for example to create bubblegram.

In medical ultrasound imaging, small encapsulated bubbles called contrast agent are used to enhance the contrast.

In thermal inkjet printing, vapor bubbles are used as actuators. They are occasionally used in other microfluidics applications as actuators.[1]

The violent collapse of bubbles (Cavitation) near solid surfaces and the resulting impinging jet constitute the mechanism used in ultrasonic cleaning. The same effect, but on a larger scale, is used in focused energy weapons such as the bazooka and the torpedo. Pistol shrimp also use a collapsing cavitation bubble as a weapon. The same effect is used to treat kidney stones in a lithotripter. Marine mammals such as dolphins and whales use bubbles for entertainment or as hunting tools. Aerators cause dissolution of gas in the liquid by injecting bubbles.

Chemical and metallurgic engineers rely on bubbles for operations such as distillation, absorption, flotation and spray drying. The complex processes involved often require consideration for mass and heat transfer, and are modelled using fluid dynamics.[2]

The star-nosed mole and the water shrew can smell underwater by rapidly breathing through their nostrils and creating a bubble. [3]

8.2.3 Pulsation

When bubbles are disturbed, they pulsate (that is, they oscillate in size) at their natural frequency. Large bubbles (negligible surface tension and thermal conductivity) undergo adiabatic pulsations, which means that no heat is transferred either from the liquid to the gas or vice versa. The natural frequency of such bubbles is determined by the equation:[4][5]

$$f_0 = \frac{1}{2\pi R_0}\sqrt{\frac{3\gamma p_0}{\rho}}$$

where:

- γ is the specific heat ratio of the gas
- R_0 is the steady state radius
- p_0 is the steady state pressure
- ρ is the mass density of the surrounding liquid

Smaller bubbles undergo isothermal pulsations. The corresponding equation for small bubbles of surface tension σ (and negligible liquid viscosity) is[5]

$$f_0 = \frac{1}{2\pi R_0}\sqrt{\frac{3p_0}{\rho} + \frac{4\sigma}{\rho R_0}}$$

Excited bubbles trapped underwater are the major source of liquid sounds, such as when a rain droplet impacts a surface of water.[6][7]

8.3 Physiology and medicine

Injury by bubble formation and growth in body tissues is the mechanism of decompression sickness, which occurs when supersaturated dissolved inert gases leave solution as bubbles during decompression. The damage can be due to mechanical deformation of tissues due to bubble growth in situ, or by blocking blood vessels where the bubble has lodged.

Arterial gas embolism can occur when a gas bubble is introduced to the circulatory system and it lodges in a blood vessel which is too small for it to pass through under the available pressure difference. This can occur as a result of decompression after hyperbaric exposure, a lung overexpansion injury, during intravenous fluid administration, or during surgery.

8.4 See also

- Sonoluminescence
- Bubble fusion
- Underwater acoustics
- Minnaert resonance

8.5 References

[1] R. J. Dijkink, J. P. van der Dennen, C. D. Ohl, A. Prosperetti,*The 'acoustic scallop': a bubble-powered actuator*, J. Micromech. Microeng. **16** 1653 (2006)

[2] Weber et al. (1978). *Bubbles, Drops and Particles*. New York: Dover Publications. ISBN 0-486-44580-1.

[3] Roxanne Khamsi. "Star-nosed mole can sniff underwater, videos reveal".

[4] Minnaert, Marcel, On musical air-bubbles and the sounds of running water, Phil. Mag. 16, 235-248 (1933).

[5] Leighton, Timothy G., The Acoustic Bubble (Academic, London, 1994).

[6] Prosperetti, Andrea; Oguz, Hasan N. (1993). "The impact of drops on liquid surfaces and the underwater noise of rain" (PDF). *Annual Review of Fluid Mechanics* **25**: 577–602. Bibcode:1993AnRFM..25..577P. doi:10.1146/annurev.fl.25.010193.003045. Retrieved 2006-12-09.

[7] Rankin, Ryan C. (June 2005). "Bubble Resonance". *The Physics of Bubbles, Antibubbles, and all That*. Retrieved 2006-12-09.

8.6 External links

- Bubble physics – touches on vapor pressure, bubble formation, bubble dynamics, cavitation, acoustic oscillations, sound of raindrops underwater, Rayleigh-Plesset equation, snapping shrimp, lithotripsy, ultrasonic cleaning, sonochemistry, sonoluminescence, medical reperfusion imaging, and microbubble therapy

Chapter 9

Synthetic aperture radar

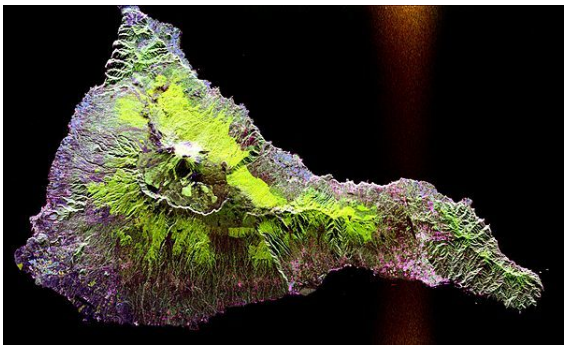

This radar image acquired by the SIR-C/X-SAR radar onboard the Space Shuttle Endeavour shows the Teide volcano. The city of Santa Cruz de Tenerife is visible as the purple and white area on the lower right edge of the island. Lava flows at the summit crater appear in shades of green and brown, while vegetation zones appear as areas of purple, green and yellow on the volcano's flanks.

Synthetic-aperture radar (SAR) is a form of radar which is used to create images of an object, such as a landscape – these images can be 2D or 3D representations of the object. SAR uses the motion of the SAR antenna over a target region to provide finer spatial resolution than is possible with conventional beam-scanning radars. SAR is typically mounted on a moving platform such as an aircraft or spacecraft, and it originated as an advanced form of side-looking airborne radar (SLAR). The distance the SAR device travels over a target creates a large "synthetic" antenna aperture (the "size" of the antenna). As a rule of thumb one can assume that the larger the aperture is, the higher the image resolution becomes, regardless whether physical aperture or synthetic aperture – this allows SAR to create high resolution images with comparatively small physical antennas.

To create a SAR image, successive pulses of radio waves are transmitted to "illuminate" a target scene, and the echo of each pulse is received and recorded. The pulses are transmitted and the echoes received using a single beam-forming antenna, with wavelengths used anywhere from a meter down to millimeters. As the SAR device onboard the aircraft or spacecraft moves, the antenna location relative to the target changes over time. Signal processing of the recorded radar echoes allows it then to combine the recordings from the multiple antenna locations – this forms the synthetic antenna aperture, and allows it to create finer resolution image than what would be possible with the given physical antenna aperture.[1]

Current (2010) airborne systems provide resolutions to about 10 cm, ultra-wideband systems provide resolutions of a few millimeters, and experimental terahertz SAR has provided sub-millimeter resolution in the laboratory.

SAR images have wide applications in remote sensing and mapping of the surfaces of both the Earth and other planets. SAR can also be implemented as inverse SAR by observing a moving target over a substantial time with a stationary antenna.

9.1 Functional principle

The surface of Venus, as imaged by the Magellan probe using SAR

9.1.1 Algorithm

The SAR algorithm, as given here, applies to phased arrays generally.

A three-dimensional array (a volume) of scene elements is defined which will represent the volume of space within which targets exist. Each element of the array is a cubical voxel representing the probability (a "density") of a reflective surface being at that location in space. (Note that two-dimensional SARs are also possible—showing only a top-down view of the target area).

Initially, the SAR algorithm gives each voxel a density of zero.

Then, for each captured waveform, the entire volume is iterated. For a given waveform and voxel, the distance from the position represented by that voxel to the antenna(e) used to capture that waveform is calculated. That distance represents a time delay into the waveform. The sample value at that position in the waveform is then added to the voxel's density value. This represents a possible echo from a target at that position. Note that there are several optional approaches here, depending on the precision of the waveform timing, among other things. For example, if phase cannot be accurately known, then only the envelope magnitude (with the help of a Hilbert transform) of the waveform sample might be added to the voxel. If polarization and phase are known in the waveform, and are accurate enough, then these values might be added to a more complex voxel that holds such measurements separately.

After all waveforms have been iterated over all voxels, the basic SAR processing is complete.

What remains, in the simplest approach, is to decide what voxel density value represents a solid object. Voxels whose density is below that threshold are ignored. Note that the threshold level chosen must at least be higher than the peak energy of any single wave—otherwise that wave peak would appear as a sphere (or ellipse, in the case of multistatic operation) of false "density" across the entire volume. Thus to detect a point on a target, there must be at least two different antenna echoes from that point. Consequently, there is a need for large numbers of antenna positions to properly characterize a target.

The voxels that passed the threshold criteria are visualized in 2D or 3D. Optionally, added visual quality can sometimes be had by use of a surface detection algorithm like marching cubes.

9.1.2 More complex operation

The basic design of a synthetic-aperture radar system can be enhanced to collect more information. Most of these methods use the same basic principle of combining many pulses to form a synthetic aperture, but may involve additional antennas or significant additional processing.

Multistatic operation

SAR requires that echo captures be taken at multiple antenna positions. The more captures taken (at different antenna locations) the more reliable the target characterization.

Multiple captures can be obtained by moving a single antenna to different locations, by placing multiple stationary antennas at different locations, or combinations thereof.

The advantage of a single moving antenna is that it can be easily placed in any number of positions to provide any number of monostatic waveforms. For example, an antenna mounted on an airplane takes many captures per second as the plane travels.

The principal advantages of multiple static antennas are that a moving target can be characterized (assuming the capture electronics are fast enough), that no vehicle or motion machinery is necessary, and that antenna positions need not be derived from other, sometimes unreliable, information. (One problem with SAR aboard an airplane is knowing precise antenna positions as the plane travels).

For multiple static antennas, all combinations of monostatic and multistatic radar waveform captures are possible. Note, however, that it is not advantageous to capture a waveform for each of both transmission directions for a given pair of antennas, because those waveforms will be identical. When multiple static antennas are used, the total number of unique echo waveforms that can be captured is

$$\frac{N^2 + N}{2}$$

where N is the number of unique antenna positions.

9.1.3 Polarimetry

Radar waves have a polarization. Different materials reflect radar waves with different intensities, but anisotropic materials such as grass often reflect different polarizations with different intensities. Some materials will also convert one polarization into another. By emitting a mixture of polarizations and using receiving antennas with a specific polarization, several images can be collected from the same series of pulses. Frequently three such RX-TX polarizations (HH-pol, VV-pol, VH-pol) are used as the three color channels in a synthesized image. This is what has been done in the picture at left. Interpretation of the resulting colors requires significant testing of known materials.

New developments in polarimetry include using the changes in the random polarization returns of some surfaces (such as grass or sand) and between two images of the same location at different times to determine where

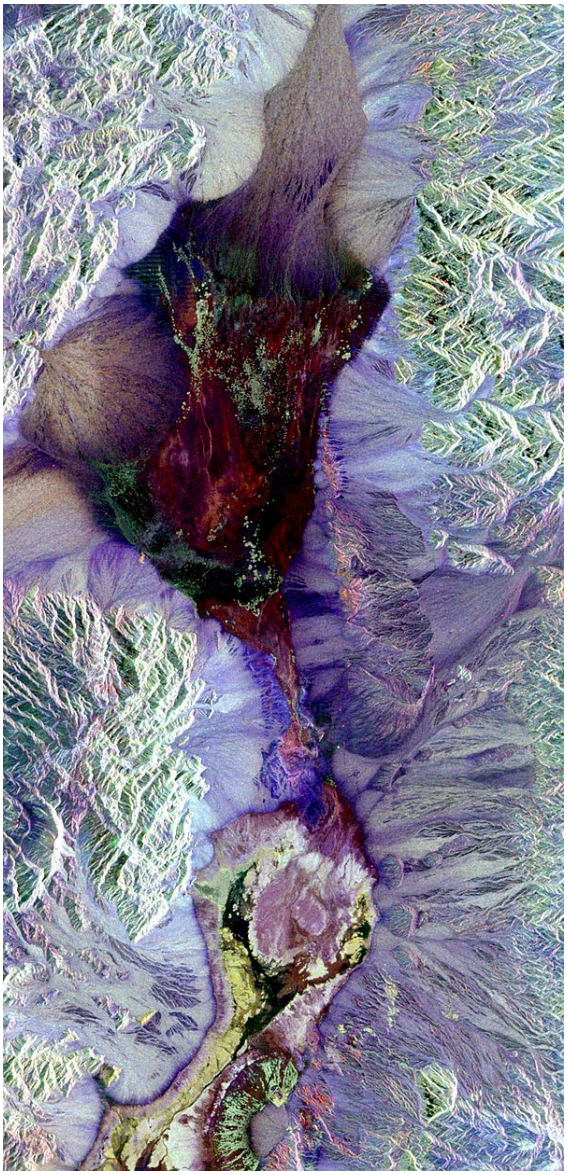

SAR image of Death Valley colored using polarimetry

changes not visible to optical systems occurred. Examples include subterranean tunneling or paths of vehicles driving through the area being imaged. Enhanced SAR sea oil slick observation has been developed by appropriate physical modelling and use of fully polarimetric and dual-polarimetric measurements.

9.1.4 Interferometry

Main article: Interferometric synthetic aperture radar

Rather than discarding the phase data, information can be extracted from it. If two observations of the same terrain from very similar positions are available, aperture synthesis can be performed to provide the resolution performance which would be given by a radar system with dimensions equal to the separation of the two measurements. This technique is called Interferometric SAR or InSAR.

If the two samples are obtained simultaneously (perhaps by placing two antennas on the same aircraft, some distance apart), then any phase difference will contain information about the angle from which the radar echo returned. Combining this with the distance information, one can determine the position in three dimensions of the image pixel. In other words, one can extract terrain altitude as well as radar reflectivity, producing a digital elevation model (DEM) with a single airplane pass. One aircraft application at the Canada Centre for Remote Sensing produced digital elevation maps with a resolution of 5 m and altitude errors also on the order of 5 m. Interferometry was used to map many regions of the Earth's surface with unprecedented accuracy using data from the Shuttle Radar Topography Mission.

If the two samples are separated in time, perhaps from two flights over the same terrain, then there are two possible sources of phase shift. The first is terrain altitude, as discussed above. The second is terrain motion: if the terrain has shifted between observations, it will return a different phase. The amount of shift required to cause a significant phase difference is on the order of the wavelength used. This means that if the terrain shifts by centimeters, it can be seen in the resulting image (a digital elevation map must be available to separate the two kinds of phase difference; a third pass may be necessary to produce one).

This second method offers a powerful tool in geology and geography. Glacier flow can be mapped with two passes. Maps showing the land deformation after a minor earthquake or after a volcanic eruption (showing the shrinkage of the whole volcano by several centimeters) have been published.

Differential interferometry

Differential interferometry (D-InSAR) requires taking at least two images with addition of a DEM. The DEM can be either produced by GPS measurements or could be generated by interferometry as long as the time between acquisition of the image pairs is short, which guarantees minimal distortion of the image of the target surface. In principle, 3 images of the ground area with similar image acquisition geometry is often adequate for D-InSar. The principle for detecting ground movement is quite simple. One interferogram is created from the first two images; this is also called the reference interferogram or topographical interferogram. A second interferogram is created that captures topography + distortion. Subtracting the latter from the reference interferogram can reveal differential fringes, indicating movement. The described 3 image D-InSAR generation technique is called 3-pass or double-difference method.

Differential fringes which remain as fringes in the differ-

ential interferogram are a result of SAR range changes of any displaced point on the ground from one interferogram to the next. In the differential interferogram, each fringe is directly proportional to the SAR wavelength, which is about 5.6 cm for ERS and RADARSAT single phase cycle. Surface displacement away from the satellite look direction causes an increase in path (translating to phase) difference. Since the signal travels from the SAR antenna to the target and back again, the measured displacement is twice the unit of wavelength. This means in differential interferometry one fringe cycle $-\pi$ to $+\pi$ or one wavelength corresponds to a displacement relative to SAR antenna of only half wavelength (2.8 cm). There are various publications on measuring subsidence movement, slope stability analysis, landslide, glacier movement, etc. tooling D-InSAR. Further advancement to this technique whereby differential interferometry from satellite SAR ascending pass and descending pass can be used to estimate 3-D ground movement. Research in this area has shown accurate measurements of 3-D ground movement with accuracies comparable to GPS based measurements can be achieved.

9.1.5 Ultra-wideband SAR

Conventional radar systems emit bursts of radio energy with a fairly narrow range of frequencies. A narrow-band channel, by definition, does not allow rapid changes in modulation. Since it is the change in a received signal that reveals the time of arrival of the signal (obviously an unchanging signal would reveal nothing about "when" it reflected from the target), a signal with only a slow change in modulation cannot reveal the distance to the target as well as can a signal with a quick change in modulation.

Ultra-wideband (UWB) refers to any radio transmission that uses a very large bandwidth – which is the same as saying it uses very rapid changes in modulation. Although there is no set bandwidth value that qualifies a signal as "UWB", systems using bandwidths greater than a sizable portion of the center frequency (typically about ten percent, or so) are most often called "UWB" systems. A typical UWB system might use a bandwidth of one-third to one-half of its center frequency. For example, some systems use a bandwidth of about 1 GHz centered around 3 GHz.

There are as many ways to increase the bandwidth of a signal as there are forms of modulation – it is simply a matter of increasing the rate of that modulation. However, the two most common methods used in UWB radar, including SAR, are very short pulses and high-bandwidth chirping. A general description of chirping appears elsewhere in this article. The bandwidth of a chirped system can be as narrow or as wide as the designers desire. Pulse-based UWB systems, being the more common method associated with the term "UWB radar", are described here.

A pulse-based radar system transmits very short pulses of electromagnetic energy, typically only a few waves or less. A very short pulse is, of course, a very rapidly changing signal, and thus occupies a very wide bandwidth. This allows far more accurate measurement of distance, and thus resolution.

The main disadvantage of pulse-based UWB SAR is that the transmitting and receiving front-end electronics are difficult to design for high-power applications. Specifically, the transmit duty cycle is so exceptionally low and pulse time so exceptionally short, that the electronics must be capable of extremely high instantaneous power to rival the average power of conventional radars. (Although it is true that UWB provides a notable gain in channel capacity over a narrow band signal because of the relationship of bandwidth in the Shannon–Hartley theorem and because the low receive duty cycle receives less noise, increasing the signal-to-noise ratio, there is still a notable disparity in link budget because conventional radar might be several orders of magnitude more powerful than a typical pulse-based radar.) So pulse-based UWB SAR is typically used in applications requiring average power levels in the microwatt or milliwatt range, and thus is used for scanning smaller, nearer target areas (several tens of meters), or in cases where lengthy integration (over a span of minutes) of the received signal is possible. Note, however, that this limitation is solved in chirped UWB radar systems.

The principal advantages of UWB radar are better resolution (a few millimeters using commercial off-the-shelf electronics) and more spectral information of target reflectivity.

9.1.6 Doppler-beam sharpening

Doppler Beam Sharpening commonly refers to the method of processing unfocused real-beam phase history to achieve better resolution than could be achieved by processing the real beam without it. Because the real aperture of the radar antenna is so small (compared to the wavelength in use), the radar energy spreads over a wide area (usually many degrees wide in a direction orthogonal (at right angles) to the direction of the platform (aircraft)). Doppler-beam sharpening takes advantage of the motion of the platform in that targets ahead of the platform return a Doppler upshifted signal (slightly higher in frequency) and targets behind the platform return a Doppler downshifted signal (slightly lower in frequency).

The amount of shift varies with the angle forward or backward from the ortho-normal direction. By knowing the speed of the platform, target signal return is placed in a specific angle "bin" that changes over time. Signals are integrated over time and thus the radar "beam" is synthetically reduced to a much smaller aperture – or more accurately (and based on the ability to distinguish smaller Doppler shifts) the system can have hundreds of very "tight" beams concurrently. This technique dramatically

improves angular resolution; however, it is far more difficult to take advantage of this technique for range resolution. (See Pulse-doppler radar).

9.1.7 Chirped (pulse-compressed) radars

A common technique for many radar systems (usually also found in SAR systems) is to "chirp" the signal. In a “chirped” radar, the pulse is allowed to be much longer. A longer pulse allows more energy to be emitted, and hence received, but usually hinders range resolution. But in a chirped radar, this longer pulse also has a frequency shift during the pulse (hence the chirp or frequency shift). When the “chirped” signal is returned, it must be correlated with the sent pulse. Classically, in analog systems, it is passed to a dispersive delay line (often a SAW device) that has the property of varying velocity of propagation based on frequency. This technique “compresses” the pulse in time – thus having the effect of a much shorter pulse (improved range resolution) while having the benefit of longer pulse length (much more signal returned). Newer systems use digital pulse correlation to find the pulse return in the signal.

9.2 Typical operation

NASA's AirSAR instrument is attached to the side of a DC-8

In a typical SAR application, a single radar antenna is attached to an aircraft or spacecraft so as to radiate a beam whose wave-propagation direction has a substantial component perpendicular to the flight-path direction. The beam is allowed to be broad in the vertical direction so it will illuminate the terrain from nearly beneath the aircraft out toward the horizon.

Resolution in the range dimension of the image is accomplished by creating pulses which define very short time intervals, either by emitting short pulses consisting of a carrier frequency and the necessary sidebands, all within a certain bandwidth, or by using longer "chirp pulses" in which frequency varies (often linearly) with time within that bandwidth. The differing times at which echoes return allow points at different distances to be distinguished.

The total signal is that from a beamwidth-sized patch of the ground. To produce a beam that is narrow in the cross-range direction, diffraction effects require that the antenna be wide in that dimension. Therefore the distinguishing, from each other, of co-range points simply by strengths of returns that persist for as long as they are within the beam width is difficult with aircraft-carryable antennas, because their beams can have linear widths only about two orders of magnitude (hundreds of times) smaller than the range. (Spacecraft-carryable ones can do 10 or more times better.) However, if both the amplitude and the phase of returns are recorded, then the portion of that multi-target return that was scattered radially from any smaller scene element can be extracted by phase-vector correlation of the total return with the form of the return expected from each such element. Careful design and operation can accomplish resolution of items smaller than a millionth of the range, for example, 30 cm at 300 km, or about one foot at nearly 200 miles (320 km).

The process can be thought of as combining the series of spatially distributed observations as if all had been made simultaneously with an antenna as long as the beamwidth and focused on that particular point. The “synthetic aperture” simulated at maximum system range by this process not only is longer than the real antenna, but, in practical applications, it is much longer than the radar aircraft, and tremendously longer than the radar spacecraft.

Image resolution of SAR in its range coordinate (expressed in image pixels per distance unit) is mainly proportional to the radio bandwidth of whatever type of pulse is used. In the cross-range coordinate, the similar resolution is mainly proportional to the bandwidth of the Doppler shift of the signal returns within the beamwidth. Since Doppler frequency depends on the angle of the scattering point’s direction from the broadside direction, the Doppler bandwidth available within the beamwidth is the same at all ranges. Hence the theoretical spatial resolution limits in both image dimensions remain constant with variation of range. However, in practice, both the errors

that accumulate with data-collection time and the particular techniques used in post-processing further limit cross-range resolution at long ranges.

The conversion of return delay time to geometric range can be very accurate because of the natural constancy of the speed and direction of propagation of electromagnetic waves. However, for an aircraft flying through the never-uniform and never-quiescent atmosphere, the relating of pulse transmission and reception times to successive geometric positions of the antenna must be accompanied by constant adjusting of the return phases to account for sensed irregularities in the flight path. SAR's in spacecraft avoid that atmosphere problem, but still must make corrections for known antenna movements due to rotations of the spacecraft, even those that are reactions to movements of onboard machinery. Locating a SAR in a manned space vehicle may require that the humans carefully remain motionless relative to the vehicle during data collection periods.

Although some references to SARs have characterized them as "radar telescopes", their actual optical analogy is the microscope, the detail in their images being smaller than the length of the synthetic aperture. In radar-engineering terms, while the target area is in the "far field" of the illuminating antenna, it is in the "near field" of the simulated one.

Returns from scatterers within the range extent of any image are spread over a matching time interval. The inter-pulse period must be long enough to allow farthest-range returns from any pulse to finish arriving before the nearest-range ones from the next pulse begin to appear, so that those do not overlap each other in time. On the other hand, the interpulse rate must be fast enough to provide sufficient samples for the desired across-range (or across-beam) resolution. When the radar is to be carried by a high-speed vehicle and is to image a large area at fine resolution, those conditions may clash, leading to what has been called SAR's ambiguity problem. The same considerations apply to "conventional" radars also, but this problem occurs significantly only when resolution is so fine as to be available only through SAR processes. Since the basis of the problem is the information-carrying capacity of the single signal-input channel provided by one antenna, the only solution is to use additional channels fed by additional antennas. The system then becomes a hybrid of a SAR and a phased array, sometimes being called a Vernier Array.

Combining the series of observations requires significant computational resources, usually using Fourier transform techniques. The high digital computing speed now available allows such processing to be done in near-real time on board a SAR aircraft. (There is necessarily a minimum time delay until all parts of the signal have been received.) The result is a map of radar reflectivity, including both amplitude and phase. The amplitude information, when shown in a map-like display, gives information about ground cover in much the same way that a black-and-white photo does. Variations in processing may also be done in either vehicle-borne stations or ground stations for various purposes, so as to accentuate certain image features for detailed target-area analysis.

Although the phase information in an image is generally not made available to a human observer of an image display device, it can be preserved numerically, and sometimes allows certain additional features of targets to be recognized. Unfortunately, the phase differences between adjacent image picture elements ("pixels") also produce random interference effects called "coherence speckle", which is a sort of graininess with dimensions on the order of the resolution, causing the concept of resolution to take on a subtly different meaning. This effect is the same as is apparent both visually and photographically in laser-illuminated optical scenes. The scale of that random speckle structure is governed by the size of the synthetic aperture in wavelengths, and cannot be finer than the system's resolution. Speckle structure can be subdued at the expense of resolution.

Before rapid digital computers were available, the data processing was done using an optical holography technique. The analog radar data were recorded as a holographic interference pattern on photographic film at a scale permitting the film to preserve the signal bandwidths (for example, 1:1,000,000 for a radar using a 0.6-meter wavelength). Then light using, for example, 0.6-micrometer waves (as from a helium–neon laser) passing through the hologram could project a terrain image at a scale recordable on another film at reasonable processor focal distances of around a meter. This worked because both SAR and phased arrays are fundamentally similar to optical holography, but using microwaves instead of light waves. The "optical data-processors" developed for this radar purpose [2][3][4] were the first effective analog optical computer systems, and were, in fact, devised before the holographic technique was fully adapted to optical imaging. Because of the different sources of range and across-range signal structures in the radar signals, optical data-processors for SAR included not only both spherical and cylindrical lenses, but sometimes conical ones.

9.3 Image appearance

Main article: Radar image

The following considerations apply also to real-aperture terrain-imaging radars, but are more consequential when resolution in range is matched to a cross-beam resolution that is available only from a SAR.

The two dimensions of a radar image are range and cross-range. Radar images of limited patches of terrain can resemble oblique photographs, but not ones taken from the

location of the radar. This is because the range coordinate in a radar image is perpendicular to the vertical-angle coordinate of an oblique photo. The apparent entrance-pupil position (or camera center) for viewing such an image is therefore not as if at the radar, but as if at a point from which the viewer's line of sight is perpendicular to the slant-range direction connecting radar and target, with slant-range increasing from top to bottom of the image.

Because slant ranges to level terrain vary in vertical angle, each elevation of such terrain appears as a curved surface, specifically a hyperbolic cosine one. Verticals at various ranges are perpendiculars to those curves. The viewer's apparent looking directions are parallel to the curve's "hypcos" axis. Items directly beneath the radar appear as if optically viewed horizontally (i.e., from the side) and those at far ranges as if optically viewed from directly above. These curvatures are not evident unless large extents of near-range terrain, including steep slant ranges, are being viewed.

When viewed as specified above, fine-resolution radar images of small areas can appear most nearly like familiar optical ones, for two reasons. The first reason is easily understood by imagining a flagpole in the scene. The slant-range to its upper end is less than that to its base. Therefore the pole can appear correctly top-end up only when viewed in the above orientation. Secondly, the radar illumination then being downward, shadows are seen in their most-familiar "overhead-lighting" direction.

Note that the image of the pole's top will overlay that of some terrain point which is on the same slant range arc but at a shorter horizontal range ("ground-range"). Images of scene surfaces which faced both the illumination and the apparent eyepoint will have geometries that resemble those of an optical scene viewed from that eyepoint. However, slopes facing the radar will be foreshortened and ones facing away from it will be lengthened from their horizontal (map) dimensions. The former will therefore be brightened and the latter dimmed.

Returns from slopes steeper than perpendicular to slant range will be overlaid on those of lower-elevation terrain at a nearer ground-range, both being visible but intermingled. This is especially the case for vertical surfaces like the walls of buildings. Another viewing inconvenience that arises when a surface is steeper than perpendicular to the slant range is that it is then illuminated on one face but "viewed" from the reverse face. Then one "sees", for example, the radar-facing wall of a building as if from the inside, while the building's interior and the rear wall (that nearest to, hence expected to be optically visible to, the viewer) have vanished, since they lack illumination, being in the shadow of the front wall and the roof. Some return from the roof may overlay that from the front wall, and both of those may overlay return from terrain in front of the building. The visible building shadow will include those of all illuminated items. Long shadows may exhibit blurred edges due to the illuminating antenna's movement during the "time exposure" needed to create the image.

Surfaces that we usually consider rough will, if that roughness consists of relief less than the radar wavelength, behave as smooth mirrors, showing, beyond such a surface, additional images of items in front of it. Those mirror images will appear within the shadow of the mirroring surface, sometimes filling the entire shadow, thus preventing recognition of the shadow.

An important fact that applies to SARs but not to real-aperture radars is that the direction of overlay of any scene point is not directly toward the radar, but toward that point of the SAR's current path direction that is nearest to the target point. If the SAR is "squinting" forward or aft away from the exactly broadside direction, then the illumination direction, and hence the shadow direction, will not be opposite to the overlay direction, but slanted to right or left from it. An image will appear with the correct projection geometry when viewed so that the overlay direction is vertical, the SAR's flight-path is above the image, and range increases somewhat downward.

Objects in motion within a SAR scene alter the Doppler frequencies of the returns. Such objects therefore appear in the image at locations offset in the across-range direction by amounts proportional to the range-direction component of their velocity. Road vehicles may be depicted off the roadway and therefore not recognized as road traffic items. Trains appearing away from their tracks are more easily properly recognized by their length parallel to known trackage as well as by the absence of an equal length of railbed signature and of some adjacent terrain, both having been shadowed by the train. While images of moving vessels can be offset from the line of the earlier parts of their wakes, the more recent parts of the wake, which still partake of some of the vessel's motion, appear as curves connecting the vessel image to the relatively quiescent far-aft wake. In such identifiable cases, speed and direction of the moving items can be determined from the amounts of their offsets. The along-track component of a target's motion causes some defocus. Random motions such as that of wind-driven tree foliage, vehicles driven over rough terrain, or humans or other animals walking or running generally render those items not focusable, resulting in blurring or even effective invisibility.

These considerations, along with the speckle structure due to coherence, take some getting used to in order to correctly interpret SAR images. To assist in that, large collections of significant target signatures have been accumulated by performing many test flights over known terrains and cultural objects.

9.4 History

9.4.1 Origin and early development (ca. 1950–1975)

Carl A. Wiley,[5] a mathematician at Goodyear Aircraft Company in Litchfield Park, Arizona, invented synthetic-aperture radar in June 1951 while working on a correlation guidance system for the Atlas ICBM program.[6] In early 1952, Wiley, together with Fred Heisley and Bill Welty, constructed a concept validation system known as DOUSER ("Doppler Unbeamed Search Radar"). During the 1950s and 1960s, Goodyear Aircraft (later Goodyear Aerospace) introduced numerous advancements in SAR technology.[7]

Independently of Wiley's work, experimental trials in early 1952 by Sherwin and others at the University of Illinois' Control Systems Laboratory showed results that they pointed out "could provide the basis for radar systems with greatly improved angular resolution" and might even lead to systems capable of focusing at all ranges simultaneously.[8]

In both of those programs, processing of the radar returns was done by electrical-circuit filtering methods. In essence, signal strength in isolated discrete bands of Doppler frequency defined image intensities that were displayed at matching angular positions within proper range locations. When only the central (zero-Doppler band) portion of the return signals was used, the effect was as if only that central part of the beam existed. That led to the term Doppler Beam Sharpening. Displaying returns from several adjacent non-zero Doppler frequency bands accomplished further "beam-subdividing" (sometimes called "unfocused radar", though it could have been considered "semi-focused"). Wiley's patent, applied for in 1954, still proposed similar processing. The bulkiness of the circuitry then available limited the extent to which those schemes might further improve resolution.

The principle was included in a memorandum[9] authored by Walter Hausz of General Electric that was part of the then-secret report of a 1952 Dept. of Defense summer study conference called TEOTA ("The Eyes of the Army"),[10] which sought to identify new techniques useful for military reconnaissance and technical gathering of intelligence. A follow-on summer program in 1953 at the University of Michigan, called Project Wolverine, identified several of the TEOTA subjects, including Doppler-assisted sub-beamwidth resolution, as research efforts to be sponsored by the Department of Defense (DoD) at various academic and industrial research laboratories. In that same year, the Illinois group produced a "strip-map" image exhibiting a considerable amount of sub-beamwidth resolution.

A more advanced focused-radar project was among several remote sensing schemes assigned in 1953 to Project Michigan, a tri-service-sponsored (Army, Navy, Air Force) program at the University of Michigan's Willow Run Research Center (WRRC), that program being administered by the Army Signal Corps. Initially called the side-looking radar project, it was carried out by a group first known as the Radar Laboratory and later as the Radar and Optics Laboratory. It proposed to take into account, not just the short-term existence of several particular Doppler shifts, but the entire history of the steadily varying shifts from each target as the latter crossed the beam. An early analysis by Dr. Louis J. Cutrona, Weston E. Vivian, and Emmett N. Leith of that group showed that such a fully focused system should yield, at all ranges, a resolution equal to the width (or, by some criteria, the half-width) of the real antenna carried on the radar aircraft and continually pointed broadside to the aircraft's path.[11]

The required data processing amounted to calculating cross-correlations of the received signals with samples of the forms of signals to be expected from unit-amplitude sources at the various ranges. At that time, even large digital computers had capabilities somewhat near the levels of today's four-function handheld calculators, hence were nowhere near able to do such a huge amount of computation. Instead, the device for doing the correlation computations was to be an optical correlator.

It was proposed that signals received by the traveling antenna and coherently detected be displayed as a single range-trace line across the diameter of the face of a cathode-ray tube, the line's successive forms being recorded as images projected onto a film traveling perpendicular to the length of that line. The information on the developed film was to be subsequently processed in the laboratory on equipment still to be devised as a principal task of the project. In the initial processor proposal, an arrangement of lenses was expected to multiply the recorded signals point-by-point with the known signal forms by passing light successively through both the signal film and another film containing the known signal pattern. The subsequent summation, or integration, step of the correlation was to be done by converging appropriate sets of multiplication products by the focusing action of one or more spherical and cylindrical lenses. The processor was to be, in effect, an optical analog computer performing large-scale scalar arithmetic calculations in many channels (with many light "rays") at once. Ultimately, two such devices would be needed, their outputs to be combined as quadrature components of the complete solution.

Fortunately (as it turned out), a desire to keep the equipment small had led to recording the reference pattern on 35 mm film. Trials promptly showed that the patterns on the film were so fine as to show pronounced diffraction effects that prevented sharp final focusing.[3]

That led Leith, a physicist who was devising the correlator, to recognize that those effects in themselves could, by natural processes, perform a significant part of the needed processing, since along-track strips of the recording operated like diametrical slices of a series of circular

optical zone plates. Any such plate performs somewhat like a lens, each plate having a specific focal length for any given wavelength. The recording that had been considered as scalar became recognized as pairs of opposite-sign vector ones of many spatial frequencies plus a zero-frequency "bias" quantity. The needed correlation summation changed from a pair of scalar ones to a single vector one.

Each zone plate strip has two equal but oppositely signed focal lengths, one real, where a beam through it converges to a focus, and one virtual, where another beam appears to have diverged from, beyond the other face of the zone plate. The zero-frequency (DC bias) component has no focal point, but overlays both the converging and diverging beams. The key to obtaining, from the converging wave component, focused images that are not overlaid with unwanted haze from the other two is to block the latter, allowing only the wanted beam to pass through a properly positioned frequency-band selecting aperture.

Each radar range yields a zone plate strip with a focal length proportional to that range. This fact became a principal complication in the design of optical processors. Consequently, technical journals of the time contain a large volume of material devoted to ways for coping with the variation of focus with range.

For that major change in approach, the light used had to be both monochromatic and coherent, properties that were already a requirement on the radar radiation. Lasers also then being in the future, the best then-available approximation to a coherent light source was the output of a mercury vapor lamp, passed through a color filter that was matched to the lamp spectrum's green band, and then concentrated as well as possible onto a very small beam-limiting aperture. While the resulting amount of light was so weak that very long exposure times had to be used, a workable optical correlator was assembled in time to be used when appropriate data became available.

Although creating that radar was a more straightforward task based on already-known techniques, that work did demand the achievement of signal linearity and frequency stability that were at the extreme state of the art. An adequate instrument was designed and built by the Radar Laboratory and was installed in a C-46 (Curtiss Commando) aircraft. Because the aircraft was bailed to WRRC by the U. S. Army and was flown and maintained by WRRC's own pilots and ground personnel, it was available for many flights at times matching the Radar Laboratory's needs, a feature important for allowing frequent re-testing and "debugging" of the continually developing complex equipment. By contrast, the Illinois group had used a C-46 belonging to the Air Force and flown by AF pilots only by pre-arrangement, resulting, in the eyes of those researchers, in limitation to a less-than-desirable frequency of flight tests of their equipment, hence a low bandwidth of feedback from tests. (Later work with newer Convair aircraft continued the Michigan group's local control of flight schedules.)

Michigan's chosen 5-foot (1.5 m)-wide World War II-surplus antenna was theoretically capable of 5-foot (1.5 m) resolution, but data from only 10% of the beamwidth was used at first, the goal at that time being to demonstrate 50-foot (15 m) resolution. It was understood that finer resolution would require the added development of means for sensing departures of the aircraft from an ideal heading and flight path, and for using that information for making needed corrections to the antenna pointing and to the received signals before processing. After numerous trials in which even small atmospheric turbulence kept the aircraft from flying straight and level enough for good 50-foot (15 m) data, one pre-dawn flight in August 1957[12] yielded a map-like image of the Willow Run Airport area which did demonstrate 50-foot (15 m) resolution in some parts of the image, whereas the illuminated beam width there was 900 feet (270 m). Although the program had been considered for termination by DoD due to what had seemed to be a lack of results, that first success ensured further funding to continue development leading to solutions to those recognized needs.

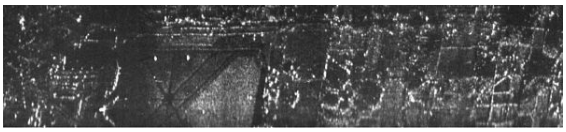

First successful focussed airborne synthetic aperture radar image, Willow Run Airport and vicinity, August 1957. Image courtesy University of Michigan.

The SAR principle was first acknowledged publicly via an April 1960 press release about the U. S. Army experimental AN/UPD-1 system, which consisted of an airborne element made by Texas Instruments and installed in a Beech L-23D aircraft and a mobile ground data-processing station made by WRRC and installed in a military van. At the time, the nature of the data processor was not revealed. A technical article in the journal of the IRE (Institute of Radio Engineers) Professional Group on Military Electronics in February 1961[13] described the SAR principle and both the C-46 and AN/UPD-1 versions, but did not tell how the data were processed, nor that the UPD-1's maximum resolution capability was about 50 feet (15 m). However, the June 1960 issue of the IRE Professional Group on Information Theory had contained a long article[14] on "Optical Data Processing and Filtering Systems" by members of the Michigan group. Although it did not refer to the use of those techniques for radar, readers of both journals could quite easily understand the existence of a connection between articles sharing some authors.

An operational system to be carried in a reconnaissance version of the F-4 "Phantom" aircraft was quickly devised and was used briefly in Vietnam, where it failed to favorably impress its users, due to the combination of its low resolution (similar to the UPD-1's), the speckly nature of

its coherent-wave images (similar to the speckliness of laser images), and the poorly understood dissimilarity of its range/cross-range images from the angle/angle optical ones familiar to military photo interpreters. The lessons it provided were well learned by subsequent researchers, operational system designers, image-interpreter trainers, and the DoD sponsors of further development and acquisition.

In subsequent work the technique's latent capability was eventually achieved. That work, depending on advanced radar circuit designs and precision sensing of departures from ideal straight flight, along with more sophisticated optical processors using laser light sources and specially designed very large lenses made from remarkably clear glass, allowed the Michigan group to advance system resolution, at about 5-year intervals, first to 15 feet (4.6 m), then 5 feet (1.5 m), and, by the mid-1970s, to 1 foot (the latter only over very short range intervals while processing was still being done optically). The latter levels and the associated very wide dynamic range proved suitable for identifying many objects of military concern as well as soil, water, vegetation, and ice features being studied by a variety of environmental researchers having security clearances allowing them access to what was then classified imagery. Similarly improved operational systems soon followed each of those finer-resolution steps.

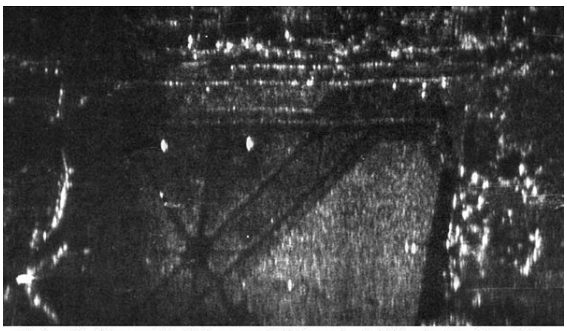

Portion of the first successful optically processed SAR image, showing Willow Run Airport, Aug 1957. Resolution varied from 50 feet to 100 feet within a beam 900 feet wide. The two large spot returns were from large corner reflectors used as test targets, appearing over-large here because their signals exceeded the dynamic range of the recording film. Widths of runways were about 150 feet. Range and cross-range scales not matched nor at right angles.

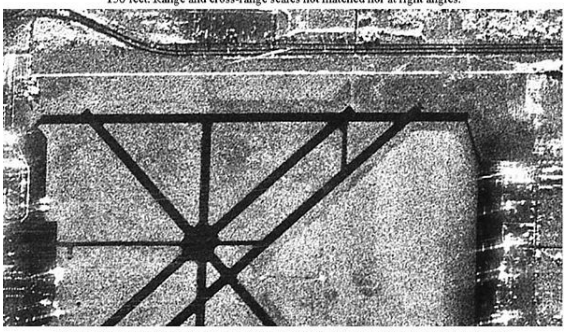

Portion of a later 15-foot SAR image, showing a part of Willow Run Airport that appeared in the upper image. The very bright line represents the airport's chain-link boundary fence. Above it is a divided highway with two paved lanes in each direction, and above that is the undivided two lanes of a paved frontage road. Note the speckle structure, which is an essential feature of coherent-wave images.

Comparison of earliest SAR image with a later improved-resolution one. Additionally, the data-processing light source had been changed from a mercury lamp to a laser. Image data courtesy of University of Michigan and Natural Resources Canada.

Even the 5-foot (1.5 m) resolution stage had over-taxed the ability of cathode-ray tubes (limited to about 2000 distinguishable items across the screen diameter) to deliver fine enough details to signal films while still covering wide range swaths, and taxed the optical processing systems in similar ways. However, at about the same time, digital computers finally became capable of doing the processing without similar limitation, and the consequent presentation of the images on cathode ray tube monitors instead of film allowed for better control over tonal reproduction and for more convenient image mensuration.

Achievement of the finest resolutions at long ranges was aided by adding the capability to swing a larger airborne antenna so as to more strongly illuminate a limited target area continually while collecting data over several degrees of aspect, removing the previous limitation of resolution to the antenna width. This was referred to as the spotlight mode, which no longer produced continuous-swath images but, instead, images of isolated patches of terrain.

It was understood very early in SAR development that the extremely smooth orbital path of an out-of-the-atmosphere platform made it ideally suited to SAR operation. Early experience with artificial earth satellites had also demonstrated that the Doppler frequency shifts of signals traveling through the ionosphere and atmosphere were stable enough to permit very fine resolution to be achievable even at ranges of hundreds of kilometers.[15] While further experimental verification of those facts by a project now referred to as the Quill satellite [16] (declassified in 2012) occurred within the second decade after the initial work began, several of the capabilities for creating useful classified systems did not exist for another two decades.

That seemingly slow rate of advances was often paced by the progress of other inventions, such as the laser, the digital computer, circuit miniaturization, and compact data storage. Once the laser appeared, optical data processing became a fast process because it provided many parallel analog channels, but devising optical chains suited to matching signal focal lengths to ranges proceeded by many stages and turned out to call for some novel optical components. Since the process depended on diffraction of light waves, it required anti-vibration mountings, clean rooms, and highly trained operators. Even at its best, its use of CRTs and film for data storage placed limits on the range depth of images.

At several stages, attaining the frequently over-optimistic expectations for digital computation equipment proved to take far longer than anticipated. For example, the SEASAT system was ready to orbit before its digital processor became available, so a quickly assembled optical recording and processing scheme had to be used to obtain timely confirmation of system operation. In 1978, the first digital SAR processor was developed by the Canadian aerospace company MacDonald Dettwiler (MDA).[17] When its digital processor was finally completed and used, the digital equipment of that time took

many hours to create one swath of image from each run of a few seconds of data.[18] Still, while that was a step down in speed, it was a step up in image quality. Modern methods now provide both high speed and high quality.

Although the above specifies the system development contributions of only a few organizations, many other groups had also become players as the value of SAR became more and more apparent. Especially crucial to the organization and funding of the initial long development process was the technical expertise and foresight of a number of both civilian and uniformed project managers in equipment procurement agencies in the federal government, particularly, of course, ones in the armed forces and in the intelligence agencies, and also in some civilian space agencies.

Since a number of publications and Internet sites refer to a young MIT physics graduate named Robert Rines as having invented fine-resolution radar in the 1940s, persons who have been exposed to those may wonder why that has not been mentioned here. Actually, none of his several radar-image-related patents [19] actually had that goal. Instead, they presumed that fine-resolution images of radar object fields could be accomplished by already-known “dielectric lenses”, the inventive parts of those patents being ways to convert those microwave-formed images to visible ones. However, that presumption incorrectly implied that such lenses and their images could be of sizes comparable to their optical-wave counterparts, whereas the tremendously larger wavelengths of microwaves would actually require the lenses to have apertures thousands of feet (or meters) wide, like the ones simulated by SARs, and the images would be comparably large. Apparently not only did that inventor fail to recognize that fact, but so also did the patent examiners who approved his several applications, and so also have those who have propagated the erroneous tale so widely. Persons seeking to understand SAR should not be misled by references to those patents.

9.4.2 Relationship to phased arrays

A technique closely related to SAR uses an array (referred to as a "phased array") of real antenna elements spatially distributed over either one or two dimensions perpendicular to the radar-range dimension. These physical arrays are truly synthetic ones, indeed being created by synthesis of a collection of subsidiary physical antennas. Their operation need not involve motion relative to targets. All elements of these arrays receive simultaneously in real time, and the signals passing through them can be individually subjected to controlled shifts of the phases of those signals. One result can be to respond most strongly to radiation received from a specific small scene area, focusing on that area to determine its contribution to the total signal received. The coherently detected set of signals received over the entire array aperture can be replicated in several data-processing channels and processed differently in each. The set of responses thus traced to different small scene areas can be displayed together as an image of the scene.

In comparison, a SAR’s (commonly) single physical antenna element gathers signals at different positions at different times. When the radar is carried by an aircraft or an orbiting vehicle, those positions are functions of a single variable, distance along the vehicle’s path, which is a single mathematical dimension (not necessarily the same as a linear geometric dimension). The signals are stored, thus becoming functions, no longer of time, but of recording locations along that dimension. When the stored signals are read out later and combined with specific phase shifts, the result is the same as if the recorded data had been gathered by an equally long and shaped phased array. What is thus synthesized is a set of signals equivalent to what could have been received simultaneously by such an actual large-aperture (in one dimension) phased array. The SAR simulates (rather than synthesizes) that long one-dimensional phased array. Although the term in the title of this article has thus been incorrectly derived, it is now firmly established by half a century of usage.

While operation of a phased array is readily understood as a completely geometric technique, the fact that a synthetic aperture system gathers its data as it (or its target) moves at some speed means that phases which varied with the distance traveled originally varied with time, hence constituted temporal frequencies. Temporal frequencies being the variables commonly used by radar engineers, their analyses of SAR systems are usually (and very productively) couched in such terms. In particular, the variation of phase during flight over the length of the synthetic aperture is seen as a sequence of Doppler shifts of the received frequency from that of the transmitted frequency. It is significant, though, to realize that, once the received data have been recorded and thus have become timeless, the SAR data-processing situation is also understandable as a special type of phased array, treatable as a completely geometric process.

The core of both the SAR and the phased array techniques is that the distances that radar waves travel to and back from each scene element consist of some integer number of wavelengths plus some fraction of a “final” wavelength. Those fractions cause differences between the phases of the re-radiation received at various SAR or array positions. Coherent detection is needed to capture the signal phase information in addition to the signal amplitude information. That type of detection requires finding the differences between the phases of the received signals and the simultaneous phase of a well-preserved sample of the transmitted illumination.

Every wave scattered from any point in the scene has a circular curvature about that point as a center. Signals from scene points at different ranges therefore arrive at a planar array with different curvatures, resulting in signal phase changes which follow different quadratic variations

across a planar phased array. Additional linear variations result from points located in different directions from the center of the array. Fortunately, any one combination of these variations is unique to one scene point, and is calculable. For a SAR, the two-way travel doubles that phase change.

In reading the following two paragraphs, be particularly careful to distinguish between array elements and scene elements. Also remember that each of the latter has, of course, a matching image element.

Comparison of the array-signal phase variation across the array with the total calculated phase variation pattern can reveal the relative portion of the total received signal that came from the only scene point that could be responsible for that pattern. One way to do the comparison is by a correlation computation, multiplying, for each scene element, the received and the calculated field-intensity values array element by array element and then summing the products for each scene element. Alternatively, one could, for each scene element, subtract each array element's calculated phase shift from the actual received phase and then vectorially sum the resulting field-intensity differences over the array. Wherever in the scene the two phases substantially cancel everywhere in the array, the difference vectors being added are in phase, yielding, for that scene point, a maximum value for the sum.

The equivalence of these two methods can be seen by recognizing that multiplication of sinusoids can be done by summing phases which are complex-number exponents of e, the base of natural logarithms.

However it is done, the image-deriving process amounts to "backtracking" the process by which nature previously spread the scene information over the array. In each direction, the process may be viewed as a Fourier transform, which is a type of correlation process. The image-extraction process we use can then be seen as another Fourier transform which is a reversal of the original natural one.

It is important to realize that only those sub-wavelength differences of successive ranges from the transmitting antenna to each target point and back, which govern signal phase, are used to refine the resolution in any geometric dimension. The central direction and the angular width of the illuminating beam do not contribute directly to creating that fine resolution. Instead, they serve only to select the solid-angle region from which usable range data are received. While some distinguishing of the ranges of different scene items can be made from the forms of their sub-wavelength range variations at short ranges, the very large depth of focus that occurs at long ranges usually requires that over-all range differences (larger than a wavelength) be used to define range resolutions comparable to the achievable cross-range resolution.

9.5 Data collection

A model of a German SAR-Lupe reconnaissance satellite inside a Cosmos-3M rocket.

Highly accurate data can be collected by aircraft overflying the terrain in question. In the 1980s, as a prototype for instruments to be flown on the NASA Space Shuttles, NASA operated a synthetic-aperture radar on a NASA Convair 990. In 1986, this plane caught fire on takeoff. In 1988, NASA rebuilt a C, L, and P-band SAR to fly on the NASA DC-8 aircraft. Called AIRSAR, it flew missions at sites around the world until 2004. Another such aircraft, the Convair 580, was flown by the Canada Center for Remote Sensing until about 1996 when it was handed over to Environment Canada due to budgetary reasons. Most land-surveying applications are now carried out by satellite observation. Satellites such as ERS-1/2, JERS-1, Envisat ASAR, and RADARSAT-1 were launched explicitly to carry out this sort of observation. Their capabilities differ, particularly in their support for interferometry, but all have collected tremendous amounts of valuable data. The Space Shuttle also carried synthetic-aperture radar equipment during the SIR-A and SIR-B missions during the 1980s, the Shuttle Radar Laboratory (SRL) missions in 1994 and the Shuttle Radar Topography Mission in 2000.

The Venera 15 and Venera 16 followed later by the Magellan space probe mapped the surface of Venus over several years using synthetic-aperture radar.

Synthetic-aperture radar was first used by NASA on JPL's Seasat oceanographic satellite in 1978 (this mission also carried an altimeter and a scatterometer); it was later

Titan - Evolving feature in Ligeia Mare (SAR; August 21, 2014).

developed more extensively on the Spaceborne Imaging Radar (SIR) missions on the space shuttle in 1981, 1984 and 1994. The Cassini mission to Saturn is currently using SAR to map the surface of the planet's major moon Titan, whose surface is partly hidden from direct optical inspection by atmospheric haze. The SHARAD sounding radar on the Mars Reconnaissance Orbiter and MARSIS instrument on Mars Express have observed bedrock beneath the surface of the Mars polar ice and also indicated the likelihood of substantial water ice in the Martian middle latitudes. The Lunar Reconnaissance Orbiter, launched in 2009, carries a SAR instrument called Mini-RF, which was designed largely to look for water ice deposits on the poles of the Moon.

The Mineseeker Project is designing a system for determining whether regions contain landmines based on a blimp carrying ultra-wideband synthetic-aperture radar. Initial trials show promise; the radar is able to detect even buried plastic mines.

SAR has been used in radio astronomy for many years to simulate a large radio telescope by combining observations taken from multiple locations using a mobile antenna.

The National Reconnaissance Office maintains a fleet of (now declassified) synthetic-aperture radar satellites commonly designated as Lacrosse or Onyx.

In February 2009, the Sentinel R1 surveillance aircraft entered service in the RAF, equipped with the SAR-based Airborne Stand-Off Radar (ASTOR) system.

The German Armed Forces' (Bundeswehr) military SAR-Lupe reconnaissance satellite system has been fully operational since 22 July 2008.

9.6 Data distribution

The Alaska Satellite Facility provides production, archiving and distribution to the scientific community of SAR data products and tools from active and past missions, including the June 2013 release of newly processed, 35-year-old Seasat SAR imagery.

CSTARS downlinks and processes SAR data (as well as other data) from a variety of satellites and supports the University of Miami Rosenstiel School of Marine and Atmospheric Science. CSTARS also supports disaster relief operations, oceanographic and meteorological research, and port and maritime security research projects.

9.7 See also

- Alaska Satellite Facility
- Aperture synthesis
- Beamforming
- Earth observation satellite
- Interferometric synthetic aperture radar (InSAR)
- Inverse synthetic aperture radar (ISAR)
- Magellan space probe
- Radar MASINT
- Remote sensing
- SAR Lupe
- Seasat
- speckle noise
- Synthetic aperture sonar* Synthetic array heterodyne detection (SAHD)
- Synthetically thinned aperture radar
- TerraSAR-X
- Terrestrial SAR Interferometry (TInSAR)
- Very Long Baseline Interferometry (VLBI)
- Wave radar

9.8 References

[1] "Introduction to Airborne RADAR", G.W. Stimson, Chapter 1 (13 pp)

[2] "Synthetic Aperture Radar", L. J. Cutrona, Chapter 23 (25 pp) of the McGraw Hill "Radar Handbook", 1970. (Written while optical data processing was still the only workable method, by the person who first led that development.)

[3] "A short history of the Optics Group of the Willow Run Laboratories", Emmett N. Leith, in *Trends in Optics: Research, Development, and Applications* (book), Anna Consortini, Academic Press, San Diego: 1996.

[4] "Sighted Automation and Fine Resolution Imaging", W. M. Brown, J. L. Walker, and W. R. Boario, IEEE Transactions on Aerospace and Electronic Systems, Vol. 40, No. 4, October 2004, pp 1426–1445.

[5] "In Memory of Carl A. Wiley", A. W. Love, *IEEE Antennas and Propagation Society Newsletter*, pp 17–18, June 1985.

[6] "Synthetic Aperture Radars: A Paradigm for Technology Evolution", C. A. Wiley, IEEE Transactions on Aerospace and Electronic Systems, v. AES-21, n. 3, pp 440–443, May 1985

[7] Gart, Jason H. "Electronics and Aerospace Industry in Cold War Arizona, 1945–1968: Motorola, Hughes Aircraft, Goodyear Aircraft." Phd diss., Arizona State University, 2006.

[8] "Some Early Developments in Synthetic Aperture Radar Systems", C. W. Sherwin, J. P. Ruina, and R. D. Rawcliffe, *IRE Transactions on Military Electronics*, April 1962, pp. 111–115.

[9] *This memo was one of about 20 published as a volume subsidiary to the following reference. No unclassified copy has yet been located. Hopefully, some reader of this article may come across a still existing one.*

[10] "Problems of Battlefield Surveillance", Report of Project TEOTA (The Eyes Of The Army), 1 May 1953, Office of the Chief Signal Officer. Defense Technical Information Center (Document AD 32532)

[11] "A Doppler Technique for Obtaining Very Fine Angular Resolution from a Side-Looking Airborne Radar" Report of Project Michigan No. 2144-5-T, The University of Michigan, Willow Run Research Center, July 1954. (No declassified copy of this historic originally confidential report has yet been located.)

[12] "High-Resolution Radar Achievements During Preliminary Flight Tests", W. A. Blikken and G.O. Hall, Institute of Science and Technology, Univ. of Michigan, 01 Sept 1957. Defense Technical Information Center (Document AD148507)

[13] "A High-Resolution Radar Combat-Intelligence System", L. J. Cutrona, W. E. Vivian, E. N. Leith, and G. O Hall; IRE Transactions on Military Electronics, April 1961, pp 127–131

[14] "Optical Data Processing and Filtering Systems", L. J. Cutrona, E. N. Leith, C. J. Palermo, and L. J. Porcello; IRE Transactions on Information Theory, June 1960, pp 386–400.

[15] An experimental study of rapid phase fluctuataions induced along a satellite to earth propagation path, Porcello, L.J., Univ. of Michigan, Apr 1964

[16] Quill (satellite)

[17] "Observation of the earth and its environment: survey of missions and sensors", Herbert J. Kramer

[18] "Principles of Synthetic Aperture Radar", S. W. McCandless and C. R. Jackson, Chapter 1 of "SAR Marine Users Manual", NOAA, 2004, p.11.

[19] U. S. Pat. Nos. 2696522, 2711534, 2627600, 2711530, and 19 others

9.9 Further reading

- The first and definitive monograph on SAR is *Synthetic Aperture Radar: Systems and Signal Processing (Wiley Series in Remote Sensing and Image Processing)* by John C. Curlander and Robert N. McDonough
- The development of synthetic-aperture radar (SAR) is examined in Gart, Jason H. "Electronics and Aerospace Industry in Cold War Arizona, 1945–1968: Motorola, Hughes Aircraft, Goodyear Aircraft." Phd diss., Arizona State University, 2006.
- A text that includes an introduction on SAR suitable for beginners is "Introduction to Microwave Remote Sensing" by Iain H Woodhouse, CRC Press, 2006.
- Moreira, A.; Prats-Iraola, P.; Younis, M.; Krieger, G.; Hajnsek, I.; Papathanassiou, K. P. (2013). "A tutorial on synthetic aperture radar". *IEEE Geoscience and Remote Sensing Magazine* **1**: 6. doi:10.1109/MGRS.2013.2248301.

9.10 External links

- Publication: SAR simulation (Electromagnetic simulation software for SAR imagery studies: www.oktal-se.fr)
- Sandia National Laboratories SAR Page (Home of miniSAR, smallest hi-res SAR)
- The Imaging Radar Home Page (NASA SAR missions)
- InSAR measurements from the Space Shuttle
- JPL InSAR Images
- GeoSAR – GeoSAR is a dualband XBand and PBand system owned and operated by Fugro EarthData
- Airborne Synthetic-Aperture Radar (AIRSAR)) (NASA Airborne SAR)
- The CCRS airborne SAR page (Canadian airborne missions)
- RADARSAT international (Canadian radar satellites)
- The ERS missions (European radar satellites)
- The ENVISAT mission (ESA's most recent SAR satellite)
- Earth Snapshot – Web Portal dedicated to Earth Observation. Includes commented satellite images, information on storms, hurricanes, fires and meteorological phenomena.

- The JERS satellites (Japanese radar satellites)
- Images from the Space Shuttle SAR instrument
- The Alaska Satellite Facility has numerous technical documents, including an introductory text on SAR theory and scientific applications
- BYU SAR projects and images Images from BYU's three SAR systems (YSAR, YINSAR, μSAR)
- NSSDC Master Catalog information on Venera 15 and 16
- NSSDC Master Catalog information on Magellan Mission
- PolsarPro Open Source Polarimetric SAR Processing Toolbox sponsored by ESA.
- Next ESA SAR Toolbox for viewing and analyzing SAR Level 1 data and higher from various missions
- Przemysłowy Instytut Telekomunikacji S.A.
- Birsen Yazici's SAR related publications at Rensselaer Polytechnic Institute

Chapter 10

Interferometric synthetic aperture radar

Interferometric synthetic aperture radar, abbreviated **InSAR** or **IfSAR**, is a radar technique used in geodesy and remote sensing. This geodetic method uses two or more synthetic aperture radar (SAR) images to generate maps of surface deformation or digital elevation, using differences in the phase of the waves returning to the satellite[1][2][3] or aircraft. The technique can potentially measure centimetre-scale changes in deformation over spans of days to years. It has applications for geophysical monitoring of natural hazards, for example earthquakes, volcanoes and landslides, and in structural engineering, in particular monitoring of subsidence and structural stability.

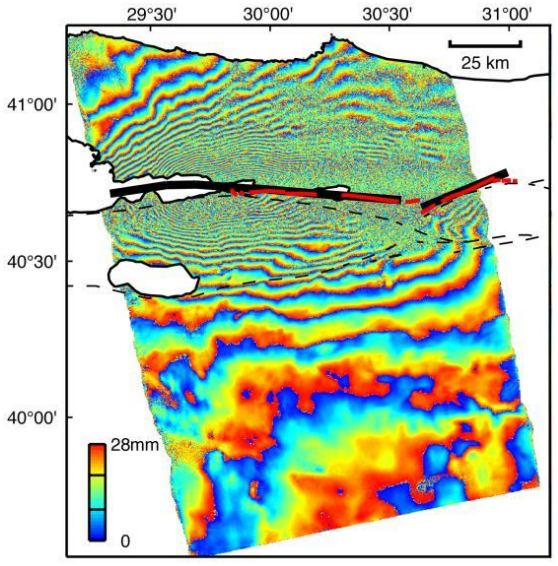

Interferogram produced using ERS-2data from 13 August and 17 September 1999, spanning the 17 August Izmit (Turkey) earthquake. (NASA/JPL-Caltech)

10.1 Technique

10.1.1 Synthetic aperture radar

Main article: Synthetic aperture radar

SAR amplitude image of Kilauea (NASA/JPL-Caltech)

Synthetic aperture radar (SAR) is a form of radar in which sophisticated processing of radar data is used to produce a very narrow effective beam. It can only be used by moving instruments over relatively immobile targets. It is a form of active remote sensing – the antenna transmits radiation which is then reflected from the target, as opposed to passive sensing, where the reflection is detected from ambient illumination. The image acquisition is therefore independent of the natural illumination and images can be taken at night. Radar uses electromagnetic radiation with microwave frequencies; the atmospheric absorption at typical radar wavelengths is very low, meaning observations are not prevented by cloud cover.

10.1.2 Phase

Most SAR applications make use of the amplitude of the return signal, and ignore the phase data. However, interferometry uses the phase of the reflected radiation. Since the outgoing wave is produced by the satellite, the phase is known, and can be compared to the phase of the return signal. The phase of the return wave depends on the distance to the ground, since the path length to the ground

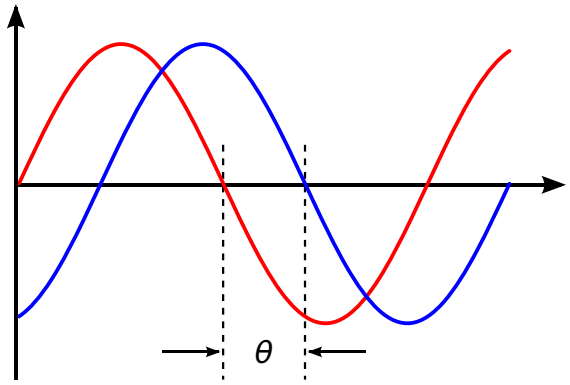

Phase difference

and back will consist of a number of whole wavelengths plus some fraction of a wavelength. This is observable as a phase difference or phase shift in the returning wave. The total distance to the satellite (i.e., the number of whole wavelengths) is not known, but the extra fraction of a wavelength can be measured extremely accurately.

In practice, the phase is also affected by several other factors, which together make the raw phase return in any one SAR image essentially arbitrary, with no correlation from pixel to pixel. To get any useful information from the phase, some of these effects must be isolated and removed. Interferometry uses two images of the same area taken from the same position (or for topographic applications slightly different positions) and finds the difference in phase between them, producing an image known as an interferogram. This is measured in radians of phase difference and, due to the cyclic nature of phase, is recorded as repeating fringes which each represent a full 2π cycle.

10.1.3 Factors affecting phase

The most important factor affecting the phase is the interaction with the ground surface. The phase of the wave may change on reflection, depending on the properties of the material. The reflected signal back from any one pixel is the summed contribution to the phase from many smaller 'targets' in that ground area, each with different dielectric properties and distances from the satellite, meaning the returned signal is arbitrary and completely uncorrelated with that from adjacent pixels. Importantly though, it is consistent – provided nothing on the ground changes the contributions from each target should sum identically each time, and hence be removed from the interferogram.

Once the ground effects have been removed, the major signal present in the interferogram is a contribution from orbital effects. For interferometry to work, the satellites must be as close as possible to the same spatial position when the images are acquired. This means that images from two satellite platforms with different orbits cannot be compared, and for a given satellite data from the same orbital track must be used. In practice the perpendicular distance between them, known as the *baseline*, is often known to within a few centimetres but can only be controlled on a scale of tens to hundreds of metres. This slight difference causes a regular difference in phase that changes smoothly across the interferogram and can be modelled and removed.

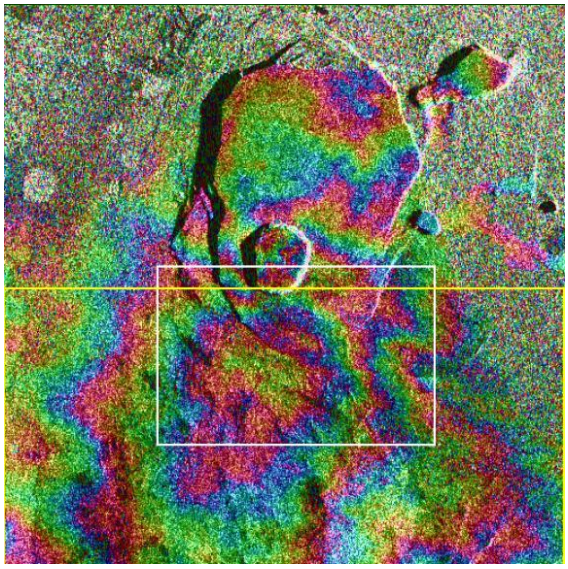

Corresponding interferogram of Kilauea, showing topographic fringes (NASA/JPL-Caltech)

The slight difference in satellite position also alters the distortion caused by topography, meaning an extra phase difference is introduced by a stereoscopic effect. The longer the baseline, the smaller the topographic height needed to produce a fringe of phase change – known as the *altitude of ambiguity*. This effect can be exploited to calculate the topographic height, and used to produce a digital elevation model (DEM).

If the height of the topography is already known, the topographic phase contribution can be calculated and removed. This has traditionally been done in two ways. In the *two-pass* method, elevation data from an externally derived DEM is used in conjunction with the orbital information to calculate the phase contribution. In the *three-pass* method two images acquired a short time apart are used to create an interferogram, which is assumed to have no deformation signal and therefore represent the topographic contribution. This interferogram is then subtracted from a third image with a longer time separation to give the residual phase due to deformation.

Once the ground, orbital and topographic contributions have been removed the interferogram contains the deformation signal, along with any remaining noise (see Difficulties below). The signal measured in the interferogram represents the change in phase caused by an increase or decrease in distance from the ground pixel to the

satellite, therefore only the component of the ground motion parallel to the satellite line of sight vector will cause a phase difference to be observed. For sensors like ERS with a small incidence angle this measures vertical motion well, but is insensitive to horizontal motion perpendicular to the line of sight (approximately north-south). It also means that vertical motion and components of horizontal motion parallel to the plane of the line of sight (approximately east-west) cannot be separately resolved.

One fringe of phase difference is generated by a ground motion of half the radar wavelength, since this corresponds to a whole wavelength increase in the two-way travel distance. Phase shifts are only resolvable relative to other points in the interferogram. Absolute deformation can be inferred by assuming one area in the interferogram (for example a point away from expected deformation sources) experienced no deformation, or by using a ground control (GPS or similar) to establish the absolute movement of a point.

10.1.4 Difficulties

A variety of factors govern the choice of images which can be used for interferometry. The simplest is data availability – radar instruments used for interferometry commonly don't operate continuously, acquiring data only when programmed to do so. For future requirements it may be possible to request acquisition of data, but for many areas of the world archived data may be sparse. Data availability is further constrained by baseline criteria. Availability of a suitable DEM may also be a factor for two-pass InSAR; commonly 90 m SRTM data may be available for many areas, but at high latitudes or in areas of poor coverage alternative datasets must be found.

A fundamental requirement of the removal of the ground signal is that the sum of phase contributions from the individual targets within the pixel remains constant between the two images and is completely removed. However, there are several factors that can cause this criterion to fail. Firstly the two images must be accurately co-registered to a sub-pixel level to ensure that the same ground targets are contributing to that pixel. There is also a geometric constraint on the maximum length of the baseline – the difference in viewing angles must not cause phase to change over the width of one pixel by more than a wavelength. The effects of topography also influence the condition, and baselines need to be shorter if terrain gradients are high. Where co-registration is poor or the maximum baseline is exceeded the pixel phase will become incoherent – the phase becomes essentially random from pixel to pixel rather than varying smoothly, and the area appears noisy. This is also true for anything else that changes the contributions to the phase within each pixel, for example changes to the ground targets in each pixel caused by vegetation growth, landslides, agriculture or snow cover.

Another source of error present in most interferograms is caused by the propagation of the waves through the atmosphere. If the wave travelled through a vacuum it should theoretically be possible (subject to sufficient accuracy of timing) to use the two-way travel-time of the wave in combination with the phase to calculate the exact distance to the ground. However, the velocity of the wave through the atmosphere is lower than the speed of light in a vacuum, and depends on air temperature, pressure and the partial pressure of water vapour.[4] It is this unknown phase delay that prevents the integer number of wavelengths being calculated. If the atmosphere was horizontally homogeneous over the length scale of an interferogram and vertically over that of the topography then the effect would simply be a constant phase difference between the two images which, since phase difference is measured relative to other points in the interferogram, would not contribute to the signal. However, the atmosphere is laterally heterogeneous on length scales both larger and smaller than typical deformation signals. This spurious signal can appear completely unrelated to the surface features of the image, however, in other cases the atmospheric phase delay is caused by vertical inhomogeneity at low altitudes and this may result in fringes appearing to correspond with the topography.

10.1.5 Persistent Scatterer InSAR

Persistent or Permanent Scatterer techniques are a relatively recent development from conventional InSAR, and rely on studying pixels which remain coherent over a sequence of interferograms. In 1999, researchers at Politecnico di Milano, Italy, developed a new multi-image approach in which one searches the stack of images for objects on the ground providing consistent and stable radar reflections back to the satellite. These objects could be the size of a pixel or, more commonly, sub-pixel sized, and are present in every image in the stack.

Politecnico di Milano patented the technology in 1999 and created the spin-off company Tele-Rilevamento Europa – TRE in 2000 to commercialize the technology and perform ongoing research.

Some research centres and other companies, like the Dutch TU Delft spin-off Hansje Brinker, were inspired to develop their own algorithms which would also overcome InSAR's limitations. In scientific literature, these techniques are collectively referred to as Persistent Scatterer Interferometry or PSI techniques. The term Persistent Scatterer Interferometry (PSI) was created by ESA to define the second generation of radar interferometry techniques.

Commonly such techniques are most useful in urban areas with lots of permanent structures, for example the PSI studies of European geohazard sites undertaken by the Terrafirma project.[5] The Terrafirma project (led by Altamira Information SL) provides a ground motion haz-

ard information service, distributed throughout Europe via national geological surveys and institutions. The objective of this service is to help save lives, improve safety, and reduce economic loss through the use of state-of-the-art PSI information. Over the last 9 years this service has supplied information relating to urban subsidence and uplift, slope stability and landslides, seismic and volcanic deformation, coastlines and flood plains.

10.2 Producing interferograms

The processing chain used to produce interferograms varies according to the software used and the precise application but will usually include some combination of the following steps.

Two SAR images are required to produce an interferogram; these may be obtained pre-processed, or produced from raw data by the user prior to InSAR processing. The two images must first be co-registered, using a correlation procedure to find the offset and difference in geometry between the two amplitude images. One SAR image is then re-sampled to match the geometry of the other, meaning each pixel represents the same ground area in both images. The interferogram is then formed by cross-multiplication of each pixel in the two images, and the interferometric phase due to the curvature of the Earth is removed, a process referred to as flattening. For deformation applications a DEM can be used in conjunction with the baseline data to simulate the contribution of the topography to the interferometric phase, this can then be removed from the interferogram.

Once the basic interferogram has been produced, it is commonly filtered using an adaptive power-spectrum filter to amplify the phase signal. For most quantitative applications the consecutive fringes present in the interferogram will then have to be *unwrapped*, which involves interpolating over the 0 to 2π phase jumps to produce a continuous deformation field. At some point, before or after unwrapping, incoherent areas of the image may be masked out. The final processing stage involves geocoding the image, which resamples the interferogram from the acquisition geometry (related to direction of satellite path) into the desired geographic projection.

10.2.1 Hardware

Spaceborne

Early exploitation of satellite-based InSAR included use of Seasat data in the 1980s, but the potential of the technique was expanded in the 1990s, with the launch of ERS-1 (1991), JERS-1 (1992), RADARSAT-1 and ERS-2 (1995). These platforms provided the stable, well-defined orbits and short baselines necessary for InSAR. More recently, the 11-day NASA STS-99 mission in February

Seasat (NASA/JPL-Caltech)

2000 used a SAR antenna mounted on the space shuttle to gather data for the Shuttle Radar Topography Mission. In 2002 ESA launched the ASAR instrument, designed as a successor to ERS, aboard Envisat. While the majority of InSAR to date has utilised the C-band sensors, recent missions such as the ALOS PALSAR, TerraSAR-X and COSMO SKYMED are expanding the available data in the L- and X-band.

Airborne

Airborne InSAR data acquisition systems are built by companies such as the American Intermap, the German AeroSensing, and the Brazilian OrbiSat.[6]

Terrestrial or ground-based

Terrestrial or ground-based SAR Interferometry (GBInSAR or TInSAR) is a remote sensing technique for the displacement monitoring of slopes, rock scarps, volcanoes, landslides, buildings, infrastructures etc. This technique is based on the same operational principles of the Satellite SAR Interferometry, but the Synthetic Aperture of the Radar (SAR) is obtained by an antenna moving on a rail instead of a satellite moving around an orbit. SAR technique allows 2D radar image of the investigated scenario to be achieved, with a high range resolution (along the instrumental line of sight) and cross-range resolution (along the scan direction). Two antennas respectively emit and receive microwave signals and, by calculating

the phase difference between two measurements taken in two different times, it is possible to compute the displacement of all the pixels of the SAR image. The accuracy in the displacement measurement is of the same order of magnitude as the EM wavelength and depends also on the specific local and atmospheric conditions.

10.3 Applications

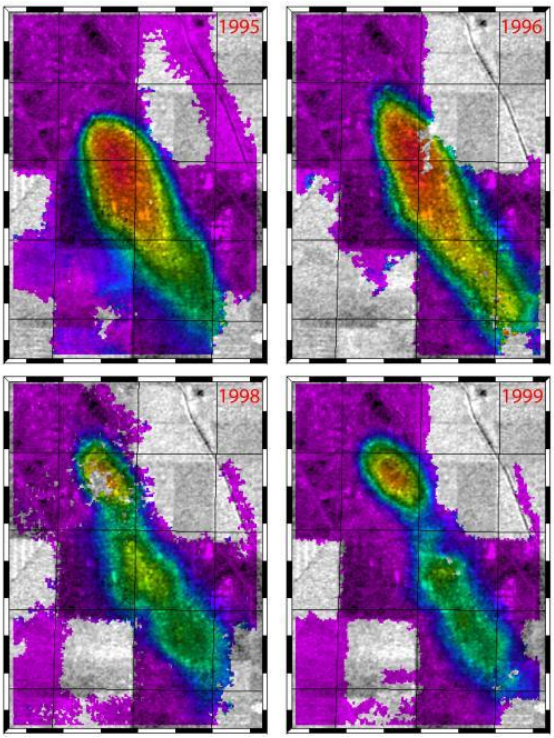

Rapid ground subsidence over the Lost Hills oil field in California. (NASA/JPL-Caltech)

10.3.1 Tectonic

InSAR can be used to measure tectonic deformation, for example ground movements due to earthquakes. It was first used for the 1992 Landers earthquake,[7] but has since been utilised extensively for a wide variety of earthquakes all over the world. In particular the 1999 Izmit and 2003 Bam earthquakes were extensively studied.[8][9] InSAR can also be used to monitor creep and strain accumulation on faults.

10.3.2 Volcanic

InSAR can be used in a variety of volcanic settings, including deformation associated with eruptions, inter-eruption strain caused by changes in magma distribution at depth, gravitational spreading of volcanic edifices, and volcano-tectonic deformation signals.[10] Early work on volcanic InSAR included studies on Mount Etna,[11] and Kilauea,[12] with many more volcanoes being studied as the field developed. The technique is now widely used for academic research into volcanic deformation, although its use as an operational monitoring technique for volcano observatories has been limited by issues such as orbital repeat times, lack of archived data, coherence and atmospheric errors.[13] Recently InSAR has been used to study rifting processes in Ethiopia.[14]

10.3.3 Subsidence

Ground subsidence from a variety of causes has been successfully measured using InSAR, in particular subsidence caused by oil or water extraction from underground reservoirs,[15] subsurface mining and collapse of old mines.[16] It can also be used for monitoring the stability of built structures,[17] and landscape features such as landslides.[18][19]

10.3.4 Ice flow

Glacial motion and deformation have been successfully measured using satellite interferometry. The technique allows remote, high-resolution measurement of changes in glacial structure, ice flow, and shifts in ice dynamics, all of which agree closely with ground observations.[20]

Kamchatka Peninsula, Landsat data draped over SRTM digital elevation model (NASA/JPL-Caltech)

10.3.5 DEM generation

Interferograms can be used to produce digital elevation maps (DEMs) using the stereoscopic effect caused by slight differences in observation position between the two images. When using two images produced by the same sensor with a separation in time, it must be assumed other phase contributions (for example from deformation or atmospheric effects) are minimal. In 1995 the two ERS satellites flew in tandem with a one-day separation for this purpose. A second approach is to use two antennas mounted some distance apart on the same platform, and acquire the images at the same time, which ensures no atmospheric or deformation signals are present. This approach was followed by NASA's SRTM mission aboard the space shuttle in 2000. InSAR-derived DEMs can be

used for later two-pass deformation studies, or for use in other geophysical applications.

10.4 See also

- Coherence (physics)
- Interferometry
- Radar
- Remote sensing
- ROI PAC
- Synthetic aperture radar
- Synthetic array heterodyne detection (SAHD)

10.5 References

[1] Massonnet, D.; Feigl, K. L. (1998), *Radar interferometry and its application to changes in the earth's surface*, *Rev. Geophys.* **36** (4): 441–500, Bibcode:1998RvGeo..36..441M, doi:10.1029/97RG03139

[2] Burgmann, R.; Rosen, P.A.; Fielding, E.J. (2000), *Synthetic aperture radar interferometry to measure Earth's surface topography and its deformation*, *Annual Review of Earth and Planetary Sciences* **28**: 169–209, Bibcode:2000AREPS..28..169B, doi:10.1146/annurev.earth.28.1.169

[3] Hanssen, Ramon F. (2001), *Radar Interferometry: Data Interpretation and Error Analysis*, Kluwer Academic, ISBN 9780792369455

[4] Zebker, H.A.; Rosen, P.A.; Hensley, S. (1997), *Atmospheric effects in interferometric synthetic aperture radar surface deformation and topographic maps*, *Journal of Geophysical Research* **102**: 7547–7563, Bibcode:1997JGR...102.7547Z, doi:10.1029/96JB03804

[5] "Terrafirma.eu.com: A pan-European ground hazard information service". Retrieved 22 January 2013.

[6]

[7] Massonnet, D.; Rossi, M.; Carmona, C.; Adragna, F.; Peltzer, G.; Feigl, K.; Rabaute, T. (1993), *The displacement field of the Landers earthquake mapped by radar interferometry*, *Nature* **364** (6433): 138–142, Bibcode:1993Natur.364..138M, doi:10.1038/364138a0

[8] "Envisat's rainbow vision detects ground moving at pace fingernails grow". European Space Agency. August 6, 2004. Retrieved 2007-03-22.

[9] "The Izmit Earthquake of 17 August 1999 in Turkey". European Space Agency. Retrieved 2007-03-22.

[10] Wadge, G. (2003), *A strategy for the observation of volcanism on Earth from space*, *Phil. Trans. Royal Soc.Lond.* **361**: 145–156

[11] Massonnet, D.; Briole, P.; Arnaud, A. (1995), *Deflation of Mount Etna monitored by spaceborne radar interferometry*, *Nature* **375** (6532): 567–570, Bibcode:1995Natur.375..567M, doi:10.1038/375567a0

[12] Rosen, P. A.; Hensley, S.; Zebker, H. A.; Webb, F. H.; Fielding, E. J. (1996), *Surface deformation and coherence measurements of Kilauea Volcano, Hawaii, from SIR C radar interferometry*, *J. Geophys. Res.* **101** (E10): 23,109–23,126, Bibcode:1996JGR...10123109R, doi:10.1029/96JE01459

[13] Stevens, N.F.; Wadge, G. (2004), *Towards operational repeat-pass SAR interferometry at active volcanoes*, *Natural Hazards* **33**: 47–76, doi:10.1023/B:NHAZ.0000035005.45346.2b

[14] Wright, T.J.; Ebinger, C.; Biggs, J.; Ayele, A.; Yirgu, G.; Keir, D.; Stork, A. (2006), *Magma-maintained rift segmentation at continental rupture in the 2005 Afar dyking episode*, *Nature* **442** (7100): 291–294, Bibcode:2006Natur.442..291W, doi:10.1038/nature04978, PMID 16855588

[15] Tomás, R., Márquez, Y., Lopez-Sanchez, J.M., Delgado, J., Blanco, P., Mallorquí, J.J., Martínez, M., Herrera, G., Mulas, J., 2005. Mapping ground subsidence induced by aquifer overexploitation using advanced Differential SAR Interferometry: Vega Media of the Segura River (SE Spain) case study. Remote Sensing of Environment 98, 269-283.

[16] Herrera, G.; Tomás, R.; Lopez-Sanchez, J.M.; Delgado, J.; Mallorqui, J.J.; Duque, S.; Mulas, J. (2007). "Advanced DInSAR analysis on mining areas: La Union case study (Murcia, SE Spain)". *Engineering Geology* **90** (3–4): 148–159. doi:10.1016/j.enggeo.2007.01.001. (subscription required (help)).

[17] Tomás, R.; García-Barba, J.; Cano, M.; Sanabria, M.P.; Ivorra, S.; Duro, J.; Herrera, G. (November 2012). "Subsidence damage assessment of a gothic church using Differential Interferometry and field data". *Structural Health Monitoring* **11** (6): 751–762. doi:10.1177/1475921712451953. (subscription required (help)).

[18] "Ground motion". European Space Agency. Retrieved 2007-03-21.

[19] Herrera, G.; Tomás, R.; Vicente, F.; Lopez-Sanchez, J.M.; Mallorquí, J.J.; Mulas, J. (October 2010). "Mapping ground movements in open pit mining areas using differential SAR interferometry". *International Journal of Rock Mechanics and Mining Sciences* **47** (7): 1114–1125. doi:10.1016/j.ijrmms.2010.07.006. (subscription required (help)).

[20] Goldstein, R.M.; Engelhardt, H.; Kamb, B.; Frolich, R. M. (1993), *Satellite radar interferometry for monitoring ice sheet motion: application to an Antarctic ice streamy*, *Science* **262** (5139): 1525–1530, Bibcode:1993Sci...262.1525G, doi:10.1126/science.262.5139.1525, PMID 17829380

10.6 Further reading

- InSAR, a tool for measuring Earth's surface deformation Matthew E. Pritchard
- USGS InSAR factsheet
- InSAR Principles, ESA publication, TM19, February 2007.
- B. Kampes, Radar Interferometry – Persistent Scatterer Technique, Kluwer Academic Publishers, Dordrecht, The Netherlands, 2006. ISBN 978-1-4020-4576-9

Chapter 11

Oil spill

Help after an oil spill

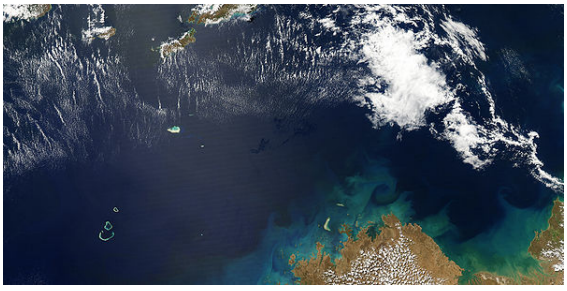

Oil slick from the Montara oil spill in the Timor Sea, September 2009

An **oil spill** is the release of a liquid petroleum hydrocarbon into the environment, especially marine areas, due to human activity, and is a form of pollution. The term is usually applied to marine oil spills, where oil is released into the ocean or coastal waters, but spills may also occur on land. Oil spills may be due to releases of crude oil from tankers, offshore platforms, drilling rigs and wells, as well as spills of refined petroleum products (such as gasoline, diesel) and their by-products, heavier fuels used by large ships such as bunker fuel, or the spill of any oily refuse or waste oil.

Spilt oil penetrates into the structure of the plumage of birds and the fur of mammals, reducing its insulating ability, and making them more vulnerable to temperature fluctuations and much less buoyant in the water. Cleanup and recovery from an oil spill is difficult and depends upon many factors, including the type of oil spilled, the temperature of the water (affecting evaporation and biodegradation), and the types of shorelines and beaches involved.[1] Spills may take weeks, months or even years to clean up.[2]

11.1 Largest oil spills

Main article: List of oil spills

Crude oil and refined fuel spills from tanker ship accidents have damaged natural ecosystems in Alaska, the Gulf of Mexico, the Galapagos Islands, France and many other places. The quantity of oil spilled during accidents has ranged from a few hundred tons to several hundred thousand tons (e.g., Deepwater Horizon Oil Spill, Atlantic Empress, Amoco Cadiz) but is a limited barometer of damage or impact. Smaller spills have already proven to have a great impact on ecosystems, such as the Exxon Valdez oil spill because of the remoteness of the site or the difficulty of an emergency environmental response.

Oil spills at sea are generally much more damaging than those on land, since they can spread for hundreds of nautical miles in a thin oil slick which can cover beaches with a thin coating of oil. This can kill sea birds, mammals, shellfish and other organisms it coats. Oil spills on land are more readily containable if a makeshift earth dam can be rapidly bulldozed around the spill site before most of the oil escapes, and land animals can avoid the oil more easily.

[1] One metric ton (tonne) of crude oil is roughly equal to 308 US gallons or 7.33 barrels approx.; 1 oil barrel (bbl) is equal to 35 imperial or 42 US gallons. Approximate conversion factors.

[2] Estimates for the amount of oil burned in the Kuwaiti oil fires range from 500,000,000 barrels (79,000,000 m^3)

to nearly 2,000,000,000 barrels (320,000,000 m^3). Between 605 and 732 wells were set ablaze, while many others were severely damaged and gushed uncontrolled for several months. It took over ten months to bring all of the wells under control. The fires alone were estimated to consume approximately 6,000,000 barrels (950,000 m^3) of oil per day at their peak.

[3] Oil spilled from sabotaged fields in Kuwait during the 1991 Persian Gulf War pooled in approximately 300 oil lakes, estimated by the Kuwaiti Oil Minister to contain approximately 25,000,000 to 50,000,000 barrels (7,900,000 m^3) of oil. According to the U.S. Geological Survey, this figure does not include the amount of oil absorbed by the ground, forming a layer of "tarcrete" over approximately five percent of the surface of Kuwait, fifty times the area occupied by the oil lakes.[5]

[4] Estimates for the Gulf War oil spill range from 4,000,000 to 11,000,000 barrels (1,700,000 m^3). The figure of 6,000,000 to 8,000,000 barrels (1,300,000 m^3) is the range adopted by the U.S. Environmental Protection Agency and the United Nations in the immediate aftermath of the war, 1991–1993, and is still current, as cited by NOAA and The New York Times in 2010.[9] This amount only includes oil discharged directly into the Persian Gulf by the retreating Iraqi forces from January 19 to 28, 1991. However, according to the U.N. report, oil from other sources not included in the official estimates continued to pour into the Persian Gulf through June, 1991. The amount of this oil was estimated to be at least several hundred thousand barrels, and may have factored into the estimates above 8,000,000 barrels (1,300,000 m^3).

11.2 Human impact

An oil spill represents an immediate fire hazard. The Kuwaiti oil fires produced air pollution that caused respiratory distress. The Deepwater Horizon explosion killed eleven oil rig workers. The fire resulting from the Lac-Mégantic derailment killed 47 and destroyed half of the town's centre.

Spilled oil can also contaminate drinking water supplies. For example, in 2013 two different oil spills contaminated water supplies for 300,000 in Miri, Malaysia;[27] 80,000 people in Coca, Ecuador,.[28] In 2000, springs were contaminated by an oil spill in Clark County, Kentucky.[29]

Contamination can have an economic impact on tourism and marine resource extraction industries. For example, the Deepwater Horizon oil spill impacted beach tourism and fishing along the Gulf Coast, and the responsible parties were required to compensate economic victims.

11.3 Environmental effects

Oil penetrates into the structure of the plumage of birds and the fur of mammals, reducing its insulating ability,

A Surf Scoter covered in oil as a result of the 2007 San Francisco Bay oil spill.

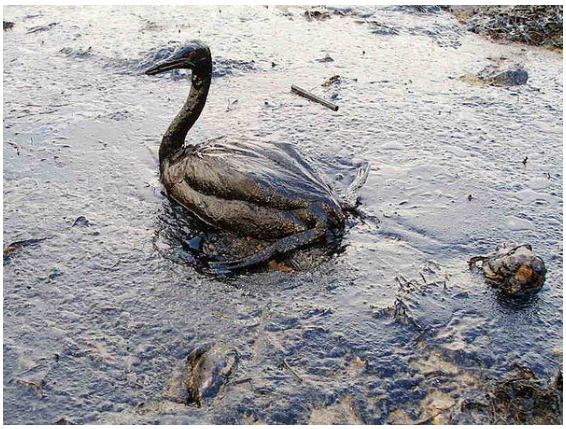

A bird covered in oil from the Black Sea oil spill.

and making them more vulnerable to temperature fluctuations and much less buoyant in the water.

Animals who rely on scent to find their babies or mothers cannot due to the strong scent of the oil. This causes a baby to be rejected and abandoned, leaving the babies to starve and eventually die. Oil can impair a bird's ability to fly, preventing it from foraging or escaping from predators. As they preen, birds may ingest the oil coating their feathers, irritating the digestive tract, altering liver function, and causing kidney damage. Together with their diminished foraging capacity, this can rapidly result in dehydration and metabolic imbalance. Some birds exposed to petroleum also experience changes in their hormonal balance, including changes in their luteinizing protein.[30] The majority of birds affected by oil spills die from complications without human intervention.[31][32] Some studies have suggested that less than one percent of oil-soaked birds survive, even after cleaning,[33] although the survival rate can also exceed ninety percent, as in the case of the Treasure oil spill.[34]

Heavily furred marine mammals exposed to oil spills are

affected in similar ways. Oil coats the fur of sea otters and seals, reducing its insulating effect, and leading to fluctuations in body temperature and hypothermia. Oil can also blind an animal, leaving it defenseless. The ingestion of oil causes dehydration and impairs the digestive process. Animals can be poisoned, and may die from oil entering the lungs or liver.

There are three kinds of oil-consuming bacteria. Sulfate-reducing bacteria (SRB) and acid-producing bacteria are anaerobic, while general aerobic bacteria (GAB) are aerobic. These bacteria occur naturally and will act to remove oil from an ecosystem, and their biomass will tend to replace other populations in the food chain.

11.4 Sources and rate of occurrence

A VLCC tanker can carry 2 million barrels (320,000 m^3) of crude oil. This is about eight times the amount spilled in the widely known *Exxon Valdez* incident. In this spill, the ship ran aground and dumped 10,800,000 US gallons (41,000 m^3) of oil into the ocean in March 1989. Despite efforts of scientists, managers, and volunteers over 400,000 seabirds, about 1,000 sea otters, and immense numbers of fish were killed.[35] Considering the volume of oil carried by sea, however, tanker owners' organisations often argue that the industry's safety record is excellent, with only a tiny fraction of a percentage of oil cargoes carried ever being spilled. The International Association of Independent Tanker Owners has observed that "accidental oil spills this decade have been at record low levels—one third of the previous decade and one tenth of the 1970s—at a time when oil transported has more than doubled since the mid 1980s."

Oil tankers are only one source of oil spills. According to the United States Coast Guard, 35.7% of the volume of oil spilled in the United States from 1991 to 2004 came from tank vessels (ships/barges), 27.6% from facilities and other non-vessels, 19.9% from non-tank vessels, and 9.3% from pipelines; 7.4% from mystery spills.[36] On the other hand, only 5% of the actual spills came from oil tankers, while 51.8% came from other kinds of vessels.[36]

The International Tanker Owners Pollution Federation has tracked 9,351 accidental spills that have occurred since 1974.[37] According to this study, most spills result from routine operations such as loading cargo, discharging cargo, and taking on fuel oil.[20] 91% of the operational oil spills are small, resulting in less than 7 metric tons per spill.[20] On the other hand, spills resulting from accidents like collisions, groundings, hull failures, and explosions are much larger, with 84% of these involving losses of over 700 metric tons.[20]

11.5 Cleanup and recovery

A U.S. Air Force Reserve plane sprays Corexit dispersant over the Deepwater Horizon oil spill in the Gulf of Mexico.

Clean-up efforts after the Exxon Valdez oil spill.

A US Navy oil spill response team drills with a "Harbour Buster high-speed oil containment system".

Cleanup and recovery from an oil spill is difficult and depends upon many factors, including the type of oil spilled, the temperature of the water (affecting evaporation and biodegradation), and the types of shorelines and beaches involved.[1]

Methods for cleaning up include:[38]

- Bioremediation: use of microorganisms[39] or

biological agents[40] to break down or remove oil; such as the bacteria Alcanivorax[41] or Methylocella Silvestris.[42]

- Bioremediation Accelerator: Oleophilic, hydrophobic chemical, containing no bacteria, which chemically and physically bonds to both soluble and insoluble hydrocarbons. The bioremediation accelerator acts as a herding agent in water and on the surface, floating molecules to the surface of the water, including solubles such as phenols and BTEX, forming gel-like agglomerations. Undetectable levels of hydrocarbons can be obtained in produced water and manageable water columns. By overspraying sheen with bioremediation accelerator, sheen is eliminated within minutes. Whether applied on land or on water, the nutrient-rich emulsion creates a bloom of local, indigenous, pre-existing, hydrocarbon-consuming bacteria. Those specific bacteria break down the hydrocarbons into water and carbon dioxide, with EPA tests showing 98% of alkanes biodegraded in 28 days; and aromatics being biodegraded 200 times faster than in nature they also sometimes use the hydrofireboom to clean the oil up by taking it away from most of the oil and burning it.[43]

- Controlled burning can effectively reduce the amount of oil in water, if done properly.[44] But it can only be done in low wind, and can cause air pollution.[45]

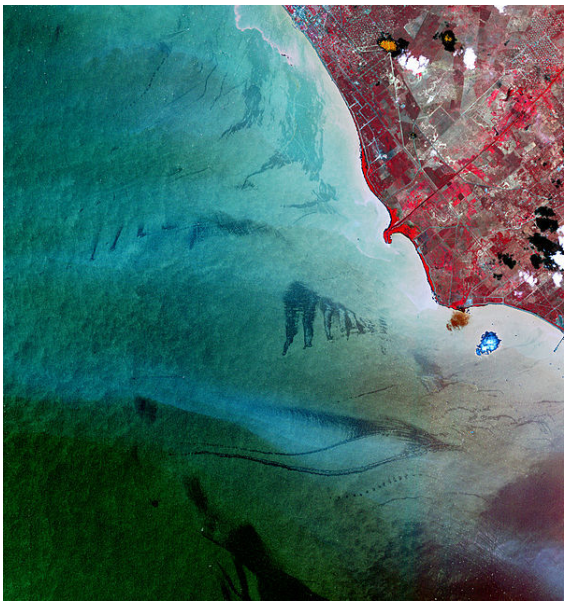

Oil slicks on Lake Maracaibo.

- Dispersants can be used to dissipate oil slicks.[46] A dispersant is either a non-surface active polymer or a surface-active substance added to a suspension, usually a colloid, to improve the separation of particles

Volunteers cleaning up the aftermath of the Prestige oil spill.

and to prevent settling or clumping. They may rapidly disperse large amounts of certain oil types from the sea surface by transferring it into the water column. They will cause the oil slick to break up and form water-soluble micelles that are rapidly diluted. The oil is then effectively spread throughout a larger volume of water than the surface from where the oil was dispersed. They can also delay the formation of persistent oil-in-water emulsions. However, laboratory experiments showed that dispersants increased toxic hydrocarbon levels in fish by a factor of up to 100 and may kill fish eggs.[47] Dispersed oil droplets infiltrate into deeper water and can lethally contaminate coral. Research indicates that some dispersants are toxic to corals.[48] A 2012 study found that Corexit dispersant had increased the toxicity of oil by up to 52 times.[49]

- Watch and wait: in some cases, natural attenuation of oil may be most appropriate, due to the invasive nature of facilitated methods of remediation, particularly in ecologically sensitive areas such as wetlands.[50]

- Dredging: for oils dispersed with detergents and other oils denser than water.

- Skimming: Requires calm waters at all times during the process.

- Solidifying: Solidifiers are composed of dry hydrophobic polymers that both adsorb and absorb. They clean up oil spills by changing the physical state of spilled oil from liquid to a semi-solid or a rubber-like material that floats on water. Solidifiers are insoluble in water, therefore the removal of the solidified oil is easy and the oil will not leach out. Solidifiers have been proven to be relatively non-toxic to aquatic and wild life and have been proven to suppress harmful vapors commonly associated with hydrocarbons such as Benzene, Xylene, Methyl Ethyl, Acetone and Naphtha. The reaction time for solidification of oil is controlled by the surf area or size of the polymer as well as the viscosity of the oil. Some

solidifier product manufactures claim the solidified oil can be disposed of in landfills, recycled as an additive in asphalt or rubber products, or burned as a low ash fuel. A solidifier called C.I.Agent (manufactured by C.I.Agent Solutions of Louisville, Kentucky) is being used by BP in granular form, as well as in Marine and Sheen Booms at Dauphin Island and Fort Morgan, Alabama, to aid in the Deepwater Horizon oil spill cleanup.

- Vacuum and centrifuge: oil can be sucked up along with the water, and then a centrifuge can be used to separate the oil from the water - allowing a tanker to be filled with near pure oil. Usually, the water is returned to the sea, making the process more efficient, but allowing small amounts of oil to go back as well. This issue has hampered the use of centrifuges due to a United States regulation limiting the amount of oil in water returned to the sea.[51]
- Beach Raking: coagulated oil that is left on the beach can be picked up by SURF RAKE beach cleaning machines by H. Barber and Sons.[52]

Equipment used includes:[44]

- Booms: large floating barriers that round up oil and lift the oil off the water
- Skimmers: skim the oil
- Sorbents: large absorbents that absorb oil
- Chemical and biological agents: helps to break down the oil
- Vacuums: remove oil from beaches and water surface
- Shovels and other road equipment: typically used to clean up oil on beaches

11.5.1 Prevention

Further information: Offshore oil spill prevention and response

- Secondary containment - methods to prevent releases of oil or hydrocarbons into environment.
- Oil Spill Prevention Containment and Countermeasures (SPCC) program by the United States Environmental Protection Agency.
- Double-hulling - build double hulls into vessels, which reduces the risk and severity of a spill in case of a collision or grounding. Existing single-hull vessels can also be rebuilt to have a double hull.
- Thick-hulled railroad transport tanks[53]

Spill response procedures should include elements such as;

- A listing of appropriate protective clothing, safety equipment, and cleanup materials required

for spill cleanup (gloves, respirators, etc.) and an explanation of their proper use;

- Appropriate evacuation zones and procedures;
- Availability of fire suppression equipment;
- Disposal containers for spill cleanup materials; and
- The first aid procedures that might be required.

[54]

11.6 Environmental Sensitivity Index (ESI) mapping

Environmental Sensitivity Index (ESI) maps are used to identify sensitive shoreline resources prior to an oil spill event in order to set priorities for protection and plan cleanup strategies.[55][56] By planning spill response ahead of time, the impact on the environment can be minimized or prevented. Environmental sensitivity index maps are basically made up of information within the following three categories: shoreline type, and biological and human-use resources.[57]

11.6.1 Shoreline type

Shoreline type is classified by rank depending on how easy the garet would be to clean up, how long the oil would persist, and how sensitive the shoreline is.[58] The floating oil slicks put the shoreline at particular risk when they eventually come ashore, covering the substrate with oil. The differing substrates between shoreline types vary in their response to oiling, and influence the type of cleanup that will be required to effectively decontaminate the shoreline. In 1995, the US National Oceanic and Atmospheric Administration extended ESI maps to lakes, rivers, and estuary shoreline types.[57] The exposure the shoreline has to wave energy and tides, substrate type, and slope of the shoreline are also taken into account—in addition to biological productivity and sensitivity. The productivity of the shoreline habitat is also taken into account when determining ESI ranking.[59] Mangroves and marshes tend to have higher ESI rankings due to the potentially long-lasting and damaging effects of both the oil contamination and cleanup actions. Impermeable and exposed surfaces with high wave action are ranked lower due to the reflecting waves keeping oil from coming onshore, and the speed at which natural processes will remove the oil.

11.6.2 Biological resources

Habitats of plants and animals that may be at risk from oil spills are referred to as "elements" and are divided by functional group. Further classification divides each element into species groups with similar life histories and behaviors relative to their vulnerability to oil spills. There are eight element groups: Birds, Reptiles, Amphibians, Fish, Invertebrates, Habitats and Plants, Wetlands, and Marine Mammals and Terrestrial Mammals. Element groups are further divided into sub-groups, for example, the 'marine mammals' element group is divided into dolphins, manatees, pinnipeds (seals, sea lions & walruses), polar bears, sea otters and whales.[57][59] Problems taken into consideration when ranking biological resources include the observance of a large number of individuals in a small area, whether special life stages occur ashore (nesting or molting), and whether there are species present that are threatened, endangered or rare.[60]

11.6.3 Human-use resources

Human use resources are divided into four major classifications; archaeological importance or cultural resource site, high-use recreational areas or shoreline access points, important protected management areas, or resource origins.[57][60] Some examples include airports, diving sites, popular beach sites, marinas, natural reserves or marine sanctuaries.

11.7 Estimating the volume of a spill

By observing the thickness of the film of oil and its appearance on the surface of the water, it is possible to estimate the quantity of oil spilled. If the surface area of the spill is also known, the total volume of the oil can be calculated.[61]

Oil spill model systems are used by industry and government to assist in planning and emergency decision making. Of critical importance for the skill of the oil spill model prediction is the adequate description of the wind and current fields. There is a worldwide oil spill modelling (WOSM) program.[62] Tracking the scope of an oil spill may also involve verifying that hydrocarbons collected during an ongoing spill are derived from the active spill or some other source. This can involve sophisticated analytical chemistry focused on finger printing an oil source based on the complex mixture of substances present. Largely, these will be various hydrocarbons, among the most useful being polyaromatic hydrocarbons. In addition, both oxygen and nitrogen heterocyclic hydrocarbons, such as parent and alkyl homologues of carbazole, quinoline, and pyridine, are present in many crude oils. As a result, these compounds have great potential to supplement the existing suite of hydrocarbons targets to fine tune source tracking of petroleum spills. Such analysis can also be used to follow weathering and degradation of crude spills.[63]

11.8 See also

- Automated Data Inquiry for Oil Spills
- Environmental issues with petroleum
- Environmental issues with shipping
- LNG spill
- Low-temperature thermal desorption
- National Oil and Hazardous Substances Pollution Contingency Plan
- Ohmsett (Oil and Hazardous Materials Simulated Environmental Test Tank)
- Oil Pollution Act of 1990 (in the US)
- Oil well
- Penguin sweater
- Project Deep Spill, the first intentional deepwater oil and gas spill
- *Pseudomonas putida* (used for degrading oil)
- S-200 (fertilizer)
- Spill containment
- Tarball

11.9 References

[1] "Lingering Lessons of the Exxon Valdez Oil Spill". Commondreams.org. 2004-03-22. Retrieved 2012-08-27.

[2] "Hindsight and Foresight, 20 Years After the Exxon Valdez Spill". NOAA. 2010-03-16. Retrieved 2010-04-30. |first1= missing |last1= in Authors list (help)

[3] United States Department of Defense *Environmental Exposure Report: Oil Well Fires* (updated August 2, 2000)

[4] CNN.com, *Kuwait still recovering from Gulf War fires*, 3 Jan. 2003.

[5] United States Geological Survey, Campbell, Robert Wellman, ed. 1999. *Iraq and Kuwait: 1972, 1990, 1991, 1997.* Earthshots: Satellite Images of Environmental Change. U.S. Geological Survey. http://earthshots.usgs.gov, revised 14 Feb. 1999.

[6] United Nations, *Updated Scientific Report on the Environmental Effects of the Conflict between Iraq and Kuwait*, 8 Mar. 1993.

[7] National Aeronautics and Space Administration, Goddard Space Flight Center News, *1991 Kuwait Oil Fires*, 21 Mar. 2003.

[8] Harvey, Steve (2010-06-13). "California's legendary oil spill". Los Angeles Times. Retrieved 2010-07-14.

[9] *Gulf Oil Spill Is Bad, but How Bad?*, last updated 20 May 2010.

[10] United States Environmental Protection Agency, *Report To Congress United States Gulf Environmental Technical Assistance From January 27 - July 31 1991*

[11] National Oceanic and Atmospheric Administration, Office of Response and Restoration, Emergency Response Division, Incident News: Arabian Gulf Spills, updated 18 May 2010.

[12] Campbell Robertson /Clifford Krauss (2 August 2010). "Gulf Spill Is the Largest of Its Kind, Scientists Say". *The New York Times*. *New York Times*. Retrieved 2 August 2010.

[13] CNN (1 July 2010). "Oil disaster by the numbers". *CNN*. Retrieved 1 July 2010.

[14] Consumer Energy Report (20 June 2010). "Internal Documents: BP Estimates Oil Spill Rate up to 100,000 Barrels Per Day". *Consumer Energy Report*. Retrieved 20 June 2010.

[15] "Big Oil Plans Rapid Response to Future Spills". Abcnews.go.com. Retrieved 2012-08-27.

[16] Khatchadourian, Raffi (March 14, 2011). "The Gulf War". *The New Yorker*.

[17] "IXTOC I". National Oceanic and Atmospheric Administration. Retrieved 2008-11-03.

[18] "Ixtoc 1 oil spill: flaking of surface mousse in the Gulf of Mexico". Nature Publishing Group. Retrieved 2008-11-03.

[19] John S. Patton, Mark W. Rigler, Paul D. Boehm & David L. Fiest (1981-03-19). "Ixtoc 1 oil spill: flaking of surface mousse in the Gulf of Mexico". *NPG (Nature Publishing Group)*. Retrieved 2007-07-29.

[20] "Major Oil Spills". International Tanker Owners Pollution Federation. Retrieved 2008-11-02.

[21] "Atlantic Empress". Centre de Documentation de Recherche et d'Expérimentations. Retrieved 2008-11-10.

[22] "Tanker Incidents". Retrieved 2009-07-19.

[23] "Oil Spill History". The Mariner Group. Retrieved 2008-11-02.

[24] "Oil Spills and Disasters". Retrieved 2008-11-16.

[25] "Amoco Cadiz". National Oceanic and Atmospheric Administration. Retrieved 2008-11-16.

[26]

[27] http://www.thestar.com.my/News/Nation/2012/03/05/Oil-spill-disrupts-water-supply.aspx

[28] Ecuador oil spill threatens Brazilian water supply

[29] Kentucky Crude Oil Spill may reach river, contaminate drinking water

[30] C. Michael Hogan (2008)., *"Magellanic Penguin"*, It can take over 1 year to solve the problem of an oil spill. GlobalTwitcher.com, ed. N. Stromberg.

[31] Dunnet, G., Crisp, D., Conan, G., Bourne, W. (1982) "Oil Pollution and Seabird Populations [and Discussion]" Philosophical Transactions of the Royal Society of London. B 297(1087): 413–427

[32] Untold Seabird Mortality due to Marine Oil Pollution, Elements Online Environmental Magazine.

[33] "Expert Recommends Killing Oil-Soaked Birds". *Spiegel Online*. May 6, 2010. Retrieved August 1, 2011.

[34] AC Wolfaardt, AJ Williams, LG Underhill, RJM Crawford & PA Whittington (2009): Review of the rescue, rehabilitation and restoration of oiled seabirds in South Africa, especially African penguins Spheniscus demersus and Cape gannets Morus capegnsis, 1983–2005, African Journal of Marine Science, 31:1, 31-54

[35] Panetta, L. E. (Chair) (2003). America's living oceans: charting a course for sea change [Electronic Version, CD] Pew Oceans Commission.

[36] United States Coast Guard (2007). "Cumulative Spill Data and Graphics". United States Coast Guard. Archived from the original on 2008-10-08. Retrieved 2008-04-10.

[37] International Tanker Owners Pollution Federation (2008). "Oil Tanker Spill Information Pack". London: International Tanker Owners Pollution Federation. Retrieved 2008-10-08.

[38] Oil spill cleanup technology Patents and patent applications

[39] "The Environmental Literacy Council - Oil Spills". Enviroliteracy.org. 2008-06-25. Retrieved 2010-06-16.

[40] "Biological Agents – Emergency Management – US EPA".

[41] , Kasai, Y et al. "Predominant Growth of Alcanivorax Strains in Oil-contaminated and Nutrient-supplemented Sea Water." Environmental Microbiology 4.3 (2002): 141-47.

[42] "Oil and natural gas eating bacteria to clear-up spills". *www.oilandgastechnology.net*. April 30, 2014.

[43] "S-200 | NCP Product Schedule | Emergency Management | US EPA". Epa.gov. Retrieved 2010-06-16.

[44] "Emergency Response: Responding to Oil Spills". *Office of Response and Restoration*. National Oceanic and Atmospheric Administration. 2007-06-20.

[45] "Oil Spills". Library.thinkquest.org. Retrieved 2012-08-27.

[46] "Spill Response - Dispersants". International Tanker Operators Pollution Federation Limited. Retrieved 2010-05-03.

[47] "Spill Response - Dispersants Kill Fish Eggs". journal Environmental Toxicology and Chemistry. Retrieved 2010-05-21.

[48] Barry, Carolyn (2007). Slick Death: Oil-spill treatment kills coral, *Science News* vol. 172, p. 67.

[49] Dispersant makes oil 52 times more toxic - Technology & science - Science - LiveScience | NBC News

[50] Pezeshki, S. R., Hester, M. W., Lin, Q. & Nyman, J. A. (2000). The effects of oil spill clean-up on dominant US Gulf coast marsh macrophytes: a review. Environmental Pollution. 108: 129-139.

[51] Fountain, Henry (2010-06-24). "Advances in Oil Spill Cleanup Lag Since Valdez". New York Times. Retrieved 2010-07-05.

[52] Iseppi, Veronica (2014-08-29). "Oil Spill Cleanup". H. Barber & Sons, Inc. Retrieved 2014-08-29.

[53] Quebec tragedy unlikely to slow oil shipments via rail - Business - The Boston Globe

[54] "Oil Spill Response Procedure". Chemstore UK. Retrieved 2014-02-25.

[55] "Environmental Sensitivity Index (ESI) Maps". Retrieved 2010-05-27.

[56] "NOAA's Ocean Service Office of Response and Restoration". Response.restoration.noaa.gov. Retrieved 2010-06-16.

[57] NOAA (2002). Environmental Sensitivity Index Guidelines, version 3.0. NOAA Technical Memorandum NOS OR&R 11. Seattle: Hazardous Response and Assessment Division, National Oceanic and Atmospheric Administration, 129p.

[58] Gundlach, E.R. and M.O. Hayes (1978). Vulnerability of Coastal Environments to Oil Spill Impacts. Marine Technology Society. 12 (4): 18-27.

[59] NOAA (2008). Introduction to Environmental Sensitivity Index maps. NOAA Technical Manual. Seattle: Hazardous Response and Assessment Division, National Oceanic and Atmospheric Administration, 56p.

[60] IMO/IPIECA (1994). Sensitivity Mapping for Oil Spill Response. International Maritime Organization/ International Petroleum Industry Environmental Conservation Association Report Series, Volume 1. 22p.

[61] *Metcalf & Eddy. Wastewater Engineering, Treatment and Reuse. 4th ed. New York: McGraw-Hill, 2003. 98.*

[62] Anderson, E.L., E. Howlett, K. Jayko, V. Kolluru, M. Reed, and M. Spaulding. 1993. The worldwide oil spill model (WOSM): an overview. Pp. 627–646 in Proceedings of the 16th Arctic and Marine Oil Spill Program, Technical Seminar. Ottawa, Ontario: Environment Canada.

[63] Wang, Z., M. Fingas, and D.S. Page. 1999. Oil spill identification. Journal of Chromatography A. 843: 369-411. doi:10.1016/S0021-9673(99)00120-X.

11.10 Further reading

Media related to Oil spills at Wikimedia Commons

- *The World Almanac and Book of Facts*, 2004
- *Oil Spill Case Histories 1967-1991*, NOAA/Hazardous Materials and Response Division, Seattle WA, 1992
- *Nelson-Smith, Oil Pollution and Marine Ecology, Elek Scientific, London, 1972; Plenum, New York, 1973*

Chapter 12

Marine pollution

While marine pollution can be obvious, as with the marine debris shown above, it is often the pollutants that cannot be seen that cause most harm.

Marine pollution occurs when harmful, or potentially harmful, effects result from the entry into the ocean of chemicals, particles, industrial, agricultural and residential waste, noise, or the spread of invasive organisms. Most sources of marine pollution are land based. The pollution often comes from nonpoint sources such as agricultural runoff, wind-blown debris and dust. Nutrient pollution, a form of water pollution, refers to contamination by excessive inputs of nutrients. It is a primary cause of eutrophication of surface waters, in which excess nutrients, usually nitrogen or phosphorus, stimulate algae growth.

Many potentially toxic chemicals adhere to tiny particles which are then taken up by plankton and benthos animals, most of which are either deposit or filter feeders. In this way, the toxins are concentrated upward within ocean food chains. Many particles combine chemically in a manner highly depletive of oxygen, causing estuaries to become anoxic.

When pesticides are incorporated into the marine ecosystem, they quickly become absorbed into marine food webs. Once in the food webs, these pesticides can cause mutations, as well as diseases, which can be harmful to humans as well as the entire food web.

Toxic metals can also be introduced into marine food webs. These can cause a change to tissue matter, biochemistry, behaviour, reproduction, and suppress growth in marine life. Also, many animal feeds have a high fish meal or fish hydrolysate content. In this way, marine toxins can be transferred to land animals, and appear later in meat and dairy products.

12.1 History

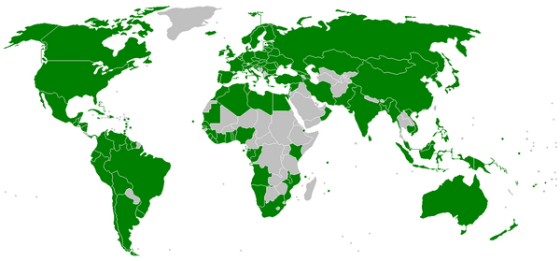

Parties to the MARPOL 73/78 convention on marine pollution

Although marine pollution has a long history, significant international laws to counter it were only enacted in the twentieth century. Marine pollution was a concern during several United Nations Conferences on the Law of the Sea beginning in the 1950s. Most scientists believed that the oceans were so vast that they had unlimited ability to dilute, and thus render pollution harmless.

In the late 1950s and early 1960s, there were several controversies about dumping radioactive waste off the

coasts of the United States by companies licensed by the Atomic Energy Commission, into the Irish Sea from the British reprocessing facility at Windscale, and into the Mediterranean Sea by the French Commissariat à l'Energie Atomique. After the Mediterranean Sea controversy, for example, Jacques Cousteau became a worldwide figure in the campaign to stop marine pollution. Marine pollution made further international headlines after the 1967 crash of the oil tanker Torrey Canyon, and after the 1969 Santa Barbara oil spill off the coast of California.

Marine pollution was a major area of discussion during the 1972 United Nations Conference on the Human Environment, held in Stockholm. That year also saw the signing of the Convention on the Prevention of Marine Pollution by Dumping of Wastes and Other Matter, sometimes called the London Convention. The London Convention did not ban marine pollution, but it established black and gray lists for substances to be banned (black) or regulated by national authorities (gray). Cyanide and high-level radioactive waste, for example, were put on the black list. The London Convention applied only to waste dumped from ships, and thus did nothing to regulate waste discharged as liquids from pipelines.[1]

12.2 Pathways of pollution

See also: Water pollution § Transport and chemical reactions of water pollutants

There are many different ways to categorize, and examine the inputs of pollution into our marine ecosystems. Patin (n.d.) notes that generally there are three main types of inputs of pollution into the ocean: direct discharge of waste into the oceans, runoff into the waters due to rain, and pollutants that are released from the atmosphere.

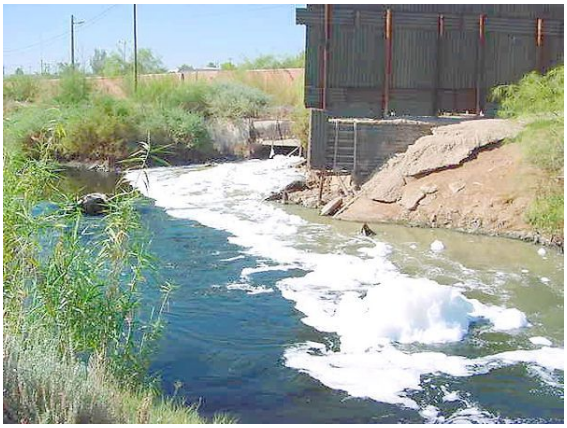

Septic river.

One common path of entry by contaminants to the sea are rivers. The evaporation of water from oceans exceeds precipitation. The balance is restored by rain over the continents entering rivers and then being returned to the sea. The Hudson in New York State and the Raritan in New Jersey, which empty at the northern and southern ends of Staten Island, are a source of mercury contamination of zooplankton (copepods) in the open ocean. The highest concentration in the filter-feeding copepods is not at the mouths of these rivers but 70 miles south, nearer Atlantic City, because water flows close to the coast. It takes a few days before toxins are taken up by the plankton.

Pollution is often classed as point source or nonpoint source pollution. Point source pollution occurs when there is a single, identifiable, and localized source of the pollution. An example is directly discharging sewage and industrial waste into the ocean. Pollution such as this occurs particularly in developing nations. Nonpoint source pollution occurs when the pollution comes from ill-defined and diffuse sources. These can be difficult to regulate. Agricultural runoff and wind blown debris are prime examples.

12.2.1 Direct discharge

Acid mine drainage in the Rio Tinto River.

See also: Sewerage, Industrial waste and Environmental issues with mining

Pollutants enter rivers and the sea directly from urban sewerage and industrial waste discharges, sometimes in the form of hazardous and toxic wastes.

Inland mining for copper, gold. etc., is another source of marine pollution. Most of the pollution is simply soil, which ends up in rivers flowing to the sea. However, some minerals discharged in the course of the mining can cause problems, such as copper, a common industrial pollutant, which can interfere with the life history and development of coral polyps.[2] Mining has a poor environmental track record. For example, according to the United States Environmental Protection Agency, mining has contaminated portions of the headwaters of over 40% of watersheds in the western continental US.[3] Much of this pollution finishes up in the sea.

12.2.2 Land runoff

Main article: Surface runoff
See also: Urban runoff, Stormwater and Nutrient pollution

Surface runoff from farming, as well as urban runoff and runoff from the construction of roads, buildings, ports, channels, and harbours, can carry soil and particles laden with carbon, nitrogen, phosphorus, and minerals. This nutrient-rich water can cause fleshy algae and phytoplankton to thrive in coastal areas; known as algal blooms, which have the potential to create hypoxic conditions by using all available oxygen.

Polluted runoff from roads and highways can be a significant source of water pollution in coastal areas. About 75 percent of the toxic chemicals that flow into Puget Sound are carried by stormwater that runs off paved roads and driveways, rooftops, yards and other developed land.[4]

12.2.3 Ship pollution

Main article: Ship pollution
See also: Ballast water discharge and the environment
Ships can pollute waterways and oceans in many ways.

A cargo ship pumps ballast water over the side.

Oil spills can have devastating effects. While being toxic to marine life, polycyclic aromatic hydrocarbons (PAHs), found in crude oil, are very difficult to clean up, and last for years in the sediment and marine environment.[5]

Oil spills are probably the most emotive of marine pollution events. However, while a tanker wreck may result in extensive newspaper headlines, much of the oil in the world's seas comes from other smaller sources, such as tankers discharging ballast water from oil tanks used on return ships, leaking pipelines or engine oil disposed of down sewers. [6]

Discharge of cargo residues from bulk carriers can pollute ports, waterways and oceans. In many instances vessels intentionally discharge illegal wastes despite foreign and domestic regulation prohibiting such actions. It has been estimated that container ships lose over 10,000 containers at sea each year (usually during storms).[7] Ships also create noise pollution that disturbs natural wildlife, and water from ballast tanks can spread harmful algae and other invasive species.[8]

Ballast water taken up at sea and released in port is a major source of unwanted exotic marine life. The invasive freshwater zebra mussels, native to the Black, Caspian and Azov seas, were probably transported to the Great Lakes via ballast water from a transoceanic vessel.[9] Meinesz believes that one of the worst cases of a single invasive species causing harm to an ecosystem can be attributed to a seemingly harmless jellyfish. *Mnemiopsis leidyi*, a species of comb jellyfish that spread so it now inhabits estuaries in many parts of the world. It was first introduced in 1982, and thought to have been transported to the Black Sea in a ship's ballast water. The population of the jellyfish shot up exponentially and, by 1988, it was wreaking havoc upon the local fishing industry. "The anchovy catch fell from 204,000 tons in 1984 to 200 tons in 1993; sprat from 24,600 tons in 1984 to 12,000 tons in 1993; horse mackerel from 4,000 tons in 1984 to zero in 1993."[8] Now that the jellyfish have exhausted the zooplankton, including fish larvae, their numbers have fallen dramatically, yet they continue to maintain a stranglehold on the ecosystem.

Invasive species can take over once occupied areas, facilitate the spread of new diseases, introduce new genetic material, alter underwater seascapes and jeopardize the ability of native species to obtain food. Invasive species are responsible for about $138 billion annually in lost revenue and management costs in the US alone.[10]

12.2.4 Atmospheric pollution

Another pathway of pollution occurs through the atmosphere. Wind blown dust and debris, including plastic bags, are blown seaward from landfills and other areas. Dust from the Sahara moving around the southern periphery of the subtropical ridge moves into the Caribbean and Florida during the warm season as the ridge builds and moves northward through the subtropical Atlantic. Dust can also be attributed to a global transport from the Gobi and Taklamakan deserts across Korea, Japan, and the Northern Pacific to the Hawaiian Islands.[12] Since 1970,

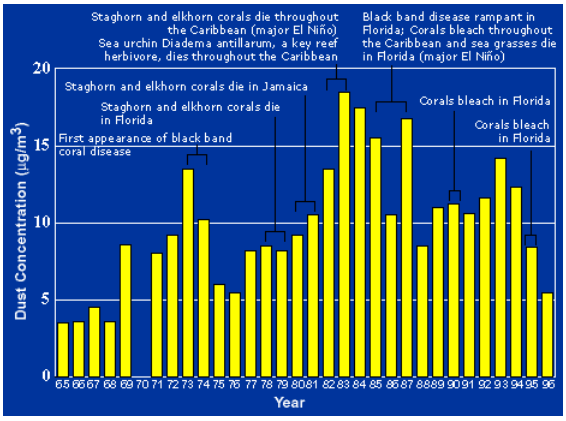

Graph linking atmospheric dust to various coral deaths across the Caribbean Sea and Florida[11]

dust outbreaks have worsened due to periods of drought in Africa. There is a large variability in dust transport to the Caribbean and Florida from year to year;[13] however, the flux is greater during positive phases of the North Atlantic Oscillation.[14] The USGS links dust events to a decline in the health of coral reefs across the Caribbean and Florida, primarily since the 1970s.[15]

Climate change is raising ocean temperatures[16] and raising levels of carbon dioxide in the atmosphere. These rising levels of carbon dioxide are acidifying the oceans.[17] This, in turn, is altering aquatic ecosystems and modifying fish distributions,[18] with impacts on the sustainability of fisheries and the livelihoods of the communities that depend on them. Healthy ocean ecosystems are also important for the mitigation of climate change.[19]

12.2.5 Deep sea mining

Main article: Deep sea mining

Deep sea mining is a relatively new mineral retrieval process that takes place on the ocean floor. Ocean mining sites are usually around large areas of polymetallic nodules or active and extinct hydrothermal vents at about 1,400 - 3,700 meters below the ocean's surface.[20] The vents create sulfide deposits, which contain precious metals such as silver, gold, copper, manganese, cobalt, and zinc.[21][22] The deposits are mined using either hydraulic pumps or bucket systems that take ore to the surface to be processed. As with all mining operations, deep sea mining raises questions about environmental damages to the surrounding areas

Because deep sea mining is a relatively new field, the complete consequences of full scale mining operations are unknown. However, experts are certain that removal of parts of the sea floor will result in disturbances to the benthic layer, increased toxicity of the water column and sediment plumes from tailings.[21] Removing parts of the sea floor disturbs the habitat of benthic organisms, possibly, depending on the type of mining and location, causing permanent disturbances.[20] Aside from direct impact of mining the area, leakage, spills and corrosion would alter the mining area's chemical makeup.

Among the impacts of deep sea mining, sediment plumes could have the greatest impact. Plumes are caused when the tailings from mining (usually fine particles) are dumped back into the ocean, creating a cloud of particles floating in the water. Two types of plumes occur: near bottom plumes and surface plumes.[20] Near bottom plumes occur when the tailings are pumped back down to the mining site. The floating particles increase the turbidity, or cloudiness, of the water, clogging filter-feeding apparatuses used by benthic organisms.[23] Surface plumes cause a more serious problem. Depending on the size of the particles and water currents the plumes could spread over vast areas.[20][24] The plumes could impact zooplankton and light penetration, in turn affecting the food web of the area.[20][24]

12.3 Types of pollution

12.3.1 Acidification

Main article: Ocean acidification

The oceans are normally a natural carbon sink, absorbing

Island with fringing reef in the Maldives. Coral reefs are dying around the world.[25]

carbon dioxide from the atmosphere. Because the levels of atmospheric carbon dioxide are increasing, the oceans are becoming more acidic.[26][27] The potential consequences of ocean acidification are not fully understood, but there are concerns that structures made of calcium carbonate may become vulnerable to dissolution, affecting corals and the ability of shellfish to form shells.[28]

Oceans and coastal ecosystems play an important role in the global carbon cycle and have removed about 25% of the carbon dioxide emitted by human activities between 2000 and 2007 and about half the anthropogenic CO_2 re-

leased since the start of the industrial revolution. Rising ocean temperatures and ocean acidification means that the capacity of the ocean carbon sink will gradually get weaker,[29] giving rise to global concerns expressed in the Monaco[30] and Manado[31] Declarations.

A report from NOAA scientists published in the journal Science in May 2008 found that large amounts of relatively acidified water are upwelling to within four miles of the Pacific continental shelf area of North America. This area is a critical zone where most local marine life lives or is born. While the paper dealt only with areas from Vancouver to northern California, other continental shelf areas may be experiencing similar effects.[32]

A related issue is the methane clathrate reservoirs found under sediments on the ocean floors. These trap large amounts of the greenhouse gas methane, which ocean warming has the potential to release. In 2004 the global inventory of ocean methane clathrates was estimated to occupy between one and five million cubic kilometres.[33] If all these clathrates were to be spread uniformly across the ocean floor, this would translate to a thickness between three and fourteen metres.[34] This estimate corresponds to 500-2500 gigatonnes carbon (Gt C), and can be compared with the 5000 Gt C estimated for all other fossil fuel reserves.[33][35]

12.3.2 Eutrophication

Main article: Eutrophication
See also: Nutrient pollution

Eutrophication is an increase in chemical nutrients, typically compounds containing nitrogen or phosphorus, in an ecosystem. It can result in an increase in the ecosystem's primary productivity (excessive plant growth and decay), and further effects including lack of oxygen and severe reductions in water quality, fish, and other animal populations.

Polluted lagoon.

The biggest culprit are rivers that empty into the ocean, and with it the many chemicals used as fertilizers in agriculture as well as waste from livestock and humans. An excess of oxygen depleting chemicals in the water can lead to hypoxia and the creation of a dead zone.[36]

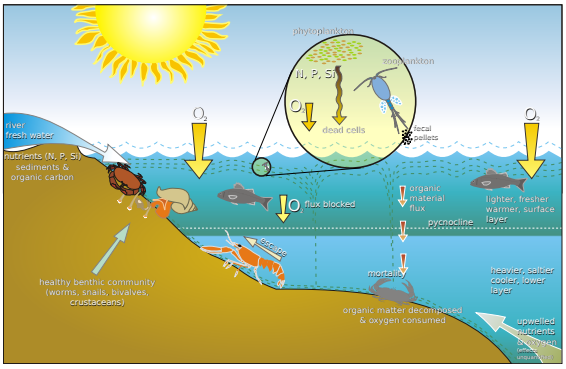

Effect of eutrophication on marine benthic life

Estuaries tend to be naturally eutrophic because land-derived nutrients are concentrated where runoff enters the marine environment in a confined channel. The World Resources Institute has identified 375 hypoxic coastal zones around the world, concentrated in coastal areas in Western Europe, the Eastern and Southern coasts of the US, and East Asia, particularly in Japan.[37] In the ocean, there are frequent red tide algae blooms[38] that kill fish and marine mammals and cause respiratory problems in humans and some domestic animals when the blooms reach close to shore.

In addition to land runoff, atmospheric anthropogenic fixed nitrogen can enter the open ocean. A study in 2008 found that this could account for around one third of the ocean's external (non-recycled) nitrogen supply and up to three per cent of the annual new marine biological production.[39] It has been suggested that accumulating reactive nitrogen in the environment may have consequences as serious as putting carbon dioxide in the atmosphere.[40]

One proposed solution to eutrophication in estuaries is to restore shellfish populations, such as oysters. Oyster reefs remove nitrogen from the water column and filter out suspended solids, subsequently reducing the likelihood or extent of harmful algal blooms or anoxic conditions.[41] Filter feeding activity is considered beneficial to water quality[42] by controlling phytoplankton density and sequestering nutrients, which can be removed from the system through shellfish harvest, buried in the sediments, or lost through denitrification.[43][44] Foundational work toward the idea of improving marine water quality through shellfish cultivation to was conducted by Odd Lindahl et al., using mussels in Sweden.[45]

12.3.3 Plastic debris

Main article: Marine debris

Marine debris is mainly discarded human rubbish which

A mute swan builds a nest using plastic garbage.

floats on, or is suspended in the ocean. Eighty percent of marine debris is plastic - a component that has been rapidly accumulating since the end of World War II.[46] The mass of plastic in the oceans may be as high as one hundred million metric tons.[47]

Discarded plastic bags, six pack rings and other forms of plastic waste which finish up in the ocean present dangers to wildlife and fisheries.[48] Aquatic life can be threatened through entanglement, suffocation, and ingestion.[49][50][51] Fishing nets, usually made of plastic, can be left or lost in the ocean by fishermen. Known as ghost nets, these entangle fish, dolphins, sea turtles, sharks, dugongs, crocodiles, seabirds, crabs, and other creatures, restricting movement, causing starvation, laceration and infection, and, in those that need to return to the surface to breathe, suffocation.[52]

Remains of an albatross containing ingested flotsam

Many animals that live on or in the sea consume flotsam by mistake, as it often looks similar to their natural prey.[53] Plastic debris, when bulky or tangled, is difficult to pass, and may become permanently lodged in the digestive tracts of these animals. Especially when evolutionary adaptions make it impossible for the likes of turtles to reject plastic bags, which resemble jellyfish when immersed in water, as they have a system in their throat to stop slippery foods from otherwise escaping.[54] Thereby blocking the passage of food and causing death through starvation or infection.[55][56]

Plastics accumulate because they don't biodegrade in the way many other substances do. They will photodegrade on exposure to the sun, but they do so properly only under dry conditions, and water inhibits this process.[57] In marine environments, photodegraded plastic disintegrates into ever smaller pieces while remaining polymers, even down to the molecular level. When floating plastic particles photodegrade down to zooplankton sizes, jellyfish attempt to consume them, and in this way the plastic enters the ocean food chain. [58] [59] Many of these long-lasting pieces end up in the stomachs of marine birds and animals,[60] including sea turtles, and black-footed albatross.[61]

Marine debris on Kamilo Beach, Hawaii, washed up from the Great Pacific Garbage Patch

Plastic debris tends to accumulate at the centre of ocean gyres. In particular, the Great Pacific Garbage Patch has a very high level of plastic particulate suspended in the upper water column. In samples taken in 1999, the mass of plastic exceeded that of zooplankton (the dominant animal life in the area) by a factor of six.[46][62] Midway Atoll, in common with all the Hawaiian Islands, receives substantial amounts of debris from the garbage patch. Ninety percent plastic, this debris accumulates on the beaches of Midway where it becomes a hazard to the bird population of the island. Midway Atoll is home to two-thirds (1.5 million) of the global population of Laysan Albatross.[63] Nearly all of these albatross have plastic in their digestive system[64] and one-third of their chicks die.[65]

Toxic additives used in the manufacture of plastic materials can leach out into their surroundings when exposed to water. Waterborne hydrophobic pollutants collect and magnify on the surface of plastic debris,[47] thus making plastic far more deadly in the ocean than it would be on land.[46] Hydrophobic contaminants are also known to bioaccumulate in fatty tissues, biomagnifying up the food chain and putting pressure on apex predators. Some plastic additives are known to disrupt the endocrine system when consumed, others can suppress the immune system or decrease reproductive rates.[62] Floating debris can

also absorb persistent organic pollutants from seawater, including PCBs, DDT and PAHs.[66] Aside from toxic effects,[67] when ingested some of these are mistaken by the animal brain for estradiol, causing hormone disruption in the affected wildlife.[61]

12.3.4 Toxins

See also: Mercury in fish

Apart from plastics, there are particular problems with other toxins that do not disintegrate rapidly in the marine environment. Examples of persistent toxins are PCBs, DDT, TBT, pesticides, furans, dioxins, phenols and radioactive waste. Heavy metals are metallic chemical elements that have a relatively high density and are toxic or poisonous at low concentrations. Examples are mercury, lead, nickel, arsenic and cadmium. Such toxins can accumulate in the tissues of many species of aquatic life in a process called bioaccumulation. They are also known to accumulate in benthic environments, such as estuaries and bay muds: a geological record of human activities of the last century.

Specific examples

- Chinese and Russian industrial pollution such as phenols and heavy metals in the Amur River have devastated fish stocks and damaged its estuary soil.[68]
- Wabamun Lake in Alberta, Canada, once the best whitefish lake in the area, now has unacceptable levels of heavy metals in its sediment and fish.
- Acute and chronic pollution events have been shown to impact southern California kelp forests, though the intensity of the impact seems to depend on both the nature of the contaminants and duration of exposure.[69][70][71][72][73]
- Due to their high position in the food chain and the subsequent accumulation of heavy metals from their diet, mercury levels can be high in larger species such as bluefin and albacore. As a result, in March 2004 the United States FDA issued guidelines recommending that pregnant women, nursing mothers and children limit their intake of tuna and other types of predatory fish.[74]
- Some shellfish and crabs can survive polluted environments, accumulating heavy metals or toxins in their tissues. For example, mitten crabs have a remarkable ability to survive in highly modified aquatic habitats, including polluted waters.[75] The farming and harvesting of such species needs careful management if they are to be used as a food.[76][77]
- Surface runoff of pesticides can alter the gender of fish species genetically, transforming male into female fish.[78]
- Heavy metals enter the environment through oil spills - such as the Prestige oil spill on the Galician coast - or from other natural or anthropogenic sources.[79]
- In 2005, the 'Ndrangheta, an Italian mafia syndicate, was accused of sinking at least 30 ships loaded with toxic waste, much of it radioactive. This has led to widespread investigations into radioactive-waste disposal rackets.[80]
- Since the end of World War II, various nations, including the Soviet Union, the United Kingdom, the United States, and Germany, have disposed of chemical weapons in the Baltic Sea, raising concerns of environmental contamination.[81][82]

12.3.5 Underwater noise

See also: Noise pollution, Acoustic ecology and Marine mammals and sonar

Marine life can be susceptible to noise or the sound pollution from sources such as passing ships, oil exploration seismic surveys, and naval low-frequency active sonar. Sound travels more rapidly and over larger distances in the sea than in the atmosphere. Marine animals, such as cetaceans, often have weak eyesight, and live in a world largely defined by acoustic information. This applies also to many deeper sea fish, who live in a world of darkness.[83] Between 1950 and 1975, ambient noise in the ocean increased by about ten decibels (that is a tenfold increase).[84]

Noise also makes species communicate louder, which is called the Lombard vocal response.[85] Whale songs are longer when submarine-detectors are on.[86] If creatures don't “speak” loud enough, their voice can be masked by anthropogenic sounds. These unheard voices might be warnings, finding of prey, or preparations of net-bubbling. When one species begins speaking louder, it will mask other species voices, causing the whole ecosystem to eventually speak louder.[87]

According to the oceanographer Sylvia Earle, “Undersea noise pollution is like the death of a thousand cuts. Each sound in itself may not be a matter of critical concern, but taken all together, the noise from shipping, seismic surveys, and military activity is creating a totally different environment than existed even 50 years ago. That high level of noise is bound to have a hard, sweeping impact on life in the sea.”[88]

12.4 Adaptation and mitigation

Aerosol can polluting a beach.

Much anthropogenic pollution ends up in the ocean. The 2011 edition of the United Nations Environment Programme Year Book identifies as the main emerging environmental issues the loss to the oceans of massive amounts of phosphorus, "a valuable fertilizer needed to feed a growing global population", and the impact billions of pieces of plastic waste are having globally on the health of marine environments.[89] Bjorn Jennssen (2003) notes in his article, "Anthropogenic pollution may reduce biodiversity and productivity of marine ecosystems, resulting in reduction and depletion of human marine food resources".[90] There are two ways the overall level of this pollution can be mitigated: either the human population is reduced, or a way is found to reduce the ecological footprint left behind by the average human. If the second way is not adopted, then the first way may be imposed as world ecosystems falter.

The second way is for humans, individually, to pollute less. That requires social and political will, together with a shift in awareness so more people respect the environment and are less disposed to abuse it.[91] At an operational level, regulations, and international government participation is needed.[92] It is often very difficult to regulate marine pollution because pollution spreads over international barriers, thus making regulations hard to create as well as enforce.[93]

Without appropriate awareness of marine pollution, the necessary global will to effectively address the issues may prove inadequate. Balanced information on the sources and harmful effects of marine pollution need to become part of general public awareness, and ongoing research is required to fully establish, and keep current, the scope of the issues. As expressed in Daoji and Dag's research,[94] one of the reasons why environmental concern is lacking among the Chinese is because the public awareness is low and therefore should be targeted. Likewise, regulation, based upon such in-depth research should be employed. In California, such regulations have already been put in place to protect Californian coastal waters from agricultural runoff. This includes the California Water Code, as well as several voluntary programs. Similarly, in India, several tactics have been employed that help reduce marine pollution, however, they do not significantly target the problem. In Chennai, sewage has been dumped further into open waters. Due to the mass of waste being deposited, open-ocean is best for diluting, and dispersing pollutants, thus making them less harmful to marine ecosystems.

12.5 See also

- Marine debris
- Nutrient pollution
- Stockholm Convention on Persistent Organic Pollutants
- Environmental effects of pesticides

12.6 Notes

[1] Hamblin, Jacob Darwin (2008) *Poison in the Well: Radioactive Waste in the Oceans at the Dawn of the Nuclear Age.* Rutgers University Press. ISBN 978-0-8135-4220-1

[2] Emma Young (2003). "Copper decimates coral reef spawning". Retrieved 26 August 2006.

[3] Environmental Protection Agency. "Liquid Assets 2000: Americans Pay for Dirty Water". Retrieved 2007-01-23.

[4] Washington State Department of Ecology. "Control of Toxic Chemicals in Puget Sound, Phase 2: Development of Simple Numerical Models", 2008

[5] Panetta, LE (Chair) (2003) *America's living oceans: charting a course for sea change* [Electronic Version, CD] Pew Oceans Commission.

[6] Farmer, Andrew. 1997. Managing Environmental Pollution.

[7] Janice Podsada (19 June 2001). "Lost Sea Cargo: Beach Bounty or Junk?". National Geographic News. Retrieved 2008-04-08.

[8] Meinesz, A. (2003) Deep Sea Invasion: The Impact of Invasive Species PBS: NOVA. Retrieved November 26, 2009

[9] Aquatic invasive species. A Guide to Least-Wanted Aquatic Organisms of the Pacific Northwest. 2001. University of Washington.

[10] Pimentel, D.; R. Zuniga and D., Morrison (2005). "Update on the environmental and economic costs associated with alien-invasive species in the United States". *Ecological Economics* **52**: 273–288. doi:10.1016/j.ecolecon.2004.10.002.

[11] Coral Mortality and African Dust: Barbados Dust Record: 1965-1996 US Geological Survey. Retrieved 10 December 2009.

[12] Duce, R.A.; Unni, C.K.; Ray, B.J.; Prospero, J.M.; Merrill, J.T. (1980). "Long-range atmospheric transport of soil dust from Asia to the tropical North Pacific:Temporal variability". *Science* **209** (4464): 1522–1524. Bibcode:1980Sci...209.1522D. doi:10.1126/science.209.4464.1522. PMID 17745962.

[13] Usinfo.state.gov. Study Says African Dust Affects Climate in U.S., Caribbean. Retrieved on 10 June 2007.

[14] Prospero, J.M.; Nees, R.T. (1986). "Impact of the North African drought and El Niño on mineral dust in the Barbados trade winds". *Nature* **320** (6064): 735–738. Bibcode:1986Natur.320..735P. doi:10.1038/320735a0.

[15] U. S. Geological Survey. Coral Mortality and African Dust. Retrieved on 10 June 2007.

[16] Observations: Oceanic Climate Change and Sea Level In: *Climate Change 2007: The Physical Science Basis*. Contribution of Working Group I to the Fourth Assessment Report of the Intergovernmental Panel on Climate Change. (15MB).

[17] Doney, S. C. (2006) "The Dangers of Ocean Acidification" *Scientific American*, March 2006.

[18] Cheung, W.W.L., et al. (2009) "Redistribution of Fish Catch by Climate Change. A Summary of a New Scientific Analysis" Pew Ocean Science Series. Oct 2009.

[19] PACFA (2009) Fisheries and Aquaculture in a Changing Climate

[20] Ahnert, A., & Borowski, C. (2000). Environmental risk assessment of anthropogenic activity in the deep sea. Journal of Aquatic Ecosystem Stress & Recovery, 7(4), 299. Retrieved from Academic Search Complete database. http://web.ebscohost.com/ehost/pdf?vid=5&hid=2&sid=4b3a30cd-c7ec-4838-ba3c-48ce12f26813%40sessionmgr12

[21] Halfar, Jochen, and Rodney M. Fujita. 2007. "Danger of Deep-Sea Mining." *Science* 316, no. 5827: 987. Academic Search Complete, EBSCOhost (accessed January 19, 2010) <http://www.sciencemag.org/cgi/content/full/316/5827/987>

[22] Glasby, G P. "Lessons Learned from Deep-Sea Mining." Science Magazine 28 July 2000: 551-53. Web. 20 Jan. 2010. <http://www.sciencemag.org/cgi/content/full/289/5479/551#ref3>

[23] Sharma R (2005) "Deep-Sea Impact Experiments and their Future Requirements" *Marine Georesources & Geotechnology*, **23**(4): 331-338Sharma, R. (2005). "Deep-Sea Impact Experiments and their Future Requirements". *Marine Georesources and Geotechnology* **23** (4): 331–338. doi:10.1080/10641190500446698.

[24] Nath B and Sharma R (2000) "Environment and Deep-Sea Mining: A Perspective" *Marine Georesources & Geotechnology*, **18**(3): 285-294Sharma, B. Nagender Nath, R. (2000). "Environment and Deep-Sea Mining: A Perspective". *Marine Georesources and Geotechnology* **18** (3): 285–294. doi:10.1080/10641190051092993.

[25] Coral reefs around the world *Guardian.co.uk*, 2 September 2009.

[26] Orr, James C.; Fabry, Victoria J.; Aumont, Olivier; Bopp, Laurent; Doney, Scott C. et al. (2005). "Anthropogenic ocean acidification over the twenty-first century and its impact on calcifying organisms" (PDF). *Nature* **437** (7059): 681–686. Bibcode:2005Natur.437..681O. doi:10.1038/nature04095. ISSN 0028-0836. PMID 16193043.

[27] Key, R.M.; Kozyr, A.; Sabine, C.L.; Lee, K.; Wanninkhof, R.; Bullister, J.; Feely, R.A.; Millero, F.; Mordy, C. and Peng, T.-H. (2004). "A global ocean carbon climatology: Results from GLODAP". *Global Biogeochemical Cycles* **18** (4): GB4031. Bibcode:2004GBioC..18.4031K. doi:10.1029/2004GB002247. ISSN 0886-6236.

[28] Raven, J. A. *et al.* (2005). Ocean acidification due to increasing atmospheric carbon dioxide. Royal Society, London, UK.

[29] UNEP, FAO, IOC (2009) Blue Carbon. The role of healthy oceans in binding carbon

[30] Monaco Declaration and Ocean Acidification A Summary for Policymakers from the Second Symposium on the Ocean in a High-CO2 World.] Intergovernmental Oceanographic Commission of UNESCO, International Geosphere-Biosphere Programme, Marine Environment Laboratories (MEL) of the International Atomic Energy Agency, Scientific Committee on Oceanic Research. 2008.

[31] Manado Ocean Declaration World Ocean Conference Ministerial/High Level Meeting. Manado, Indonesia, 11–14 May 2009.

[32] Feely, Richard; Christopher L. Sabine, J. Martin Hernandez-Ayon, Debby Ianson, Burke Hales. (2008). "Evidence for Upwelling of Corrosive "Acidified" Seawater onto the Continental Shelf". *Science* **320** (5882): 1490–2. Bibcode:2008Sci...320.1490F. doi:10.1126/science.1155676. PMID 18497259.

[33] Milkov, AV (2004). "Global estimates of hydrate-bound gas in marine sediments: how much is really out there?". *Earth-Sci Rev* **66** (3–4): 183–197. Bibcode:2004ESRv...66..183M. doi:10.1016/j.earscirev.2003.11.002.

[34] The oceans occupy 361 million sq km

[35] USGS World Energy Assessment Team, 2000. US Geological Survey world petroleum assessment 2000—description and results. USGS Digital Data Series DDS-60.

[36] Gerlach: Marine Pollution, Springer, Berlin (1975)

[37] Selman, Mindy (2007) *Eutrophication: An Overview of Status, Trends, Policies, and Strategies.* World Resources Institute.

[38] "The Gulf of Mexico Dead Zone and Red Tides". Retrieved 2006-12-27.

[39] Duce, R A and 29 others (2008) *Impacts of Atmospheric Anthropogenic Nitrogen on the Open Ocean* Science. Vol 320, pp 893–89

[40] *Addressing the nitrogen cascade* Eureka Alert, 2008.

[41] Kroeger, Timm. 2012. Dollars and Sense: Economic Benefits and Impacts from two Oyster Reef Restoration Projects in the Northern Gulf of Mexico. TNC Report. http://www.nature.org/ourinitiatives/regions/northamerica/oyster-restoration-study-kroeger.pdf

[42] Burkholder, JoAnn M. and Sandra E. Shumway. 2011. Bivalve shellfish aquaculture and eutrophication. In: Shellfish Aquaculture and the Environment. Ed. Sandra E. Shumway. John Wiley & Sons.

[43] Kaspar, H.F., et al. 1985. Effects of mussel aquaculture on the nitrogen cycle and benthic communities in Kenepuru Sound, Marlborough Sounds, New Zealand. Marine Biology 85:127-136.

[44] Newell, R.IE, J.C. Cornwell & M.S. Owens. 2002. Influence of simulated bivalve biodepositon and microphytobenthos on sediment nitrogen dynamics, a laboratory study. Limnology & Oceanography 47:1367-1379.

[45] Lindahl. O., et al. 2005. Improving marine water quality by mussel farming-a profitable solution for Swedish society. Ambio 131-138.

[46] Alan Weisman (2007). *The World Without Us*. St. Martin's Thomas Dunne Books. ISBN 0-312-34729-4.

[47] "Plastic Debris: from Rivers to Sea" (PDF). Algalita Marine Research Foundation. Retrieved 2008-05-29.

[48] "Research | AMRF/ORV Alguita Research Projects" Algalita Marine Research Foundation. Macdonald Design. Accessed 19 May 2009.

[49] UNEP (2005) Marine Litter: An Analytical Overview

[50] Six pack rings hazard to wildlife

[51] Louisiana Fisheries - Fact Sheets

[52] "'Ghost fishing' killing seabirds". BBC News. 28 June 2007. Retrieved 2008-04-01.

[53] Kenneth R. Weiss (2 August 2006). "Plague of Plastic Chokes the Seas". Los Angeles Times. Archived from the original on 2008-03-25. Retrieved 2008-04-01.

[54] Venema, Vibeke. "The Dutch boy mopping up a sea of plastic". *BBC*. BBC Magazine. Retrieved 2014-10-18.

[55] Charles Moore (November 2003). "Across the Pacific Ocean, plastics, plastics, everywhere". Natural History. Retrieved 2008-04-05.

[56] Sheavly & Register, 2007, p. 3.

[57] Alan Weisman (Summer 2007). "Polymers Are Forever". Orion magazine. Retrieved 2008-07-01.

[58] Thompson, Richard C.; Olsen, Y; Mitchell, RP; Davis, A; Rowland, SJ; John, AW; McGonigle, D; Russell, AE (7 May 2004). "Lost at Sea: Where Is All the Plastic?,". *Science* **304** (5672): 843–6. doi:10.1126/science.1094559. PMID 15131299. Retrieved 2008-07-19.

[59] Moore, Charles; Moore, S. L.; Leecaster, M. K.; Weisberg, S. B. (April 2001). "A Comparison of Plastic and Plankton in the North Pacific Central Gyre" (PDF). *Marine Pollution Bulletin* (2001-12-01) **42** (12): 1297–1300. doi:10.1016/S0025-326X(01)00114-X. PMID 11827116.

[60] Moore, Charles (November 2003). "Across the Pacific Ocean, plastics, plastics, everywhere". Natural History Magazine.

[61] Moore, Charles (2002-10-02). "Great Pacific Garbage Patch". Santa Barbara News-Press.

[62] "Plastics and Marine Debris". Algalita Marine Research Foundation. 2006. Retrieved 2008-07-01.

[63] "Midway's albatross population stable | The Honolulu Advertiser | Hawaii's Newspaper". The Honolulu Advertiser. 2005-01-17. Retrieved 2012-05-20.

[64] Chris Jordan (November 11, 2009). "Midway: Message from the Gyre". Retrieved 2009-11-13.

[65] "Q&A: Your Midway questions answered". *BBC News*. 28 March 2008. Retrieved 12 May 2010.

[66] Rios, L.M.; Moore, C. and Jones, P.R. (2007). "Persistent organic pollutants carried by Synthetic polymers in the ocean environment". *Marine Pollution Bulletin* **54** (8): 1230–1237. doi:10.1016/j.marpolbul.2007.03.022. PMID 17532349.

[67] Tanabe, S.; Watanabe, M., Minh, T.B., Kunisue, T., Nakanishi, S., Ono, H. and Tanaka, H. (2004). "PCDDs, PCDFs, and coplanar PCBs in albatross from the North Pacific and Southern Oceans: Levels, patterns, and toxicological implications". *Environmental Science & Technology* **38** (2): 403–413. Bibcode:2004EnST...38..403T. doi:10.1021/es034966x. PMID 14750714.

[68] "Indigenous Peoples of the Russian North, Siberia and Far East: Nivkh" by Arctic Network for the Support of the Indigenous Peoples of the Russian Arctic

[69] Grigg, R.W. and R.S. Kiwala. 1970. Some ecological effects of discharged wastes on marine life. California Department of Fish and Game 56: 145-155.

[70] Stull, J.K. 1989. Contaminants in sediments near a major marine outfall: history, effects and future. OCEANS '89 Proceedings 2: 481-484.

[71] North, W.J., D.E. James and L.G. Jones. 1993. History of kelp beds (*Macrocystis*) in Orange and San Diego Counties, California. Hydrobiologia 260/261: 277-283.

[72] Tegner, M.J., P.K. Dayton, P.B. Edwards, K.L. Riser, D.B. Chadwick, T.A. Dean and L. Deysher. 1995. Effects of a large sewage spill on a kelp forest community: catastrophe or disturbance? Marine Environmental Research 40: 181-224.

[73] Carpenter, S.R.; Caraco, R.F.; Cornell, D.F.; Howarth, R.W.; Sharpley, A.N.; Smith, V.N. (1998). "Nonpoint pollution of surface waters with phosphorus and nitrogen". *Ecological Applications* **8** (3): 559–568. doi:10.1890/1051-0761(1998)008[0559:NPOSWW]2.0.CO;2. ISSN 1051-0761.

[74] "What You Need to Know About Mercury in Fish and Shellfish". March 2004. Retrieved 2007-05-19.

[75] Stephen Gollasch (2006-03-03). "Ecology of *Eriocheir sinensis*".

[76] Hui, Clifford A. et al. (2005). "Mercury burdens in Chinese mitten crabs (Eriocheir sinensis) in three tributaries of southern San Francisco Bay, California, USA". *Environmental Pollution* (Elsevier) **133** (3): 481–487. doi:10.1016/j.envpol.2004.06.019. PMID 15519723.

[77] Silvestre, F. et al. (2004). "Uptake of cadmium through isolated perfused gills of the Chinese mitten crab, Eriocheir sinensis". *Comparative Biochemistry and Physiology - Part A: Molecular & Integrative Physiology* (Elsevier) **137** (1): 189–196. doi:10.1016/S1095-6433(03)00290-3.

[78] *Science News.* "DDT treatment turns male fish into mothers." 2000-02-05. (By subscription only.)

[79] Perez-Lopez *et al.* (2006)

[80] (Italian) Parla un boss: Così lo Stato pagava la 'ndrangheta per smaltire i rifiuti tossici, by Riccardo Bocca, L'Espresso, August 5, 2005

[81] Chemical Weapon Time Bomb Ticks in the Baltic Sea *Deutsche Welle*, 1 February 2008.

[82] Activities 2006: Overview Baltic Sea Environment Proceedings No. 112. Helsinki Commission.

[83] Noise pollution *Sea.org*. Retrieved 24 October 2009.

[84] Ross, (1993) On Ocean Underwater Ambient Noise. Institute of Acoustics Bulletin, St Albans, Herts, UK: Institute of Acoustics, 18.

[85] Glossary *Discovery of Sounds in the Sea*. Retrieved 23 December 2009.

[86] Fristrup, KM; Hatch, LT; Clark, CW (2003). "Variation in humpback whale (*Megaptera novaeangliae*) song length in relation to low-frequency sound broadcasts". *Journal of the Acoustical Society of America* **113** (6): 3411–3424. Bibcode:2003ASAJ..113.3411F. doi:10.1121/1.1573637. PMID 12822811.

[87] Effects of Sound on Marine Animals *Discovery of Sounds in the Sea*. Retrieved 23 December 2009.

[88] Natural Resources Defense Council Press Release (1999) Sounding the Depths: Supertankers, Sonar, and the Rise of Undersea Noise, Executive Summary. New York, N.Y.: www.nrdc.org.

[89] Fertilizer and plastic pollution are main emerging issues in 2011 UNEP Year Book, 17 February 2011. *News Centre*, United Nations Environment Programme, The Hague.

[90] Jenssen BM (2003) "Marine pollution: the future challenge is to link human and wildlife studies" *Environ Health Perspect.* **111**(4): A198–A199.

[91] Kullenberg G (1999) "Approaches to addressing the problems of pollution of the marine environment: an overview" *Ocean & Coastal Management*, **42**(12): 999-1018Kullenberg, G (1999). "Approaches to addressing the problems of pollution of the marine environment: an overview". *Ocean & Coastal Management* **42** (12): 999–1018. doi:10.1016/S0964-5691(99)00059-9.

[92] Matthews G (1973) "Pollution of the oceans: An international problem?" *Ocean Management*, **1**: 161-170Matthews, G (1973). "Pollution of the oceans: An international problem?". *Ocean Management* **1**: 161–170. doi:10.1016/0302-184X(73)90010-3.

[93] Warner R (2009) *Protecting the oceans beyond national jurisdiction: strengthening the international law framework* Volume 3 of *Legal aspects of sustainable development*, Brill, ISBN 978-90-04-17262-3.

[94] Daoji L and Daler D (2004) "Ocean pollution from land-based sources: East China Sea, China" *Ambio*, **33**: 1–2. Royal Swedish Academy of Sciences.

12.7 References

- Ahn, YH; Hong, GH; Neelamani, S; Philip, L and Shanmugam, P (2006) *Assessment of Levels of coastal marine pollution of Chennai city, southern India.* Water Resource Management, 21(7), 1187-1206.
- Daoji, L and Dag, D (2004) *Ocean pollution from land-based sources: East China sea.* AMBIO – A Journal of the Human Environment, 33(1/2), 107-113.
- Dowrd, BM; Press, D and Los Huertos, M (2008) *Agricultural non-point sources: water pollution policy: The case of California's central coast. Agriculture, Ecosystems & Environment*, 128(3), 151-161.
- Laws, Edward A (2000) *Aquatic Pollution* John Wiley and Sons. ISBN 978-0-471-34875-7
- Sheavly, SB and Register, KM (2007) *Marine debris and plastics: Environmental concerns, sources, impacts and solutions.* Journal of Polymers & the Environment, 15(4), 301-305.
- Slater, D (2007) *Affluence and effluents.* Sierra 92(6), 27

- UNEP/GPA (2006) *The State of the Marine Environment: Trends and processes* United Nations Environment Programme, Global Programme of Action, The Hague. 2006 ISBN 92-807-2708-7.
- UNEP (2007) *Land-based Pollution in the South China Sea*. UNEP/GEF/SCS Technical Publication No 10.

12.8 External links

- Coastal Pollution Information from the Coastal Ocean Institute, Woods Hole Oceanographic Institution
- Mercury pollution
- How Oil Spill Absorbent Products Work
- Facts about Marine Mercury Pollution from Oceana.org
- Science News / Marine Pollution Spawns 'wonky Babies'
- Plastics at SEA: North Atlantic Expedition
- Plastic Trash Plagues the Ocean, Trashing the Ocean, Oil's Impact on Marine Invertebrates on the Smithsonian Ocean Portal
- How the oceans can clean themselves – TED Talk

Chapter 13

Geodesy

An old geodetic pillar (1855) at Ostend, Belgium

A Munich archive with lithography plates of maps of Bavaria

Geodesy (/dʒiːˈɒdɪsi/),[1] — also known as **geodetics** or **geodetics engineering** — a branch of applied mathematics [2] and earth sciences, is the scientific discipline that deals with the measurement and representation of the Earth, including its gravitational field, in a three-dimensional time-varying space. Geodesists also study geodynamical phenomena such as crustal motion, tides, and polar motion. For this they design global and national control networks, using space and terrestrial techniques while relying on datums and coordinate systems.

13.1 Definition

Geodesy — from the Greek word γεωδαισία or *geodaisia* (literally, "division of the Earth") — is primarily concerned with positioning within the temporally varying gravity field. Somewhat obsolete nowadays, geodesy in the German-speaking world is divided into "Higher Geodesy" ("Erdmessung" or "höhere Geodäsie"), which is concerned with measuring the Earth on the global scale, and "Practical Geodesy" or "Engineering Geodesy" ("Ingenieurgeodäsie"), which is concerned with measuring specific parts or regions of the Earth, and which includes surveying.

The shape of the Earth is to a large extent the result of its rotation, which causes its equatorial bulge, and the competition of geological processes such as the collision of plates and of volcanism, resisted by the Earth's gravity field. This applies to the solid surface, the liquid surface (dynamic sea surface topography) and the Earth's atmosphere. For this reason, the study of the Earth's gravity field is called physical geodesy by some.

13.2 History

Main article: History of geodesy

13.3 Geoid and reference ellipsoid

See also: Geoid

The geoid is essentially the figure of the Earth abstracted from its topographical features. It is an idealized equilibrium surface of sea water, the mean sea level surface in the absence of currents, air pressure variations etc. and continued under the continental masses. The geoid, unlike the reference ellipsoid, is irregular and too complicated to serve as the computational surface on which to solve geometrical problems like point positioning. The geometrical separation between the geoid and the reference ellipsoid is called the geoidal undulation. It varies globally between ±110 m, when referred to the GRS 80 ellipsoid.

A reference ellipsoid, customarily chosen to be the same size (volume) as the geoid, is described by its semi-major axis (equatorial radius) a and flattening f. The quantity $f = (a-b)/a$, where b is the semi-minor axis (polar radius), is a purely geometrical one. The mechanical ellipticity of the Earth (dynamical flattening, symbol J_2) can be determined to high precision by observation of satellite orbit perturbations. Its relationship with the geometrical flattening is indirect. The relationship depends on the internal density distribution, or, in simplest terms, the degree of central concentration of mass.

The 1980 Geodetic Reference System (GRS80) posited a 6,378,137 m semi-major axis and a 1:298.257 flattening. This system was adopted at the XVII General Assembly of the International Union of Geodesy and Geophysics (IUGG). It is essentially the basis for geodetic positioning by the Global Positioning System and is thus also in widespread use outside the geodetic community.

The numerous other systems which have been used by diverse countries for their maps and charts are gradually dropping out of use as more and more countries move to global, geocentric reference systems using the GRS80 reference ellipsoid.

13.4 Coordinate systems in space

See also: Geodetic system

The locations of points in three-dimensional space are most conveniently described by three cartesian or rectangular coordinates, X, Y and Z . Since the advent of satellite positioning, such coordinate systems are typically geocentric: the Z axis is aligned with the Earth's (conventional or instantaneous) rotation axis.

Prior to the era of satellite geodesy, the coordinate systems associated with a geodetic datum attempted to be geocentric, but their origins differed from the geocentre by hundreds of metres, due to regional deviations in the direction of the plumbline (vertical). These regional geodetic datums, such as ED50 (European Datum 1950) or NAD27 (North American Datum 1927) have ellipsoids associated with them that are regional 'best fits' to the geoids within their areas of validity, minimising the deflections of the vertical over these areas.

It is only because GPS satellites orbit about the geocentre, that this point becomes naturally the origin of a coordinate system defined by satellite geodetic means, as the satellite positions in space are themselves computed in such a system.

Geocentric coordinate systems used in geodesy can be divided naturally into two classes:

1. Inertial reference systems, where the coordinate axes retain their orientation relative to the fixed stars, or equivalently, to the rotation axes of ideal gyroscopes; the X axis points to the vernal equinox
2. Co-rotating, also ECEF ("Earth Centred, Earth Fixed"), where the axes are attached to the solid body of the Earth. The X axis lies within the Greenwich observatory's meridian plane.

The coordinate transformation between these two systems is described to good approximation by (apparent) sidereal time, which takes into account variations in the Earth's axial rotation (length-of-day variations). A more accurate description also takes polar motion into account, a phenomenon closely monitored by geodesists.

13.4.1 Coordinate systems in the plane

In surveying and mapping, important fields of application of geodesy, two general types of coordinate systems are used in the plane:

1. Plano-polar, in which points in a plane are defined by a distance s from a specified point along a ray having a specified direction α with respect to a base line or axis;
2. Rectangular, points are defined by distances from two perpendicular axes called x and y . It is geodetic practice—contrary to the mathematical convention—to let the x axis point to the North and the y axis to the East.

Rectangular coordinates in the plane can be used intuitively with respect to one's current location, in which case the x axis will point to the local North. More formally, such coordinates can be obtained from three-dimensional coordinates using the artifice of a map projection. It is *not* possible to map the curved surface of the Earth onto a flat map surface without deformation. The compromise most often chosen—called a conformal projection—preserves angles and length ratios, so that small circles are mapped as small circles and small squares as squares.

An example of such a projection is UTM (Universal Transverse Mercator). Within the map plane, we have rectangular coordinates x and y . In this case the North

direction used for reference is the *map* North, not the *local* North. The difference between the two is called meridian convergence.

It is easy enough to "translate" between polar and rectangular coordinates in the plane: let, as above, direction and distance be α and s respectively, then we have

$$\begin{aligned} x &= s\cos\alpha \\ y &= s\sin\alpha \end{aligned}$$

The reverse transformation is given by:

$$\begin{aligned} s &= \sqrt{x^2+y^2} \\ \alpha &= \arctan(y/x). \end{aligned}$$

13.5 Heights

In geodesy, point or terrain *heights* are "above sea level", an irregular, physically defined surface. Therefore a height should ideally *not* be referred to as a coordinate. It is more like a physical quantity, and though it can be tempting to treat height as the vertical coordinate z , in addition to the horizontal coordinates x and y , and though this actually is a good approximation of physical reality in small areas, it quickly becomes invalid for regional considerations.

Heights come in the following variants:

1. Orthometric heights
2. Normal heights
3. Geopotential heights

Each has its advantages and disadvantages. Both orthometric and normal heights are heights in metres above sea level, whereas geopotential numbers are measures of potential energy (unit: $m^2\ s^{-2}$) and not metric. Orthometric and normal heights differ in the precise way in which mean sea level is conceptually continued under the continental masses. The reference surface for orthometric heights is the geoid, an equipotential surface approximating mean sea level.

None of these heights is in any way related to **geodetic** or **ellipsoidial** heights, which express the height of a point above the reference ellipsoid. Satellite positioning receivers typically provide ellipsoidal heights, unless they are fitted with special conversion software based on a model of the geoid.

13.6 Geodetic data

Because geodetic point coordinates (and heights) are always obtained in a system that has been constructed itself using real observations, geodesists introduce the concept of a *geodetic datum*: a physical realization of a coordinate system used for describing point locations. The realization is the result of *choosing* conventional coordinate values for one or more *datum points*.

In the case of height datums, it suffices to choose *one* datum point: the reference bench mark, typically a tide gauge at the shore. Thus we have vertical datums like the NAP (Normaal Amsterdams Peil), the North American Vertical Datum 1988 (NAVD88), the Kronstadt datum, the Trieste datum, and so on.

In case of plane or spatial coordinates, we typically need several datum points. A regional, ellipsoidal datum like ED50 can be fixed by prescribing the undulation of the geoid and the deflection of the vertical in *one* datum point, in this case the Helmert Tower in Potsdam. However, an overdetermined ensemble of datum points can also be used.

Changing the coordinates of a point set referring to one datum, so to make them refer to another datum, is called a *datum transformation*. In the case of vertical datums, this consists of simply adding a constant shift to all height values. In the case of plane or spatial coordinates, datum transformation takes the form of a similarity or *Helmert transformation*, consisting of a rotation and scaling operation in addition to a simple translation. In the plane, a Helmert transformation has four parameters; in space, seven.

13.6.1 A note on terminology

In the abstract, a coordinate system as used in mathematics and geodesy is, e.g., in ISO terminology, referred to as a *coordinate system*. International geodetic organizations like the IERS (International Earth Rotation and Reference Systems Service) speak of a *reference system*.

When these coordinates are realized by choosing datum points and fixing a geodetic datum, ISO uses the terminology *coordinate reference system*, while IERS speaks of a *reference frame*. A datum transformation again is referred to by ISO as a *coordinate transformation*. (ISO 19111: Spatial referencing by coordinates).

13.7 Point positioning

Point positioning is the determination of the coordinates of a point on land, at sea, or in space with respect to a coordinate system. Point position is solved by computation from measurements linking the known positions of terrestrial or extraterrestrial points with the unknown terrestrial position. This may involve transformations between or among astronomical and terrestrial coordinate systems.

The known points used for point positioning can be

Geodetic Control Mark (example of a deep benchmark)

triangulation points of a higher order network, or GPS satellites.

Traditionally, a hierarchy of networks has been built to allow point positioning within a country. Highest in the hierarchy were triangulation networks. These were densified into networks of traverses (polygons), into which local mapping surveying measurements, usually with measuring tape, corner prism and the familiar red and white poles, are tied.

Nowadays all but special measurements (e.g., underground or high precision engineering measurements) are performed with GPS. The higher order networks are measured with static GPS, using differential measurement to determine vectors between terrestrial points. These vectors are then adjusted in traditional network fashion. A global polyhedron of permanently operating GPS stations under the auspices of the IERS is used to define a single global, geocentric reference frame which serves as the "zero order" global reference to which national measurements are attached.

For surveying mappings, frequently Real Time Kinematic GPS is employed, tying in the unknown points with known terrestrial points close by in real time.

One purpose of point positioning is the provision of known points for mapping measurements, also known as (horizontal and vertical) control. In every country, thousands of such known points exist and are normally documented by the national mapping agencies. Surveyors involved in real estate and insurance will use these to tie their local measurements to.

13.8 Geodetic problems

Main article: Geodesics on an ellipsoid

In geometric geodesy, two standard problems exist:

13.8.1 First (direct) geodetic problem

> Given a point (in terms of its coordinates) and the direction (azimuth) and distance from that point to a second point, determine (the coordinates of) that second point.

13.8.2 Second (inverse) geodetic problem

> Given two points, determine the azimuth and length of the line (straight line, arc or geodesic) that connects them.

In the case of plane geometry (valid for small areas on the Earth's surface) the solutions to both problems reduce to simple trigonometry. On the sphere, the solution is significantly more complex, e.g., in the inverse problem the azimuths will differ between the two end points of the connecting great circle, arc, i.e. the geodesic.

On the ellipsoid of revolution, geodesics may be written in terms of elliptic integrals, which are usually evaluated in terms of a series expansion; for example, see Vincenty's formulae.

In the general case, the solution is called the geodesic for the surface considered. The differential equations for the geodesic can be solved numerically.

13.9 Geodetic observational concepts

Here we define some basic observational concepts, like angles and coordinates, defined in geodesy (and astronomy as well), mostly from the viewpoint of the local observer.

- The *plumbline* or *vertical* is the direction of local gravity, or the line that results by following it.
- The *zenith* is the point on the celestial sphere where the direction of the gravity vector in a point, extended upwards, intersects it. More correct is to call it a <direction> rather than a point.
- The *nadir* is the opposite point (or rather, direction), where the direction of gravity extended downward intersects the (invisible) celestial sphere.
- The celestial *horizon* is a plane perpendicular to a point's gravity vector.
- *Azimuth* is the direction angle within the plane of the horizon, typically counted clockwise from the North (in geodesy and astronomy) or South (in France).
- *Elevation* is the angular height of an object above the horizon, Alternatively zenith distance, being equal to 90 degrees minus elevation.

- *Local topocentric coordinates* are azimuth (direction angle within the plane of the horizon) and elevation angle (or zenith angle) and distance.
- The North *celestial pole* is the extension of the Earth's (precessing and nutating) instantaneous spin axis extended Northward to intersect the celestial sphere. (Similarly for the South celestial pole.)
- The *celestial equator* is the intersection of the (instantaneous) Earth equatorial plane with the celestial sphere.
- A *meridian plane* is any plane perpendicular to the celestial equator and containing the celestial poles.
- The *local meridian* is the plane containing the direction to the zenith and the direction to the celestial pole.

13.10 Geodetic measurements

Main articles: Satellite geodesy, Geodetic astronomy, Surveying and Gravimetry

The level is used for determining height differences and

Project manager Stephen Merkowitz talks about his work with NASA's Space Geodesy Project, including a brief overview of the four fundamental techniques of space geodesy: GPS, VLBI, SLR, and DORIS.

height reference systems, commonly referred to mean sea level. The traditional spirit level produces these practically most useful heights above sea level directly; the more economical use of GPS instruments for height determination requires precise knowledge of the figure of the geoid, as GPS only gives heights above the GRS80 reference ellipsoid. As geoid knowledge accumulates, one may expect use of GPS heighting to spread.

The theodolite is used to measure horizontal and vertical angles to target points. These angles are referred to the local vertical. The tacheometer additionally determines, electronically or electro-optically, the distance to target, and is highly automated to even robotic in its operations. The method of free station position is widely used.

For local detail surveys, tacheometers are commonly employed although the old-fashioned rectangular technique using angle prism and steel tape is still an inexpensive alternative. Real-time kinematic (RTK) GPS techniques are used as well. Data collected are tagged and recorded digitally for entry into a Geographic Information System (GIS) database.

Geodetic GPS receivers produce directly three-dimensional coordinates in a geocentric coordinate frame. Such a frame is, e.g., WGS84, or the frames that are regularly produced and published by the International Earth Rotation and Reference Systems Service (IERS).

GPS receivers have almost completely replaced terrestrial instruments for large-scale base network surveys. For Planet-wide geodetic surveys, previously impossible, we can still mention Satellite Laser Ranging (SLR) and Lunar Laser Ranging (LLR) and Very Long Baseline Interferometry (VLBI) techniques. All these techniques also serve to monitor Earth rotation irregularities as well as plate tectonic motions.

Gravity is measured using gravimeters. Basically, there are two kinds of gravimeters. *Absolute* gravimeters, which nowadays can also be used in the field, are based directly on measuring the acceleration of free fall (for example, of a reflecting prism in a vacuum tube). They are used for establishing the vertical geospatial control. Most common *relative* gravimeters are spring based. They are used in gravity surveys over large areas for establishing the figure of the geoid over these areas. Most accurate relative gravimeters are *superconducting* gravimeters, and these are sensitive to one thousandth of one billionth of the Earth surface gravity. Twenty-some superconducting gravimeters are used worldwide for studying Earth tides, rotation, interior, and ocean and atmospheric loading, as well as for verifying the Newtonian constant of gravitation.

13.11 Units and measures on the ellipsoid

Geographical latitude and longitude are stated in the units degree, minute of arc, and second of arc. They are *angles*, not metric measures, and describe the *direction* of the local normal to the reference ellipsoid of revolution. This is *approximately* the same as the direction of the plumbline, i.e., local gravity, which is also the normal to the geoid surface. For this reason, astronomical position determination – measuring the direction of the plumbline by astronomical means – works fairly well provided an ellipsoidal model of the figure of the Earth is used.

One geographical mile, defined as one minute of arc on the equator, equals 1,855.32571922 m. One nautical mile is one minute of astronomical latitude. The radius of curvature of the ellipsoid varies with latitude, being the longest at the pole and the shortest at the equator as is the nautical mile.

A metre was originally defined as the 10-millionth part of the length of a meridian (the target was not quite reached in actual implementation, so that is off by 200 ppm in the current definitions). This means that one kilometre is roughly equal to (1/40,000) * 360 * 60 meridional minutes of arc, which equals 0.54 nautical mile, though this is not exact because the two units are defined on different bases (the international nautical mile is defined as exactly 1,852 m, corresponding to a rounding of 1000/0.54 m to four digits).

13.12 Temporal change

In geodesy, temporal change can be studied by a variety of techniques. Points on the Earth's surface change their location due to a variety of mechanisms:

- Continental plate motion, plate tectonics
- Episodic motion of tectonic origin, esp. close to fault lines
- Periodic effects due to Earth tides
- Postglacial land uplift due to isostatic adjustment
- Various anthropogenic movements due to, for instance, petroleum or water extraction or reservoir construction.

The science of studying deformations and motions of the Earth's crust and the solid Earth as a whole is called geodynamics. Often, study of the Earth's irregular rotation is also included in its definition.

Techniques for studying geodynamic phenomena on the global scale include:

- satellite positioning by GPS and other such systems,
- Very Long Baseline Interferometry (VLBI)
- satellite and lunar laser ranging
- Regionally and locally, precise levelling,
- precise tacheometers,
- monitoring of gravity change,
- Interferometric synthetic aperture radar (InSAR) using satellite images, etc.

13.13 Famous geodesists

13.13.1 Mathematical geodesists before 1900

- Pythagoras 580–490 BC, ancient Greece[3]
- Eratosthenes 276–194 BC, ancient Greece
- Hipparchus ca. 190–120 BC, ancient Greece
- Posidonius ca. 135–51 BC, ancient Greece
- Claudius Ptolemy 83–c.168 AD, Roman Empire (Roman Egypt)
- Al-Ma'mun 786–833, Baghdad (Iraq/Mesopotamia)
- Abu Rayhan Biruni 973–1048, Khorasan (Iran/Samanid Dynasty)
- Muhammad al-Idrisi 1100–1166, (Arabia & Sicily)
- Regiomontanus 1436–1476, (Germany/Austria)
- Abel Foullon 1513–1563 or 1565, (France)
- Pedro Nunes 1502–1578 (Portugal)
- Gerhard Mercator 1512–1594 (Belgium & Germany)
- Snellius (Willebrord Snel van Royen) 1580–1626, Leiden (Netherlands)
- Christiaan Huygens 1629–1695 (Netherlands)
- Pierre Bouguer 1698–1758, (France & Peru)
- Pierre de Maupertuis 1698–1759 (France)
- Alexis Clairaut 1713–1765 (France)
- Johann Heinrich Lambert 1728–1777 (France)
- Roger Joseph Boscovich 1711–1787, (Rome/ Berlin/ Paris)
- Ino Tadataka 1745-1818, (Tokyo)
- Georg von Reichenbach 1771–1826, Bavaria (Germany)
- Pierre-Simon Laplace 1749–1827, Paris (France)
- Adrien Marie Legendre 1752–1833, Paris (France)
- Johann Georg von Soldner 1776–1833, Munich (Germany)
- George Everest 1830–1843 (England & India)
- Friedrich Wilhelm Bessel 1784–1846, Königsberg (Germany)
- Heinrich Christian Schumacher 1780–1850 (Germany & Estonia)
- Carl Friedrich Gauß 1777–1855, Göttingen (Germany)
- Friedrich Georg Wilhelm Struve 1793–1864, Dorpat and Pulkovo (Russian Empire)

- J. H. Pratt 1809–1871, London (England)
- Friedrich H. C. Paschen 1804–1873, Schwerin (Germany)
- Johann Benedikt Listing 1808–1882 (Germany)
- Johann Jacob Baeyer 1794–1885, Berlin (Germany)
- Sir George Biddell Airy 1801–1892, Cambridge & London
- Karl Maximilian von Bauernfeind 1818–1894, Munich (Germany)
- Wilhelm Jordan 1842–1899, (Germany)
- Hervé Faye 1814–1902 (France)
- George Gabriel Stokes 1819–1903 (England)
- Carlos Ibáñez e Ibáñez de Ibero 1825-1891 Barcelona (Spain)
- Henri Poincaré 1854–1912, Paris (France)
- Alexander Ross Clarke 1828–1914, London (England)
- Charles Sanders Peirce 1839–1914 (United States)
- Friedrich Robert Helmert 1843–1917, Potsdam (Germany)
- Heinrich Bruns 1848–1919, Berlin (Germany)
- Loránd Eötvös 1848–1919 (Hungary)

13.13.2 Twentieth century

- John Fillmore Hayford, 1868–1925, (US)
- Alfred Wegener, 1880–1930, (Germany and Greenland)
- William Bowie, 1872–1940, (US)
- Friedrich Hopfner, 1881–1949, Vienna, (Austria)
- Tadeusz Banachiewicz, 1882–1954, (Poland)
- Felix Andries Vening-Meinesz, 1887–1966, (Netherlands)
- Martin Hotine, 1898–1968, (England)
- Yrjö Väisälä, 1889–1971, (Finland)
- Veikko Aleksanteri Heiskanen, 1895–1971, (Finland and US)
- Karl Ramsayer, 1911–1982, Stuttgart, (Germany)
- Harold Jeffreys, 1891–1989, London, (England)
- Reino Antero Hirvonen, 1908–1989, (Finland)
- Mikhail Sergeevich Molodenskii, 1909–1991, (Russia)
- Hellmut Schmid, 1914–1998, (Switzerland)
- William M. Kaula, 1926–2000, Los Angeles, (US)
- John A. O'Keefe, 1916–2000, (US)
- Thaddeus Vincenty, 1920–2002, (Poland)
- Willem Baarda, 1917–2005, (Netherlands)
- Irene Kaminka Fischer, 1907–2009, (US)
- Arne Bjerhammar, 1917–2011, (Sweden)
- Karl-Rudolf Koch 1935, Bonn, (Germany)
- Helmut Moritz, 1933, Graz, (Austria)
- Petr Vaníček, 1935, Fredericton, (Canada)
- Erik Grafarend, 1939, Stuttgart, (Germany)

13.13.3 Unlisted

This list is incomplete; you can help by expanding it.

13.14 See also

Fundamentals Geodynamics · Geomatics · Cartography · Geodesics on an ellipsoid · Physical geodesy · Adjustment of observations

Concepts Datum · Distance · Figure of the Earth · Geoid · Geodetic system · Geog. coord. system · Horizontal position representation · Map projection · Reference ellipsoid · Satellite geodesy · Spatial reference system

Geodesy community **International organizations** International Association of Geodesy (IAG) · European Petroleum Survey Group (EPSG) · International Federation of Surveyors (FIG) · International Geodetic Student Organisation (IGSO)

Governmental agencies **USA** **NOAA-NGS** · **NGA** · **USGS**

Technologies GNSS · GPS · Space techniques

Standards ED50 · ETRS89 · NAD83 · NAVD88 · SAD69 · SRID · UTM · WGS84

History History of geodesy · NAVD29

Other Surveying · Meridian arc · Lenart Sphere

13.15 References

[1] *OED*

[2] Merriam-Webster Dictionary

[3] DEFENSE MAPPING AGENCY TECHNICAL REPORT 80-003

13.16 Further reading

- F. R. Helmert, *Mathematical and Physical Theories of Higher Geodesy*, Part 1, ACIC (St. Louis, 1964). This is an English translation of *Die mathematischen und physikalischen Theorieen der höheren Geodäsie*, Vol 1 (Teubner, Leipzig, 1880).
- F. R. Helmert, *Mathematical and Physical Theories of Higher Geodesy*, Part 2, ACIC (St. Louis, 1964). This is an English translation of *Die mathematischen und physikalischen Theorieen der höheren Geodäsie*, Vol 2 (Teubner, Leipzig, 1884).
- B. Hofmann-Wellenhof and H. Moritz, *Physical Geodesy*, Springer-Verlag Wien, 2005. (This text is an updated edition of the 1967 classic by W.A. Heiskanen and H. Moritz).
- W. Kaula, *Theory of Satellite Geodesy : Applications of Satellites to Geodesy*, Dover Publications, 2000. (This text is a reprint of the 1966 classic).
- Vaníček P. and E.J. Krakiwsky, *Geodesy: the Concepts*, pp. 714, Elsevier, 1986.
- Torge, W (2001), *Geodesy* (3rd edition), published by de Gruyter, isbn=3-11-017072-8.
- Thomas H. Meyer, Daniel R. Roman, and David B. Zilkoski. “What does *height* really mean?" (This is a series of four articles published in *Surveying and Land Information Science, SaLIS*.)
  - “Part I: Introduction” *SaLIS* Vol. 64, No. 4, pages 223–233, December 2004.
  - “Part II: Physics and gravity” *SaLIS* Vol. 65, No. 1, pages 5–15, March 2005.
  - “Part III: Height systems” *SaLIS* Vol. 66, No. 2, pages 149–160, June 2006.
  - “Part IV: GPS heighting” *SaLIS* Vol. 66, No. 3, pages 165–183, September 2006.

13.17 External links

- Geodetic awareness guidance note, Geodesy Subcommittee, Geomatics Committee, International Association of Oil & Gas Producers

Chapter 14

Physical geodesy

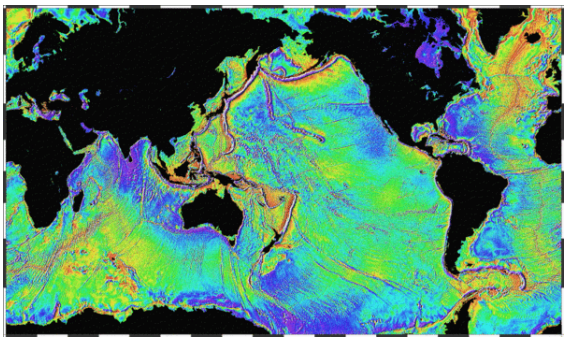

Ocean basins mapped with satellite altimetry. Seafloor features larger than 10 km are detected by resulting gravitational distortion of sea surface. (1995, NOAA)

Physical geodesy is the study of the physical properties of the gravity field of the Earth, the geopotential, with a view to their application in geodesy.

14.1 Measurement procedure

Traditional geodetic instruments such as theodolites rely on the gravity field for orienting their vertical axis along the local plumb line or local vertical direction with the aid of a spirit level. After that, vertical angles (zenith angles or, alternatively, elevation angles) are obtained with respect to this local vertical, and horizontal angles in the plane of the local horizon, perpendicular to the vertical.

Levelling instruments again are used to obtain geopotential differences between points on the Earth's surface. These can then be expressed as "height" differences by conversion to metric units.

14.2 The geopotential

The Earth's gravity field can be described by a potential as follows:

$$\mathbf{g} = \nabla W = \operatorname{grad} W = \frac{\partial W}{\partial X}\mathbf{i} + \frac{\partial W}{\partial Y}\mathbf{j} + \frac{\partial W}{\partial Z}\mathbf{k}$$

which expresses the gravitational acceleration vector as the gradient of W , the potential of gravity. The vector triad $\{\mathbf{i}, \mathbf{j}, \mathbf{k}\}$ is the orthonormal set of base vectors in space, pointing along the X, Y, Z coordinate axes.

Note that both gravity and its potential contain a contribution from the centrifugal pseudo-force due to the Earth's rotation. We can write

$$W = V + \Phi$$

where V is the potential of the *gravitational* field, W that of the *gravity* field, and Φ that of the centrifugal force field.

The centrifugal force is given by

$$\mathbf{g}_c = \omega^2 \mathbf{p},$$

where

$$\mathbf{p} = X\mathbf{i} + Y\mathbf{j} + 0 \cdot \mathbf{k}$$

is the vector pointing to the point considered straight from the Earth's rotational axis. It can be shown that this pseudo-force field, in a reference frame co-rotating with the Earth, has a potential associated with it that looks like this:

$$\Phi = \frac{1}{2}\omega^2(X^2 + Y^2).$$

This can be verified by taking the gradient (∇) operator of this expression.

Here, X , Y and Z are geocentric coordinates.

14.3 Units of gravity and geopotential

Gravity is commonly measured in units of $\mathrm{m{\cdot}s^{-2}}$ (metres per second squared). This also can be expressed (multiplying by the gravitational constant **G** in order to change units) as newtons per kilogram of attracted mass.

Potential is expressed as gravity times distance, $m^2 \cdot s^{-2}$. Travelling one metre in the direction of a gravity vector of strength 1 $m \cdot s^{-2}$ will increase your potential by 1 $m^2 \cdot s^{-2}$. Again employing G as a multipier, the units can be changed to joules per kilogram of attracted mass.

A more convenient unit is the GPU, or geopotential unit: it equals 10 $m^2 \cdot s^{-2}$. This means that travelling one metre in the vertical direction, i.e., the direction of the 9.8 $m \cdot s^{-2}$ ambient gravity, will *approximately* change your potential by 1 GPU. Which again means that the difference in geopotential, in GPU, of a point with that of sea level can be used as a rough measure of height "above sea level" in metres.

14.4 The normal potential

To a rough approximation, the Earth is a sphere, or to a much better approximation, an ellipsoid. We can similarly approximate the gravity field of the Earth by a spherically symmetric field:

$$W \approx \frac{GM}{R}$$

of which the *equipotential surfaces*—the surfaces of constant potential value—are concentric spheres.

It is more accurate to approximate the geopotential by a field that has *the Earth reference ellipsoid* as one of its equipotential surfaces, however. The most recent Earth reference ellipsoid is GRS80, or Geodetic Reference System 1980, which the Global Positioning system uses as its reference. Its geometric parameters are: semi-major axis a = 6378137.0 m, and flattening f = 1/298.257222101.

A geopotential field U is constructed, being the sum of a gravitational potential Ψ and the known centrifugal potential Φ , that *has the GRS80 reference ellipsoid as one of its equipotential surfaces*. If we also require that the enclosed mass is equal to the known mass of the Earth (including atmosphere) $GM = 3986005 \times 10^8$ $m^3 \cdot s^{-2}$, we obtain for the *potential at the reference ellipsoid:*

$$U_0 = 62636860.850 \text{ m}^2 \text{ s}^{-2}$$

Obviously, this value depends on the assumption that the potential goes asymptotically to zero at infinity ($R \to \infty$), as is common in physics. For practical purposes it makes more sense to choose the zero point of normal gravity to be that of the reference ellipsoid, and refer the potentials of other points to this.

14.5 Disturbing potential and geoid

Once a clean, smooth geopotential field U has been constructed matching the known GRS80 reference ellipsoid with an equipotential surface (we call such a field a *normal potential*) we can subtract it from the true (measured) potential W of the real Earth. The result is defined as **T**, the *disturbing potential*:

$$T = W - U$$

The disturbing potential **T** is numerically a great deal smaller than **U** or **W**, and captures the detailed, complex variations of the true gravity field of the actually existing Earth from point-to-point, as distinguished from the overall global trend captured by the smooth mathematical ellipsoid of the normal potential.

Due to the irregularity of the Earth's true gravity field, the equilibrium figure of sea water, or the geoid, will also be of irregular form. In some places, like west of Ireland, the geoid—mathematical mean sea level—sticks out as much as 100 m above the regular, rotationally symmetric reference ellipsoid of GRS80; in other places, like close to Ceylon, it dives under the ellipsoid by nearly the same amount. The separation between these two surfaces is called the undulation of the geoid, symbol N , and is closely related to the disturbing potential.

According to the famous Bruns formula, we have

$$N = T/\gamma\,,$$

where γ is the force of gravity computed from the normal field potential U .

In 1849, the mathematician George Gabriel Stokes published the following formula named after him:

$$N = \frac{R}{4\pi\gamma_0} \iint_\sigma \Delta g\, S(\psi)\, d\sigma.$$

In this formula, Δg stands for *gravity anomalies*, differences between true and normal (reference) gravity, and S is the *Stokes function*, a kernel function derived by Stokes in closed analytical form. (Note that determining N anywhere on Earth by this formula requires Δg to be known *everywhere on Earth*. Welcome to the role of international co-operation in physical geodesy.)

The geoid, or mathematical mean sea surface, is defined not only on the seas, but also under land; it is the equilibrium water surface that would result, would sea water be allowed to move freely (e.g., through tunnels) under the land. Technically, an *equipotential surface* of the true geopotential, chosen to coincide (on average) with mean sea level.

As mean sea level is physically realized by tide gauge bench marks on the coasts of different countries and continents, a number of slightly incompatible "near-geoids" will result, with differences of several decimetres to over one metre between them, due to the dynamic sea surface topography. These are referred to as *vertical* or *height datums*.

For every point on Earth, the local direction of gravity or vertical direction, materialized with the plumb line, is *perpendicular* to the geoid. On this is based a method, *astrogeodetic levelling*, for deriving the local figure of the geoid by measuring *deflections of the vertical* by astronomical means over an area.

14.6 Gravity anomalies

Main article: Gravity anomaly

Above we already made use of *gravity anomalies* Δg . These are computed as the differences between true (observed) gravity $g = \|\vec{g}\|$, and calculated (normal) gravity $\gamma = \|\vec{\gamma}\| = \|\nabla U\|$. (This is an oversimplification; in practice the location in space at which γ is evaluated will differ slightly from that where g has been measured.) We thus get

$$\Delta g = g - \gamma.$$

These anomalies are called free-air anomalies, and are the ones to be used in the above Stokes equation.

In geophysics, these anomalies are often further reduced by removing from them the *attraction of the topography*, which for a flat, horizontal plate (Bouguer plate) of thickness H is given by

$$a_B = 2\pi G\rho H,$$

The Bouguer reduction to be applied as follows:

$$\Delta g_B = \Delta g_{FA} - a_B,$$

so-called Bouguer anomalies. Here, Δg_{FA} is our earlier Δg , the free-air anomaly.

In case the terrain is not a flat plate (the usual case!) we use for H the local terrain height value but apply a further correction called the terrain correction (*TC*).

14.7 See also

- LAGEOS
- Friedrich Robert Helmert
- Geophysics
- Gravity of Earth
- gravimetry
- satellite geodesy

14.8 References

- B. Hofmann-Wellenhof and H. Moritz, **Physical Geodesy,** Springer-Verlag Wien, 2005. (This text is an updated edition of the 1967 classic by W.A. Heiskanen and H. Moritz).

Chapter 15

Gravity of Earth

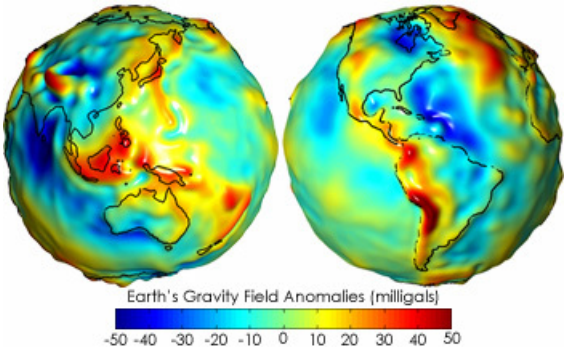

*Earth's gravity measured by NASA's GRACE mission, showing deviations from the theoretical gravity of an idealized smooth Earth, the so-called earth ellipsoid. Red shows the areas where gravity is stronger than the smooth, standard value, and blue reveals areas where gravity is weaker. (**Animated version.**)*[1]

The **gravity of Earth**, which is denoted by ***g***, refers to the acceleration that the Earth imparts to objects on or near its surface. In SI units this acceleration is measured in metres per second squared (in symbols, m/s^2 or m·s^{-2}) or equivalently in newtons per kilogram (N/kg or N·kg^{-1}). It has an approximate value of 9.81 m/s^2, which means that, ignoring the effects of air resistance, the speed of an object falling freely near the Earth's surface will increase by about 9.81 metres (32.2 ft) per second every second. This quantity is sometimes referred to informally as *little g* (in contrast, the gravitational constant *G* is referred to as *big G*).

There is a direct relationship between gravitational acceleration and the downwards weight force experienced by objects on Earth, given by the equation $F = ma$ (*force* = *mass* × *acceleration*). However, other factors such as the rotation of the Earth also contribute to the net acceleration.

The precise strength of Earth's gravity varies depending on location. The nominal "average" value at the Earth's surface, known as standard gravity is, by definition,[2] 9.80665 m/s^2 (about 32.1740 ft/s^2). This quantity is denoted variously as g_n, g_e (though this sometimes means the normal equatorial value on Earth, 9.78033 m/s^2), g_0, gee, or simply *g* (which is also used for the variable local value). The symbol *g* should not be confused with g, the abbreviation for gram (which is not italicized).[3][4]

15.1 Variation in gravity and apparent gravity

A perfect sphere of spherically uniform density (density varies solely with distance from centre) would produce a gravitational field of uniform magnitude at all points on its surface, always pointing directly towards the sphere's centre. However, the Earth deviates slightly from this ideal, and there are consequently slight deviations in both the magnitude and direction of gravity across its surface. Furthermore, the net force exerted on an object due to the Earth, called "effective gravity" or "apparent gravity", varies due to the presence of other factors, such as inertial response to the Earth's rotation. A scale or plumb bob measures only this effective gravity.

Parameters affecting the apparent or actual strength of Earth's gravity include latitude, altitude, and the local topography and geology.

Apparent gravity on the earth's surface varies by around 0.7%, from 9.7639 m/s^2 on the Nevado Huascarán mountain in Peru to 9.8337 m/s^2 at the surface of the Arctic Ocean.[5] In large cities, it ranges from 9.766 in Kuala Lumpur, Mexico City, and Singapore to 9.825 in Oslo and Helsinki.

15.1.1 Latitude

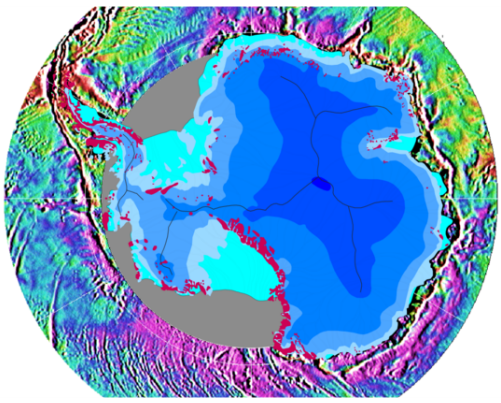

The differences of Earth's gravity around the Antarctic continent.

The surface of the Earth is rotating, so it is not an inertial frame of reference. At latitudes nearer the Equator, the outward centrifugal force produced by Earth's rotation is larger than at polar latitudes. This counteracts the Earth's gravity to a small degree – up to a maximum of 0.3% at the Equator – and reduces the apparent downward acceleration of falling objects.

The second major reason for the difference in gravity at different latitudes is that the Earth's equatorial bulge (itself also caused by inertia) causes objects at the Equator to be farther from the planet's centre than objects at the poles. Because the force due to gravitational attraction between two bodies (the Earth and the object being weighed) varies inversely with the square of the distance between them, an object at the Equator experiences a weaker gravitational pull than an object at the poles.

In combination, the equatorial bulge and the effects of the Earth's inertia mean that sea-level gravitational acceleration increases from about 9.780 m/s^2 at the Equator to about 9.832 m/s^2 at the poles, so an object will weigh about 0.5% more at the poles than at the Equator.[6][7]

The same two factors influence the direction of the effective gravity. Anywhere on Earth away from the Equator or poles, effective gravity points not exactly toward the centre of the Earth, but rather perpendicular to the surface of the geoid, which, due to the flattened shape of the Earth, is somewhat toward the opposite pole. About half of the deflection is due to inertia, and half because the extra mass around the Equator causes a change in the direction of the true gravitational force relative to what it would be on a spherical Earth.

15.1.2 Altitude

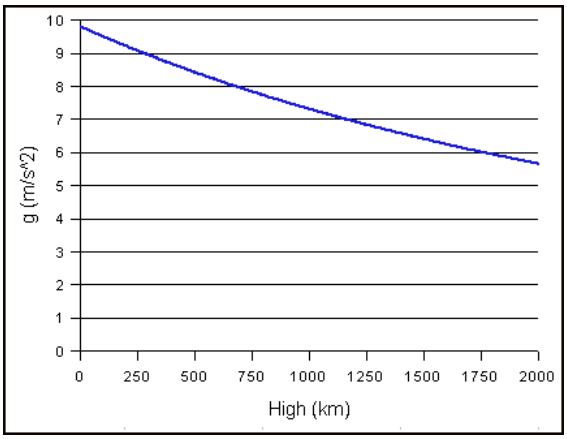

The graph shows the variation in gravity relative to the height of an object

Gravity decreases with altitude as one rises above the earth's surface because greater altitude means greater distance from the Earth's center. All other things being equal, an increase in altitude from sea level to 9,000 metres (30,000 ft) causes a weight decrease of about 0.29%. (An additional factor affecting apparent weight is the decrease in air density at altitude, which lessens an object's buoyancy.[8] This would increase a person's apparent weight at an altitude of 9,000 metres by about 0.08%)

It is a common misconception that astronauts in orbit are weightless because they have flown high enough to "escape" the Earth's gravity. In fact, at an altitude of 400 kilometres (250 mi), equivalent to a typical orbit of the Space Shuttle, gravity is still nearly 90% as strong as at the Earth's surface. Weightlessness actually occurs because orbiting objects are in free-fall.[9]

The effect of ground elevation depends on the density of the ground (see Slab correction section). A person flying at 30 000 ft above sea level over mountains will feel more gravity than someone at the same elevation but over the sea. However, a person standing on the earth's surface feels less gravity when the elevation is higher.

The following formula approximates the Earth's gravity variation with altitude:

$$g_h = g_0 \left(\frac{r_\mathrm{e}}{r_\mathrm{e} + h} \right)^2$$

Where

- gh is the gravitational acceleration at height h above sea level.
- r_e is the Earth's mean radius.
- g_0 is the standard gravitational acceleration.

This formula treats the Earth as a perfect sphere with a radially symmetric distribution of mass; a more accurate mathematical treatment is discussed below.

15.1.3 Depth

See also: Shell theorem

An approximate depth dependence of density in the Earth can be obtained by assuming that the mass is spherically symmetric (it depends only on depth, not on latitude or longitude). In such a body, the gravitational acceleration is towards the center. The gravity at a radius r depends only on the mass inside the sphere of radius r; all the contributions from outside cancel out. This is a consequence of the inverse-square law of gravitation. Another consequence is that the gravity is the same as if all the mass were concentrated at the center of the Earth. Thus, the gravitational acceleration at this radius is[10]

$$g(r) = -\frac{GM(r)}{r^2}.$$

where G is the gravitational constant and $M(r)$ is the total mass enclosed within radius r. If the Earth had a constant density ρ, the mass would be $M(r) = (4/3)\pi\rho r^3$ and the dependence of gravity on depth would be

$$g(r) = \frac{4\pi}{3} G\rho r.$$

g at depth d is given by g'=g(1-d/R) where g is acceleration due to gravity on surface of the earth, d is depth and R is radius of Earth. If the density decreased linearly with increasing radius from a density ϱ_0 at the centre to ϱ_1 at the surface, then $\varrho(r) = \varrho_0 - (\varrho_0 - \varrho_1)\, r / r_\mathrm{e}$, and the dependence would be

$$g(r) = \frac{4\pi}{3} G\rho_0 r - \pi G \left(\rho_0 - \rho_1\right) \frac{r^2}{r_\mathrm{e}}.$$

The actual depth dependence of density and gravity, inferred from seismic travel times (see Adams–Williamson equation), is shown in the graphs below.

15.1.4 Local topography and geology

See also: Physical geodesy

Local variations in topography (such as the presence of mountains) and geology (such as the density of rocks in the vicinity) cause fluctuations in the Earth's gravitational field, known as gravitational anomalies. Some of these anomalies can be very extensive, resulting in bulges in sea level, and throwing pendulum clocks out of synchronisation.

The study of these anomalies forms the basis of gravitational geophysics. The fluctuations are measured with highly sensitive gravimeters, the effect of topography and other known factors is subtracted, and from the resulting data conclusions are drawn. Such techniques are now used by prospectors to find oil and mineral deposits. Denser rocks (often containing mineral ores) cause higher than normal local gravitational fields on the Earth's surface. Less dense sedimentary rocks cause the opposite.

15.1.5 Other factors

In air, objects experience a supporting buoyancy force which reduces the apparent strength of gravity (as measured by an object's weight). The magnitude of the effect depends on air density (and hence air pressure); see Apparent weight for details.

The gravitational effects of the Moon and the Sun (also the cause of the tides) have a very small effect on the apparent strength of Earth's gravity, depending on their relative positions; typical variations are 2 μm/s^2 (0.2 mGal) over the course of a day.

15.1.6 Comparative gravities in various cities around the world

The table below shows the gravitational acceleration in various cities around the world;[12] amongst these listed cities, it is lowest in Kandy, Sri Lanka (9.775 m/s^2 32.07 ft/s^2) and highest in Anchorage, Alaska (9.826 m/s^2 32.24 ft/s^2). A difference of about 0.5%.

15.1.7 Mathematical models

Latitude model

If the terrain is at sea level, we can estimate g:

$$g_\phi = 9.780327 \left(1 + 0.0053024 \sin^2\phi - 0.0000058 \sin^2 2\phi\right) \frac{\mathrm{m}}{\mathrm{s}^2}$$

where

$$g_\phi = \text{acceleration in m·s}^{-2} \text{ at latitude : } \phi$$

This is the International Gravity Formula 1967, the 1967 Geodetic Reference System Formula, Helmert's equation or Clairaut's formula.[13]

Helmert's equation may be written equivalently to the version above as either:

$$g_\phi = \left(9.8061999 - 0.0259296 \cos(2\phi) + 0.0000567 \cos^2(2\phi)\right) \frac{\mathrm{m}}{\mathrm{s}^2}$$

or

$$g_\phi = \left(9.780327 + 0.0516323 \sin^2(\phi) + 0.0002269 \sin^4(\phi)\right) \frac{\mathrm{m}}{\mathrm{s}^2}$$

An alternate formula for g as a function of latitude is the WGS (World Geodetic System) 84 Ellipsoidal Gravity Formula:

$$g_\phi = \left(9.7803267714 \frac{1 + 0.00193185138639 \sin^2\phi}{\sqrt{1 - 0.00669437999013 \sin^2\phi}}\right) \frac{\mathrm{m}}{\mathrm{s}^2}$$

The difference between the WGS-84 formula and Helmert's equation is less than $0.68{\cdot}10^{-6}$ m·s^{-2}.

Free air correction

The first correction to be applied to the model is the free air correction (FAC) that accounts for heights above sea level. Near the surface of the Earth (sea level), gravity decreases with height such that linear extrapolation would give zero gravity at a height of one half the radius is 9.8 m·s^{-2} per 3,200 km.[14]

Using the mass and radius of the Earth:

$$r_{\text{Earth}} = 6.371 \times 10^6\,\text{m}$$

$$m_{\text{Earth}} = 5.9736 \times 10^{24}\,\text{kg}$$

The FAC correction factor (Δg) can be derived from the definition of the acceleration due to gravity in terms of G, the Gravitational Constant (see Estimating *g* from the law of universal gravitation, below):

$$g_0 = G\,m_{\text{Earth}}/r_{\text{Earth}}^2 = 9.8331\ \frac{\text{m}}{\text{s}^2}$$

where:

$$G = 6.67428 \times 10^{-11}\ \frac{\text{m}^3}{\text{kg}\cdot\text{s}^2}.$$

At a height *h* above the nominal surface of the earth *gh* is given by:

$$g_h = G\,m_{\text{Earth}}/\left(r_{\text{Earth}} + h\right)^2$$

So the FAC for a height *h* above the nominal earth radius can be expressed:

$$\Delta g_h = \left[G\,m_{\text{Earth}}/\left(r_{\text{Earth}} + h\right)^2\right] - \left[G\,m_{\text{Earth}}/r_{\text{Earth}}^2\right]$$

This expression can be readily used for programming or inclusion in a spreadsheet. Collecting terms, simplifying and neglecting small terms ($h << r_{\text{Earth}}$), however yields the good approximation:

$$\Delta g_h \approx -\frac{G\,m_{\text{Earth}}}{r_{\text{Earth}}^2} \times \frac{2\,h}{r_{\text{Earth}}}$$

Using the numerical values above and for a height *h* in metres:

$$\Delta g_h \approx -3.084 \times 10^{-6}\,h$$

Grouping the latitude and FAC altitude factors the expression most commonly found in the literature is:

$$g_{\phi,h} = 9.780327\left(1 + 0.0053024\sin^2\phi - 0.0000058\sin^2 2\phi\right) - 3.086\times10^{-6}h$$

where $g_{\phi,h}$ = acceleration in m·s^{-2} at latitude ϕ and altitude *h* in metres. Alternatively (with the same units for *h*) the expression can be grouped as follows:

$$g_{\phi,h} = 9.780327\left[\left(1 + 0.0053024\sin^2\phi - 0.0000058\sin^2 2\phi\right) - 3.155\times10^{-7}h\right]\ \frac{\text{m}}{\text{s}^2}$$

Slab correction

> Note: The section uses the galileo (symbol: "Gal"), which is a cgs unit for acceleration of 1 centimetre/second^2.

For flat terrain above sea level a second term is added for the gravity due to the extra mass; for this purpose the extra mass can be approximated by an infinite horizontal slab, and we get $2\pi G$ times the mass per unit area, i.e. 4.2×10^{-10} m^3·s^{-2}·kg^{-1} (0.042 μGal·kg^{-1}·m^2)) (the Bouguer correction). For a mean rock density of 2.67 g·cm^{-3} this gives 1.1×10^{-6} s^{-2} (0.11 mGal·m^{-1}). Combined with the free-air correction this means a reduction of gravity at the surface of ca. 2 μm·s^{-2} (0.20 mGal) for every metre of elevation of the terrain. (The two effects would cancel at a surface rock density of 4/3 times the average density of the whole earth. The density of the whole earth is 5.515 g·cm^{-3}, so standing on a slab of something like iron whose density is over 7.35 g·cm^{-3} would increase one's weight.)

For the gravity below the surface we have to apply the free-air correction as well as a double Bouguer correction. With the infinite slab model this is because moving the point of observation below the slab changes the gravity due to it to its opposite. Alternatively, we can consider a spherically symmetrical Earth and subtract from the mass of the Earth that of the shell outside the point of observation, because that does not cause gravity inside. This gives the same result.

15.2 Estimating *g* from the law of universal gravitation

From the law of universal gravitation, the force on a body acted upon by Earth's gravity is given by

$$F = G\frac{m_1 m_2}{r^2} = \left(G\frac{m_1}{r^2}\right) m_2$$

where *r* is the distance between the centre of the Earth and the body (see below), and here we take m_1 to be the mass of the Earth and m_2 to be the mass of the body.

Additionally, Newton's second law, *F* = *ma*, where *m* is mass and *a* is acceleration, here tells us that

$$F = m_2 g$$

Comparing the two formulas it is seen that:

$$g = G\frac{m_1}{r^2}$$

So, to find the acceleration due to gravity at sea level, substitute the values of the gravitational constant, *G*, the

Earth's mass (in kilograms), m_1, and the Earth's radius (in metres), r, to obtain the value of g:

$$g = G\frac{m_1}{r^2} = (6.6742\times10^{-11})\frac{5.9736 \times 10^{24}}{(6.37101 \times 10^6)^2} = 9.822\text{m}\cdot\text{s}^{-2}$$

Note that this formula only works because of the mathematical fact that the gravity of a uniform spherical body, as measured on or above its surface, is the same as if all its mass were concentrated at a point at its centre. This is what allows us to use the Earth's radius for r.

The value obtained agrees approximately with the measured value of g. The difference may be attributed to several factors, mentioned above under "Variations":

- The Earth is not homogeneous
- The Earth is not a perfect sphere, and an average value must be used for its radius
- This calculated value of g only includes true gravity. It does not include the reduction of constraint force that we perceive as a reduction of gravity due to the rotation of Earth, and some of gravity being "used up" in providing the centripetal acceleration

There are significant uncertainties in the values of r and m_1 as used in this calculation, and the value of G is also rather difficult to measure precisely.

If G, g and r are known then a reverse calculation will give an estimate of the mass of the Earth. This method was used by Henry Cavendish.

15.3 Comparative gravities of the Earth, Sun, Moon, and planets

The table below shows comparative gravitational accelerations at the surface of the Sun, the Earth's moon, each of the planets in the Solar System and their major moons, Pluto, and Eris. The "surface" is taken to mean the cloud tops of the gas giants (Jupiter, Saturn, Uranus and Neptune). For the Sun, the surface is taken to mean the photosphere. The values in the table have not been derated for the inertia effect of planet rotation (and cloud-top wind speeds for the gas giants) and therefore, generally speaking, are similar to the actual gravity that would be experienced near the poles. For reference the time it would take an object to fall 100 metres, the height of a skyscraper, is shown, along with the maximum speed reached. Air resistance is neglected.

15.4 See also

- Earth's magnetic field
- Gravitation
- Gravity anomaly, Bouguer anomaly
- Gravitation of the Moon
- Gravitational acceleration
- Gravity Field and Steady-State Ocean Circulation Explorer
- Gravity Recovery and Climate Experiment
- Newton's law of universal gravitation

15.5 References

[1] NASA/JPL/University of Texas Center for Space Research. "PIA12146: GRACE Global Gravity Animation". *Photojournal*. NASA Jet Propulsion Laboratory. Retrieved 30 December 2013.

[2] *The international system of units (SI)* (2008 ed.). United States Department of Commerce, NIST Special Publication 330. p. 51.

[3] Bureau International des Poids et Mesures (2006). "Chapter 5". "The International System of Units (SI)". 8th ed. Retrieved 2009-11-25. "Unit names are normally printed in roman (upright) type ... Symbols for quantities are generally single letters set in an italic font, although they may be qualified by further information in subscripts or superscripts or in brackets."

[4] "SI Unit rules and style conventions". National Institute For Standards and Technology (USA). September 2004. Retrieved 2009-11-25. "Variables and quantity symbols are in italic type. Unit symbols are in roman type."

[5] Hirt,Claessens et. al. (Aug 6, 2013). "New ultra-high resolution picture of Earth's gravity field". *Geophysical Research Letters DOI: 10.1002/grl.50838*.

[6] Boynton, Richard (2001). "*Precise Measurement of Mass*". "Sawe Paper No. 3147". Arlington, Texas: S.A.W.E., Inc. Retrieved 2007-01-21.

[7] "Curious About Astronomy?", Cornell University, retrieved June 2007

[8] "I feel 'lighter' when up a mountain but am I?", National Physical Laboratory FAQ

[9] "The G's in the Machine", NASA, see "Editor's note #2"

[10] Tipler, Paul A. (1999). *Physics for scientists and engineers.* (4th ed. ed.). New York: W.H. Freeman/Worth Publishers. pp. 336–337. ISBN 9781572594913.

[11] A. M. Dziewonski, D. L. Anderson (1981). "Preliminary reference Earth model". *Physics of the Earth and Planetary Interiors* **25** (4): 297–356. Bibcode:1981PEPI...25..297D. doi:10.1016/0031-9201(81)90046-7. ISSN 0031-9201.

[12] Gravitational Fields Widget as of Oct 25th, 2012 – WolframAlpha

[13] International Gravity formula

[14] The rate is calculated by differentiating $g(r)$ with respect to r and evaluating at r=$r\mathrm{E}_{\mathrm{arth}}$.

[15] This value excludes the adjustment for centrifugal force due to Earth's rotation and is therefore greater than the 9.80665 m/s^2 value of standard gravity.

15.6 External links

- Altitude gravity calculator
- GRACE – Gravity Recovery and Climate Experiment
- GGMplus high resolution data (2013)

Chapter 16

Gravity anomaly

Not to be confused with Gravitational anomaly.

A **gravity anomaly** is the difference between the observed acceleration of a planet's gravity and a value predicted from a model. A location with a positive anomaly exhibits more gravity than predicted, while a negative anomaly exhibits a lower value than predicted. The anomaly is the body or effect that causes the deviation from the "ideal" gravity model. Many data corrections must be made to the measured gravity value in order to extract the response of the local anomaly, or local geology, which is typically the goal of applied geophysics.

16.1 Causes

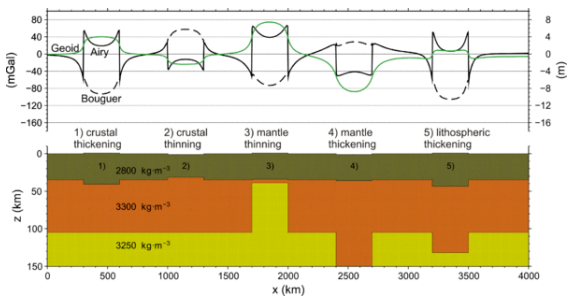

Gravity and geoid anomalies caused by various crustal and lithospheric thickness changes relative to a reference configuration. All settings are under local isostatic compensation.

Lateral variations in gravity anomalies are related to anomalous density distributions within the Earth. Gravity measures help us to understand the internal structure of the planet. Synthetic calculations show that the gravity anomaly signature of a thickened crust (for example, in orogenic belts produced by continental collision) is negative and larger in absolute value, relative to a case where thickening affects the entire lithosphere.

The Bouguer anomalies usually are negative in the mountains because of isostasy: the rock density of their roots is lower, compared with the surrounding earth's mantle. Typical anomalies in the Central Alps are −150 milligals (−1.5 mm/s^2). Rather local anomalies are used in applied geophysics: if they are positive, this may indicate metallic ores. At scales between entire mountain ranges and ore bodies, Bouguer anomalies may indicate rock types. For example, the northeast-southwest trending high across central New Jersey (see figure) represents a graben of Triassic age largely filled with dense basalts. Salt domes are typically expressed in gravity maps as lows, because salt has a low density compared to the rocks the dome intrudes. Anomalies can help to distinguish sedimentary basins whose fill differs in density from that of the surrounding region - see Gravity Anomalies of Britain and Ireland for example.

16.2 Geodesy and geophysics

In geodesy and geophysics, the usual theoretical model is the gravity on the surface of a reference ellipsoid such as WGS84.

To understand the nature of the gravity anomaly due to the subsurface, a number of corrections must be made to the measured gravity value:

1. The *theoretical gravity* (smoothed normal gravity) should be removed in order to leave only local effects.
2. The elevation of the point where each gravity measurement was taken must be reduced to a reference datum to compare the whole profile. This is called the *Free-air Correction*, and when combined with the removal of theoretical gravity leaves the free-air anomaly .
3. the normal gradient of gravity (rate of change of gravity by change of elevation), as in free air, usually 0.3086 milligals per meter, or the *Bouguer gradient* of 0.1967 mGal/m (19.67 μm/(s^2·m) which considers the mean rock density (2.67 g/cm^3) beneath the point; this value is found by subtracting the gravity due to the Bouguer plate, which is 0.1119 mGal/m (11.19 μm/(s^2·m)) for this density. Simply, we have to correct for the effects of any material between the point where gravimetry was done and the geoid. To do this we model the material in between as being

made up of an infinite number of slabs of thickness *t*. These slabs have no lateral variation in density, but each slab may have a different density than the one above or below it. This is called the *Bouguer correction*.

4. and (in special cases) a digital terrain model (DTM). A terrain correction, computed from a model structure, accounts for the effects of rapid lateral change in density, e.g. edge of plateau, cliffs, steep mountains, etc.

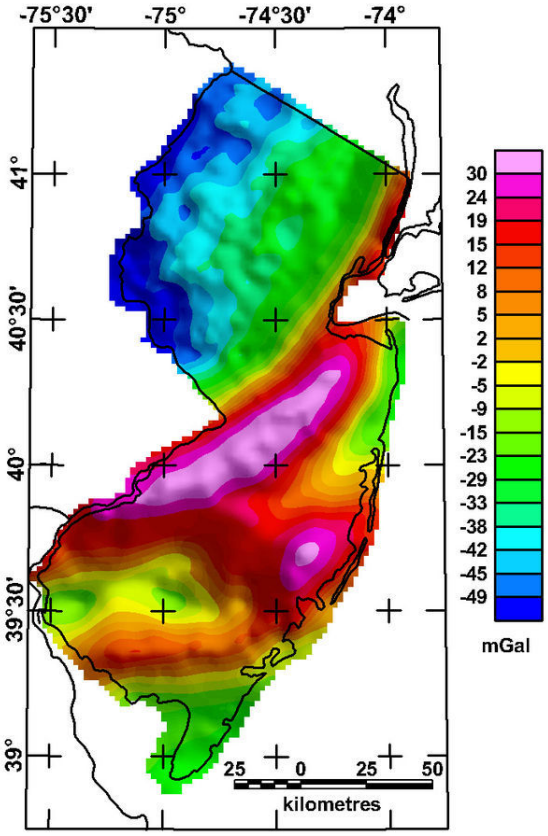

(Bouguer) gravity anomaly map of the state of New Jersey (USGS)

For these reductions, different methods are used:

- The gravity changes as we move away from the surface of the Earth. For this reason, we must compensate with the free-air anomaly (or Faye's anomaly): application of the *normal gradient* 0.3086 mGal/m, but no terrain model. This anomaly means a downward shift of the point, together with the whole shape of the terrain. This simple method is ideal for many geodetic applications.
- simple Bouguer anomaly: downward reduction just by the Bouguer gradient (0.1967). This anomaly handles the point as if it is located on a flat plain.
- **refined** (or **complete**) Bouguer anomaly (usual abbreviation ΔgB): the DTM is considered as accurate as possible, using a standard density of 2.67 g/cm^3 (granite, limestone). Bouguer anomalies are ideal for geophysics because they show the effects of different rock densities in the subsurface.
  - The difference between the two - the differential gravitational effect of the unevenness of the terrain - is called the terrain effect. It is always negative (up to 100 milligals).
  - The difference between *Faye anomaly* and ΔgB is called *Bouguer reduction* (attraction of the terrain).
- **special methods** like that of Poincare-Prey, using an interior gravity gradient of about 0.009 milligal per meter (90 nm/(s^2·m)). These methods are valid for the gravity within boreholes or for special geoid computations.

16.3 Satellite measurements

Large-scale gravity anomalies can be detected from space. The Gravity Recovery and Climate Experiment (GRACE) consists of two satellites that can detect gravitational changes across the Earth.

16.4 Astronomy

Any region of space with higher than expected mass density will produce a gravity anomaly. Observations of gravity anomalies on galactic and intergalactic scales lead to the assumption of dark matter.

16.5 See also

- Gravimetry
- Physical geodesy
- Vertical deflection

16.6 External links

- Bouguer anomaly theory
- Bouguer anomalies of Belgium. The blue regions are related to deficit masses in the subsurface - e.g. lower rock density beneath the mountains

Chapter 17

Gravity Recovery and Climate Experiment

The **Gravity Recovery And Climate Experiment** (**GRACE**), a joint mission of NASA and the German Aerospace Center, has been making detailed measurements of Earth's gravity field anomalies since its launch in March 2002.

Gravity is determined by mass. By measuring gravity anomalies, GRACE shows how mass is distributed around the planet and how it varies over time. Data from the GRACE satellites is an important tool for studying Earth's ocean, geology, and climate.

GRACE is a collaborative endeavor involving the Center for Space Research at the University of Texas, Austin; NASA's Jet Propulsion Laboratory, Pasadena, Calif.; the German Space Agency and Germany's National Research Center for Geosciences, Potsdam.[1] The Jet Propulsion Laboratory is responsible for the overall mission management under the NASA ESSP program.

The principal investigator is Dr. Byron Tapley of the University of Texas Center for Space Research, and the co-principal investigator is Dr. Christoph Reigber of the GeoForschungsZentrum (GFZ) Potsdam.[2]

The GRACE satellites were launched from Plesetsk Cosmodrome, Russia on a Rockot (SS-19 + Breeze upper stage) launch vehicle, on March 17, 2002.

As of November 2012 the craft was expected to remain in a slowly decaying orbit until 2015 or 2016.[3]

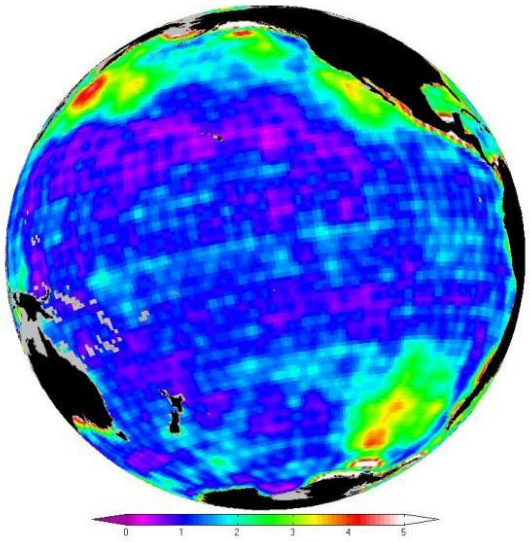

Variations in ocean bottom pressure measured by GRACE

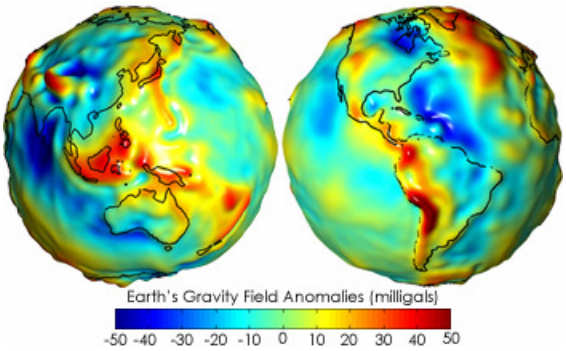

Gravity anomaly map from GRACE

17.1 Discoveries and applications

The monthly gravity anomalies maps generated by Grace are up to 1,000 times more accurate than previous maps, substantially improving the accuracy of many techniques used by oceanographers, hydrologists, glaciologists, geologists and other scientists to study phenomena that influence climate.[4]

From the thinning of ice sheets to the flow of water through aquifers and the slow currents of magma inside Earth, measurements of the amount of mass involved provided by GRACE help scientists better understand these important natural processes.

Among the first important applications for GRACE data was to improve the understanding of global ocean circulation. The hills and valleys in the ocean's surface are due to currents and variations in Earth's gravity field. GRACE enables separation of those two effects to better measure ocean currents and their effect on climate. GRACE data are also critical in helping to determine the cause of sea level rise, whether it is the result of mass being added to the ocean, from melting glaciers, for example, or from thermal expansion of warming water or changes

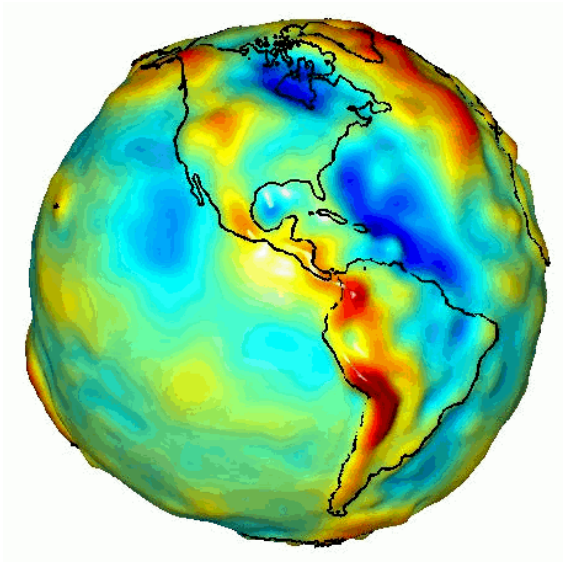

Gravity anomaly map from GRACE as a rotating globe

in salinity.[5]

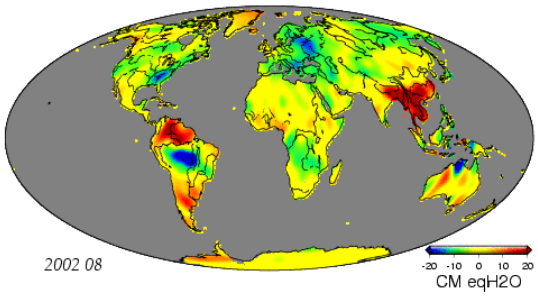

Global Gravity Anomaly Animation over land from GRACE

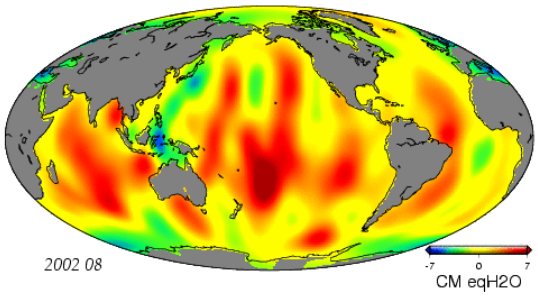

Global Gravity Anomaly Animation over oceans from GRACE

As of February 2012, the data obtained by GRACE are the most precise gravimetric data yet recorded: they have been used to re-analyse data obtained from the LAGEOS experiment to try to measure the relativistic frame-dragging effect. In 2006, a team of researchers led by Ralph von Frese and Laramie Potts used GRACE data to discover the 480-kilometer (300 mi) wide Wilkes Land crater in Antarctica, which probably formed about 250 million years ago.[6] GRACE has been used to map the hydrologic cycle in the Amazon River basin and the location and magnitude of post-glacial rebound from changes in the free air gravity anomaly. GRACE data has also been used to analyze the shifts in the Earth's crust caused by the earthquake that created the 2004 Indian Ocean tsunami.[7] Scientists have recently developed a new way to calculate ocean bottom pressure—as important to oceanographers as atmospheric pressure is to meteorologists—using GRACE data.[8]

17.2 How GRACE works

GRACE is the first Earth-monitoring mission in the history of space flight whose key measurement is not derived from electromagnetic waves either reflected off, emitted by, or transmitted through Earth's surface and/or atmosphere. Instead, the mission uses a microwave ranging system to accurately measure changes in the speed and distance between two identical spacecraft flying in a polar orbit about 220 kilometers (140 mi) apart, 500 kilometers (310 mi) above Earth. The ranging system is sensitive enough to detect separation changes as small as 10 micrometres (approximately one-tenth the width of a human hair) over a distance of 220 kilometers.[9]

As the twin GRACE satellites circle the globe 15 times a day, they sense minute variations in Earth's gravitational pull. When the first satellite passes over a region of slightly stronger gravity, a gravity anomaly, it is pulled slightly ahead of the trailing satellite. This causes the distance between the satellites to increase. The first spacecraft then passes the anomaly, and slows down again; meanwhile the following spacecraft accelerates, then decelerates over the same point.

By measuring the constantly changing distance between the two satellites and combining that data with precise positioning measurements from Global Positioning System (GPS) instruments, scientists can construct a detailed map of Earth's gravity anomalies.

The two satellites (nicknamed "Tom" and "Jerry") constantly maintain a two-way microwave-ranging link between them. Fine distance measurements are made by comparing frequency shifts of the link. As a cross-check, the vehicles measure their own movements using accelerometers. All of this information is then downloaded to ground stations. To establish baseline positions and fulfill housekeeping functions, the satellites also use star cameras, magnetometers, and GPS receivers. The GRACE vehicles also have optical corner reflectors to enable laser ranging from ground stations, bridging the range between spacecraft positions and Doppler ranges.

17.3 Spacecraft

The spacecraft were manufactured by Astrium of Germany, using its "Flexbus" platform. The microwave RF systems, and attitude determination and control sys-

tem algorithms were provided by Space Systems/Loral. The star cameras used to measure the spacecraft attitude were provided by Technical University of Denmark. The instrument computer along with a highly precise BlackJack GPS receiver and digital signal processing system has been provided by JPL in Pasadena. The highly precise accelerometer that is needed to separate atmospheric and solar wind effects from the gravitation data was manufactured by ONERA.

17.4 GRACE Follow On

The GeoForschungsZentrum (GFZ) Potsdam has announced a follow on of the GRACE mission. GRACE-FO mission will be a collaboration between GFZ and NASA and is scheduled to be launched in August 2017 on a Dnepr from Baikonur Cosmodrome.[10] The orbit and the design of GRACE-FO will be very similar to GRACE; the distance between the two spacecraft of GRACE-FO will be measured also with lasers (the original GRACE used microwave ranging) as a technological experiment in preparation for future satellites.[11][12]

17.5 See also

- Geoid
- Gravity Field and Steady-State Ocean Circulation Explorer (GOCE, March 2009 to Nov 2013)
- Gravity Recovery and Interior Laboratory (GRAIL, a similar probe intended to map the moon)

17.6 References

[1] "Grace Space Twins Set to Team Up to Track Earth's Water and Gravity". NASA/JPL.

[2] "Mission Overview". University of Texas. 19 Nov 2008. Retrieved 2009-07-30.

[3] "GRACE Orbit Lifetime Prediction".

[4] "New Gravity Mission on Track to Map Earth's Shifty Mass". NASA/JPL.

[5] "NASA Missions Help Dissect Sea Level Rise". NASA/JPL.

[6] "Big Bang in Antarctica--Killer Crater Found Under Ice". Ohio State University.

[7] Chang, Kenneth (August 8, 2006). "Before the '04 Tsunami, an Earthquake So Violent It Even Shook Gravity". The New York Times. Retrieved May 4, 2010.

[8] "Gravity data sheds new light on ocean, climate". NASA/JPL.

[9] "GRACE Launch Press Kit". NASA/JPL.

[10] "Gravity Recovery and Climate Experiment Follow On - Launch Vehicle". NASA JPL. Retrieved 20 November 2014.

[11] "Development, Operation and Analysis of Gravity Field Satellite Missions". GFZ Helmholtz Centre Potsdam.

[12] "Airbus Defence and Space to build two new research satellites for NASA". EADS Astrium.

17.7 External links

- GRACE mission home page (Primary Investigator)
- GRACE Tellus (JPL)
- GRACE mission home page (co Primary Investigator) (language: German)
- GRACE Mission Profile by NASA's Solar System Exploration
- *Science@NASA* article about GRACE
- *Weighing Earth's Water from Space* Estimating ground water using GRACE (written for non-scientists)
- Report by BBC showing early results
- GPS World Discussion of instrumentation

Chapter 18

Ocean current

This article is about ocean currents. For other uses, see Current (disambiguation).

An **ocean current** is a continuous, directed movement of seawater generated by the forces acting upon this mean flow, such as breaking waves, wind, Coriolis effect, cabbeling, temperature and salinity differences, with tides caused by the gravitational pull of the Moon and the Sun. Depth contours, shoreline configurations and interaction with other currents influence a current's direction and strength.

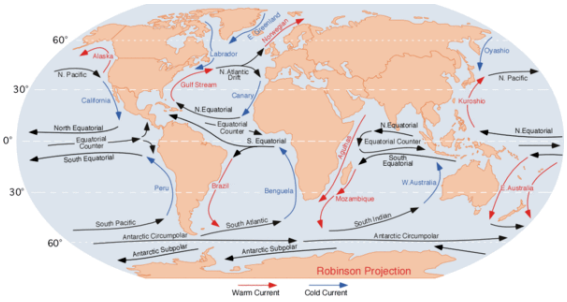

The ocean currents.

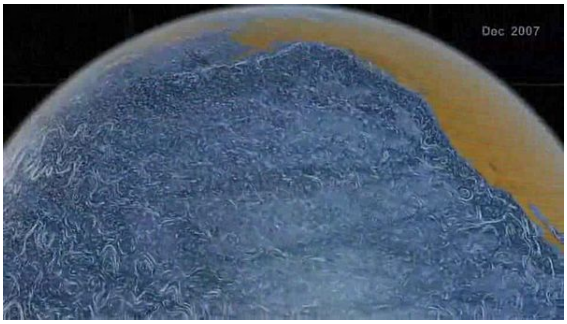

Distinctive white lines trace the flow of surface currents around the world.

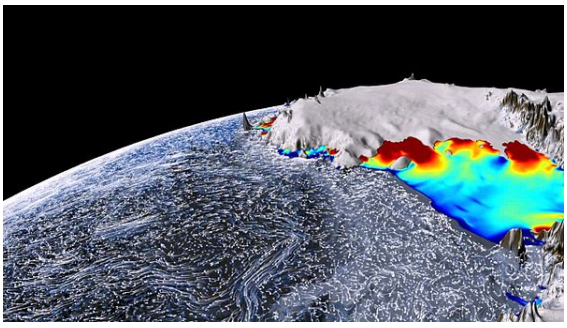

Animation of circulation around ice shelves of Antarctica.

Ocean currents can flow for great distances, and together they create the great flow of the global conveyor belt which plays a dominant part in determining the climate of many of the Earth's regions. Perhaps the most striking example is the Gulf Stream, which makes northwest Europe much more temperate than any other region at the same latitude. Another example is Lima, Peru where the climate is cooler (sub-tropical) than the tropical latitudes in which the area is located, due to the effect of the Humboldt Current. Ocean currents influence the temperature of the regions through which they travel. warm currents increase the temperature of the coasts along which they move. sea breezes that blow over warm currents get warmed in turn and absorb moisture.

18.1 Function

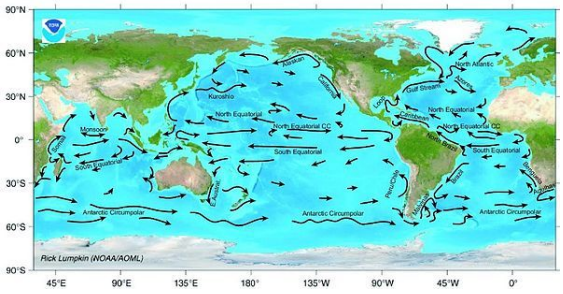

Major ocean surface currents, (Source: NOAA)

Surface ocean currents are sometimes wind driven and develop their typical clockwise spirals in the northern hemisphere counter clockwise rotation in the southern hemisphere because of the imposed wind stresses. In wind driven current, the Ekman spiral effect results in the currents flowing at an angle to the driving winds. The areas of surface ocean currents move somewhat with the seasons; this is most notable in equatorial currents.

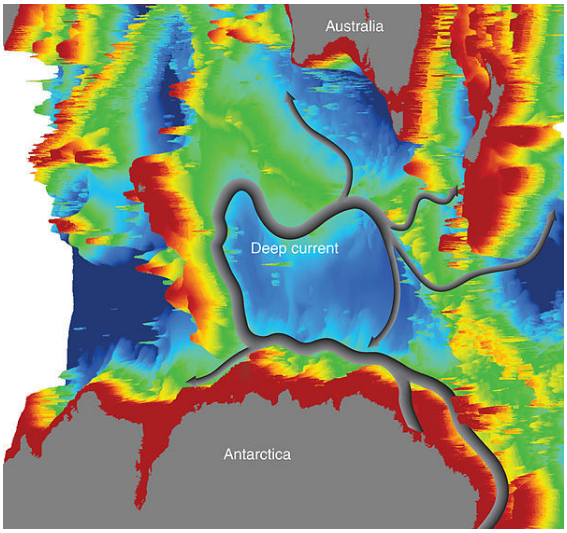

The bathymetry of the Kerguelen Plateau in the Southern Ocean governs the course of the new current part of the global network of ocean currents (Source:CSIRO)

Ocean basins generally have a non-symmetric surface current, in that the eastern equatorward-flowing branch is broad and diffuse whereas the western poleward flowing branch is very narrow. These western boundary currents (of which the Gulf Stream is an example) are a consequence of the rotation of the Earth.

Deep ocean currents are driven by density and temperature gradients. Thermohaline circulation, also known as the ocean's conveyor belt which refers to the deep ocean density driven ocean basin currents. These currents, that flow under the surface of the ocean and are thus hidden from immediate detection, are called submarine rivers. These are currently being researched using a fleet of underwater robots called Argo. Upwelling and downwelling areas in the oceans are areas where significant vertical movement of ocean water is observed.

The South Equatorial Currents of the Atlantic and Pacific straddle the equator. Though the Coriolis effect is weak near the equator (and absent at the equator), water moving in the currents on either side of the equator is deflected slightly poleward and replaced by deeper water. Thus, equatorial upwelling occurs in these westward flowing equatorial surface currents. Upwelling is an important process because this water from within and below the pycnocline is often rich in the nutrients needed by marine organisms for growth. By contrast, generally poor conditions for growth prevail in most of the open tropical ocean, because strong layering isolates deep, nutrient rich water from the sunlit ocean surface.

Surface currents make up about 8% of all the water in the ocean. Surface currents are generally restricted to the upper 400 m (1,300 ft) of the ocean. The movement of deep water in the ocean basins is by density driven forces and gravity. The density difference is a function of different temperatures and salinity. Deep waters sink into the deep ocean basins at high latitudes where the temperatures are cold enough to cause the density to increase.

Ocean currents are measured in sverdrup (sv), where 1 sv is equivalent to a volume flow rate of 1,000,000 m^3 (35,000,000 cu ft) per second.

18.2 Surface currents

18.3 Thermohaline circulation

Further information: Deep ocean water and Thermohaline circulation

Horizontal and vertical currents also exist below the pycnocline in the ocean's deeper waters. The movement of water due to differences in density as a function of water temperature and salinity is called thermohaline circulation. Ripple marks in sediments, scour lines, and the erosion of rocky outcrops on deep-ocean floors are evidence that relatively strong, localized bottom currents exist. Some of these currents may move as rapidly as 60 centimeters (24 inches) per second.

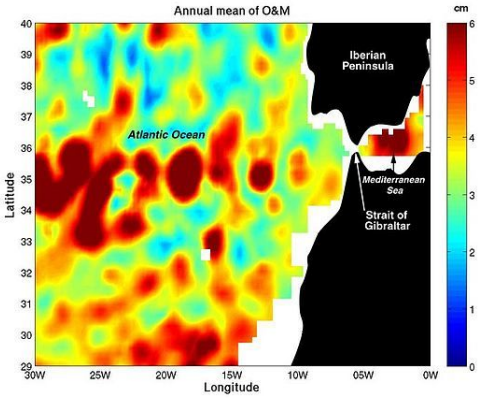

Coupling data collected by NASA/JPL by several different satellite-borne sensors, researchers have been able to "break through" the ocean's surface to detect "Meddies" -- super-salty warm-water eddies that originate in the Mediterranean Sea and then sink more than a half-mile underwater in the Atlantic Ocean. The Meddies are shown in red in this scientific figure.

These currents are strongly influenced by bottom topography, since dense, bottom water must forcefully flow around seafloor projections. Thus, they are sometimes called contour currents. Bottom currents generally move equator-ward at or near the western boundaries of ocean basins (below the western boundary surface currents). The deep-water masses are not capable of moving water at speeds comparable to that of wind-driven surface currents. Water in some of these currents may move only 1 to 2 meters per day. Even at that slow speed, the Coriolis effect modifies their pattern of flow.

18.3.1 Downwelling of deep water in polar regions

Antarctic Bottom Water is the most distinctive of the deep-water masses. It is characterized by a salinity of 34.65‰, a temperature of −0.5°C (30°F), and a density of 1.0279 grams per cubic centimeter. This water is noted for its extreme density (the densest in the world ocean), for the great amount of it produced near Antarctic coasts, and for its ability to migrate north along the seafloor. Most Antarctic Bottom Water forms near the Antarctic coast south of South America during winter. Salt is concentrated in pockets between crystals of pure water and then squeezed out of the freezing mass to form a frigid brine. Between 20 million and 50 million cubic meters of this brine form every second. The water's great density causes it to sink toward the continental shelf, where it mixes with nearly equal parts of water from the southern Antarctic Circumpolar Current. The mixture settles along the edge of Antarctica's continental shelf, descends along the slope, and spreads along the deep-sea bed, creeping north in slow sheets. Antarctic Bottom Water flows many times as slowly as the water in surface currents: in the Pacific it may take a thousand years to reach the equator. Antarctic Bottom Water also flows into the Atlantic Ocean basin, where it flows north at a faster rate than in the Pacific. Antarctic Bottom Water has been identified as high as 40º N on the Atlantic floor.

A small amount of dense bottom water also forms in the northern polar ocean. Although, the topography of the Arctic Ocean basin prevents most of the bottom water from escaping, with the exception of deep channels formed in the submarine ridges between Scotland, Iceland, and Greenland. These channels allow the cold, dense water formed in the Arctic to flow into the North Atlantic to form North Atlantic Deep Water. North Atlantic Deep Water forms when the relatively warm and salty North Atlantic Ocean cools as cold winds from northern Canada sweep over it. Exposed to the chilled air, water at the latitude of Iceland releases heat, cools from 10°C to 2°C, and sinks. Gulf Stream water that sinks in the north is replaced by warm water flowing clockwise along the U.S. east coast in the North Atlantic gyre.

18.4 Importance

Knowledge of surface ocean currents is essential in reducing costs of shipping, since traveling with them reduces fuel costs. In the sail-ship era knowledge was even more essential. A good example of this is the Agulhas Current, which long prevented Portuguese sailors from reaching India. Even today, the round-the-world sailing competitors employ surface currents to their benefit. Ocean currents are also very important in the dispersal of many life forms. An example is the life-cycle of the European Eel.

Ocean currents are important in the study of marine debris, and vice versa. These currents also affect temperatures throughout the world. For example, the current that brings warm water up the north Atlantic to northwest Europe stops ice from forming by the shores, which would block ships from entering and exiting ports, the currents have a decisive role in influencing the climate of the regions they flow through. The cold currents that flow from the polar and sub-polar regions, bring in a lot of plankton. Since this is the food of the fish you can find a lot of fish where these currents pass through.

18.5 OSCAR: Near-realtime global ocean surface current data set

The 'OSCAR near-realtime global ocean circulation data set' is based on NOAA and NASA satellite data (sea level altimetry, surface vector winds, and SST). The data set extends from 1993–present and is available at 1-degree and 1/3-degree resolution. The OSCAR data are continuously updated on an interactive website from which users can create customized graphics and download the data. A section of the website provides validation studies in the form of graphics comparing OSCAR data with moored buoys and global drifters.

OSCAR data are used extensively in climate studies. Monthly maps and anomalies have been published in the monthly Climate Diagnostic Bulletin since 2001, and are used routinely to monitor ENSO and to test prediction models. OSCAR currents are routinely used to evaluate the surface currents in Global Circulation Models (GCMs), for example in NCEP Global Ocean Data Assimilation System (GODAS) and European Centre for Medium-Range Weather Forecasts (ECMWF).[1]

18.6 See also

- Deep ocean water
- Currentology
- Thermohaline circulation
- Fish migration
- List of ocean circulation models
- Oceanic gyres
- Physical oceanography
- Marine current power
- Latitude of the Gulf Stream and the Gulf Stream north wall index

18.7 References

[1] OSCAR website

- Hansen, B.; Østerhus, S; Quadfasel, D; Turrell, W (2004). "Already the day after tomorrow?". *Science* **305** (5686): 953–954. doi:10.1126/science.1100085. PMID 15310882.
- Kerr, Richard A. (2004). "A slowing cog in the North Atlantic ocean's climate machine". *Science* **304** (5669): 371–372. doi:10.1126/science.304.5669.371a. PMID 15087513.
- Munday, Phillip L.; Jones, Geoffrey P.; Pratchett, Morgan S.; Williams, Ashley J. (2008). "Climate change and the future for coral reef fishes". *Fish and Fisheries* **9** (3): 261–285. doi:10.1111/j.1467-2979.2008.00281.x.
- Rahmstorf, S. (2003). "Thermohaline circulation: The current climate". *Nature* **421** (6924): 699–699. doi:10.1038/421699a. PMID 12610602.
- Roemmich, D. (2007). "Physical oceanography: Super spin in the southern seas". *Nature* **449** (7158): 34–35. doi:10.1038/449034a. PMID 17805284.

18.8 External links

- NOAA Ocean Surface Current Analyses - Realtime (OSCAR) Near-realtime Global Ocean Surface Currents derived from satellite altimeter and scatterometer data.
- RSMAS Ocean Surface Currents
- Coastal Ocean Current Monitoring Program
- Ocean Motion and Surface Currents
- Data Visualizer from OceanMotion.org
- Changes in Ocean Circulation - Cluster of Excellence "Future Ocean", Kiel

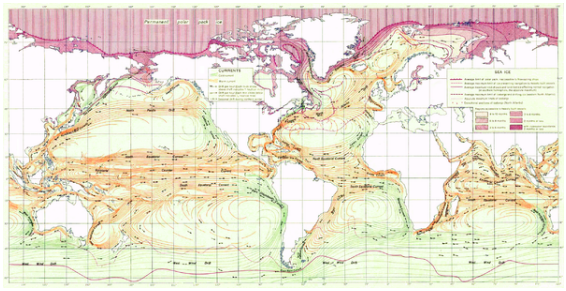

A 1943 map of the world's ocean currents.

Chapter 19

Rayleigh–Taylor instability

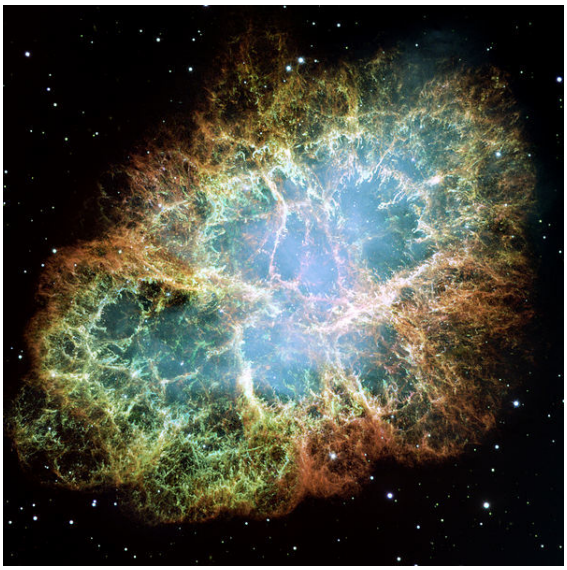

RT fingers evident in the Crab Nebula

The **Rayleigh–Taylor instability**, or **RT instability** (after Lord Rayleigh and G. I. Taylor), is an instability of an interface between two fluids of different densities which occurs when the lighter fluid is pushing the heavier fluid.[1][2] Examples include supernova explosions in which expanding core gas is accelerated into denser shell gas,[3][4] instabilities in plasma fusion reactors,[5] and the common terrestrial example of a denser fluid such as water suspended above a lighter fluid such as oil in the Earth's gravitational field.[2]

To model the last example, consider two completely plane-parallel layers of immiscible fluid, the more dense on top of the less dense one and both subject to the Earth's gravity. The equilibrium here is unstable to any perturbations or disturbances of the interface: if a parcel of heavier fluid is displaced downward with an equal volume of lighter fluid displaced upwards, the potential energy of the configuration is lower than the initial state. Thus the disturbance will grow and lead to a further release of potential energy, as the more dense material moves down under the (effective) gravitational field, and the less dense material is further displaced upwards. This was the set-up as studied by Lord Rayleigh.[2] The important insight by G. I. Taylor was his realisation that this situation is equivalent to the situation when the fluids are accelerated, with the less dense fluid accelerating into the more dense fluid.[2] This occurs deep underwater on the surface of an expanding bubble and in a nuclear explosion.[6]

As the RT instability develops, the initial perturbations progress from a linear growth phase into a non-linear or "exponential" growth phase, eventually developing "plumes" flowing upwards (in the gravitational buoyancy sense) and "spikes" falling downwards. In general, the density disparity between the fluids determines the structure of the subsequent non-linear RT instability flows (assuming other variables such as surface tension and viscosity are negligible here). The difference in the fluid densities divided by their sum is defined as the Atwood number, A. For A close to 0, RT instability flows take the form of symmetric "fingers" of fluid; for A close to 1, the much lighter fluid "below" the heavier fluid takes the form of larger bubble-like plumes.[1]

This process is evident not only in many terrestrial examples, from salt domes to weather inversions, but also in astrophysics and electrohydrodynamics. RT instability structure is also evident in the Crab Nebula, in which the expanding pulsar wind nebula powered by the Crab pulsar is sweeping up ejected material from the supernova explosion 1000 years ago.[7] The RT instability has also recently been discovered in the Sun's outer atmosphere, or solar corona, when a relatively dense solar prominence overlies a less dense plasma bubble.[8] This latter case is an exceptionally clear example of the magnetically modulated RT instability.[9][10]

Note that the RT instability is not to be confused with the Plateau-Rayleigh instability (also known as Rayleigh instability) of a liquid jet. This instability, sometimes called the hosepipe (or firehose) instability, occurs due to surface tension, which acts to break a cylindrical jet into a stream of droplets having the same volume but lower surface area.

Many people have witnessed the RT instability by looking at a lava lamp, although some might claim this is more accurately described as an example of Rayleigh–Bénard convection due to the active heating of the fluid layer at the bottom of the lamp.

19.1 Linear stability analysis

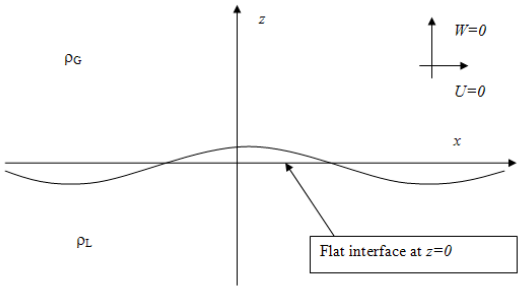

Base state of the Rayleigh–Taylor instability. Gravity points downwards.

The inviscid two-dimensional Rayleigh–Taylor (RT) instability provides an excellent springboard into the mathematical study of stability because of the exceptionally simple nature of the base state.[11] This is the equilibrium state that exists before any perturbation is added to the system, and is described by the mean velocity field $U(x,z) = W(x,z) = 0$, where the gravitational field is $\mathbf{g} = -g\hat{\mathbf{z}}$. An interface at $z = 0$ separates the fluids of densities ρ_G in the upper region, and ρ_L in the lower region. In this section it is shown that when the heavy fluid sits on top, the growth of a small perturbation at the interface is exponential, and takes place at the rate[2]

$$\exp(\gamma t)\,, \qquad \text{with} \quad \gamma = \sqrt{\mathcal{A}g\alpha} \quad \text{and} \quad \mathcal{A} = \frac{\rho_{\text{heavy}} - \rho_{\text{light}}}{\rho_{\text{heavy}} + \rho_{\text{light}}},$$

where γ is the temporal growth rate, α is the spatial wavenumber and $\mathcal{A}$ is the Atwood number.

Details of the linear stability analysis[11] A similar derivation appears in,[9] §92, pp. 433–435.

The perturbation introduced to the system is described by a velocity field of infinitesimally small amplitude, $(u'(x,z,t), w'(x,z,t))$. Because the fluid is assumed incompressible, this velocity field has the streamfunction representation

$$\mathbf{u}' = (u'(x,z,t), w'(x,z,t)) = (\psi_z, -\psi_x),$$

where the subscripts indicate partial derivatives. Moreover, in an initially stationary incompressible fluid, there is no vorticity, and the fluid stays irrotational, hence $\nabla \times \mathbf{u}' = 0$. In the streamfunction representation, $\nabla^2\psi = 0$. Next, because of the translational invariance of the system in the x-direction, it is possible to make the ansatz

$$\psi(x,z,t) = e^{i\alpha(x-ct)}\Psi(z)\,,$$

where α is a spatial wavenumber. Thus, the problem reduces to solving the equation

$$\left(D^2 - \alpha^2\right)\Psi_j = 0, \quad D = \frac{d}{dz}, \quad j = L, G.$$

The domain of the problem is the following: the fluid with label 'L' lives in the region $-\infty < z \leq 0$, while the fluid with the label 'G' lives in the upper half-plane $0 \leq z < \infty$. To specify the solution fully, it is necessary to fix conditions at the boundaries and interface. This determines the wave speed c, which in turn determines the stability properties of the system.

The first of these conditions is provided by details at the boundary. The perturbation velocities w_i' should satisfy a no-flux condition, so that fluid does not leak out at the boundaries $z = \pm\infty$. Thus, $w_L' = 0$ on $z = -\infty$, and $w_G' = 0$ on $z = \infty$. In terms of the streamfunction, this is

$$\Psi_L(-\infty) = 0, \qquad \Psi_G(\infty) = 0.$$

The other three conditions are provided by details at the interface $z = \eta(x,t)$.

Continuity of vertical velocity: At $z = \eta$, the vertical velocities match, $w_L' = w_G'$. Using the streamfunction representation, this gives

$$\Psi_L(\eta) = \Psi_G(\eta)\,.$$

Expanding about $z = 0$ gives

$$\Psi_L(0) = \Psi_G(0) + \text{H.O.T.},$$

where H.O.T. means 'higher-order terms'. This equation is the required interfacial condition.

The free-surface condition: At the free surface $z = \eta(x,t)$, the kinematic condition holds:

$$\frac{\partial\eta}{\partial t} + u'\frac{\partial\eta}{\partial x} = w'(\eta)\,.$$

Linearizing, this is simply

$$\frac{\partial\eta}{\partial t} = w'(0)\,,$$

where the velocity $w'(\eta)$ is linearized on to the surface $z = 0$. Using the normal-mode and streamfunction representations, this condition is $c\eta = \Psi$, the second interfacial condition.

Pressure relation across the interface: For the case with surface tension, the pressure difference over the interface at $z = \eta$ is given by the Young–Laplace equation:

$$p_G\left(z=\eta\right)-p_L\left(z=\eta\right)=\sigma\kappa,$$

where σ is the surface tension and κ is the curvature of the interface, which in a linear approximation is

$$\kappa=\nabla^2\eta=\eta_{xx}.$$

Thus,

$$p_G\left(z=\eta\right)-p_L\left(z=\eta\right)=\sigma\eta_{xx}.$$

However, this condition refers to the total pressure (base+perturbed), thus

$$\left[P_G\left(\eta\right)+p'_G\left(0\right)\right]-\left[P_L\left(\eta\right)+p'_L\left(0\right)\right]=\sigma\eta_{xx}.$$

(As usual, The perturbed quantities can be linearized onto the surface *z=0.*) Using hydrostatic balance, in the form

$$P_L=-\rho_L gz+p_0,\qquad P_G=-\rho_G gz+p_0,$$

this becomes

$$p'_G-p'_L=g\eta\left(\rho_G-\rho_L\right)+\sigma\eta_{xx},\qquad \text{on} z=0.$$

The perturbed pressures are evaluated in terms of streamfunctions, using the horizontal momentum equation of the linearised Euler equations for the perturbations,

$$\frac{\partial u'_i}{\partial t}=-\frac{1}{\rho_i}\frac{\partial p'_i}{\partial x}\text{ with }i=L,G,$$

to yield

$$p'_i=\rho_i cD\Psi_i,\qquad i=L,G.$$

Putting this last equation and the jump condition on $p'_G-p'_L$ together,

$$c\left(\rho_G D\Psi_G-\rho_L D\Psi_L\right)=g\eta\left(\rho_G-\rho_L\right)+\sigma\eta_{xx}.$$

Substituting the second interfacial condition $c\eta=\Psi$ and using the normal-mode representation, this relation becomes

$$c^2\left(\rho_G D\Psi_G-\rho_L D\Psi_L\right)=g\Psi\left(\rho_G-\rho_L\right)-\sigma\alpha^2\Psi,$$

where there is no need to label Ψ (only its derivatives) because $\Psi_L=\Psi_G$ at $z=0$.

Solution

Now that the model of stratified flow has been set up, the solution is at hand. The streamfunction equation $\left(D^2-\alpha^2\right)\Psi_i=0$, with the boundary conditions $\Psi\left(\pm\infty\right)$ has the solution

$$\Psi_L=A_L e^{\alpha z},\qquad \Psi_G=A_G e^{-\alpha z}.$$

The first interfacial condition states that $\Psi_L=\Psi_G$ at $z=0$, which forces $A_L=A_G=A$. The third interfacial condition states that

$$c^2\left(\rho_G D\Psi_G-\rho_L D\Psi_L\right)=g\Psi\left(\rho_G-\rho_L\right)-\sigma\alpha^2\Psi.$$

Plugging the solution into this equation gives the relation

$$Ac^2\alpha\left(-\rho_G-\rho_L\right)=Ag\left(\rho_G-\rho_L\right)-\sigma\alpha^2 A.$$

The *A* cancels from both sides and we are left with

$$c^2=\frac{g}{\alpha}\frac{\rho_L-\rho_G}{\rho_L+\rho_G}+\frac{\sigma\alpha}{\rho_L+\rho_G}.$$

To understand the implications of this result in full, it is helpful to consider the case of zero surface tension. Then,

$$c^2=\frac{g}{\alpha}\frac{\rho_L-\rho_G}{\rho_L+\rho_G},\qquad \sigma=0,$$

and clearly

- If $\rho_G<\rho_L$, $c^2>0$ and c is real. This happens when the

lighter fluid sits on top;

- If $\rho_G>\rho_L$, $c^2<0$ and c is purely imaginary. This happens

when the heavier fluid sits on top.

Now, when the heavier fluid sits on top, $c^2<0$, and

$$c=\pm i\sqrt{\frac{g\mathcal{A}}{\alpha}},\qquad \mathcal{A}=\frac{\rho_G-\rho_L}{\rho_G+\rho_L},$$

where $\mathcal{A}$ is the Atwood number. By taking the positive solution, we see that the solution has the form

$$\Psi\left(x,z,t\right)=Ae^{-\alpha|z|}\exp\left[i\alpha\left(x-ct\right)\right]=A\exp\left(\alpha\sqrt{\frac{g\tilde{\mathcal{A}}}{\alpha}}t\right)\exp\left(i\alpha x-\right.$$

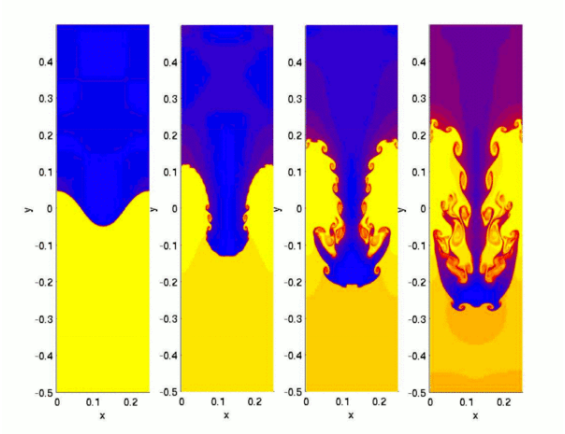

Hydrodynamics simulation of a single "finger" of the Rayleigh–Taylor instability[12] Note the formation of Kelvin–Helmholtz instabilities, in the second and later snapshots shown (starting initially around the level $y = 0$), as well as the formation of a "mushroom cap" at a later stage in the third and fourth frame in the sequence.

and this is associated to the interface position η by: $c\eta = \Psi$. Now define $B = A/c$.

The time evolution of the free interface elevation $z = \eta(x,t)$, initially at $\eta(x,0) = \Re\{B\ \exp(i\alpha x)\}$, is given by:

$$\eta = \Re\left\{B\ \exp\left(\sqrt{\mathcal{A}g\alpha}\,t\right)\exp(i\alpha x)\right\}$$

which grows exponentially in time. Here B is the amplitude of the initial perturbation, and $\Re\{\cdot\}$ denotes the real part of the complex valued expression between brackets.

In general, the condition for linear instability is that the imaginary part of the "wave speed" c be positive. Finally, restoring the surface tension makes c^2 less negative and is therefore stabilizing. Indeed, there is a range of short waves for which the surface tension stabilizes the system and prevents the instability forming.

19.2 Late-time behaviour

The analysis of the previous section breaks down when the amplitude of the perturbation is large. The growth then becomes non-linear as the spikes and bubbles of the instability tangle and roll up into vortices. Then, as in the figure, numerical simulation of the full problem is required to describe the system.

19.3 See also

- Richtmyer–Meshkov instability
- Kelvin–Helmholtz instability
- Mushroom cloud
- Plateau–Rayleigh instability
- Salt fingering
- Hydrodynamic stability
- Kármán vortex street
- Fluid thread breakup

19.4 Notes

[1] Sharp, D.H. (1984). "An Overview of Rayleigh-Taylor Instability". *Physica D* **12**: 3–18. Bibcode:1984PhyD...12....3S. doi:10.1016/0167-2789(84)90510-4.

[2] Drazin (2002) pp. 50–51.

[3] Wang, C.-Y. & Chevalier R. A. (2000). "Instabilities and Clumping in Type Ia Supernova Remnants". arXiv:astro-ph/0005105v1.

[4] Hillebrandt, W.; Höflich, P. (1992). "Supernova 1987a in the Large Magellanic Cloud". In R. J. Tayler. *Stellar Astrophysics*. CRC Press. pp. 249–302. ISBN 0-7503-0200-3.. See page 274.

[5] Chen, H. B.; Hilko, B.; Panarella, E. (1994). "The Rayleigh–Taylor instability in the spherical pinch". *Journal of Fusion Energy* **13** (4): 275–280. Bibcode:1994JFuE...13..275C. doi:10.1007/BF02215847.

[6] John Pritchett (1971). "EVALUATION OF VARIOUS THEORETICAL MODELS FOR UNDERWATER EXPLOSION". U.S. Government. p. 86. Retrieved October 9, 2012.

[7] Hester, J. Jeff (2008). "The Crab Nebula: an Astrophysical Chimera". *Annual Review of Astronomy and Astrophysics* **46**: 127–155. Bibcode:2008ARA&A..46..127H. doi:10.1146/annurev.astro.45.051806.110608.

[8] Berger, Thomas E.; Slater, Gregory; Hurlburt, Neal; Shine, Richard; Tarbell, Theodore; Title, Alan; Lites, Bruce W.; Okamoto, Takenori J.; Ichimoto, Kiyoshi; Katsukawa, Yukio; Magara, Tetsuya; Suematsu, Yoshinori; Shimizu, Toshifumi (2010). "Quiescent Prominence Dynamics Observed with the Hinode Solar Optical Telescope. I. Turbulent Upflow Plumes". *The Astrophysical Journal* **716** (2): 1288–1307. Bibcode:2010ApJ...716.1288B. doi:10.1088/0004-637X/716/2/1288.

[9] Chandrasekhar, S. (1981). *Hydrodynamic and Hydromagnetic Instabilties*. Dover. ISBN 0-486-64071-X.. See Chap. X.

[10] Hillier, A. et al.; Berger, Thomas; Isobe, Hiroaki; Shibata, Kazunari. "Numerical Simulations of the Magnetic Rayleigh-Taylor Instability in the Kippenhahn-Schl{\"u}ter Prominence Model. I. Formation of Upflows". *The Astrophysical Journal* **716**: 120–133. Bibcode:2012ApJ...746..120H. doi:10.1088/0004-637X/746/2/120.

[11] Drazin (2002) pp. 48–52.

[12] Li, Shengtai and Hui Li. "Parallel AMR Code for Compressible MHD or HD Equations". Los Alamos National Laboratory. Retrieved 2006-09-05.

19.5 References

19.5.1 Original research papers

- Rayleigh, Lord (John William Strutt) (1883). "Investigation of the character of the equilibrium of an incompressible heavy fluid of variable density". *Proceedings of the London Mathematical Society* **14**: 170–177. doi:10.1112/plms/s1-14.1.170. (Original paper is available at: https://www.irphe.univ-mrs.fr/~{}clanet/otherpaperfile/articles/Rayleigh/rayleigh1883.pdf .)
- Taylor, Sir Geoffrey Ingram (1950). "The instability of liquid surfaces when accelerated in a direction perpendicular to their planes". *Proceedings of the Royal Society of London. Series A, Mathematical and Physical Sciences* **201** (1065): 192–196. Bibcode:1950RSPSA.201..192T. doi:10.1098/rspa.1950.0052.

19.5.2 Other

- Chandrasekhar, Subrahmanyan (1981). *Hydrodynamic and Hydromagnetic Stability*. Dover Publications. ISBN 978-0-486-64071-6.
- Drazin, P. G. (2002). *Introduction to hydrodynamic stability*. Cambridge University Press. ISBN 0-521-00965-0. xvii+238 pages.
- Drazin, P. G.; Reid, W. H. (2004). *Hydrodynamic stability* (2nd ed.). Cambridge: Cambridge University Press. ISBN 0-521-52541-1. 626 pages.

19.6 External links

- Java demonstration of the RT instability in fluids
- Actual images and videos of RT fingers
- Experiments on Rayleigh-Taylor experiments at the University of Arizona
- plasma Rayleigh-Taylor instability experiment at California Institute of Technology

Chapter 20

Kelvin–Helmholtz instability

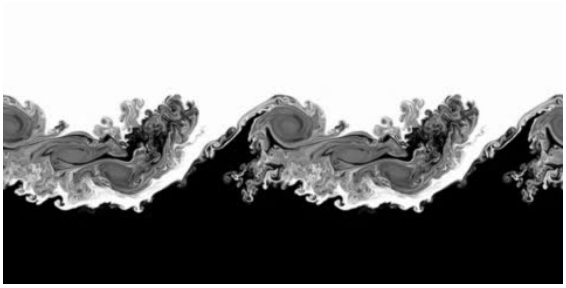

Numerical simulation of a temporal Kelvin–Helmholtz instability

The **Kelvin–Helmholtz instability** (after Lord Kelvin and Hermann von Helmholtz) can occur when there is velocity shear in a single continuous fluid, or where there is a velocity difference across the interface between two fluids. An example is wind blowing over water: The instability manifests in waves on the water surface. More generally, clouds, the ocean, Saturn's bands, Jupiter's Red Spot, and the sun's corona show this instability.[1]

The theory predicts the onset of instability and transition to turbulent flow in fluids of different densities moving at various speeds. Helmholtz studied the dynamics of two fluids of different densities when a small disturbance, such as a wave, was introduced at the boundary connecting the fluids.

A KH instability rendered visible by clouds over Mount Duval in Australia

For some short enough wavelengths, if surface tension is ignored, two fluids in parallel motion with different velocities and densities yield an interface that is unstable for all speeds. Surface tension stabilises the short wavelength instability however, and theory predicts stability until a velocity threshold is reached. The theory with surface tension included broadly predicts the onset of wave formation in the important case of wind over water.

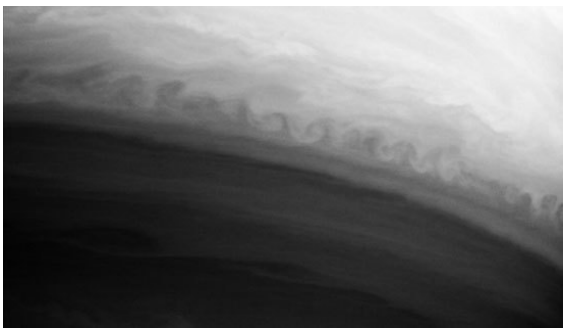

A KH instability on the planet Saturn, formed at the interaction of two bands of the planet's atmosphere

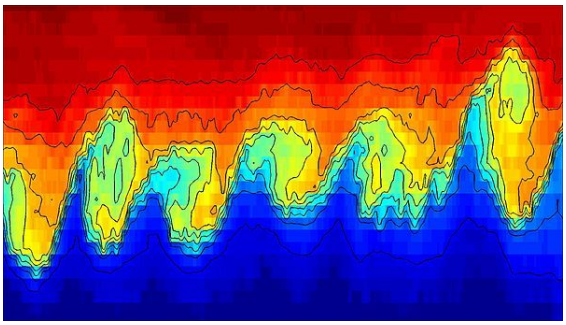

Kelvin-Helmholtz billows 500m deep in the Atlantic Ocean

In gravity, for a continuously varying distribution of density and velocity (with the lighter layers uppermost, so that the fluid is RT-stable), the dynamics of the KH instability is described by the Taylor–Goldstein equation and its onset is given by a Richardson number, Ri. Typically the layer is unstable for Ri<0.25. These effects are common in cloud layers. The study of this instability is applicable in plasma physics, for example in inertial confinement fusion and the plasma–beryllium interface.

Numerically, the KH instability is simulated in a temporal or a spatial approach. In the temporal approach, experimenters consider the flow in a periodic (cyclic) box "moving" at mean speed (absolute instability). In the spatial approach, experimenters simulate a lab experiment with natural inlet and outlet conditions (convective instability).

20.1 See also

- Rayleigh–Taylor instability
- Richtmyer–Meshkov instability
- Mushroom cloud
- Plateau–Rayleigh instability
- Kármán vortex street
- Taylor–Couette flow
- Fluid mechanics
- Fluid dynamics

20.2 Notes

[1] Fox, Karen C. "NASA's Solar Dynamics Observatory Catches "Surfer" Waves on the Sun". *NASA-The Sun-Earth Connection: Heliophysics*. NASA.

20.3 References

- Lord Kelvin (William Thomson) (1871). "Hydrokinetic solutions and observations". *Philosophical Magazine* **42**: 362–377.
- Hermann von Helmholtz (1868). "Über discontinuierliche Flüssigkeits-Bewegungen [On the discontinuous movements of fluids]". *Monatsberichte der Königlichen Preussische Akademie der Wissenschaften zu Berlin* [Monthly Reports of the Royal Prussian Academy of Philosophy in Berlin] ***23**: 215–228.*
- Article describing discovery of K-H waves in deep ocean: Broad, William J. (April 19, 2010). "In Deep Sea, Waves With a Familiar Curl". New York Times. Retrieved April 2010.

20.4 External links

- Hwang, K.-J.; Goldstein, Kuznetsova, Wang, Viñas, Sibeck (2012). "The first in situ observation of Kelvin-Helmholtz waves at high-latitude magnetopause during strongly dawnward interplanetary magnetic field conditions". *J. Geophys. Res.* **117** (A08233). Bibcode:2012JGRA..117.8233H. doi:10.1029/2011JA017256.
- Giant Tsunami-Shaped Clouds Roll Across Alabama Sky - Natalie Wolchover, Livescience via Yahoo.com
- Tsunami Cloud Hits Florida Coastline
- Vortex formation in free jet - YouTube video showing Kelvin Helmholz waves on the edge of a fre jet visualised in a scientific experiment.

{{int:Coll-attribution-page|

- **Vector calculus identities** *Source:* http://en.wikipedia.org/wiki/Vector%20calculus%20identities?oldid=635104707 *Contributors:* Michael Hardy, Tobias Bergemann, Giftlite, MFNickster, Chris Howard, Kri, Roboto de Ajvol, YurikBot, Twin Bird, Gillis, That Guy, From That Show!, SmackBot, Maksim-e, Droll, Metacomet, Nbarth, Akriasas, Jim.belk, Hvn0413, Stikonas, JayZ, Andreas Rejbrand, Vyznev Xnebara, Mhschwar, Pklepec, Anupam, Dachande, Ben pcc, MER-C, Jheiv, Mark87, K61824, Catslash, Aielyn, Uncle Dick, Hologram0110, Freiddie, JohnBlackburne, LokiClock, Philip Trueman, Badgerific, Spinningspark, Narchy, Jurlinga, Breeet, Alexbot, Brews ohare, Crowsnest, XLinkBot, WikiDao, Addbot, Arbitrarily0, Luckas-bot, ⍰⍰, Citation bot, Srinivas.zinka, ⍰⍰, FrescoBot, Songjie509, Sławomir Biały, X Legende x, Syockit, Quondum, Isarra, Donner60, ClueBot NG, MerlIwBot, Helpful Pixie Bot, Aannoonn, F=q(E+v^B), Sethyvenatem, Paul Sunman, Mark viking, Koala021202, Samuello1228, Ginsuloft, I2000s, Alex&Jones1878, Tommyl89, Alexis.angelidis, Branko Malesevic and Anonymous: 88
- **Flow velocity** *Source:* http://en.wikipedia.org/wiki/Flow%20velocity?oldid=610818007 *Contributors:* MFNickster, Mauxb, Krishnavedala, Alaibot, Dolphin51, ClueBot, Ideal gas equation, Crowsnest, Addbot, LilHelpa, Imveracious, Seattle, ClueBot NG, Helpful Pixie Bot, BG19bot and Anonymous: 11
- **Laminar flow** *Source:* http://en.wikipedia.org/wiki/Laminar%20flow?oldid=617537696 *Contributors:* Mav, Gareth Owen, Peterlin, David spector, Tim Starling, Mac, Rob Hooft, Charles Matthews, Robbot, BenFrantzDale, Rick Block, Christopherlin, Dj245, Sonett72, NathanHurst, Marsian, Pegasi195, Jhertel, Linmhall, Sligocki, Kenyob, Nuno Tavares, Before My Ken, Eleassar777, GregorB, Isnow, Emerson7, RuM, PinkPig, Shandolad, Quiddity, Williamborg, AySz88, FayssalF, Margosbot, Chobot, Antilived, Dj Capricorn, Siddhant, YurikBot, Zaidpjd, RussBot, Nick, BeastRHIT, StuRat, Vicarious, Jjhunt, SmackBot, Rex the first, Verne Equinox, Bluebot, Thumperward, Crwesq@gmail.com, Jaganath, Mgiganteus1, Peterlewis, Deviatorz, Beetstra, Ryanjunk, Wikixoox, Tawkerbot2, AbsolutDan, Van helsing, Phydend, Alaibot, Thijs!bot, Headbomb, Micahgoulart, AntiVandalBot, Akradecki, Mikenorton, JAnDbot, Jjdreese, Arch dude, Cardamon, Easyl, Loz97, Vijay2000, Salih, Jayden54, Green453, Xelous, VolkovBot, Larryisgood, TXiKiBoT, FMasic, Andy Dingley, Leckiesmum, Natox, SieBot, BotMultichill, Alexecutor, Dolphin51, Struway2, ClueBot, Flixxy, EMBaero, Donebythesecondlaw, Alexbot, Three-quarter-ten, Fergnatz, BOTarate, Darkicebot, Jovianeye, Bye12, Addbot, ChenzwBot, Splodgeness, Luckas-bot, Newportm, Daniele Pugliesi, Mostiquera, Bluerasberry, LilHelpa, Obersachsebot, BookWormHR, Abce2, Doremo, Gryllida, Viatr0nic, Defender of torch, RjwilmsiBot, EmausBot, John of Reading, Orphan Wiki, Rami radwan, Raspberrycoulis, ZéroBot, Thebousse, AvicAWB, Suslindisambiguator, Jamie-NJITWILL, ResearchRave, ClueBot NG, Senthilvel32, Twillisjr, Helpful Pixie Bot, Drsimonz, Bibcode Bot, Vagobot, Techocontra, Tadpoleleesie, Junaji, Tritario, Monkbot and Anonymous: 92
- **Chaos theory** *Source:* http://en.wikipedia.org/wiki/Chaos%20theory?oldid=635241664 *Contributors:* AxelBoldt, Tobias Hoevekamp, Sodium, Mav, Zundark, Gareth Owen, Arvindn, Roadrunner, SimonP, David spector, Heron, Gumpu, Edward, Michael Hardy, Tez, Lexor, Isomorphic, Chinju, Karada, Iluvcapra, Ahoerstemeier, William M. Connolley, Snoyes, Darkwind, Kevin Baas, Evercat, Smack, Schneelocke, Charles Matthews, Adam Bishop, Dino, Dysprosia, Jitse Niesen, Doradus, Munford, K1Bond007, Jose Ramos, Fairandbalanced, Bevo, Traroth, Banno, JorgeGG, Phil Boswell, Robbot, Bernhard Bauer, Goethean, Gandalf61, Chopchopwhitey, MathMartin, Sverdrup, Academic Challenger, Ojigiri, Zubras, Paul Murray, Dave Bass, Dbroadwell, Wile E. Heresiarch, Tobias Bergemann, Enochlau, Decumanus, Giftlite, Smjg, Fennec, Gene Ward Smith, Vir4030, Kim Bruning, Everyking, Curps, Sunny256, Pucicu, Chowbok, Utcursch, LucasVB, Antandrus, Mako098765, Quarl, Vanished user 1234567890, Karol Langner, Rdsmith4, Oneiros, Pmanderson, Zfr, Sam Hocevar, Lumidek, Jmeppley, Joyous!, Barnaby dawson, TheObtuseAngleOfDoom, Shiftchange, Discospinster, Rich Farmbrough, TedPavlic, Avriette, Guanabot, Vsmith, Lulu of the Lotus-Eaters, Fluzwup, Paul August, Bender235, Neurophyre, Loren36, Fenice, Brian0918, El C, Pjrich, Alereon, AJP, Rwh, Semper discens, Billymac00, John Vandenberg, Thomas G Graf, Flammifer, Obradovic Goran, Mdd, Cyrloc, Msh210, Defunkt, Prashmail, Alansohn, Arthena, Keenan Pepper, CommodoreMan, Lectonar, WhiteC, BryanD, Sligocki, Hu, Bart133, PaePae, Helixblue, HenkvD, Evil Monkey, Cal 1234, RainbowOfLight, DV8 2XL, Embryomystic, Kazvorpal, Dan100, OleMaster, Simetrical, Linas, Ramsremedies, Scriberius, Igny, VanFullOfMidgets, LOL, Scid, Guardian of Light, KickAir8P~, Ruud Koot, MONGO, Kelisi, GregorB, XaosBits, Graham87, Magister Mathematicae, Anarchivist, Jorunn, Rjwilmsi, Joakim Munkhammar, KYPark, XP1, TheRingess, Brighterorange, Scartol, The wub, Bhadani, Yamamoto Ichiro, Mathbot, Greg321, Sunayana, Nivix, RexNL, Nabarry, Incompetnce, Smithbrenon, Nicholasink, Chobot, Evilphoenix, Bgwhite, Cactus.man, Gwernol, YurikBot, Wavelength, Deeptrivia, Pmg, Hillman, Nmondal, Splash, JabberWok, Prokaryote1234, Stephenb, Jugander, Chaos, Alex Bakharev, Rsrikanth05, David R. Ingham, Dtrebbien, Grafen, Winonanick, JocK, Dhollm, Raven4x4x, Moe Epsilon, Zwobot, Epipelagic, Romarin, Dlyons493, Suso, Bota47, Dan131m, Cat2020, Zunaid, WAS 4.250, Phgao, Ninly, Imaninjapirate, Arthur Rubin, GraemeL, DGaw, Madrazz, Vicarious, Reject, Kungfuadam, DVD R W, Soir, Benjamindees, Marquez, SmackBot, 4dhayman, ManaUser, Maksim-e, Sethmasters, Stellea, The hoodie, InverseHypercube, KnowledgeOfSelf, Unyoyega, C.Fred, Rosaak, Thunderboltz, Flux.books, PeterSymonds, Sbonsib, Skizzik, GwydionM, Izehar, Bluebot, Persian Poet Gal, RDBrown, Telempe, Alex brollo, SchfiftyThree, GabrielPere, Complexica, Bazonka, Sudharsansn, CSWarren, DHN-bot, Jdthood, Yanksox, Hellfire81, QuimGil, Gorgeorgeus, Can't sleep, clown will eat me, Aremith, Jahiegel, Rrburke, Spectrogram, Nakon, Anmnd, Mini-Geek, Thismarty, Profyorke, Wybot, DMacks, SashatoBot, Lambiam, Mukadderat, Luigi-ish, Kuru, Lakinekaki, Lapaz, Buchanan-Hermit, Joshua Andersen, Chodorkovskiy, Dumelow, Jim.belk, IronGargoyle, Mosgiel, Atomic Duck!, Brazucs, Dicklyon, Xiaphias, Invisifan, Candybars, Dr.K., Dfred, Inquisitus, Rlinfinity, Xionbox, Asyndeton, Mdanziger, PSOfan2000, Iridescent, Shoeofdeath, Cumi, Rhetth, Daveyork, Experiment123, Tawkerbot2, Chetvorno, Timrem, PurpleRain, CRGreathouse, Crownjewel82, Aherunar, Avanu, TheTito, Neelix, Grein, Mct mht, CX, Yaris678, Gogo Dodo, Lugnuts, Pascal.Tesson, Alpharius, Tawkerbot4, DumbBOT, Chrislk02, Romon, Letranova, Thijs!bot, Epbr123, Hervegirod, UXs, Sagaciousuk, Scientio, Oliver202, Headbomb, Zardoze, Perrygogas, West Brom 4ever, James086, Nezzadar, Charukesi, Universal Hero, Widenet, Gfalco, Northumbrian, AntiVandalBot, Devanshi.shah, Ben pcc, Doc Tropics, Jcsellak, Jj137, JAnDbot, Ashishval44, Husond, Gandhi gaurav, MER-C, Sophie means wisdom, Igodard, Hut 8.5, MSBOT, Kirrages, Captain head, Peteymills, Coffee2theorems, Jill.marleigh, Magioladitis, Diderot7, VoABot II, Catslash, JamesBWatson, Mbc362, Carlylecastle, Brewhaha@edmc.net, Brother Francis, Catgut, Ensign beedrill, Mjkelley79, David Eppstein, Kotinopoulos, Vssun, JoergenB, DerHexer, JaGa, Bryt, Waitati, Cocytus, Stephenchou0722, DancingPenguin, MartinBot, Arjun01, Poeloq, InnocuousPseudonym, Tomasao, Ayonbd2000, Erkan Yilmaz, J.delanoy, Oshron, Trusilver, AstroHurricane001, MikeBaharmast, Maurice Carbonaro, Zakholdsworth, Thegreenj, JAK2112, Salih, Katalaveno, Enuja, QuasiAbstract, V.V zzzzz, Coppertwig, Chiswick Chap, NewEnglandYankee, Policron, MKoltnow, Zojj, MetsFan76, TottyBot, Ahshabazz, Lamp90, Prot D, Yodler, JavierMC, Nnnagig, Cmarnold, Idioma-bot, JLBernstein, Funandtrvl, Phlounder, Yoeb137, Torcini, Mimigary, Pleasantville, DSRH, Tunnels of Set, Jeff G., JohnBlackburne, AlnoktaBOT, HeckXX, Richardseel, DancingMan, Philip Trueman, TXiKiBoT, Gggggdxn, Red Act, A4bot, Tagalong99, IPSOS, Voorlandt, Magmi, Corvus cornix, Garravogue, Rubseb, PDFbot, Katimawan2005, 3p1416, Kızılsungur, Inductiveload, Kaiketsu, Kilmer-san, Wolfrock, Jacob501, Sheildofthunder, The The Fool on the Hill, Blazen nite, HiDrNick, Symane, SamuraiGabe, Radagast3, Maxlittle2007, SieBot, Tosun, Cwkmail, This, that and the other, Zsniew, Revent, Vanished User 8a9b4725f8376, Africangenesis, Warhammer 8, Somecreepyoldguy, Prestonmag, Trang Oul, Oxymoron83, AngelOfSadness, KoshVorlon, Michael Courtney, Fratrep, Convictionist, StaticGull, Szalagloria, Mike2vil, Abmcdonald, Tojuro, Tommi Ronkainen, Wikiskimmer, SUPERSONICOOHHHOHOH, Escape

Orbit, Stu, Francvs, Apsimpson02, Axel-Rega, ClueBot, Avenged Eightfold, The Thing That Should Not Be, Sijokjoseph, Plastikspork, Ribbon Salminen, Herakles01, Abrfreek777, Der Golem, Gommert, Ksmadden, Niceguyedc, JJIG, LizardJr8, ChandlerMapBot, Lbertolotti, Paulcmnt, Djr32, Feline Hymnic, IPrussian, Echion2, Jmlipton, Mikaey, Niyse, La Pianista, Flower Priest, Versus22, SoxBot III, Vanished user uih38riiw4hjlsd, Nori Llane, Un Piton, Wbblaze4, Golddragon24, XLinkBot, Jovianeye, Rror, Colliric, Addbot, Mortense, Rakeshfern, TheDestitutionOfOrganizedReligion, Melab-1, The Equilibrium, Otisjimmy1, DougsTech, Fgnievinski, Ronhjones, Funky Fantom, SomeUsr, Glane23, Nutter13, Ytbau, Debresser, Favonian, XFreakonaLeashX, SpBot, LinkFA-Bot, Lipehauss, Freakonaleashnj, Tassedethe, Bwrs, LarryJeff, Lightbot, Gail, Zorrobot, Jarble, Jamesevi, Megaman en m, Vicky sekar, CS2020, Legobot, Luckas-bot, Yobot, Dgurubaran, AnomieBOT, Kristen Eriksen, IRP, Collieuk, Aeortiz, Kingpin13, Flewis, Materialscientist, Jacksonroberts25, To Fight a Vandal, Citation bot, Srinivas, Onesius, Ruby2010, Spidermanizdabest, Xqbot, TitusCarus, CathNek, GrouchoBot, Damienivan, 7h3 3L173, RibotBOT, SassoBot, Energybender, Smallman12q, A. di M., Frozenevolution, FrescoBot, Justinodem, Thayts, Sławomir Biały, Argumzio, Kwiki, Citation bot 1, Milly.mortimer, Theory2reality, Pinethicket, SimmonsNorwood, Therealfozzy, MastiBot, FoxBot, Koolguy1029, Anonwhymus, Wotnow, Willihans, Redfan45x, Math.geek3.1415926, Inferior Olive, Duoduoduo, DARTH SIDIOUS 2, RjwilmsiBot, DSP-user, CanadianPenguin, Orphan Wiki, Karsh07007, KurtLC, Jaguar6cy, Perfect Introvert, AppuruPan, Slightsmile, AgRince, Mussermaster, K6ka, Koryds2008, Earthh, Hhhippo, Ida Shaw, Hugo.cavalcante, Shuipzv3, Askedonty, JPfreak, Arbnos, Wayne Slam, Music Sorter, Donner60, Inka 888, Bill william compton, Subanm, AnthonyMarkes, Mr Schneebly, Support.and.Defend, Mikhail Ryazanov, ClueBot NG, Guswfla1, Marechal Ney, Davidcarfi, Timflutre, Minki6656, Helpful Pixie Bot, Richardjb25, Lottsy, Bibcode Bot, Jeraphine Gryphon, Rhysjeans, BG19bot, LangdonAlger29, Cispyre, Birdtracks, FiveColourMap, Yowanvista, HMman, Westcoastg24, Brad7777, Packman744, Randomguess, BattyBot, Ema--or, DIY Sunrise, Ruidilao, Prayforrain, Hamzaata, Trololol115, Zirconzx, Illia Connell, Dexbot, Theillusionking, Pal.bjartan, Sundarsharath, TheKing44, Patrick.knoll96, Anthaceorote, NerdGirl1988, Ydoc52, Ufoneda, Paulpgh, Penitence, Docirish7, VAggarwal, Nigellwh, Francois-Pier, Irte, Anrnusna, TheSawyerBean, Sheddow, JaconaFrere, Masdpofham, Jsmk, Monkbot, Rebusch, ChaoticPoet, Garfield Garfield, Purgy Purgatorio, Loraof, TheOddsMaker and Anonymous: 967

- **Fractal** *Source:* http://en.wikipedia.org/wiki/Fractal?oldid=635484215 *Contributors:* AxelBoldt, Lee Daniel Crocker, Brion VIBBER, Archibald Fitzchesterfield, Mav, Zundark, Piotr Gasiorowski, Mirwin, XJaM, PierreAbbat, The Ostrich, Hhanke, Miguel, SimonP, Edemaine, Heron, Aafuss, Arj, Youandme, JDG, Olivier, Frecklefoot, Lir, Infrogmation, Michael Hardy, Jdandr2, Wapcaplet, Ixfd64, Firebirth, TakuyaMurata, Arpingstone, Card, Ahoerstemeier, William M. Connolley, Theresa knott, Ijon, DropDeadGorgias, Glenn, Aragorn2, Llull, Evercat, Lancevortex, Schneelocke, Flajann, Revolver, Charles Matthews, Nostrum, Dino, Jitse Niesen, WhisperToMe, Timc, CB-Dunkerson, Tpbradbury, Maximus Rex, Hyacinth, Morwen, Saltine, Bevo, Xyb, Shizhao, Khym Chanur, Raul654, AnonMoos, Jeffq, Robbot, Ke4roh, Fredrik, Chris 73, Matt me, RedWolf, Bkalafut, Lowellian, Gandalf61, Chopchopwhitey, Sverdrup, Texture, Timrollpickering, Paul Murray, Fuelbottle, Seth Ilys, Gregorsamsa11, Superm401, MikeCapone, Tobias Bergemann, David Gerard, Cedars, Stirling Newberry, Matthew Stannard, Giftlite, Elf, Wolfkeeper, Everyking, Anville, Wikibob, Frencheigh, DO'Neil, Andris, Avsa, Eequor, Macrakis, Foobar, Gzornenplatz, Matt Crypto, Chameleon, SWAdair, Bobblewik, PhiloVivero, Utcursch, Shibboleth, Antandrus, Rajasekaran Deepak, ClockworkLunch, Kaldari, Joizashmo, MacGyverMagic, IYY, APH, MarkBurnett, Maximaximax, Kevin B12, Jawed, Eranb, Eric B. and Rakim, Urhixidur, Joyous!, Grunt, Mike Rosoft, Shiftchange, Mormegil, DanielCD, Discospinster, Haruki, Rich Farmbrough, TedPavlic, Pak21, Michal Jurosz, Solkoll, User2004, AlexKepler, Jamadagni, Michael Zimmermann, Nard the Bard, Paul August, Pban92, Bender235, ESkog, Kaisershatner, Neko-chan, Brian0918, EastNile, El C, Shanes, Mkosmul, RoyBoy, ~K, Bobo192, Reinyday, Cohesion, Sidjaggi, QTxVi4bEMRbrNqOorWBV, Blotwell, Bert Hickman, Rambus, Davidgothberg, MPerel, Gsklee, Nsaa, Mdd, Danski14, Sswn, Alansohn, Julesruis, Gargaj, Arthena, Rgclegg, Darrenthebaron, Craigy144, Weezer Ohio, ABCD, Hu, Snowolf, Malber, Yogi de, DRJacobson, Twisp, JCSP, Danhash, Uffish, Dirac1933, Lerdsuwa, DV8 2XL, Redvers, Oleg Alexandrov, Levan, JordanSamuels, Lkinkade, Novacatz, Woohookitty, TigerShark, Camw, LOL, TheNightFly, Duncan.france, Kelisi, SDC, Plrk, DocRuby, Cshirky, Mekong Bluesman, DaveApter, Kobi L, Aidje, Runis57, Graham87, Magister Mathematicae, Electricmoose, MC MasterChef, FreplySpang, Grammarbot, Saperaud, JVz, MarSch, Jamesrskemp, TheRingess, Salix alba, SpNeo, Mbutts, Feil0014, Titoxd, FlaBot, Mathbot, ZoneSeek, Crazycomputers, Who, Fragglet, Gparker, RexNL, Gurch, Ayla, Nimur, Physchim62, Chobot, Visor, ShadowHntr, WriterHound, Gwernol, The Rambling Man, YurikBot, Wavelength, Sceptre, Adamhauner, RussBot, Sarranduin, AVM, Hellbus, RadioFan, Stephenb, Gaius Cornelius, Chaos, Wimt, Wiki alf, Raven4x4x, Moe Epsilon, Charron, Tony1, Supten, Cheeser1, Cat2020, BazookaJoe, Sandstein, JonathanD, Zzuuzz, RDF, Theda, Arthur Rubin, Josh3580, Ianbolland, Reyk, BorgQueen, Paul Erik, Bo Jacoby, Roke, Choi9999, Yakudza, SmackBot, RDBury, GBarnett, Mujahideen, Unschool, Nadimghaznavi, Nihonjoe, Ravage386, KnowledgeOfSelf, Vald, Chairman S., Mdd4696, Jonathan Karlsson, BiT, Gilliam, Benjaminevans82, Ohnoitsjamie, Skizzik, RobertM525, Qtoktok, Full Shunyata, RDBrown, MalafayaBot, Ida noeman, DHN-bot, Colonies Chris, Gbok, Max David, OrphanBot, Pevarnj, Gunjankg, Nakon, TheLimbicOne, Aelffin, Infovoria, Dreadstar, Kirils, Dr. Gabriel Gojon, Acdx, Kukini, SashatoBot, Lambiam, Wvbailey, Harryboyles, Lakinekaki, Rigadoun, Ocee, Rijkbenik, Sir Nicholas de Mimsy-Porpington, Ivanip, Johnsen953, JoshuaZ, Noegenesis, Samirdmonte, Thegreatdr, Ben Moore, Hvgard, 16@r, Grumpyyoungman01, Fractalmichel, Tasc, GilbertoSilvaFan, Waggers, Dhp1080, Farzaad, H, AntOnTrack, Hu12, Kevin R Johnson, Jason7825, Pegasus1138, Aeternus, Tó campos, Neoking, FakeTango, Courcelles, Padvi, Experiment123, Tawkerbot2, Lasserempe, Generalcp702, Fdot, JForget, InvisibleK, Edward Vielmetti, Ninetyone, Basawala, ShelfSkewed, David Traver, Karenjc, Nauticashades, Badseed, Slazenger, Doctormatt, Cydebot, MC10, SyntaxError55, Tawkerbot4, Christian75, Optimist on the run, Junglerolf, Victoriaedwards, PamD, Ael 2, Riojajar, Letranova, Epbr123, Barticus88, Wikid77, Ante Aikio, Hervegirod, Dafydd Williams, Marek69, John254, Drewboy64, Bunzil, Big Bird, Elert, AntiVandalBot, Seaphoto, QuiteUnusual, Quintote, Danger, Tillman, Alphachimpbot, Derouch, Byrgenwulf, Qwerty Binary, Myanw, Kaini, JAnDbot, MER-C, Fetchcomms, Dizzydog11235, Plm209, Beaumont, LittleOldMe, S0uj1r0, Penubag, Bongwarrior, VoABot II, Santisan, Nitku, Bubba hotep, Catgut, Indon, Animum, Dobi, Seberle, David Eppstein, Gregly, Martynas Patasius, GermanX, Vishvax, Ineffable3000, Denis tarasov, MartinBot, Geometricarts, NAHID, Reguiieee, Gcranston, EdwardHades, CommonsDelinker, Alexnevzorov, Fconaway, Jwoehr, Lilac Soul, LedgendGamer, Erkan Yilmaz, Pravirmalik, J.delanoy, Prokofiev2, Gandreas, Rayquaza11, Uncle Dick, McFarty, Maurice Carbonaro, Semajdraehs, Power Gear, Bot-Schafter, 5theye, Silver The Slammer, Nemo bis, C quest000, Chiswick Chap, WHeimbigner, Nwbeeson, SJP, Robertgreer, Submanifold, Gtg204y, Idioma-bot, Funandtrvl, Signalhead, Mbheyman, VolkovBot, Thedjatclubrock, Kriplozoik, Nikhil Varma, Sssmok1, TXiKiBoT, Zurishaddai, Arnon Chaffin, Voorlandt, Anna Lincoln, Una Smith, Auaug, Everything counts, Modocc, Hristos, Simzer, Kmhkmh, Emc2rocks, Synthebot, Murrogh, White Witch of Narnia, Lampica, Koldito, Chilti, Duckmackay, Logan, Ishboyfay, GirasoleDE, Dark Jackalope, SieBot, Bjtaylor01, Gopher292, Tresiden, Pengyanan, Caltas, Paul beaulieu, Kkrouni, Nikos.salingaros, LeadSongDog, Soler97, Andersmusician, SiegeLord, Keilana, Maphyche, Zucchini Marie, Oda Mari, Arbor to SJ, Rolandnine, Rhanyeia, Poop78432, BlueCerinthe, Oxymoron83, Faradayplank, Hobartimus, Svick, Eglash, Jons63, Arkixml, WikipedianMarlith, Casp7, ClueBot, Rumping, Fyyer, Foxj, The Thing That Should Not Be, JASONQUANTUM1, Hadrianheugh, JuPitEer, Meekywiki, Ryoutou, Lbertolotti, Edo 555, Patalbwil, Tamaratrouts, Wavedoc1, Sun Creator, Mr45acp, Francisco Albani, Jackrm, Sarsaparilla, ChrisHodgesUK, Ori benjamin, Aitias, Vanished User 1004, Jeflecastin, XLinkBot, Gonzonoir, Rortaruiter, XalD, Ehsan Nikooee, Addbot, DOI bot, Betterusername, Landon1980, SunDragon34, Twsntwsntwsm, Download, CarsracBot, Delaszk, LinkFA-Bot, Tide rolls, ScAvenger, Luckas Blade, Zorrobot, David0811, Jarble, Tinso1, Legobot, Luckas-bot, Yobot, Pink!Teen, Squish7, Synchronism, AnomieBOT, Accuruss, AdjustShift, Aditya, Kingpin13, Jacksonroberts25, Citation bot,

Dromioofephesus, LilHelpa, PavelSolin, Xqbot, Mgroover, Hayley Tales, Hip2BSquare, Ptrf, Puvircho, Spw0766, Xenodream, Abce2, Web420, RibotBOT, FillerBrushMan, Locobot, Baba11111, WaysToEscape, Samwb123, Sesu Prime, Prari, FrescoBot, LucienBOT, Polynomial123, Harry f seldon, Citation bot 4, Pinethicket, Arctic Night, Hamtechperson, Moreinfopleasenow, Xxslorexx, Sumant Sethi, Mikejbau, Jandalhandler, Keri, Dr. Snew, Tatasz, Jordgette, Willihans, Clarkcj12, ???, Percyzhang, Satdeep gill, DARTH SIDIOUS 2, Mean as custard, RjwilmsiBot, Utrytr, Calcyman, Beyond My Ken, BertSeghers, DSP-user, Afteread, Skamecrazy123, Der Künstler, Spennyize, Rusfuture, ScottyBerg, RA0808, Awall2012, Ochristi, FatPope, Tommy2010, Wikipelli, K6ka, Cegalegolog99, TheLunarFrog, Josve05a, Empty Buffer, Fred Gandt, Muffiewrites, Dubravka2, Fractus-1, TyA, Gut Monk, James Krug, Maschen, Scientific29, Orange Suede Sofa, Foldedwater, FeatherPluma, Dllu, Signalizing, ClueBot NG, Elcubano91, A520, -sche, Austinlittle93, Teichlersmith, Widr, Calumcjr, Helpful Pixie Bot, Ahmad.829, Yiliangchen0113, DBigXray, BG19bot, DrJimothyCatface, Papadim.G, M0rphzone, Smitty121981, MSa1, MaxxyXD, Zhenxinghua, Yra-yra12, Lekro, Tigris35711, Achowat, Akarpe, Ezhu94, Josep m batlle, BattyBot, Justincheng12345-bot, HueSatLum, Khazar2, Dexbot, Cwobeel, DeniseKShull, Czech is Cyrillized, Brirush, Seaman4516, FairyTale'sEnd, Polytope4d, Feniakaidan, Vanamonde93, Josep m batlle2, GailTheOx, Frac2012, Ignaciokriche, Ben christianson, QuahogClamMan, Anupama Srinivas, Wamiq, Ashorocetus, NorthBySouthBaranof, Revolverc24, Jackmcbarn, Francois-Pier, Metingle, Dkapetansky, Antideregister, Moogooshoe, Ali salsa, BethNaught, Shastamist, AKFS Editor, Garfield Garfield, Shira201, Loraof, Almondeve and Anonymous: 805

- **Wind wave** *Source:* http://en.wikipedia.org/wiki/Wind%20wave?oldid=632160235 *Contributors:* The Anome, Lir, Michael Hardy, Ahoerstemeier, Kils, Zimbres, Charles Matthews, Omegatron, Slawojarek, Robbot, Paranoid, FredR, Texture, Fuelbottle, Giftlite, DocWatson42, Wolfkeeper, Cantus, Lst27, Antandrus, DRE, GeoGreg, Sonett72, Clemwang, DanielCD, Noisy, Discospinster, Rich Farmbrough, Igorivanov, ESkog, Pt, Sfahey, RoyBoy, Andrewpmack, Jag123, Jumbuck, AzaToth, Pippu d'Angelo, LadyInGrey, Snowolf, BRW, RPH, Gene Nygaard, Oleg Alexandrov, Boothy443, UFu, Alvis, Woohookitty, TigerShark, Fbv65edel, Isnow, BD2412, Qwertyus, Chun-hian, MC MasterChef, Jorunn, Zbxgscqf, XLerate, Matt Deres, Yamamoto Ichiro, Ardhuin, Old Moonraker, Latka, Mathbot, Krun, Srleffler, Kri, Chobot, Bornhj, DVdm, Benjamin Gatti, Bgwhite, Gwernol, Wingchi, The Rambling Man, Siddhant, Sceptre, Dmharvey, Kiwimhm, SatuSuro, Gaius Cornelius, Wimt, Y6y6y6, Inike, Larsinio, Hmette, Samuel Huang, Epipelagic, Brucevdk, Tetracube, Daniel C, Closedmouth, Arthur Rubin, AlexD, Eaefremov, SmackBot, Alan Pascoe, Nihonjoe, Marc Lacoste, Leki, Zephyris, Ohnoitsjamie, Kdliss, Chris the speller, Bluebot, KaragouniS, Persian Poet Gal, JDCMAN, DHN-bot, Darth Panda, Audriusa, Jahiegel, LC Revelation, Wine Guy, Ritchie333, Flyguy649, T-borg, Akral, Caudex Rax, NickPenguin, Liljohn, Wikiklaas, Kukini, Harryboyles, Cdills, John, Drahcir, Swlenz, Accurizer, Smith609, LACameraman, Neddyseagoon, Ryulong, Marysunshine, Gveret Tered, Vargklo, Fedir, Fnfal, Mika1h, MaxEnt, Cydebot, Steel, Alvesgaspar, Rracecarr, Emustonen, Blindman shady, Nol888, Rosser1954, Ayzmo, CieloEstrellado, Epbr123, Andyjsmith, Hugo.arg, Marek69, James086, StudentJCase, Dfrg.msc, NERIUM, D.H, Nick Number, AntiVandalBot, Luna Santin, Autocracy, Danger, Malcolm, JAnDbot, BlindEagle, Bencherlite, KyleAndMelissa22, VoABot II, Email4mobile, Markey2, User A1, JaGa, MartinBot, Floor Anthoni, CommonsDelinker, Tgeairn, J.delanoy, Rgoodermote, Boom&zoom, Maison mere des rumeurs, Salih, Skinny McGee, NewEnglandYankee, Touch Of Light, Dhaluza, RB972, Warlordwolf, Skimx, JavierMC, Random Passer-by, Mwarner94, Idioma-bot, VolkovBot, Jennavecia, Aesopos, Pivari, WikiCantona, AppleJordan, Enviroboy, Sylent, RaseaC, AlanS, Thatsuperguy11, SieBot, Coffee, Winchelsea, Mbz1, Caltas, Yintan, Mimihitam, Atani, Antonio Lopez, Steven Zhang, Lightmouse, Dillard421, Bschaeffer, Martarius, ClueBot, The Thing That Should Not Be, PACO193, Taikanatur, Elisabethnost, Shustov, DragonBot, Excirial, Ottawa4ever, Aitias, SoxBot III, Crowsnest, Erodium, HokiePE, Lemmey, Addbot, Ziggzagoon, DOI bot, EjsBot, Mr. Wheely Guy, Vishnava, CanadianLinuxUser, NjardarBot, CarsracBot, Ferroequus, Inln93, Xev lexx, Sionnach1, Arbitrarily0, س‌ع‌ی, Meltingsidewalk123, Luckas-bot, Yobot, THEN WHO WAS PHONE?, KamikazeBot, Chasingseconds, Carlsotr, Maxis ftw, ARAGONESE35, Xqbot, Scholar743, TechBot, Anna Frodesiak, GrouchoBot, Fargo21, Josemanimala, A.amitkumar, Thehelpfulbot, Bernard94, Dave3457, FrescoBot, Jatlas, Truthspeaketh, Chulp, John85, Pinethicket, Rokaszil, Jivee Blau, Calmer Waters, December21st2012Freak, Hickorybark, WPPilot, Dcs002, Fdentale, Rolands75, EmausBot, Eekerz, Immunize, Sir jasper, Dewritech, GoingBatty, Wikipelli, AvicBot, Imperial Monarch, Bahudhara, Kgsbot, ClueBot NG, Lolfriend, Ulflund, O.Koslowski, Widr, Helpful Pixie Bot, Bibcode Bot, BG19bot, Garfl, AvocatoBot, IMollerCamU, Snow Blizzard, Shawn Worthington Laser Plasma, Mdann52, SquallBLi, Claushade, Smalleditor, Sspacce, FrigidNinja, JamesMoose, Jwratner1, Chuck bodeen, Anrnusna, Seung Yang, Sjyang80, Emrah6565, Karthik Easvur, Lippolop and Anonymous: 318
- **Mixing (process engineering)** *Source:* http://en.wikipedia.org/wiki/Mixing%20(process%20engineering)?oldid=634681393 *Contributors:* Michael Hardy, Ike9898, Hyacinth, Chowbok, Rhobite, Vsmith, CanisRufus, Linas, Ae-a, Jeff3000, RussBot, Witger, Tony1, Fram, SmackBot, Peterlewis, Wizard191, RSido, Khamar, Escarbot, Lanfrasa, Swpb, Nyttend, STBot, Extransit, KylieTastic, VolkovBot, Krzysiulek, Moonriddengirl, Addbot, Daniele Pugliesi, Materialscientist, Erik9bot, BenzolBot, Jujutacular, Fiftytwo thirty, Rlreid1, GoingBatty, Paulienkonniger, TheodoreNg, FusionFluid, ClueBot NG, Backonceagain, Widr, Bibcode Bot, AgaRed, Sls1234, Kwardle33, Jodosma, Monkbot, Vieque and Anonymous: 16
- **Liquid bubble** *Source:* http://en.wikipedia.org/wiki/Liquid%20bubble?oldid=618052172 *Contributors:* Edward, Michael Hardy, Omegatron, David.Monniaux, Robbot, Nurg, Academic Challenger, Giftlite, Alansohn, Stemonitis, Mindmatrix, CharlesC, Sjö, SchuminWeb, Gurch, Shaddack, NawlinWiki, Leptictidium, Dspradau, Hydrogen Iodide, Melchoir, Gilliam, SchfiftyThree, J. Spencer, Dasyati, Ninjagecko, Igoldste, JForget, MaxEnt, Michaelas10, Odie5533, Alaibot, Epbr123, Dgies, SummerPhD, David Shankbone, Res2216firestar, JAnDbot, Instinct, Andonic, VoABot II, Allstarecho, DerHexer, JaGa, STBot, Tgeairn, J.delanoy, Salih, Cobi, 28bytes, Soliloquial, Blurpeace, Amwyll Rwden, Enviroboy, Thunderbird2, Roger Jeurissen, SieBot, Josh the Nerd, Yintan, Keilana, Anchor Link Bot, Pinkadelica, ClueBot, Niceguyedc, Excirial, CrazyChemGuy, PixelBot, Eeekster, Vivio Testarossa, SchreiberBike, Katanada, SoxBot III, Vizka-Longtooth, Shinobi167, Jetsetpainter, Pielvr43, Addbot, RobinClay, DOI bot, ThePenguinStrangler, Chzz, TStein, Tide rolls, Zorrobot, Arbitrarily0, Luckas-bot, Yobot, Jjjjasminex, Kristen Eriksen, Daniele Pugliesi, MichaelRogersMacKenzie, Blue horizon 666, Sionus, Pianogrl97, RibotBOT, FrescoBot, Courtwashere, Gwenwood, Sleepingdogg, Wireless Keyboard, Redbubble, Pbsouthwood, SkyMachine, TBloemink, TjBot, J36miles, EmausBot, Orphan Wiki, NotAnonymous0, ZéroBot, Bahudhara, Dondervogel 2, Rails, DASHBotAV, Dgal001, ClueBot NG, 123Hedgehog456, Rawrorawr, Widr, Kierasmells, Bibcode Bot, Keephallow, Jjjane, Klilidiplomus, Achowat, The Illusive Man, ChrisGualtieri, Killer199208, Snotbag1234, CensoredScribe, Monkbot, DrTCz, Bellarocks21703, Blenderbottles and Anonymous: 98
- **Synthetic aperture radar** *Source:* http://en.wikipedia.org/wiki/Synthetic%20aperture%20radar?oldid=635105747 *Contributors:* Axelboldt, Michael Hardy, Aarchiba, Charles Matthews, Echoray, Rnbc, Topbanana, Stormie, Rbruels, Dominick, DavidCary, Laudaka, BenFrantzDale, Ferkelparade, Zigger, Ssd, Ukexpat, Brianhe, TedPavlic, Loren36, Matt McIrvin, Alansohn, Hu, OwenX, Uncle G, BlaiseFEgan, Rnt20, Drbogdan, Coneslayer, FlaBot, Maayanh, Kapitolini, Chobot, Banaticus, YurikBot, Phantomsteve, Test-tools, Grafen, Brandon, Alison.philp, Fitzsimons, DisambigBot, Segv11, SmackBot, Eskimbot, Chris the speller, MalafayaBot, Viewfinder, Colonies Chris, Dual Freq, Милан Јелисавчић, Glloq, Vina-iwbot, Khazar, John, Pierre cb, Novangelis, Dl2000, Iridescent, Eyliu, LaMa, Lavaka, SkyWalker, Ssircar, Quibik, Thijs!bot, ContivityGoddess, Uruiamme, Ekimd, HolyT, Soulbot, Indon, BilCat, Axlq, R'n'B, Rebell18190, Naniwako, STBotD, TXiKiBoT, Eve Hall, !dea4u, AlleborgoBot, SieBot, Avayak, WereSpielChequers, Boydrh, MichaelVernonDavis, Fleem, Alaimbeer, Alexbot, Ajoly, XLinkBot, RP459, Addbot, Fgnievinski, VSteiger, Lightbot, Acchen, Ben Ben, Legobot, Luckas-bot, Yobot, Pmallas,

Bunnyhop11, Punctilius, AnomieBOT, Piano non troppo, Xqbot, .45Colt, Phyrlight, Rosegate, Mmigliaccio, Rc3002, AstaBOTh15, Rapsar, HarmonicSeries, Dinamik-bot, Ashishindemand, EmausBot, John of Reading, GoingBatty, Rppeabody, Charvatg, Whatnick, Crown Prince, Oldteched, CocuBot, Braincricket, Op47, Ninney, Qpzdwrit, 220 of Borg, Fortiain, Kalmiopsiskid, DoctorKubla, Dexbot, Mogism, Arallen3, Tony Mach, Aladdin Ali Baba, John.f.paramino and Anonymous: 115

- **Interferometric synthetic aperture radar** *Source:* http://en.wikipedia.org/wiki/Interferometric%20synthetic%20aperture%20radar?oldid=635592485 *Contributors:* Hankwang, Ezhiki, Chowbok, Proberts2003, Brianhe, Keenan Pepper, Stephan Leeds, Woohookitty, Rjwilmsi, Seidenstud, Malcolma, Raistolo, SmackBot, RedSpruce, Chris the speller, Bluebot, Mwtoews, MGlosenger, Bumbulski, Quibik, Rosarinagazo, Dawnseeker2000, Mikenorton, Peppergrower, Naniwako, KylieTastic, Ghettobeamer, Eve Hall, Baumfreund-FFM, Spinningspark, Bob.lanahan, Marikan, XLinkBot, NPA Group, Addbot, Fgnievinski, LaaknorBot, م‌انی, Yobot, KamikazeBot, AnomieBOT, Materialscientist, Citation bot, Quebec99, Iszdfb, Urbanbricks, Topherwhelan, Almandine gloss, Phyrlight, Whanrott, Citation bot 1, Trappist the monk, RjwilmsiBot, EmausBot, John of Reading, Werieth, Jpvandijk, RockMagnetist, Whatnick, FeatherPluma, Marvistavenicec, Helpful Pixie Bot, Bibcode Bot, BG19bot, Qpzdwrit, NotWith, EricJFielding, Villemv, Aladdin Ali Baba, Gcooksley, ChiaraTRE, Roberto Tom, Danperiz, Vieque, Secretlady and Anonymous: 30
- **Oil spill** *Source:* http://en.wikipedia.org/wiki/Oil%20spill?oldid=635290061 *Contributors:* AxelBoldt, Bryan Derksen, Tarquin, SimonP, Shii, Olivier, D, Norm, Kku, Ixfd64, Karada, Skysmith, SebastianHelm, Ahoerstemeier, Mac, Theresa knott, Mark Foskey, Glenn, Nikai, Evercat, Varitek, Fuzheado, WhisperToMe, Haukurth, Dragons flight, Morwen, Tempshill, SEWilco, Nickshanks, HarryHenryGebel, Johnleemk, Robinstocks, Hello, Sunray, Bkell, Cyrius, Alan Liefting, Giftlite, Seabhcan, Tom harrison, SWAdair, Edcolins, Utcursch, Pgan002, Andycjp, Geni, Lexie67, Antandrus, Beland, OverlordQ, Jossi, Oneiros, Paulscrawl, Gscshoyru, Adashiel, Danh, Ta bu shi da yu, Myfanwy, Jkl, Jpg, Discospinster, Rich Farmbrough, Vsmith, JimR, Xezbeth, Mjpieters, Chadlupkes, Edgarde, Bender235, NeilTarrant, JoeSmack, Brian0918, Bobdoe, Maclean25, Ruyn, AlexTheMartian, Bobo192, Longhair, Smalljim, Func, Orbst, Viriditas, Bighead, AKGhetto, Giraffedata, (aeropagitica), Krellis, Nsaa, Stephen G. Brown, Danski14, Alansohn, Anthony Appleyard, Andrewpmk, Echuck215, InShaneee, Hu, Bart133, Hohum, Snowolf, Mudshark, Isaac, RainbowOfLight, Gene Nygaard, Dan100, Ceyockey, Zntrip, Stemonitis, LOL, Rtdrury, Bbatsell, Bluemoose, GregorB, Wayward, Xiong Chiamiov, NeonGeniuses, Emerson7, Mandarax, NickF, Kbdank71, Csnewton, Saperaud, Rjwilmsi, 40 Watt, Cxbrx, TexasDawg, Vegaswikian, DonSiano, CQJ, Bhadani, Tbone, Yamamoto Ichiro, FlaBot, RobertG, RexNL, TeaDrinker, Alphachimp, Silivrenion, Mstroeck, King of Hearts, ...adam..., Chobot, Korg, Bgwhite, Dj Capricorn, WriterHound, Gwernol, The Rambling Man, Wavelength, Sceptre, Kollision, Phantomsteve, RussBot, Rxnd, Stephenb, David Woodward, Rsrikanth05, Pseudomonas, Salsb, ALoopingIcon, NawlinWiki, Wiki alf, Grafen, Duran, Harksaw, Howcheng, Dureo, Patrick Neylan, Bobbo, Brian Crawford, Xdenizen, DAJF, Raven4x4x, Moe Epsilon, Speedevil, Nick C, Zwobot, Epipelagic, Syrthiss, Darkfred, Speedoflight, Kibblesnbits, Mugunth Kumar, Sperril, 21655, Closedmouth, Josh3580, Dspradau, Chrishmt0423, Fram, Peter, Repayne, Spliffy, Allens, Katieh5584, Codeine, Cfwschmidt, NetRolller 3D, Luk, SmackBot, Indyguy, KnowledgeOfSelf, Ma8thew, Vald, Eskimbot, Frymaster, Yamaguchi??, Gilliam, Ohnoitsjamie, Skizzik, TRosenbaum, AppleMacD, Fetofs, Persian Poet Gal, Ian13, Jprg1966, PureRED, Baa, Bill Slawski, Gracenotes, Scwlong, Rogermw, Can't sleep, clown will eat me, Shalom Yechiel, Sephiroth BCR, Snowmanradio, Rrburke, Ebaksa, Stevenmitchell, Popsup, Theanphibian, Decltype, Nakon, Tomtefarbror, Evenfiel, Illnab1024, Gbinal, Wizardman, Springnuts, Kukini, ArglebargleIV, Rory096, Nick carson, CharlesDexterWard, JuicyKnowledge, Scientizzle, Znixon, J 1982, Gobonobo, Javit, IronGargoyle, Ben Moore, Mathewignash, Alethiophile, Optakeover, Meco, Waggers, Camp3rstrik3r, Nwwaew, Geologyguy, P199, Fredwerner, YipYip, Politepunk, DabMachine, HisSpaceResearch, Iridescent, Joseph Solis in Australia, Skapur, Jcpalma, J Di, Theflyer, CapitalR, Blehfu, Ewulp, Courcelles, Tawkerbot2, Falconus, SkyWalker, Xcentaur, JForget, CmdrObot, Ale jrb, Lavateraguy, Makeemlighter, JohnCD, Baiji, Dgw, N2e, 345Kai, .Koen, Lokal Profil, Phatom87, Slazenger, Gogo Dodo, Travelbird, TicketMan, Odie5533, Tawkerbot4, Christian75, DumbBOT, Omicronpersei8, Billtubbs, Pustelnik, JimmB, Phi*n!x, Mattisse, Thijs!bot, Epbr123, Barticus88, Wikid77, Qwyrxian, Azimuth1, GentlemanGhost, Lanky, Mojo Hand, Headbomb, Marek69, Jcarle, John254, Tapir Terrific, E. Ripley, Calathan, Passa, Danielfolsom, Hmrox, AntiVandalBot, Widefox, Seaphoto, Opelio, Prolog, Dr. Blofeld, Mackan79, Joe Schmedley, Incantation, Bmaples, CombatWombat42, Damien o'connell, MER-C, Planetary, Dybryd, Blood Red Sandman, Hamsterlopithecus, Natureguy1980, Maias, LittleOldMe, Acroterion, Gert7, S0uj1r0, Meeples, Bongwarrior, VoABot II, AndriusG, AuburnPilot, AtticusX, JNW, JamesBWatson, Appraiser, Harel, Jim Douglas, Avicennasis, Catgut, Cgingold, Joshlim, 28421u2232nfenfcenc, Allstarecho, Beagel, Highcount, Halogenated, DerHexer, Philg88, Esanchez7587, Meodudlye, Almadenbuff, Marcelcarroll, S3000, Hdt83, MartinBot, Prgrmr@wrk, Cadillacregan, Rettetast, CommonsDelinker, AlexiusHoratius, Cyrus Andiron, Tgeairn, Rossarbeer, J.delanoy, Rebell18190, Uncle Dick, Ginsengbomb, Nothingofwater, Rubenwikipedia, Katalaveno, Ncmvocalist, Jeepday, OAC, Milkyface, (jarbarf), RenniePet, HiLo48, Plasticup, Cmichael, Natl1, Gtg204y, Tatortitz, Ja 62, Iabpm, Xiahou, Levydav, Funandtrvl, Spellcast, Xenonice, Deor, Johnfos, DSRH, Jeff G., Willow177, Barneca, Philip Trueman, Drunkenmonkey, TXiKiBoT, Oil Treatment International, Hqb, Censol, Templationist, Yksin, Killjoy966, Retiono Virginian, IronMaidenRocks, Edge2001, Chaan, Lucas j barker, From-cary, Drappel, Joren, Raymondwinn, Bob f it, Hannes Röst, Madhero88, Mwilso24, Greswik, Plazak, Squaretex, Turgan, Princess Fatima, !dea4u, Insanity Incarnate, Davidkhill, Brianga, Mike4ty4, Monty845, Onceonthisisland, Logan, NHRHS2010, Steven Weston, D. Recorder, Phil Polychaete, HowardMorland, SPQRobin, Aalox, Kksinter, Crudlique, Tpb, SieBot, Tiddly Tom, Dawn Bard, Caltas, Matthew Yeager, BlooxEinjeru, Yintan, Bonebuster, Bobmaster123, 123nec, Accu700, Accu20, Keilana, Chmyr, Happysailor, Nopetro, Wilson44691, CutOffTies, Yerpo, 123321123321123321t, Lightmouse, Nec123, Tombomp, Techman224, Padgadfgad, Danelo, Soccer93, DanniellaWB, La Parka Your Car, StaticGull, Johnson487682, Philly jawn, Sjyoo96, Mygerardromance, Tony Webster, Superbeecat, Jons63, Snarkosis, Loren.wilton, ClueBot, Burks88, The Thing That Should Not Be, Rjd0060, Cptmurdok, Arakunem, Drmies, Mild Bill Hiccup, CounterVandalismBot, JTSchreiber, Rowan747, Niceguyedc, Bubbles28, Edknol, Morwinyon, Arunsingh16, PMDrive1061, Excirial, Jusdafax, Eeekster, SpikeToronto, Vivio Testarossa, Jason526, Thehowitzer, Environnement2100, Xocasgv, Tuandoan, Thingg, Aitias, Halgin, Introductory adverb clause, NJGW, Qwfp, DumZiBoT, Aj00200, XLinkBot, Crash8552000, Spitfire, Stickee, Jovianeye, Mopenv, Avoided, Nikegirl101, Skarebo, Noctibus, Wulfgang, JCDenton2052, Athrun Atreides, HexaChord, Imperial Star Destroyer, Mojska, Metodicar, Luwilt, Addbot, Willking1979, Offenbach, Captain-tucker, Next-Genn-Gamer, AkhtaBot, Blethering Scot, Vernk, Misterx2000, Shirtwaist, CanadianLinuxUser, Download, Monster133, DreamHaze, Edwinseah, Favonian, Truefreedo, 84user, Zurukea, Tide rolls, OlEnglish, Avono, K12kk45kk53, Arxiloxos, Luckas-bot, ZX81, Yobot, Falky, THEN WHO WAS PHONE?, CinchBug, IW.HG, Umbertoumm, Isola20, AnomieBOT, Noq, 1exec1, Daniele Pugliesi, Killiondude, Jim1138, Dwayne, Piano non troppo, Ipatrol, Kingpin13, Bluerasberry, Joliv22, Materialscientist, RobertEves92, Rtyq2, FinneJager, Maxis ftw, Pseade, GB fan, Neurolysis, ArthurBot, LovesMacs, Xqbot, Lizard617, Intelati, Hockeykidd, JimVC3, Capricorn42, Nasnema, HelioSmith, Hikili, Roochieboy, Tad Lincoln, Anna Frodesiak, Sam1dotdot, AbigailAbernathy, Hi878, The Grand Rans, Frosted14, Call me Bubba, Twirligig, Silvia879, Minkypinky8, Tennesseefan67, Hmayoral, Manuelt15, Shadowjams, Miyagawa, Eugene-elgato, PM800, Starphi, Frozenjangofett, Erik9, Asfarer, Manman523, Dougofborg, FrescoBot, LucienBOT, Originalwana, Tranletuhan, Brianback, Turaliscool, Snowman837, ZbeeblebroxIV, VI, Igna, Girlwithgreeneyes, Finalius, Jamesooders, A little insignificant, Sopher99, Simple Bob, Tintenfischlein, Cubs197, Bobmcpee, Pinethicket, Pink Bull, Elockid, Edderso, Abductive, 10metreh, Calmer Waters, Tinton5, Slabree, Hariehkr, ContinueWithCaution, Piandcompany, Fumitol, EdoDodo, Bassbasketball03, Reconsider the static, December21st2012Freak, Gryllida, TobeBot, Yunshui, Pjoseph 98, Lotje, Vrenator, TBloemink,

Reaper Eternal, Clarabearasarah, Specs112, Weedwhacker128, Suffusion of Yellow, Tbhotch, Minimac, DARTH SIDIOUS 2, Mean as custard, The Utahraptor, RjwilmsiBot, Ripchip Bot, P Aculeius, CatJar, DASHBot, Xenon2, Steve03Mills, J36miles, EmausBot, John of Reading, Orphan Wiki, Immunize, Cephlasparks, Smokin yall out, IncognitoErgoSum, RA0808, Bubbletea98, Poiuytrfg, Solarra, Tommy2010, Wikipelli, K6ka, Djembayz, Nomaphi123, Fæ, Lateg, Azuris, Sellcott, Mrubin22, Holbi, Marybethholleman, H3llBot, Leo de Beo, Jj beast, Missiledragon, Edgarsonneborg, FinalRapture, Blood thir, Natasha1689, CosmicJake, Oilint, Wedontneedoil, Sphingomonas, Semajbobby123456789, Jamshid33, TyA, Ohlssons, Robnesbitt, Computerclass14, Greco32, Tp01386, Jimkearn, IGeMiNix, EAlphaBear, L Kensington, Andm32, Msaizan, Pad0215, Joe8789, Donner60, Environment101, Littlet1219, Autoerrant, Chicagooilscandal, Theuglygirl123, DASHBotAV, 28bot, Petrb, M6rr47, ClueBot NG, Dibbey, Satellizer, Weldone1234567, Muon, Marechal Ney, Widr, Reify-tech, Vibhijain, Helpful Pixie Bot, Nikdum, Electriccatfish2, Calabe1992, BG19bot, Kit kat2141, Jackerjr, Petrarchan47, Mr. watermelon man, Wiki13, MusikAnimal, Mark Arsten, Deepakmr14, Altaïr, Kejting, Pieplzrolyat, Kirsten951533, PlasmaTime, Achowat, Pratyya Ghosh, Hshah1998, ChrisGualtieri, Jionpedia, Mtcgold, Abraun3, Lakahata13, K7L, Snipepwner, Webclient101, LeFapOnymous, Lugia2453, Rockhuntress, Graphium, Little green rosetta, Mrelephantboyman, Akindo01, Reatlas, Sammyb123123, Aatifazeem, Rajat.danger, Diane Wagenbrenner, CensoredScribe, ɑb, Littledmanic, Coatface, G S Palmer, Amandacariip, Marickaburke, Demoniccathandler, RXG TDA, Nicoatxo, Crappycrap2003, Evabryn, Newtocambridge, Jizzburgerunited, Phaldistimus, Justin.gazzola and Anonymous: 1215

- **Marine pollution** *Source:* http://en.wikipedia.org/wiki/Marine%20pollution?oldid=633335973 *Contributors:* Infrogmation, William M. Connolley, Kils, Haukurth, Pakaran, Koba-chan, Alan Liefting, Andycjp, Adashiel, TheObtuseAngleOfDoom, Rich Farmbrough, Vsmith, Kaszeta, AKGhetto, Nsaa, Alansohn, Snowolf, Velella, Gene Nygaard, Stephen, Woohookitty, Mazca, Mandarax, Niffweed17, Rjwilmsi, Seidenstud, Jivecat, Mahlum, RexNL, Chobot, Wavelength, Kollision, Phantomsteve, CambridgeBayWeather, Epipelagic, Mkill, DeadEyeArrow, Sandstein, Zzuuzz, Arthur Rubin, KGasso, Katieh5584, Tom Morris, BomBom, SmackBot, Gjs238, Gilliam, Jprg1966, Miquonranger03, CSWarren, Onceler, OrphanBot, Rrburke, Flyguy649, Nakon, Valenciano, Ex nihil, NJA, Caiaffa, Squirepants101, Dean1970, DabMachine, Neelix, Jayen466, PKT, Dasani, N5iln, Headbomb, MikeLynch, Barek, Andonic, Bongwarrior, VoABot II, Rivertorch, Cgingold, Trusilver, Inomyabcs, Jeff G., Philip Trueman, Censol, Templationist, Dirkbb, Falcon8765, Michael Frind, Caltas, Elfino, Miguel.mateo, ClueBot, The Thing That Should Not Be, Pakaraki, Footballfan190, Hotcrocodile, Usmanmumtazbutt, Monfornot, Addbot, Willking1979, Jojhutton, Raywil, MrOllie, Favonian, Cubanonradar, Tide rolls, Anxietycello, OlEnglish, Zorrobot, Benjohn65, PlankBot, Luckas-bot, Themfromspace, Alchimista, Nukesea, Ayrton Prost, Backslash Forwardslash, AnomieBOT, The High Fin Sperm Whale, Citation bot, Quebec99, LilHelpa, Xqbot, JimVC3, Capricorn42, Brandon5485, MerlLinkBot, Elemesh, Marinecreatures, Citation bot 1, Luthiens submarine, Pinethicket, BRUTE, Vrenator, Djrao25, RjwilmsiBot, Valentin Zahrnt, EmausBot, Trofobi, Tommy2010, Thecheesykid, Oceans and oceans, ZéroBot, Fæ, Lesliebre, H3llBot, Wayne Slam, Cskok, Tsuchiya Hikaru, L Kensington, Fagopyrum, Petrb, ClueBot NG, Vacation9, Jga49143, Widr, Mintyzoozoos, Camstool, Helpful Pixie Bot, Titodutta, Bibcode Bot, AvocatoBot, Shellfishbiologist, Francis Meyrick, Jonadin93, BattyBot, Justincheng12345-bot, DerickDiamond, Pazqual3, Webclient101, Jonnieroxursox, Epicgenius, Eyesnore, Christiandasilva, Bbmusicman, Nathec12, Zenibus, TheEpTic, Danielleblake1, TerryAlex, Farash Luthfy 05 and Anonymous: 209
- **Geodesy** *Source:* http://en.wikipedia.org/wiki/Geodesy?oldid=623456295 *Contributors:* Mav, The Anome, Youandme, Edward, Patrick, Michael Hardy, Ixfd64, SebastianHelm, Egil, Looxix, Ellywa, Mac, Smack, Redjar, Natevw, Robbot, Hankwang, Chris 73, Altenmann, Romanm, Ojigiri, Radagast, Giftlite, DocWatson42, DavidCary, Kmote, Joe Kress, Leonard G., Mboverload, Evolt, Pgan002, JoJan, APH, OwenBlacker, Icairns, Simoneau, Mrtrey99, Sam Hocevar, Lumidek, Neutrality, Vermeer, Ta bu shi da yu, Geof, Pyrop, Rich Farmbrough, Guanabot, Vsmith, ESkog, El C, Walden, Kwamikagami, Aude, Art LaPella, Muntfish, CDN99, Maurreen, Syd1435, Clyde frogg, Caeruleancentaur, Mpeisenbr, Hawei, Zer T, Keenan Pepper, GJeffery, Dirac1933, Gene Nygaard, Oleg Alexandrov, Kokoriko, Pdn, Eilthireach, Obersachse, Graham87, Amorrow, Dpv, Daniel Collins, FlaBot, SchuminWeb, David.Gaya, Ryan Hardy, Srleffler, WouterBot, Jaraalbe, YurikBot, Borgx, StuffOfInterest, KSmrq, DanMS, Lord Voldemort, NawlinWiki, AlexD, Busstop, Junglecat, GrinBot, XieChengnuo, SmackBot, Unyoyega, Jagged 85, Eskimbot, Mattsnibbs, TimBentley, Silly rabbit, Ras, CDV, Tsca.bot, OrphanBot, Radagast83, RandomP, David G. Smith, Jbergquist, DMacks, Aaker, SashatoBot, Cronholm144, JorisvS, Tasc, Dicklyon, Geologyguy, Dan Gluck, Iridescent, MFago, Joseph Solis in Australia, Audiosmurf, Avg, CmdrObot, Destrius, MarsRover, Cydebot, Nimar, Krauss, Arb, Thijs!bot, N5iln, Nyd, EdJohnston, D.H, Jmsanta-de, Tomenes, LachlanA, Alphachimpbot, Mikenorton, Deflective, Quentar, MickeyWiki, Magioladitis, Tenzing347, Ac44ck, NatureA16, Dontdoit, Niels G. Mortensen, Speck-Made, R'n'B, Farnil, Athaenara, Geonarva, Lunokhod, JonMcLoone, Treisijs, Greg-si, Idioma-bot, Vedran8080, Macedonian, Markusbela, TXiKiBoT, Eve Hall, A4bot, Cognoscibilis, The Tetrast, Don de la Muncha, Mikael R, Yk Yk Yk, AdRock, SieBot, Toddst1, Cffk, OKBot, Jaan, Vergos, Steve.hawtin, Eyeintheskye, ImageRemovalBot, SlackerMom, TrigWorks, Geoeg, Sun Creator, Arjayay, TheRedPenOfDoom, Dekisugi, Corkgkagj, Scooter171, XLinkBot, T68492, BodhisattvaBot, A. Ardalan, SilvonenBot, RP459, Cloudruns, Vikpfeifer, Addbot, Iwanttotubereallybad, Fgnievinski, OlEnglish, Legobot, Luckas-bot, PMLawrence, KamikazeBot, مرحبـــوب عالم, AnomieBOT, Bsimmons666, Iszdfb, Njchoi, Obersachsebot, MauritsBot, Xqbot, Poetaris, Turk oğlan, Omnipaedista, RibotBOT, Coosbane, Originalwana, Jc3s5h, Peter Mercator, J. Sketter, Redrose64, Saimyooo, RedBot, Robo Cop, FoxBot, Mjsmale, Nascar1996, EmausBot, GoingBatty, ZéroBot, Ruislick0, Persian Aviator, Jay-Sebastos, Ego White Tray, ⁇⁇, RockMagnetist, 28bot, ClueBot NG, Cheers!, Frietjes, Titodutta, Mark Arsten, Ninney, Psychap, Stanislav.grigas, Bnland, Pdecalculus, Ya yahya, Plazmic, JeanLucMargot, Oren Stembel and Anonymous: 190
- **Physical geodesy** *Source:* http://en.wikipedia.org/wiki/Physical%20geodesy?oldid=586073716 *Contributors:* Bryan Derksen, The Anome, Heron, Michael Hardy, Snoyes, Julesd, SEWilco, Vermeer, Geof, Gene Nygaard, Oleg Alexandrov, Linas, Marudubshinki, Srleffler, RDBury, Sbharris, Fuhghettaboutit, Jbergquist, MegaHasher, Michel M Verstraete, MFago, Christian75, Roberta F., D.H, Dontdoit, SieBot, Anchor Link Bot, Geoeg, Awickert, Mxbuck, Kbdankbot, Addbot, Rubinbot, Amin Hashem, Advancedxu, FrB.TG and Anonymous: 11
- **Gravity of Earth** *Source:* http://en.wikipedia.org/wiki/Gravity%20of%20Earth?oldid=634863828 *Contributors:* Patrick, Julesd, Charles Matthews, Dcoetzee, Jeepien, Dragons flight, Roachmeister, Dunning, Rei, Indefatigable, Denelson83, Ancheta Wis, Wolfkeeper, Brockert, Bobblewik, Irene1949, Eregli bob, Geof, Discospinster, Vsmith, ArnoldReinhold, Xezbeth, ZeroOne, EmilJ, Afed, Bobo192, MPerel, Eric Kvaalen, Arthena, Keenan Pepper, Velella, RainbowOfLight, Allen McC., Gene Nygaard, LukeSurl, HenryLi, Siafu, Firsfron, Shreevatsa, Xinghuei, StradivariusTV, WadeSimMiser, Lawe, Zeromaru, Rjwilmsi, SMC, ElKevbo, Roboto de Ajvol, YurikBot, Petiatil, Wimt, NawlinWiki, Moe Epsilon, AdiJapan, 21655, Nemu, Dspradau, Smurrayinchester, Sbyrnes321, SmackBot, Blue520, LuNatic, Hibernian, Cygnus78, Egsan Bacon, Tamfang, Jhausauer, Lord Vader, Mwtoews, DMacks, Sadi Carnot, Krashlandon, J 1982, Accurizer, Bjankuloski06en, Rahul14 1991, Ckatz, Geologyguy, Novangelis, Teodozjan, Nialsh, Quaeler, Iridescent, StephenBuxton, Kielvon, Anon user, CmdrObot, Antipika, CWY2190, Ruslik0, Green caterpillar, Erzbischof, Johnlogic, Skybon, Rivemont, Starylon, Rracecarr, Shirulashem, Epbr123, Headbomb, Marek69, Greg L, Seaphoto, Memset, Mikenorton, JAnDbot, CosineKitty, Snolygoster, OhanaUnited, LittleOldMe, Bongwarrior, VoABot II, Sarahj2107, Email4mobile, Alanbrowne, DerHexer, NatureA16, Naohiro19, Glrx, R'n'B, CommonsDelinker, J.delanoy, Aveh8, GeoWriter, McSly, Lunokhod, ColinClark, Qbk, Rising*From*Ashes, Izno, CardinalDan, TimeHorse, VolkovBot, Larryisgood, Nburden, Sagittarian Milky Way, Muro de Aguas, Calwiki, Brian eye, Grahamwild, LeaveSleaves, RadiantRay, Entropy1963, Insanity Incarnate, ExtonGuy, Adaviel, Dawn Bard, The way, the truth, and the light, Keilana, Wilson44691, Prestonmag, Bagatelle,

SieBot, Mbz1, PerryTachett, ClueBot, Pcirrus, Tanketz, Alexbot, Mleconte, Crowsnest, PSimeon, Nathan Johnson, Addbot, Luckas-bot, Yobot, Ptbotgourou, AnomieBOT, Bdubb12, Thehelpfulbot, Jujutacular, Bjarkeoveandersen, Ivica Vlahović, RjwilmsiBot, EmausBot, Az29, Pen7777, Lhibbeler, FoxBee, Xonqnopp, ClueBot NG, Helpful Pixie Bot, Bibcode Bot, BattyBot and Anonymous: 32

|

- **File:A_Swarm_of_Ancient_Stars_-_GPN-2000-000930.jpg** *Source:* http://upload.wikimedia.org/wikipedia/commons/6/6a/A_Swarm_of_Ancient_Stars_-_GPN-2000-000930.jpg *License:* Public domain *Contributors:* Great Images in NASA Description *Original artist:* NASA, The Hubble Heritage Team, STScI, AURA
- **File:Accreting_coast_Image6.svg** *Source:* http://upload.wikimedia.org/wikipedia/commons/4/48/Accreting_coast_Image6.svg *License:* Public domain *Contributors:* self-made SVG, based on the public domain PNG [1] by User:Feydey *Original artist:* Surachit
- **File:Aerosolcan_pullution.jpg** *Source:* http://upload.wikimedia.org/wikipedia/commons/2/2c/Aerosolcan_pullution.jpg *License:* Public domain *Contributors:* Own work *Original artist:* [//commons.wikimedia.org/w/index.php?title=User:T3rminatr&action=edit&redlink=1 T3rminatr]
- **File:Agitated_vessel.svg** *Source:* http://upload.wikimedia.org/wikipedia/commons/b/be/Agitated_vessel.svg *License:* CC-BY-SA-3.0 *Contributors:* Own work *Original artist:* Aushulz
- **File:Aguas_del_lago_de_Maracaibo_contaminadas_por_Lemna_03.JPG** *Source:* http://upload.wikimedia.org/wikipedia/commons/5/5b/Aguas_del_lago_de_Maracaibo_contaminadas_por_Lemna_03.JPG *License:* CC0 *Contributors:* Own work *Original artist:* Wilfredor
- **File:AirSAR-instrument-on-aircraft.jpg** *Source:* http://upload.wikimedia.org/wikipedia/commons/a/a6/AirSAR-instrument-on-aircraft.jpg *License:* Public domain *Contributors:* ? *Original artist:* ?
- **File:Air_bubbles_in_a_pool_as_a_man_surfaces_for_air.jpg** *Source:* http://upload.wikimedia.org/wikipedia/commons/6/6b/Air_bubbles_in_a_pool_as_a_man_surfaces_for_air.jpg *License:* CC-BY-SA-3.0 *Contributors:* David Shankbone *Original artist:* David Shankbone
- **File:Airplane_vortex_edit.jpg** *Source:* http://upload.wikimedia.org/wikipedia/commons/f/fe/Airplane_vortex_edit.jpg *License:* Public domain *Contributors:* This image or video was catalogued by Langley Research Center of the United States National Aeronautics and Space Administration (NASA) under **Photo ID:** EL-1996-00130 AND **Alternate ID:** L90-5919.
  Original artist: NASA Langley Research Center (NASA-LaRC), Edited by Fir0002
- **File:Ambox_content.png** *Source:* http://upload.wikimedia.org/wikipedia/en/f/f4/Ambox_content.png *License:* ? *Contributors:*
  Derived from Image:Information icon.svg *Original artist:*
  El T (original icon); David Levy (modified design); Penubag (modified color)
- **File:Animated_fractal_mountain.gif** *Source:* http://upload.wikimedia.org/wikipedia/commons/6/6d/Animated_fractal_mountain.gif *License:* Public domain *Contributors:* self made based in own JAVA animation *Original artist:* António Miguel de Campos - en:User:Tó campos
- **File:Antarctic_bottom_water.svg** *Source:* http://upload.wikimedia.org/wikipedia/commons/e/e7/Antarctic_bottom_water.svg *License:* CC-BY-SA-4.0 *Contributors:* *Original artist:* Fred the Oyster
- **File:Apophysis-100303-104.jpg** *Source:* http://upload.wikimedia.org/wikipedia/en/1/10/Apophysis-100303-104.jpg *License:* PD *Contributors:*
  I (Gut Monk (talk)) created this work entirely by myself. *Original artist:*
  Gut Monk (talk)
- **File:Aviacionavion.png** *Source:* http://upload.wikimedia.org/wikipedia/commons/6/68/Aviacionavion.png *License:* Public domain *Contributors:*
- Turkmenistan.airlines.frontview.arp.jpg *Original artist:* Turkmenistan.airlines.frontview.arp.jpg: elfuser
- **File:BML_N=200_P=32.png** *Source:* http://upload.wikimedia.org/wikipedia/commons/f/f6/BML_N%3D200_P%3D32.png *License:* CC-BY-SA-3.0 *Contributors:* Own work *Original artist:* Purpy Pupple
- **File:Barbadosdustgraph.gif** *Source:* http://upload.wikimedia.org/wikipedia/en/2/20/Barbadosdustgraph.gif *License:* ? *Contributors:* ? *Original artist:* ?
- **File:Barnsley_fern_plotted_with_VisSim.PNG** *Source:* http://upload.wikimedia.org/wikipedia/commons/7/76/Barnsley_fern_plotted_with_VisSim.PNG *License:* CC-BY-SA-3.0 *Contributors:* Own work, using model written by Mike Borrello *Original artist:* DSP-user
- **File:Big_wave_breaking_in_Santa_Cruz.jpg** *Source:* http://upload.wikimedia.org/wikipedia/commons/2/2a/Big_wave_breaking_in_Santa_Cruz.jpg *License:* CC-BY-SA-3.0 *Contributors:* Own work *Original artist:* Brocken Inaglory
- **File:Bottle2.gif** *Source:* http://upload.wikimedia.org/wikipedia/commons/3/33/Bottle2.gif *License:* Public domain *Contributors:*
- File:Bottle.gif *Original artist:*
- yorickm (see Bottle.gif)
- **File:C-130_support_oil_spill_cleanup.jpg** *Source:* http://upload.wikimedia.org/wikipedia/commons/6/61/C-130_support_oil_spill_cleanup.jpg *License:* Public domain *Contributors:* US Air Force public affairs story direct link *Original artist:* Technical Sergeant Adrian Cadiz
- **File:CSIRO_ScienceImage_11128_The_bathymetry_of_the_Kerguelen_Plateau_in_the_Southern_Ocean_governs_the_course_of_the_new_current_part_of_the_global_network_of_ocean_currents.jpg** *Source:* http://upload.wikimedia.org/wikipedia/commons/5/5e/CSIRO_ScienceImage_11128_The_bathymetry_of_the_Kerguelen_Plateau_in_the_Southern_Ocean_governs_the_course_of_the_new_current_part_of_the_global_network_of_ocean_currents.jpg *License:* CC-BY-3.0 *Contributors:* http://www.scienceimage.csiro.au/image/11128 *Original artist:* division, CSIRO
- **File:Chaos_Sensitive_Dependence.svg** *Source:* http://upload.wikimedia.org/wikipedia/commons/8/8e/Chaos_Sensitive_Dependence.svg *License:* Public domain *Contributors:* Own work *Original artist:* Radagast3
- **File:Chaos_Topological_Mixing.png** *Source:* http://upload.wikimedia.org/wikipedia/commons/d/dc/Chaos_Topological_Mixing.png *License:* Public domain *Contributors:* Own work *Original artist:* Radagast3

- **File:Circulation_of_Ocean_Currents_Around_the_Western_Antarctic_Ice_Shelves.ogv** *Source:* http://upload.wikimedia.org/wikipedia/commons/c/cd/Circulation_of_Ocean_Currents_Around_the_Western_Antarctic_Ice_Shelves.ogv *License:* Public domain *Contributors:* Goddard Multimedia *Original artist:* NASA/Goddard Space Flight Center
- **File:Close-up_of_Lake_Maracaibo,_Venezuela.jpg** *Source:* http://upload.wikimedia.org/wikipedia/commons/b/bb/Close-up_of_Lake_Maracaibo%2C_Venezuela.jpg *License:* Public domain *Contributors:* NASA Earth Observatory *Original artist:* Image courtesy NASA Earth Observatory
- **File:Commons-logo.svg** *Source:* http://upload.wikimedia.org/wikipedia/en/4/4a/Commons-logo.svg *License:* ? *Contributors:* ? *Original artist:* ?
- **File:Compare_images.JPG** *Source:* http://upload.wikimedia.org/wikipedia/commons/3/35/Compare_images.JPG *License:* CC-BY-SA-3.0 *Contributors:* Own work based on image data courtesy of University of Michigan and Natural Resources Canada. *Original artist:* Oldteched
- **File:Complex-adaptive-system.jpg** *Source:* http://upload.wikimedia.org/wikipedia/commons/0/00/Complex-adaptive-system.jpg *License:* Public domain *Contributors:* Own work by Acadac : Taken from en.wikipedia.org, where Acadac was inspired to create this graphic after reading: *Original artist:* Acadac
- {{int:Coll-image-attribution|File:Corrientes-oceanicas.gif|http://upload.wikimedia.org/wikipedia/commons/0/06/Corrientes-oceanicas.gif|Public domain|http://blue.utb.edu/paullgj/geog3333/lectures/physgeog.html, [http://skyblue.utb.edu/paullgj/geog3333/lectures/oceancurrents-1.gif original image]|Dr. Michael Pidwirny (see http://www.physicalgeography.net)}}
- **File:Crab_Nebula.jpg** *Source:* http://upload.wikimedia.org/wikipedia/commons/0/00/Crab_Nebula.jpg *License:* Public domain *Contributors:* HubbleSite: gallery, release. *Original artist:* NASA, ESA, J. Hester and A. Loll (Arizona State University)
- **File:DCG_chart.svg** *Source:* http://upload.wikimedia.org/wikipedia/commons/e/e9/DCG_chart.svg *License:* Public domain *Contributors:* Own work (Original text: *I (Srinivas.zinka (talk)) created this work entirely by myself.*) *Original artist:* Srinivas.zinka (talk)
- **File:Death-valley-sar.jpg** *Source:* http://upload.wikimedia.org/wikipedia/commons/2/20/Death-valley-sar.jpg *License:* Public domain *Contributors:* http://photojournal.jpl.nasa.gov/catalog/PIA01349 *Original artist:* NASA/JPL
- **File:Deep_Oceanic_Kelvin-Helmholtz_billows.jpg** *Source:* http://upload.wikimedia.org/wikipedia/commons/b/b7/Deep_Oceanic_Kelvin-Helmholtz_billows.jpg *License:* CC-BY-SA-3.0 *Contributors:* Own work *Original artist:* Lgostiau
- **File:Deep_water_wave.gif** *Source:* http://upload.wikimedia.org/wikipedia/commons/4/4a/Deep_water_wave.gif *License:* GFDL *Contributors:* Own work *Original artist:* Kraaiennest
- **File:Deep_water_wave.png** *Source:* http://upload.wikimedia.org/wikipedia/commons/6/61/Deep_water_wave.png *License:* CC-BY-SA-3.0-2.5-2.0-1.0 *Contributors:*
- Deep_water_wave.gif *Original artist:* Deep_water_wave.gif: Kraaiennest
- **File:Double-compound-pendulum.gif** *Source:* http://upload.wikimedia.org/wikipedia/commons/4/45/Double-compound-pendulum.gif *License:* Public domain *Contributors:* Own work *Original artist:* Catslash
- **File:EarthGravityPREM.svg** *Source:* http://upload.wikimedia.org/wikipedia/commons/5/50/EarthGravityPREM.svg *License:* CC-BY-SA-3.0-2.5-2.0-1.0 *Contributors:* http://geophysics.ou.edu/solid_earth/prem.html
Original artist: Con-struct
- **File:Edit-clear.svg** *Source:* http://upload.wikimedia.org/wikipedia/en/f/f2/Edit-clear.svg *License:* Public domain *Contributors:* The *Tango! Desktop Project*. *Original artist:*
The people from the Tango! project. And according to the meta-data in the file, specifically: “Andreas Nilsson, and Jakub Steiner (although minimally).”
- **File:Erdgvarp.png** *Source:* http://upload.wikimedia.org/wikipedia/commons/0/04/Erdgvarp.png *License:* CC-BY-SA-3.0 *Contributors:* ? *Original artist:* ?
- **File:Experimental_chamber_for_studying_chemotaxis_in_response_to_laminar_flow.ogv** *Source:* http://upload.wikimedia.org/wikipedia/commons/6/6d/Experimental_chamber_for_studying_chemotaxis_in_response_to_laminar_flow.ogv *License:* CC-BY-2.5 *Contributors:* Video S1 from Readman G, Owen S, Murrell J, Knowles T (2013). "Do Fish Perceive Anaesthetics as Aversive?". *PLOS ONE*. DOI:10.1371/journal.pone.0073773. PMC: 3781131. *Original artist:* Readman G, Owen S, Murrell J, Knowles T
- **File:Exxon_Valdez_Cleanup.jpg** *Source:* http://upload.wikimedia.org/wikipedia/commons/7/7d/Exxon_Valdez_Cleanup.jpg *License:* Public domain *Contributors:* http://www.dodmedia.osd.mil/DVIC_View/Still_Details.cfm?SDAN=DNSC8907300&JPGPath=/Assets/Still/1989/Navy/DN-SC-89-07300.JPG *Original artist:* PH2 POCHE
- **File:Fernando_noronha.jpg** *Source:* http://upload.wikimedia.org/wikipedia/commons/5/58/Fernando_noronha.jpg *License:* CC-BY-2.0 *Contributors:* Fernando de Noronha *Original artist:* Roberto Garrido from Salvador, Brasil
- **File:Finite_subdivision_of_a_radial_link.png** *Source:* http://upload.wikimedia.org/wikipedia/commons/d/d6/Finite_subdivision_of_a_radial_link.png *License:* CC-BY-SA-3.0 *Contributors:* Own work *Original artist:* Brirush
- **File:FirstSARimage.JPG** *Source:* http://upload.wikimedia.org/wikipedia/commons/2/2b/FirstSARimage.JPG *License:* CC-BY-SA-3.0 *Contributors:* Own work based on data from Radar Laboratory, Willow Run Labs, University of Michigan. *Original artist:* Oldteched
- **File:Flag_of_Angola.svg** *Source:* http://upload.wikimedia.org/wikipedia/commons/9/9d/Flag_of_Angola.svg *License:* Public domain *Contributors:* Drawn by User:SKopp *Original artist:* User:SKopp
- **File:Flag_of_France.svg** *Source:* http://upload.wikimedia.org/wikipedia/en/c/c3/Flag_of_France.svg *License:* ? *Contributors:* ? *Original artist:* ?
- **File:Flag_of_Iran.svg** *Source:* http://upload.wikimedia.org/wikipedia/commons/c/ca/Flag_of_Iran.svg *License:* Public domain *Contributors:* URL http://www.isiri.org/portal/files/std/1.htm and an English translation / interpretation at URL http://flagspot.net/flags/ir'.html *Original artist:* Various
- **File:Flag_of_Kuwait.svg** *Source:* http://upload.wikimedia.org/wikipedia/commons/a/aa/Flag_of_Kuwait.svg *License:* Public domain *Contributors:* Own work *Original artist:* SKopp
- **File:Flag_of_Mexico.svg** *Source:* http://upload.wikimedia.org/wikipedia/commons/f/fc/Flag_of_Mexico.svg *License:* Public domain *Contributors:* This vector image was created with Inkscape. *Original artist:* **Alex Covarrubias**, 9 April 2006
- **File:Flag_of_South_Africa_1928-1994.svg** *Source:* http://upload.wikimedia.org/wikipedia/commons/6/67/Flag_of_South_Africa_1928-1994.svg *License:* Public domain *Contributors:* SVG based on this image *Original artist:* Parliament of South Africa
- **File:Flag_of_Trinidad_and_Tobago.svg** *Source:* http://upload.wikimedia.org/wikipedia/commons/6/64/Flag_of_Trinidad_and_Tobago.svg *License:* Public domain *Contributors:* ? *Original artist:* ?

- **File:Flag_of_Uzbekistan.svg** *Source:* http://upload.wikimedia.org/wikipedia/commons/8/84/Flag_of_Uzbekistan.svg *License:* Public domain *Contributors:* Own work *Original artist:* O'zbekiston Respublikasining Davlat bayrog'i. The officially defined colours are Pantone 313C for blue and 361C for green (source: [1], [2]). Drawn by User:Zscout370.
- **File:Flag_of_the_United_States.svg** *Source:* http://upload.wikimedia.org/wikipedia/en/a/a4/Flag_of_the_United_States.svg *License:* ? *Contributors:* ? *Original artist:* ?
- **File:Fluidized_Bed_Reactor_Graphic.svg** *Source:* http://upload.wikimedia.org/wikipedia/commons/9/91/Fluidized_Bed_Reactor_Graphic.svg *License:* Public domain *Contributors:* Own work based on Fluidized Bed Reactor Graphic.JPG (user:Hughesy127) *Original artist:* This vector image was created with Inkscape.
- **File:Folder_Hexagonal_Icon.svg** *Source:* http://upload.wikimedia.org/wikipedia/en/4/48/Folder_Hexagonal_Icon.svg *License:* Cc-by-sa-3.0 *Contributors:* ? *Original artist:* ?
- **File:Fractal_Broccoli.jpg** *Source:* http://upload.wikimedia.org/wikipedia/commons/4/4f/Fractal_Broccoli.jpg *License:* Public domain *Contributors:* http://pdphoto.org/PictureDetail.php?mat=pdef&pg=8232 *Original artist:* Jon Sullivan
- **File:Fractal_defrosting_patterns_on_Mars.jpg** *Source:* http://upload.wikimedia.org/wikipedia/commons/1/1c/Fractal_defrosting_patterns_on_Mars.jpg *License:* Public domain *Contributors:* http://hirise.lpl.arizona.edu/ESP_029614_1105 *Original artist:* NASA HiRISE camera, Mars Reconnaissance Orbiter.
- **File:Fractal_fern_explained.png** *Source:* http://upload.wikimedia.org/wikipedia/commons/4/4b/Fractal_fern_explained.png *License:* Public domain *Contributors:* Own work *Original artist:* António Miguel de Campos
- **File:Frost_patterns_2.jpg** *Source:* http://upload.wikimedia.org/wikipedia/commons/0/0a/Frost_patterns_2.jpg *License:* CC-BY-SA-3.0 *Contributors:* Own work *Original artist:* Schnobby
- **File:GRACE_artist_concept.jpg** *Source:* http://upload.wikimedia.org/wikipedia/commons/e/e6/GRACE_artist_concept.jpg *License:* Public domain *Contributors:* http://photojournal.jpl.nasa.gov/catalog/PIA04235 *Original artist:* NASA
- **File:GRACE_globe_animation.gif** *Source:* http://upload.wikimedia.org/wikipedia/commons/7/78/GRACE_globe_animation.gif *License:* Public domain *Contributors:* http://photojournal.jpl.nasa.gov/catalog/PIA12146 *Original artist:* NASA/JPL/University of Texas Center for Space Research.
- **File:GRACE_ocean_bottom_pressure.jpg** *Source:* http://upload.wikimedia.org/wikipedia/commons/1/19/GRACE_ocean_bottom_pressure.jpg *License:* Public domain *Contributors:* http://photojournal.jpl.nasa.gov/catalog/PIA12188 *Original artist:* NASA/JPL
- **File:Geodetic_Control_Mark.jpg** *Source:* http://upload.wikimedia.org/wikipedia/commons/6/6f/Geodetic_Control_Mark.jpg *License:* GFDL *Contributors:* Own work *Original artist:* Junglecat
- **File:Geodetisch_station1855.jpg** *Source:* http://upload.wikimedia.org/wikipedia/commons/8/85/Geodetisch_station1855.jpg *License:* CC-BY-SA-3.0 *Contributors:* ? *Original artist:* ?
- **File:Geoids_sm.jpg** *Source:* http://upload.wikimedia.org/wikipedia/commons/5/56/Geoids_sm.jpg *License:* Public domain *Contributors:* ? *Original artist:* ?
- **File:Global_Gravity_Anomaly_Animation_over_LAND.gif** *Source:* http://upload.wikimedia.org/wikipedia/commons/1/15/Global_Gravity_Anomaly_Animation_over_LAND.gif *License:* Public domain *Contributors:* ? *Original artist:* ?
- **File:Global_Gravity_Anomaly_Animation_over_OCEANS.gif** *Source:* http://upload.wikimedia.org/wikipedia/commons/b/b4/Global_Gravity_Anomaly_Animation_over_OCEANS.gif *License:* Public domain *Contributors:* ? *Original artist:* ?
- **File:Global_Wave_Height_Speed.jpg** *Source:* http://upload.wikimedia.org/wikipedia/en/2/20/Global_Wave_Height_Speed.jpg *License:* ? *Contributors:* Source: NASA Official website, [1]. *Original artist:* ?
- **File:Glue1_800x600.jpg** *Source:* http://upload.wikimedia.org/wikipedia/commons/6/69/Glue1_800x600.jpg *License:* CC-BY-SA-3.0 *Contributors:* ? *Original artist:* ?
- **File:Gravity,_geoid_anomaly_synthetic_cases_with_local_isostasy_2.gif** *Source:* http://upload.wikimedia.org/wikipedia/commons/9/9f/Gravity%2C_geoid_anomaly_synthetic_cases_with_local_isostasy_2.gif *License:* CC-BY-SA-3.0 *Contributors:* Own work *Original artist:* Gaianauta
- **File:HD-Rayleigh-Taylor.gif** *Source:* http://upload.wikimedia.org/wikipedia/commons/d/d6/HD-Rayleigh-Taylor.gif *License:* Public domain *Contributors:* "Parallel AMR Code for Compressible MHD or HD Equations" *Original artist:* Shengtai Li, Hui Li
- **File:Harbour_Buster_high-speed_oil_containment_system.jpg** *Source:* http://upload.wikimedia.org/wikipedia/commons/5/5d/Harbour_Buster_high-speed_oil_containment_system.jpg *License:* Public domain *Contributors:* http://www.navy.mil/view_single.asp?id=61744 *Original artist:* U.S. Navy photo by Mr. Paul Farley/Released
- **File:Helmet_logo_for_Underwater_Diving_portal.png** *Source:* http://upload.wikimedia.org/wikipedia/commons/5/5e/Helmet_logo_for_Underwater_Diving_portal.png *License:* ? *Contributors:* Kask-nurka.jpg
Original artist: Kask-nurka.jpg: User:Julo
- **File:Izmit_interferogram.jpg** *Source:* http://upload.wikimedia.org/wikipedia/commons/c/cc/Izmit_interferogram.jpg *License:* Public domain *Contributors:* http://photojournal.jpl.nasa.gov/catalog/PIA00557 *Original artist:* NASA/JPL-Caltech
- **File:JerkCircuit01.png** *Source:* http://upload.wikimedia.org/wikipedia/commons/8/87/JerkCircuit01.png *License:* Public domain *Contributors:* ? *Original artist:* ?
- **File:Julia_set_(indigo).png** *Source:* http://upload.wikimedia.org/wikipedia/commons/b/bd/Julia_set_%28indigo%29.png *License:* Public domain *Contributors:* ? *Original artist:* ?
- **File:Kamilo_Beach2_Courtesy_Algalita_dot_org.jpg** *Source:* http://upload.wikimedia.org/wikipedia/commons/f/f9/Kamilo_Beach2_Courtesy_Algalita_dot_org.jpg *License:* Public domain *Contributors:* Courtesy Algalita.org *Original artist:* Algalita.org
- **File:KarperienFractalBranch.jpg** *Source:* http://upload.wikimedia.org/wikipedia/commons/b/b7/KarperienFractalBranch.jpg *License:* CC-BY-SA-3.0 *Contributors:* Own work *Original artist:* Audrey Karperien
- **File:Karperien_Strange_Attractor_200.gif** *Source:* http://upload.wikimedia.org/wikipedia/commons/5/5e/Karperien_Strange_Attractor_200.gif *License:* CC-BY-SA-3.0 *Contributors:* Own work *Original artist:* Akarpe

- **File:Kelvin-Helmholtz_Instability.ogv** *Source:* http://upload.wikimedia.org/wikipedia/commons/d/d8/Kelvin-Helmholtz_Instability.ogv *License:* Public domain *Contributors:*
- KHI.gif *Original artist:* KHI.gif: Bdubb12
- **File:Koch_Snowflake_Animated_Fractal.gif** *Source:* http://upload.wikimedia.org/wikipedia/en/e/e7/Koch_Snowflake_Animated_Fractal.gif *License:* CC-BY-SA-3.0 *Contributors:*

  I created this using Xaos and the Gimp

  Original artist:

  Nadimghaznavi
- **File:Laminar_flow.gif** *Source:* http://upload.wikimedia.org/wikipedia/commons/0/06/Laminar_flow.gif *License:* Public domain *Contributors:* HyperPhysicsh http://hyperphysics.phy-astr.gsu.edu/hbase/pfric.html *Original artist:* R Nave Georgia State University
- **File:Laminar_flow_profile.gif** *Source:* http://upload.wikimedia.org/wikipedia/commons/5/59/Laminar_flow_profile.gif *License:* Public domain *Contributors:* HyperPhysics http://hyperphysics.phy-astr.gsu.edu/hbase/pfric.html *Original artist:* R Nave Georgia State University
- **File:Laysan_albatross_chick_remains.jpg** *Source:* http://upload.wikimedia.org/wikipedia/commons/0/01/Laysan_albatross_chick_remains.jpg *License:* Public domain *Contributors:* [1] *Original artist:* Forest & Kim Starr (USGS)
- **File:Litography_archive_of_the_Bayerisches_Vermessungsamt.jpg** *Source:* http://upload.wikimedia.org/wikipedia/commons/3/38/Litography_archive_of_the_Bayerisches_Vermessungsamt.jpg *License:* CC-BY-SA-3.0 *Contributors:* ? *Original artist:* ?
- **File:LogisticMap_BifurcationDiagram.png** *Source:* http://upload.wikimedia.org/wikipedia/commons/7/7d/LogisticMap_BifurcationDiagram.png *License:* Public domain *Contributors:* Own work *Original artist:* PAR
- **File:Lorenz_attractor_yb.svg** *Source:* http://upload.wikimedia.org/wikipedia/commons/5/5b/Lorenz_attractor_yb.svg *License:* CC-BY-SA-3.0 *Contributors:* ? *Original artist:* ?
- **File:Lost_Hills_Subsidence_interferogram.jpg** *Source:* http://upload.wikimedia.org/wikipedia/commons/8/8f/Lost_Hills_Subsidence_interferogram.jpg *License:* Public domain *Contributors:* http://photojournal.jpl.nasa.gov/catalog/PIA03458 *Original artist:* JPL, Producer ID:MRPS97478
- **File:MARPOL_73-78_signatories.png** *Source:* http://upload.wikimedia.org/wikipedia/commons/a/ab/MARPOL_73-78_signatories.png *License:* Public domain *Contributors:* Own work *Original artist:* Jrockley
- **File:Machine_for_incorporating_liquids_and_finely-ground_solids.JPG** *Source:* http://upload.wikimedia.org/wikipedia/commons/7/7a/Machine_for_incorporating_liquids_and_finely-ground_solids.JPG *License:* Public domain *Contributors:* The elements of chemical engineering (1906) *Original artist:* Jacob Grossmann
- **File:Magnetic_Stirrer.JPG** *Source:* http://upload.wikimedia.org/wikipedia/commons/3/32/Magnetic_Stirrer.JPG *License:* CC-BY-SA-3.0 *Contributors:* photo taken by self *Original artist:* User:Ruhrfisch
- **File:Maldives_-_Kurumba_Island.jpg** *Source:* http://upload.wikimedia.org/wikipedia/commons/5/5b/Maldives_-_Kurumba_Island.jpg *License:* Public domain *Contributors:* Own work *Original artist:* PalawanOz
- **File:Mandelbrot-similar-x1.jpg** *Source:* http://upload.wikimedia.org/wikipedia/commons/2/2e/Mandelbrot-similar-x1.jpg *License:* GPL *Contributors:* ? *Original artist:* ?
- **File:Mandelbrot-similar-x100.jpg** *Source:* http://upload.wikimedia.org/wikipedia/commons/4/42/Mandelbrot-similar-x100.jpg *License:* CC-BY-SA-3.0 *Contributors:* ? *Original artist:* ?
- **File:Mandelbrot-similar-x2000.jpg** *Source:* http://upload.wikimedia.org/wikipedia/commons/8/82/Mandelbrot-similar-x2000.jpg *License:* CC-BY-SA-3.0 *Contributors:* ? *Original artist:* ?
- **File:Mandelbrot-similar-x6.jpg** *Source:* http://upload.wikimedia.org/wikipedia/commons/e/ed/Mandelbrot-similar-x6.jpg *License:* GPL *Contributors:* ? *Original artist:* ?
- **File:Meddes-20060320-browse.jpg** *Source:* http://upload.wikimedia.org/wikipedia/en/f/f7/Meddes-20060320-browse.jpg *License:* ? *Contributors:*

  NASA Official website, [1]. *Original artist:* ?
- **File:Merge-arrows.svg** *Source:* http://upload.wikimedia.org/wikipedia/commons/5/52/Merge-arrows.svg *License:* Public domain *Contributors:* ? *Original artist:* ?
- **File:Mergefrom.svg** *Source:* http://upload.wikimedia.org/wikipedia/commons/0/0f/Mergefrom.svg *License:* Public domain *Contributors:* ? *Original artist:* ?
- **File:Mixing_-_flusso_assiale_e_radiale.jpg** *Source:* http://upload.wikimedia.org/wikipedia/commons/7/7e/Mixing_-_flusso_assiale_e_radiale.jpg *License:* CC-BY-SA-3.0 *Contributors:* Own work *Original artist:* Aushulz
- **File:Munk_ICCE_1950_Fig1.svg** *Source:* http://upload.wikimedia.org/wikipedia/commons/d/db/Munk_ICCE_1950_Fig1.svg *License:* CC-BY-3.0 *Contributors:* http://journals.tdl.org/ICCE/article/view/904 *Original artist:* Walter H. Munk
- **File:Nj_cboug.jpg** *Source:* http://upload.wikimedia.org/wikipedia/commons/8/8a/Nj_cboug.jpg *License:* Public domain *Contributors:* ? *Original artist:* ?
- **File:Nrborderborderentrythreecolorsmay05-1-.JPG** *Source:* http://upload.wikimedia.org/wikipedia/commons/8/8a/Nrborderborderentrythreecolorsmay05-1-.JPG *License:* Public domain *Contributors:* Calexico New River Committee (CNRC) *Original artist:* CNRC
- **File:Nuvola_apps_edu_mathematics_blue-p.svg** *Source:* http://upload.wikimedia.org/wikipedia/commons/3/3e/Nuvola_apps_edu_mathematics_blue-p.svg *License:* GPL *Contributors:* Derivative work from Image:Nuvola apps edu mathematics.png and Image:Nuvola apps edu mathematics-p.svg *Original artist:* David Vignoni (original icon); Flamurai (SVG convertion); bayo (color)
- **File:Obvious_water_pollution.jpeg** *Source:* http://upload.wikimedia.org/wikipedia/commons/d/dd/Obvious_water_pollution.jpeg *License:* CC-BY-2.5 *Contributors:* ? *Original artist:* ?
- **File:Ocean_currents_1943_(borderless)3.png** *Source:* http://upload.wikimedia.org/wikipedia/commons/6/67/Ocean_currents_1943_%28borderless%293.png *License:* Public domain *Contributors:* Edited version of File:Ocean currents 1943 (borderless).png *Original artist:* US army
- **File:Ocean_gravity_map.gif** *Source:* http://upload.wikimedia.org/wikipedia/commons/8/8c/Ocean_gravity_map.gif *License:* Public domain *Contributors:* http://www.ngdc.noaa.gov/mgg/bathymetry/predicted/explore.HTML *Original artist:* NOAA

- **File:Ocean_surface_currents.jpg** *Source:* http://upload.wikimedia.org/wikipedia/commons/c/cc/Ocean_surface_currents.jpg *License:* Public domain *Contributors:* here *Original artist:* NOAA
- **File:Ocean_wave_phases_numbered.png** *Source:* http://upload.wikimedia.org/wikipedia/commons/3/3d/Ocean_wave_phases_numbered.png *License:* CC0 *Contributors:* Own work *Original artist:* Ingvald Straume
- **File:Office-book.svg** *Source:* http://upload.wikimedia.org/wikipedia/commons/a/a8/Office-book.svg *License:* Public domain *Contributors:* This and myself. *Original artist:* Chris Down/Tango project
- **File:OiintLaTeX.svg** *Source:* http://upload.wikimedia.org/wikipedia/commons/8/86/OiintLaTeX.svg *License:* CC0 *Contributors:* Own work *Original artist:* Maschen
- **File:Oil-spill.jpg** *Source:* http://upload.wikimedia.org/wikipedia/commons/2/2e/Oil-spill.jpg *License:* Public domain *Contributors:* US Gov NOAA *Original artist:* US Gov NOAA
- **File:Oil_Slick_in_the_Timor_Sea_September-2009.jpg** *Source:* http://upload.wikimedia.org/wikipedia/commons/0/02/Oil_Slick_in_the_Timor_Sea_September-2009.jpg *License:* Public domain *Contributors:* Transferred from en.wikipedia; transferred to Commons by User:Bobamnertiopsis using CommonsHelper.
Original artist: NASA Earth Observatory. Original uploader was Mattisse at en.wikipedia
- **File:Oiled_Bird_-_Black_Sea_Oil_Spill_111207.jpg** *Source:* http://upload.wikimedia.org/wikipedia/commons/f/fc/Oiled_Bird_-_Black_Sea_Oil_Spill_111207.jpg *License:* ? *Contributors:* ? *Original artist:* ?
- **File:Oiled_bird_3.jpg** *Source:* http://upload.wikimedia.org/wikipedia/commons/3/3f/Oiled_bird_3.jpg *License:* CC-BY-SA-3.0-2.5-2.0-1.0 *Contributors:* Own work *Original artist:* Brocken Inaglory
- **File:OintclockwiseLaTeX.svg** *Source:* http://upload.wikimedia.org/wikipedia/commons/8/8e/OintclockwiseLaTeX.svg *License:* CC0 *Contributors:* Own work *Original artist:* Maschen
- **File:OintctrclockwiseLaTeX.svg** *Source:* http://upload.wikimedia.org/wikipedia/commons/b/bd/OintctrclockwiseLaTeX.svg *License:* CC0 *Contributors:* Own work *Original artist:* Maschen
- **File:Orbital_wave_motion-Wiegel_Johnson_ICCE_1950_Fig_6.png** *Source:* http://upload.wikimedia.org/wikipedia/commons/3/32/Orbital_wave_motion-Wiegel_Johnson_ICCE_1950_Fig_6.png *License:* CC-BY-3.0 *Contributors:* http://journals.tdl.org/ICCE/article/view/905 *Original artist:* R.L. Wiegel & J.W. Johnson
- **File:PIA02740_lrg.jpg** *Source:* http://upload.wikimedia.org/wikipedia/commons/2/2c/PIA02740_lrg.jpg *License:* Public domain *Contributors:* ? *Original artist:* ?
- **File:PIA18430-SaturnMoon-Titan-EvolvingFeature-20140821.jpg** *Source:* http://upload.wikimedia.org/wikipedia/commons/e/e1/PIA18430-SaturnMoon-Titan-EvolvingFeature-20140821.jpg *License:* Public domain *Contributors:* http://photojournal.jpl.nasa.gov/jpeg/PIA18430.jpg *Original artist:* NASA/JPL-Caltech/ASI/Cornell
- **File:Perpetual_Ocean.ogv** *Source:* http://upload.wikimedia.org/wikipedia/commons/7/79/Perpetual_Ocean.ogv *License:* Public domain *Contributors:* http://svs.gsfc.nasa.gov/vis/a000000/a003800/a003827/prepetual_ocean_1080p30.mp4 *Original artist:* NASA/Goddard Space Flight Center
- **File:Phase_shift.svg** *Source:* http://upload.wikimedia.org/wikipedia/commons/5/55/Phase_shift.svg *License:* CC-BY-SA-3.0 *Contributors:* Own work *Original artist:* Peppergrower
- **File:Pollution_swan.jpg** *Source:* http://upload.wikimedia.org/wikipedia/commons/4/47/Pollution_swan.jpg *License:* Public domain *Contributors:* ? *Original artist:* ?
- **File:Portal-puzzle.svg** *Source:* http://upload.wikimedia.org/wikipedia/en/f/fd/Portal-puzzle.svg *License:* Public domain *Contributors:* ? *Original artist:* ?
- **File:Porto_Covo_pano_April_2009-4.jpg** *Source:* http://upload.wikimedia.org/wikipedia/commons/c/c7/Porto_Covo_pano_April_2009-4.jpg *License:* CC-BY-SA-3.0 *Contributors:* Own work *Original artist:* Alvesgaspar
- **File:PrestigeVolunteersInGaliciaCoast.jpg** *Source:* http://upload.wikimedia.org/wikipedia/commons/4/4a/PrestigeVolunteersInGaliciaCoast.jpg *License:* CC-BY-SA-3.0 *Contributors:* Own work *Original artist:* Viajero at English Wikipedia
- **File:Question_book-new.svg** *Source:* http://upload.wikimedia.org/wikipedia/en/9/99/Question_book-new.svg *License:* Cc-by-sa-3.0 *Contributors:*
Created from scratch in Adobe Illustrator. Based on Image:Question book.png created by User:Equazcion *Original artist:*
Tkgd2007
- **File:RadialDensityPREM.jpg** *Source:* http://upload.wikimedia.org/wikipedia/commons/8/89/RadialDensityPREM.jpg *License:* CC-BY-3.0 *Contributors:* Own work, Paper: http://www.gps.caltech.edu/uploads/File/People/dla/DLApepi81.pdf *Original artist:* AllenMcC.
- **File:Recording_Current_Meter.jpg** *Source:* http://upload.wikimedia.org/wikipedia/commons/e/e8/Recording_Current_Meter.jpg *License:* CC-BY-SA-3.0 *Contributors:* Personal photograph taken in the National Maritime Museum, London, UK *Original artist:* Rémi Kaupp
- **File:Rio_tinto_river_CarolStoker_NASA_Ames_Research_Center.jpg** *Source:* http://upload.wikimedia.org/wikipedia/commons/b/b0/Rio_tinto_river_CarolStoker_NASA_Ames_Research_Center.jpg *License:* Public domain *Contributors:* ACD03-0051-13 from http://www.nasa.gov/centers/ames/news/releases/2003/03images/tinto/tinto.html *Original artist:* Carol Stoker, NASA
- **File:RocketSunIcon.svg** *Source:* http://upload.wikimedia.org/wikipedia/commons/d/d6/RocketSunIcon.svg *License:* ? *Contributors:* Self made, based on File:Spaceship and the Sun.jpg *Original artist:* Me
- **File:Rti_base.png** *Source:* http://upload.wikimedia.org/wikipedia/en/a/a9/Rti_base.png *License:* PD *Contributors:* ? *Original artist:* ?
- **File:S.Carpet_Animated_Fractal.gif** *Source:* http://upload.wikimedia.org/wikipedia/commons/1/13/S.Carpet_Animated_Fractal.gif *License:* CC-BY-SA-3.0 *Contributors:* Created with Xaos and the Gimp *Original artist:* Nadimghaznavi
- **File:SAR-Lupe.jpg** *Source:* http://upload.wikimedia.org/wikipedia/commons/4/4b/SAR-Lupe.jpg *License:* GFDL *Contributors:* http://ru.wikipedia.org/wiki/%D0%A4%D0%B0%D0%B9%D0%BB:SarLupe.JPG *Original artist:* Marshall80
- **File:SAR_Kilauea.jpg** *Source:* http://upload.wikimedia.org/wikipedia/commons/6/61/SAR_Kilauea.jpg *License:* Public domain *Contributors:* http://photojournal.jpl.nasa.gov/catalog/PIA01763 *Original artist:* JPL
- **File:SAR_Kilauea_topo_interferogram.jpg** *Source:* http://upload.wikimedia.org/wikipedia/commons/1/11/SAR_Kilauea_topo_interferogram.jpg *License:* Public domain *Contributors:* http://photojournal.jpl.nasa.gov/catalog/PIA01762 *Original artist:* JPL

- **File:Saturn_Kelvin_Helmholtz.jpg** *Source:* http://upload.wikimedia.org/wikipedia/commons/2/27/Saturn_Kelvin_Helmholtz.jpg *License:* Public domain *Contributors:* http://photojournal.jpl.nasa.gov/catalog/PIA06502 *Original artist:* NASA
- **File:Scheme_eutrophication-en.svg** *Source:* http://upload.wikimedia.org/wikipedia/commons/d/dd/Scheme_eutrophication-en.svg *License:* Public domain *Contributors:* Vectorized version of Image:Eutrophication.jpg *Original artist:* Hans Hillewaert
- **File:Seasat.jpg** *Source:* http://upload.wikimedia.org/wikipedia/commons/7/7f/Seasat.jpg *License:* Public domain *Contributors:* http://www.jpl.nasa.gov/missions/missionImages.cfm?missionType=Seasat&fullTitle=Artist%27s%20Concept%20of%20Seasatt&missionID=223 direct link to the picture: http://www.jpl.nasa.gov/images/spacecraft/seasat/craft2-browse.jpg *Original artist:* Image Credit: NASA/JPL
- **File:Shallow_water_wave.png** *Source:* http://upload.wikimedia.org/wikipedia/commons/8/8e/Shallow_water_wave.png *License:* CC-BY-SA-3.0 *Contributors:*
- Shallow_water_wave.gif *Original artist:* Shallow_water_wave.gif: Kraaiennest
- **File:Ship_pumping_ballast_water.jpg** *Source:* http://upload.wikimedia.org/wikipedia/commons/a/a4/Ship_pumping_ballast_water.jpg *License:* Public domain *Contributors:* http://www.uscg.mil/hq/g-m/mso/ans.htm *Original artist:* US Coast Guard
- **File:Sjyang_waveGeneration.png** *Source:* http://upload.wikimedia.org/wikipedia/commons/4/4b/Sjyang_waveGeneration.png *License:* CC-BY-SA-3.0 *Contributors:* Own work *Original artist:* Seung Joon Yang
- **File:Soda_bubbles_macro.jpg** *Source:* http://upload.wikimedia.org/wikipedia/commons/1/1f/Soda_bubbles_macro.jpg *License:* Public domain *Contributors:* From en:Image:Soda bubbles macro.jpg *Original artist:* en:User:Spiff
- **File:Southern_ocean_gravity_hg.png** *Source:* http://upload.wikimedia.org/wikipedia/commons/a/a9/Southern_ocean_gravity_hg.png *License:* Public domain *Contributors:* Antarctic continent: own work; gravity field: NOAA/NGDC (Marks, McAdoo & Smith) *Original artist:* Hannes Grobe, AWI
- **File:SpongeDiver.jpg** *Source:* http://upload.wikimedia.org/wikipedia/commons/8/81/SpongeDiver.jpg *License:* Public domain *Contributors:* Own work *Original artist:* Bryan Shrode
- **File:Square1.jpg** *Source:* http://upload.wikimedia.org/wikipedia/commons/5/55/Lichtenberg_figure_in_block_of_Plexiglas.jpg *License:* Attribution *Contributors:* en:Image:Square1.jpg *Original artist:* Bert Hickman
- **File:Stephen_Merkowitz_NASA'{}s_Space_Geodesy_Project.ogv** *Source:* http://upload.wikimedia.org/wikipedia/commons/9/9f/Stephen_Merkowitz_NASA%27s_Space_Geodesy_Project.ogv *License:* Public domain *Contributors:* Goddard Multimedia *Original artist:* NASA/Goddard Space Flight Center
- **File:Stokes_sphere.svg** *Source:* http://upload.wikimedia.org/wikipedia/commons/a/ae/Stokes_sphere.svg *License:* CC-BY-SA-3.0 *Contributors:* self-made Based on: G.K. Batchelor (1967) *An introduction to fluid dynamics*, Cambridge University Press. Pages 230–235. *Original artist:* Kraaiennest
- **File:Stylised_Lithium_Atom.svg** *Source:* http://upload.wikimedia.org/wikipedia/commons/e/e1/Stylised_Lithium_Atom.svg *License:* CC-BY-SA-3.0 *Contributors:* ? *Original artist:* ?
- **File:Symbol_list_class.svg** *Source:* http://upload.wikimedia.org/wikipedia/en/d/db/Symbol_list_class.svg *License:* Public domain *Contributors:* ? *Original artist:* ?
- **File:TEIDE.JPG** *Source:* http://upload.wikimedia.org/wikipedia/commons/a/a8/TEIDE.JPG *License:* Public domain *Contributors:* ? *Original artist:* ?
- **File:Text_document_with_red_question_mark.svg** *Source:* http://upload.wikimedia.org/wikipedia/commons/a/a4/Text_document_with_red_question_mark.svg *License:* Public domain *Contributors:* Created by bdesham with Inkscape; based upon Text-x-generic.svg from the Tango project. *Original artist:* Benjamin D. Esham (bdesham)
- **File:Textile_cone.JPG** *Source:* http://upload.wikimedia.org/wikipedia/commons/7/7d/Textile_cone.JPG *License:* CC-BY-SA-3.0 *Contributors:* Location: Cod Hole, Great Barrier Reef, Australia *Original artist:* Photographer: Richard Ling (richard@research.canon.com.au)
- **File:TwoLorenzOrbits.jpg** *Source:* http://upload.wikimedia.org/wikipedia/commons/4/44/TwoLorenzOrbits.jpg *License:* CC-BY-2.5 *Contributors:* ? *Original artist:* ?
- **File:USA_tar_bubble_la_brea_CA.jpg** *Source:* http://upload.wikimedia.org/wikipedia/commons/0/0c/USA_tar_bubble_la_brea_CA.jpg *License:* CC-BY-SA-2.5 *Contributors:* Own work *Original artist:* Daniel Schwen
- **File:Uniform_Triangle_Mass_Center_grade_5_fractal.gif** *Source:* http://upload.wikimedia.org/wikipedia/commons/0/0c/Uniform_Triangle_Mass_Center_grade_5_fractal.gif *License:* CC-BY-3.0 *Contributors:* by programming it in java then editing it with gimp
  Previously published: yes, on my own web site: http://www.kriche.com.ar/root/programming/recursion/fractals.ht *Original artist:* Ignaciokriche
- **File:Upwelling.svg** *Source:* http://upload.wikimedia.org/wikipedia/commons/e/ee/Upwelling.svg *License:* Public domain *Contributors:*
- File:Upwelling.jpg *Original artist:* Lichtspiel
- **File:Venus_globe.jpg** *Source:* http://upload.wikimedia.org/wikipedia/commons/8/85/Venus_globe.jpg *License:* Public domain *Contributors:* http://photojournal.jpl.nasa.gov/catalog/PIA00104 *Original artist:* NASA
- **File:Von_Koch_curve.gif** *Source:* http://upload.wikimedia.org/wikipedia/commons/f/fd/Von_Koch_curve.gif *License:* Public domain *Contributors:* self made based in own JAVA animation *Original artist:* António Miguel de Campos
- **File:Wavecloudsduval.jpg** *Source:* http://upload.wikimedia.org/wikipedia/commons/e/e3/Wavecloudsduval.jpg *License:* CC-BY-SA-3.0 *Contributors:* English Wikipedia http://en.wikipedia.org/wiki/Image:Wavecloudsduval.jpg *Original artist:* GRAHAMUK, user of the English language Wikipedia
- **File:Waves_in_pacifica_1.jpg** *Source:* http://upload.wikimedia.org/wikipedia/commons/4/45/Waves_in_pacifica_1.jpg *License:* GFDL *Contributors:* Own work *Original artist:* Brocken Inaglory
- **File:Wea00810.jpg** *Source:* http://upload.wikimedia.org/wikipedia/commons/6/63/Wea00810.jpg *License:* Public domain *Contributors:* http://www.photolib.noaa.gov/bigs/wea00810.jpg *Original artist:* NOAA
- **File:Wedge_Newport_Hurricane_Marie_photo_D_Ramey_Logan.jpg** *Source:* http://upload.wikimedia.org/wikipedia/commons/b/bc/Wedge_Newport_Hurricane_Marie_photo_D_Ramey_Logan.jpg *License:* CC-BY-SA-4.0 *Contributors:* Own work *Original artist:* WPPilot
- **File:Wedge_Video_D_Ramey_Logan.ogv** *Source:* http://upload.wikimedia.org/wikipedia/commons/b/be/Wedge_Video_D_Ramey_Logan.ogv *License:* CC-BY-SA-4.0 *Contributors:* Own work *Original artist:* WPPilot
- **File:Wiki_letter_w.svg** *Source:* http://upload.wikimedia.org/wikipedia/en/6/6c/Wiki_letter_w.svg *License:* Cc-by-sa-3.0 *Contributors:* ? *Original artist:* ?

- **File:Wiki_letter_w_cropped.svg** *Source:* http://upload.wikimedia.org/wikipedia/commons/1/1c/Wiki_letter_w_cropped.svg *License:* CC-BY-SA-3.0 *Contributors:*
- Wiki_letter_w.svg *Original artist:* Wiki_letter_w.svg: Jarkko Piiroinen
- **File:Wikibooks-logo-en-noslogan.svg** *Source:* http://upload.wikimedia.org/wikipedia/commons/d/df/Wikibooks-logo-en-noslogan.svg *License:* CC-BY-SA-3.0 *Contributors:* Own work *Original artist:* User:Bastique, User:Ramac et al.
- **File:Wiktionary-logo-en.svg** *Source:* http://upload.wikimedia.org/wikipedia/commons/f/f8/Wiktionary-logo-en.svg *License:* Public domain *Contributors:* Vector version of Image:Wiktionary-logo-en.png. *Original artist:* Vectorized by Fvasconcellos (talk · contribs), based on original logo tossed together by Brion Vibber
- **File:Yellowstone_mud_pot_p1090998.jpg** *Source:* http://upload.wikimedia.org/wikipedia/commons/3/34/Yellowstone_mud_pot_p1090998.jpg *License:* CC-BY-SA-3.0 *Contributors:* ? *Original artist:* ?

|

- Creative Commons Attribution-Share Alike 3.0

}}